PROCESSES AND STRATEGIES FOR SOLID STATE
Q-SWITCH LASER MARKING OF POLYMERS

PROCESSES AND STRATEGIES FOR SOLID STATE
Q-SWITCH LASER MARKING OF POLYMERS

PROEFSCHRIFT

ter verkrijging van
de graad van doctor aan de Universiteit Twente
op gezag van de rector magnificus
prof.dr. W.H.M. Zijm
volgens besluit van het College voor Promoties
in het openbaar te verdedigen
op vrijdag 26 oktober 2007 om 16.45 uur

door

Johan Bosman

geboren op 2 april 1968

te Meppel

Dit proefschrift is goedgekeurd door
prof. dr. ir. J. Meijer, promotor.

Preface

The work presented here is a part of the work I have done for the past ten years at the Philips Centre for Industrial Technology (CFT). The CFT changed its name to Applied Technologies (Apptech). In these past ten years I have been lucky to participate and contribute to the development of solid state lasers for industrial use. The development in laser material processing has been interesting with lots of new developments. New wavelengths, higher pulse energies and shorter pulses enabled an almost unlimited range of processes. The development of new laser processes and applications is still going on. The industrial applications are in 2007 entering the pico second range and will soon step over to femto second systems making the laser as an industrial tool even more versatile and flexible. This thesis focuses only on a part of the applications of lasers in industry, but a visible one: laser marking with Q-switch solid state lasers on polymers.

Acknowledgements

Summary

The overview of all laser marking processes for a wide range of materials shows the versatile aspect of laser technology. The statement that all materials can be written by laser is temping but not correct. The writing of liquids and gasses is possible but not practical. The overview of processes for laser marking is therefore a practical guide for the use of laser marking.

Flexibility and a readable contrast are the key items for the application of laser marking. The low thermal conductivity and high transparency of polymers makes the laser the best tool to get energy into a volume of a polymer. By using different wavelengths this absorption is selective. This enables selective bleaching of pigments for full colour laser marking.

Samenvatting

Het overzicht van alle laser mark processen voor een breed scala aan materialen geeft de veelzijdigheid van laser technologie weer. De uitspraak dat alle materialen gemarkeerd kunnen worden is verleidelijk maar niet correct. Het beschrijven van vloeistoffen en gassen is mogelijk maar niet praktisch. Het overzicht van de laser markeerprocessen is daarom een praktische gids voor het gebruik van laser markeren.

Flexibiliteit en een leesbaar contrast zijn de belangrijkste elementen voor de toepassing van laser markeren. De geringe thermische geleiding en grote licht doorlaatbaarheid van kunststoffen zorgen ervoor dat de laser een goed toe te passen gereedschap is om energie binnen in een polymeer volume te krijgen. Door verschillende golflengten te gebruiken is deze energie absorptie selectief. Hierdoor kan het worden gebruikt om pigmenten te bleken voor laser marken

SYMBOLS AND NOTATION

Symbols	Description	Units
a	Thermal diffusivity ($a = k / \rho\, c_p$)	$m^2\,s^{-1}$
A	Transversal area in resonator	m^2
c	Speed of light in vacuum ($2.9979246\ 10^8$)	$m\,s^{-1}$
c_P	Thermal capacity at constant pressure	$J\,kg^{-1}\,K^{-1}$
d	Diameter of laser spot	m
d_x, d_y	Length (width) of laser spot in x (y) direction	m
d_{vect}	Minimum distance between two non parallel vectors	m
E_{dis}	Dissociation energy	K
E_p	Pulse energy	J
E	Photon energy	eV
F	Laser fluence	$J\,m^{-2}$
f	Focal length lens	m
f_Q	Laser pulse frequency	s^{-1}
h	Planck's constant ($6.62176\ 10^{-34}$)	$W\,s^2$
$I(x,y)$	Laser beam intensity profile	$W\,m^{-2}$
I_0	Laser beam intensity (x = 0, y = 0)	$W\,m^{-2}$
k	Thermal conductivity	$W\,m^{-1}\,K^{-1}$
k	Boltzmann's constant ($1.28066\ 10^{-23}$)	$W\,s\,K^{-1}$
L	Optical length resonator	m
M^2	Times-diffraction limited factor, or beam quality ($M^2 \geq 1$)	-
N_A	Avogadro's number ($6.02205\ 10^{23}$)	mol^{-1}
m	Mass	kg
n	Index of refraction	-
P	Laser power	W
Q	Total energy release during laser pulse	J
R_L	Reflectivity	-
R_{loss}	Resonator loss	-
R	Gas constant (8.3143)	$J\,mol^{-1}K^{-1}$
T	Temperature, Temperature rise	K
$T_{\frac{1}{2}}$	Half lifetime temperature	K
t	Time	s
t_p	Pulse width or length of laser pulse (FWHH, full width at half height)	s
t_{start}	Time before scanner starts moving	s
t_{stop}	Time after scanner stops	s
v	Laser beam velocity (scan)	$m\,s^{-1}$
w	Waist radius	m
x	Coordinate (in direction of beam translation)	m
Δx	Distance between two laser spots	m

Δy	Distance between two lines	m
y	Coordinate (perpendicular to direction of beam translation)	m
z	Coordinate (in direction of laser beam, depth)	m
α	Linear absorption coefficient	m^{-1}
α_{inout}	Angle between the incoming ray and the outgoing ray	rad
β	Scattering distribution parameter	-
γ	Non linear absorption coefficient	m^{-2}
α_s	Scatter coefficient	m^{-1}
δ_o	Optical penetration depth	m
δ_h	Thermal penetration depth	m
ε	Emissivity	-
ξ	Mie parameter	-
Θ	Angle of incidence	rad
	Rotation angle galvanometer	rad
λ	Wavelength	m
λ_0	Wavelength in vacuum	m
ρ	Density	$kg\ m^{-3}$
σ	Stefan-Boltzmann constant ($5.67051\ 10^{-8}$)	$W\ m^{-2}\ K^{-4}$
τ_λ	Spectral transmittance	m^{-1}
σ	Absorption cross-section for two photon excitation	m^2
Φ	Photon intensity per unit area per unit time	$m^{-2}\ s^{-1}$

Contents

xiv

Chapter 1   Introduction

1.1   Laser engraving

The growing need to identify and trace products in a production line but also during its entire lifetime requires a permanent marking. Laser engraving is the best and most applied technique to make such permanent marks on a wide range of materials. The high process yield enables the use of a laser engraving machine at the end of the production line. At this stage of production the product has it's highest value and so will be the costs of any loss of yield. For IC marking the most used technology is laser engraving. This is a one step process. There is no post - or pre processing necessary. One aspect of laser engraving that should not be neglected is the laser safety. The use of concentrated laser energy could easily damage eyes. Therefore the use of laser engraving is regulated in the international laser safety norm IEC 60825 –1.
The wide range of laser systems available nowadays enables laser engraving for every material. Whether it is a colour change or a structural change that changes the reflection of the surface.
The major advantages of laser engraving are:

- Small character features possible, laser can be focused easily below 30 μm spot diameter.

- Marking of difficult printable materials like Polypropylene and Glass.

- High temperature resistance of the marks, because no additive material is necessary for direct laser engraving.

- No chemicals.

- Low and predictable maintenance and costs of the laser engraving machine.

- Curved surfaces and difficult places like the bottom of a hole or around a pin are possible.

Industrial marking applications can be characterised as one production cycle (first time right), limited available writable area, human and machine readability, low costs, low and predictable maintenance and information content always as much as possible. In a growing number of cases laser engraving is the answer for all these demands. The importance of laser marking will grow because the reduction of the laser engraving systems price will increase the number of economical viable applications. Combined with the availability of other wavelengths and pulse lengths more marking applications will be feasible.

1.2   Processes and strategy

Laser engraving has found a major application field in polymer engraving. The use of laser in this field is often governed by trial and error. This thesis was started as more insight was needed to use the full potential of laser engraving.

The focus is on the production technical aspects of laser engraving and the introduction of processing strategies. Less attention is paid to the complex chemical processes that can be observed when using laser as a tool to chance the visible material appearance. The goal is to identify guidelines that can be used to control the laser engraving process in a production environment and to catalogue the different phenomenon of laser polymer interaction and their use for laser engraving.

1.3   Outline of the Thesis

This thesis is divided into six parts. Five of them relate to the use of solid-state Q-switch lasers for engraving and decoration applications in polymers. Although this thesis is focused on polymer materials it was felt necessary to give an overview of the complete field of laser engraving and decoration for all the different material classes, including fruit and eggs. The laser material interaction processes are described for these different materials. Resulting in a matrix containing all laser engraving applications (Chapter 2).

The thermal nature of laser marking polymers introduces effects like non-uniform colouring of the polymer and increase of marking line width. The reason of this behavior can be explained by looking at the unique aspects of polymers with respect to the low absorption, low thermal diffusion combined with the optical and degradation behavior. This results in a complete different laser processing compared to metal laser processing (Chapter 3).

The important aspects of industrial laser marking are: a constant, readable and uniform mark written within the available time limited by the production cycle. To achieve this scan strategy is used to ensure that no time is lost to unnecessary movements and the thermal behavior of the polymer can be compensated to avoid unwanted thermal effects (Chapter 4).

Solid-state Q-switch lasers are the most important class with regard to laser engraving. A wide range of pulse widths and pulse energies combinations are available. Chapter 5 uses the pulse width and pulse energy characteristic of solid-state lasers to reduce the amount of experiments normally used for process design. This enables a more machine independent process design. It is also used to compare different solid-state Q-switch lasers and to describe new developments like higher pulse frequencies enabling faster engraving.

Chapter 6 and Chapter 7 focus on two specific laser marking processes in polymers: bleaching of pigments and the reduction of titanium dioxide (TiO_2).

Chapter 8 describes possible new applications and developments in the field of laser marking.

Chapter 2   The art of laser-marking

2.1   Introduction laser–marking

Philips uses laser marking when flexible information is needed to identify and trace its products. The wide range of Philips' products enabled me to gather in the past twelve years much information about laser marking. The innovative side of Philips' products also made it possible to develop new ways of laser marking and to expand the application of lasers in marking. This chapter gives an overview of the wide range of applications where laser marking can be used. Some of the applications are mature but also new ones are presented. A lot of the application descriptions are based on own work done in the paste twelve years for Philips factories, Philips Research and in the Brite-Euram projects Syladec and Licopal.

2.2   Laser-marking processes

The goal of laser-marking is to generate a visual contrast. This contrast can be achieved in two ways, either a change in colour or a change in the specular reflection (gloss) (Klimt 1988). A wide variety of materials (glass, ceramics, silicon and polymers) can be marked using laser (Meier and Weinfurtner 1990). There are a number of different processes that change the colour or the specular reflection of materials under laser exposure. However, it is possible to distinguish the same principle for different classes of materials. For example, the removal of material by vaporization (ablation) can be used for metals, glass, silicon, ceramics, and polymers. Table 2.1 shows the combination of processes and materials. This overview shows the versatility of the polymer group. The effect of the processes, either colour-change or specular reflection (**Colour**/**Reflection**) is also shown in this table. The table can be used if a specific marking application has to be developed. The specific properties of a material determine which process will prevail. Often this will not be one isolated process. In practice, due to the laser-intensity distribution and the subsequent reaction of material, more than one process will take place. The processes given in Table 2.1 are detailed in the following paragraphs. The last paragraph describes materials that can be classified as natural materials. These materials like apple skin and textiles shouldn't be omitted in this overview of laser marking because they form a considerable application field.

Table 2.1: Laser-marking processes.
R = Reflection, *change in reflection*
C = Colour, *change in colour*
- *= low contrast, + = normal contrast, ++ = very good contrast*

Materials / Processes	Metal (2.5)	Glass (2.6)	Silicon (2.7)	Ceramics (2.8)	Polymers (2.9)
Ablation	R +	R +	R +	R -	R -
Fragmentation		R +			
Oxidation	C ++				R -
Melting	R +	R +	R +	R -	R -
Alloying/doping	C +	C +		C +	C ++
Reduction		C +		C +	C ++
Optical breakdown		R +			R +
Foaming					C ++
Bleaching					C +
Colour-forming		C++			C ++
Transfer	C +	C +		C +	C ++
Carbonisation					C ++
Unzipping					R +
Dehydration	C ++				C ++

2.3   Equipment for laser marking

Almost all types of lasers are used for marking. An overview is given in Table 2.2. The solid-state lasers, including Q-switched, pulsed, and continuous, form an important group of laser systems used for marking and engraving. The power range of the CO_2 lasers used for marking is large. Next to the low-power CO_2 laser (< 10 W) high power systems up to several kW (Dijk 2004) are used for marking steel plates. The pulsed TEA CO_2 laser (10 W, t_p 70 ns) for example is widely used for marking beer-bottle labels (Nilson 1982). Excimer lasers are used for making small micro-marks on glasses (Daniels and Schuerle 1989). Such marks are made often for counterfeiting reasons. The labelling of cables, for example for the use in aircraft, is another application area of the excimer laser marking (Dance 1990). The typical spot diameter of some lasers is far below 80 μm, which is the threshold for the naked eye. Such small marks are often used for machine vision systems. Using such a small spot for human readable codes is possible if multiple lines are used to create wider lines. The extra lines increase the total writing time. A much faster approach is to increase the spot width by using a longer focal length lens or another beam expander. As also the resolution decreases, the latter can only be done to a limited size. Readability and appearance could become a problem.

Table 2.2: Overview of lasers used for marking & engraving.

Wavelength	Laser type	Typical Pulse/cont., (t_p pulse width)	Typical spot diameter or mask resolution.
SOLID-STATE			
1064 nm	Nd:YAG	Q-switched/pulse/cont. , t_p 150 ns	80 μm
	Nd:YVO$_4$ or Vanadate	Q-switched, t_p 10 ns	50 μm
	Fibre laser	cont. 100 W	50 μm
		Pulsed 20 W, t_p 50 ns	50 μm
532 nm	2nd Nd:YAG	Q-switched/cont. , t_p 150 ns	50 μm
	2nd Nd:Vanadate	Q-switched, t_p 10 ns	30 μm
355 nm	3rd Nd:YAG	Q-switched , t_p 100 ns	20 μm
	3rd Nd:Vanadate	Q-switched/mode-locked, t_p 10 ns	20 μm
266 nm	4th Nd:YAG	Q-switched, , t_p 10 ns	15 μm
GAS LASER			
10.6 μm	CO$_2$ sealed tube.	cont. 20 W	150 μm
	CO$_2$ TEA	pulsed 10 – 20 W, t_p 70 ns	200 μm, marking res.
	CO$_2$ fast axial	cont. 1 – 10 kW	300 μm
457.9 nm	Ar-ion	cont. 60 mW	2 μm
488 nm	Ar-ion	cont. 300 mW	2 μm
514.5 nm	Ar-ion	cont. 300 mW	2 μm
632.8 nm	He-Ne	cont. 30 mW	50 μm
510.5 / 578.2 nm	Cu vapour	Pulsed 25 W, t_p 30 ns	20 μm
EXCIMER			Mask resolution:
351 nm	XeF	Pulsed	<1 μm
308 nm	XeCl	Pulsed	<1 μm
248 nm	KrF	Pulsed	<1 μm
248 nm	KrF	Femto	<1 μm
222 nm	KrCl	Pulsed	<1 μm
193 nm	ArF	Pulsed	<1 μm
157 nm	F$_2$	Pulsed	<1 μm

2.4   Beam handling methods

Beam handling is an essential aspect of laser marking. There are three different methods: 1. polygon systems, 2. mask projection and 3. beam deflection systems. An overview is given in Table 2.3.

The term laser-engraving refers to the applications using beam deflection systems while the term laser-marking is often used as a more common name for all methods including the mask projection applications.

Table 2.3: Beam handling methods.

Beam handling method	Specifics	Elements
Polygon		Polygon mirror
Masks	Fixed masks	Transmission mask
		Reflective mask
		Diffractive mask
	Software driven masks	LCD mask
		Micro mirrors
Beam deflection systems	Mechanical	XY translation tables
		Galvanometric mirrors
	Optical	Acousto-optic deflection

Figure 2.1 show the schematic overview of three most used beam handling methods.

2.4.1   Polygon scanner

A polygon scanner enables high speeds, but no vector-oriented scanning. The laser-beam is deflected in one direction by a rotating polygon mirror. The effectiveness of polygon scanners is therefore limited. The laser energy has to be modulated by a mask to write patterns and an additional movement is required to allow a scan in two dimensions.

2.4.2   Fixed masks

The projection of a shaped mask is very effective if used with a pulsed laser. This mask can stay fixed or exchanged between pulses. In this way texts can be written on a moving product. The maximum speed for this type of marking is limited by the maximum shift of the product during a pulse. For example, if a laser with pulse duration of 10 ns is used, and a maximum shift of 1 μm is allowed, then the maximum speed will be 100 m/s. This could mark a text on a TGV train travelling at 360 km/hour. The frequency of the laser will be 66 kHz for 1 mm characters with 0.5 mm character spacing. While the time to change the mask would be 15 μs. Typical applications are marking of beer bottles labels (by removing ink from the paper label), marking cables and marking of electronic components.

Instead of a transmission mask also reflective masks are used which reflect the required mark. The unused part of the beam is scattered out of the imaging system. This type of mask don't need the characteristic dams that are used for metal transmission masks. The dams allow only semi open characters. For excimer applications often quartz transmission masks are used or diffractive masks. The diffractive masks use interference to create the pattern.

One major disadvantage of the transmission masks is the loss of energy due to the partial transmission. Professor Olsen developed an optical system to re-use the reflected energy from the mask. A concave mirror placed in the beam path above the mask increases the amount of energy through the mask (Bastue and Olsen 1996).

1. Incoming laser beam
2. Polygon
3. Deflected laser beam

1. Laser beam
2. Beam expander
3. Galvo motor + mirror
4. fΘ lens
5. Focal plane

1. Laser beam
2. Mask
3. Lens
4. Image plane
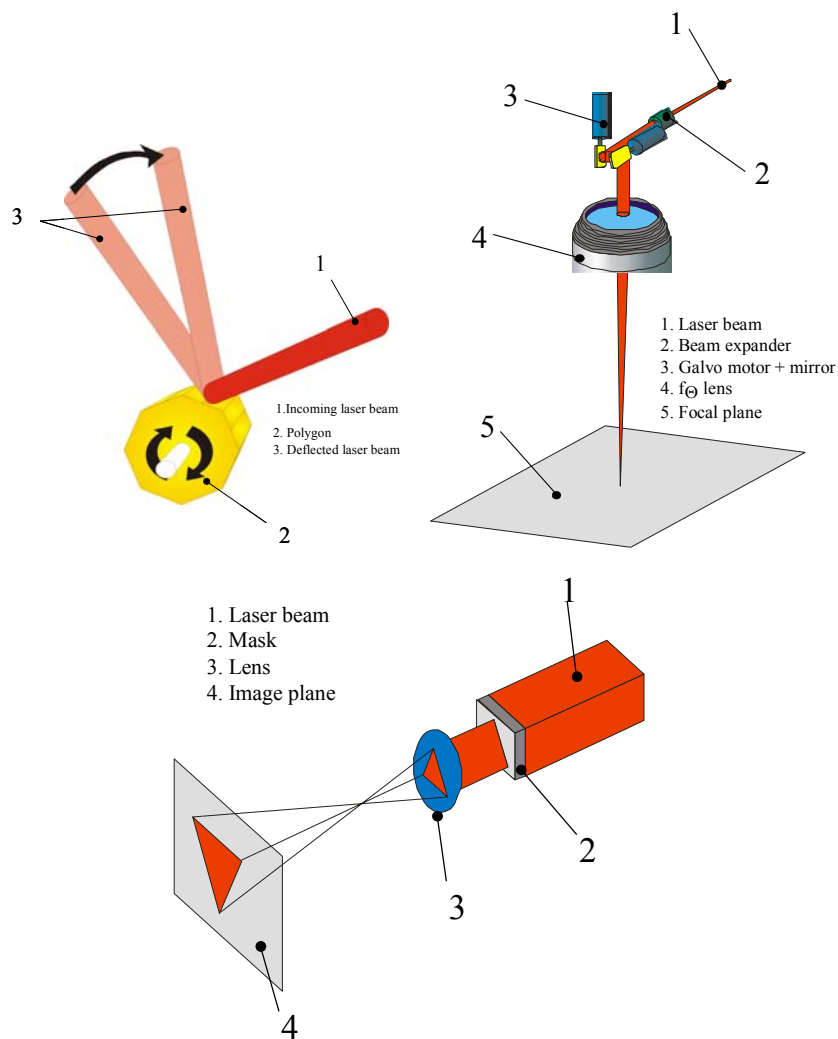
Figure 2.1: Top left, polygon scanner, Top right, galvanometric mirror system,
Bottom, mask
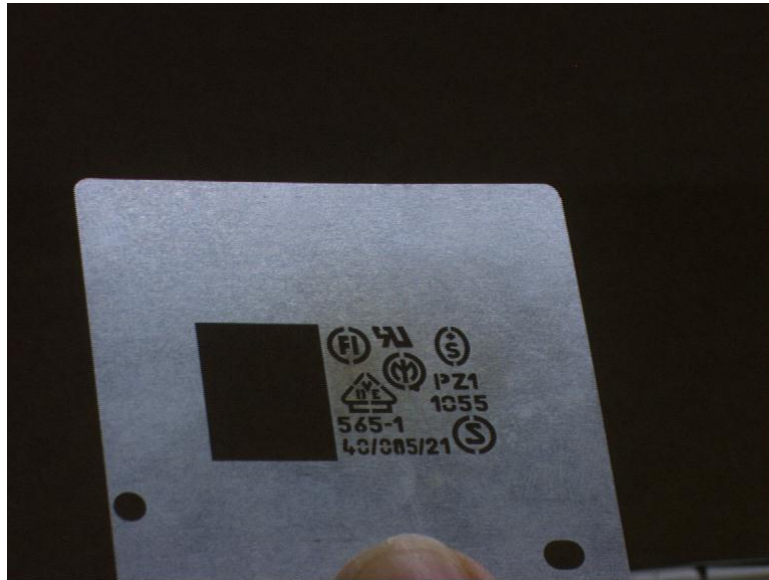
Figure 2.2: Mask with semi open characters used for component marking by TEA CO$_2$ laser.

2.4.3   Software driven masks.

The first introduction of software driven masks was made by the company Komatsu in 1995. These masks are based on Liquid-Crystal-technology (Masashi 1995) and have a limited lifetime due to the absorption of laser energy. Kuntze reported in 2003 the use of a micro mirror array as mask for an excimer laser (Kuntze, Panzner et al. 2003). This type of flexible mask could reach a higher marking speed than high speed galvanometric systems without loosing its flexibility.

2.4.4   Beam deflections by galvanometric mirrors.

The most common method is to focus the laser beam to a small spot and to move either the product or the laser beam. The high speed that is needed to write within an acceptable period favours the deflection of the laser beam as a way to write patterns on a product. The mass of the two mirrors is often less than a complete XY-table needed for the product movement. Figure 2.1 shows a schematic view of a beam-deflection unit or scanner. The laser beam is first expanded resulting in decreased laser intensity at the mirrors and a smaller focus diameter. After the expansion the beam is deflected by two galvanometric mirrors, and subsequently focused by a scan lens (fΘ lens). The fΘ lens has a flat focal plane and a linear relation between the deflection angle and its deviation in the X-direction. For small deflection angles a normal thin lens can be

used. This gives a smaller spot size but at large deflection angles the linear relationship between deflection and angle becomes invalid.

The two separate mirrors introduce a distortion of the scan field due to the different distances to the lens. The vector path can compensate this distortion to a certain extend. The distance between the separate mirrors makes also the lens design more difficult and rotation dependant.

A single mirror scanner would be a more effective solution. Special for large apertures the size of the second mirror limits the fast movements. The second mirror has to be so big because it should deflect a line projected by the first mirror. A single mirror scanner was demonstrated in the Amulet project by Hafez and Janssen (Hafez, Slider et al. 2000). The challenge of a single mirror unit is to full independence of both scan directions.

The vector-oriented way of writing, and the use of programmable deflection units, enables a high flexibility. Together with higher pulse frequencies more and complex codes become possible.

The effective use of these high frequency systems is limited by the maximum speed of the scanning systems. For example, if a laser delivers pulses at 100 kHz, and the distance between the pulses has to be 80 μm, this already requires a scanner with a linear speed of 8 m/s. This means an angular velocity for a 160mm fϴ-lens of approximately 50 rad/s. A typical galvanometric system (2005) with an aperture of 7 mm is specified to reach speeds of 18.8 rad/s and a step response of 0.25 ms for 1/10 of the full scale (Scanlab 2004).

The high pulse rates of the new generation solid-state lasers will enable laser processes beyond the 100 kHz mark. Meaning that higher speeds would enable high resolution marks for example for full and individual traceability of automotive parts.

2.4.5   Beam deflection by an acousto-optic deflector/modulator.

Almost all Q-switch lasers use an acousto-optic modulator to generate the Q-switch pulses by blocking the resonator. This enables the build-up of the inversion. This inversion is released by de-blocking the resonator causing an avalanche like build up of the laser pulse.

When the incident and the diffracted beam are equally inclined to the acoustic wave a constructive interference occurs because the phase difference becomes zero. This angle is called the Bragg angle (Scruby and Drain 1990; Brimrose 2003). The small angle of deflection of the available crystals is the reason why an acousto-optic (AO) deflector isn't used for standard engraving applications. A way to use best of both worlds (galvanometric scanner and AO deflector) is to combine the fast but small angle deflection of the AO deflector and the larger angle of the galvanometric scanner. If a galvanometric scanner travels at its highest possible speed errors are made. For example the highest forces act on the mirrors during the writing of small characters. The small radii and abrupt stops of these characters need a high bandwidth scanner. The AO deflector can be used to compensate these errors by measuring the response and a real time correction. Another way is to avoid the high frequencies by filtering them out and feed this high frequency signal to the AO deflector. The AO deflector and modulator is already used in high frequency laser systems (>200 kHz) were the modulation of the laser causes instabilities. The AO deflector is used as a shutter enabling the laser to run freely at its most stable point, unaffected by the modulation needed for the writing. Although the AO is an extra element in the system the advantage of a highly stable laser pulse train compensates this. Nippon telegraph and telephone corporation has grown a KTN crystal ($KTa_{1-x}Nb_xO_3$) with a high electro-optic effect.

The main application is the use in waveguides for optical modulators. Only 1/10 of the standard voltage is needed (Fujiura 2005). The KTN material is well known but is very difficult to grow.
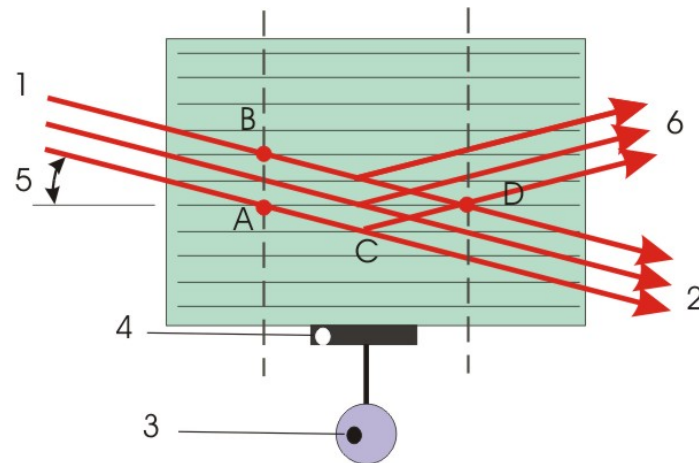
1 Incident laser beam
2 Zero Order beam
3 Electrical input
4 Transducer
5 Bragg angle
6 Diffracted beam

Figure 2.3: AO deflector, length ACD =BD.

The size NTT showed enables the use of the KTN material for laser scanners. The material enables a 100 times faster response time and reduces the size of the scanner considerable. At this moment (2007) there are no scanners based on this material commercially available according to Kazuo Fujiura (Fujiura 2007). A test setup at NTT showed a 12° angle. This angle is acceptable for some applications. A conventional scanner has a scan angle of ±20°. The AO scanner would enable two axis scanning in one device enabling a more efficient lens design as the lens doesn't have to optimised for two different mirror distances. Especially for larger apertures this would be a big advantage.

2.5   Marking of metals

Marking of metal objects has found a major application field in tools for medical applications. Laser technology was the only process that could meet the high demands of marking each tool uniquely. Surgical tools have to be cleaned and sterilised at a high temperature, and the marking

should last the tool's lifetime. If the marks are cut into the metal, bacteria could survive. Laser-generated oxide layers made it possible to have a durable mark without the risk of contamination. The effectiveness of laser marking, and its ability for integration in automated production lines, further stimulated the use of laser marking on metal objects. The processes used for laser marking of metals range from the high-power, deep-penetration marking used for security codes in the automotive industry, to the low-energy fine marking of precision products.

2.5.1   Metal ablation

Ablative marking removes a surface layer of a metal product. Sometimes an extra layer is applied for marking only. The ablation removes that layer, generating a colour difference. Without the extra layer the ablative mark is seen by its difference in specula reflection.

If no precaution is made to prevent re-deposition alongside the mark, an extra cleaning step is necessary which might change the mark appearance, because the ablative product will be oxidised, see Figure 2.4 top. By removing this coloured debris the mark will be less visible. Toth (1999) showed that the ablation of thin metal films involves all three phases (melt phase, solid phase and gas phase). The re-solidified droplets can be difficult to remove. To prevent contamination a protective coating could be applied before laser marking and removed afterwards. PVA (poly vinyl alcohol) as used in hair spray is a good method to protect even optical grade metals. It can be removed using warm water. That metal ablation can be controlled also in depth shows the application of marking 3D spectacle moulds, see Figure 2.6 bottom. By controlling both pulse energy and focus position the depth of the marking is controlled within 100 nm. For these applications different depth are necessary for different types of moulds. Figure 2.4 bottom shows a white light interferic measurement of a micro mark made in Stavax. The mark is made with a 3rd harmonic Nd:YAG with a 3 μm spot diameter. The line width of 10 mm is achieved by placing two lines with a 3 μm distance.

A frequently used method is the ablation of a black anodised layer on Aluminium. This gives a white appearance on a black background, see Figure 2.5 left. After the removal of the anodised layer a new layer can be re-grown and subsequently dyed with a contrasting colour. After hydration this mark is permanent (Hamano and Kato 1994) ,see Figure 2.5 right.

Creating a rough background can increase the low contrast of a laser mark on aluminium, see Figure 2.6 top.

Prichystal showed that it is possible to drill blind holes in aluminium and to stop when only a small layer of aluminium is still hiding the holes. The small layer of aluminium is so thin that light can travel through it. To avoid any deformation a grid of larger blind holes is drilled first with a bigger diameter and after that the smaller holes to the surface can be drilled. A sensor setup stops the process just before breaking though the aluminium (Prichystal, Hansen et al. 2005).
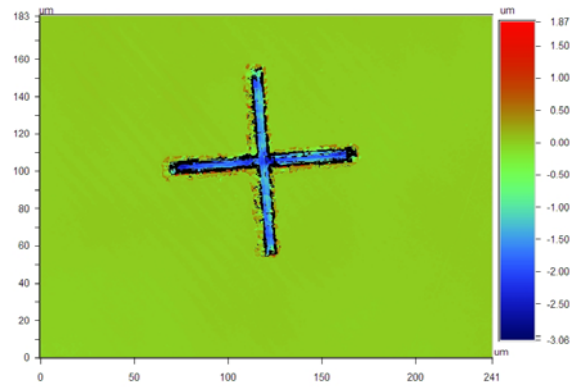
Figure 2.4: Top, metal engraving of steel, the different colours are due to oxidation [Q-switched Nd:YAG]. Bottom, micro marking with nanosecond laser line width 10 μm polished Stavax (30 mm fθ lens) [3rd Q-switched Nd:YAG, 355 nm].

Figure 2.5:Left, anodised aluminium ablation[2nd Q-switched Nd:YAG, 532 nm]. Right, grey logo in the middle is applied by re-growth of previously ablated anodised layer on Aluminium [Q-switched Nd:YVO$_4$].
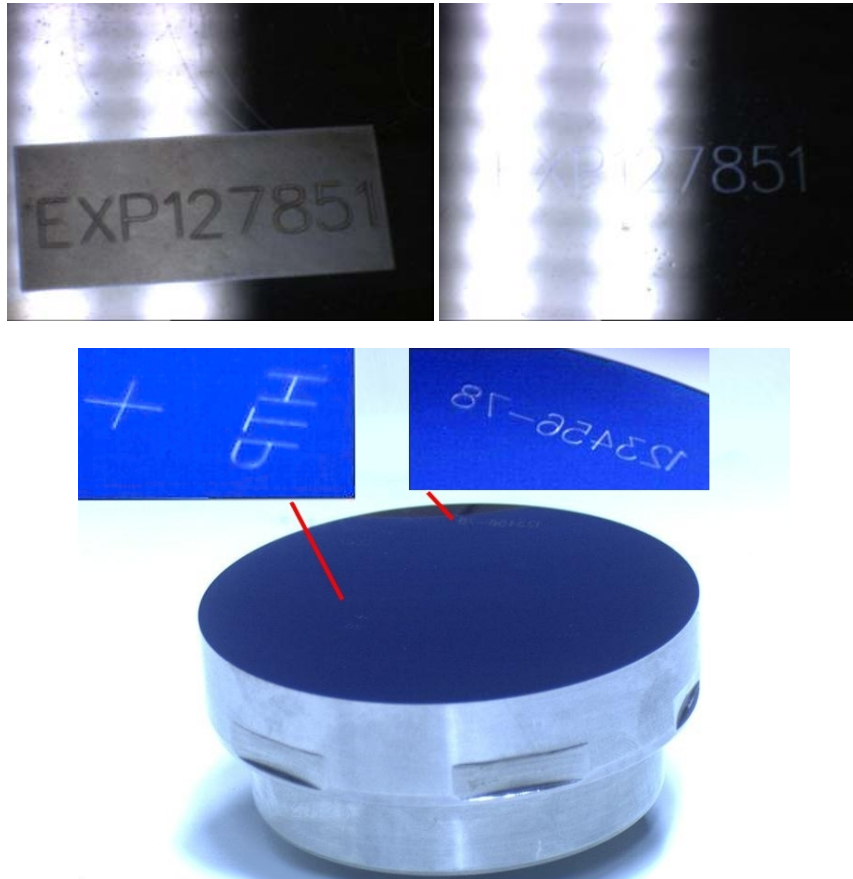
Figure 2.6: Top, rough background to enhance contrast of mark on polished stavax (1.5 mm height) [3rd harmonic Q-switched Nd:YAG laser, 355 nm].
Bottom, spectacle mould [Q-switched Nd:YVO$_4$].

2.5.2   Metal oxidation

A beautiful concept of marking of metals is to oxidise the metal surface locally by the influence of laser irradiation. The oxide layer is formed with a certain thickness. By interference of light this thin layer creates the typical interference colour. By changing the laser parameters and scan settings the temperature and also the oxide layer thickness can be tuned to the desired colour (Nanai, Vajtai et al. 1996), see Figure 2.7 top left.

The use of patterned oxidised layers to create colours is used by Nagata (1994). Nagata used laser beam interference to irradiate a metal surface to generate a fine pattern (oxide or nitrogen) in a high temperature Oxygen or Nitrogen atmosphere. The small feature size diffracts light as a function of the wavelength. The interference pattern can also be made under atmospheric conditions using a copper vapour laser. The period of the interference pattern (typical 1 μm) is determined by the angle between the two identical laser beams and the wavelength that is used,

see Figure 2.7 top right. Aluminium gives under normal atmospheric conditions a white mark. Under an argon atmosphere (1 bar) the marking is black with the same laser settings as used for the white mark.
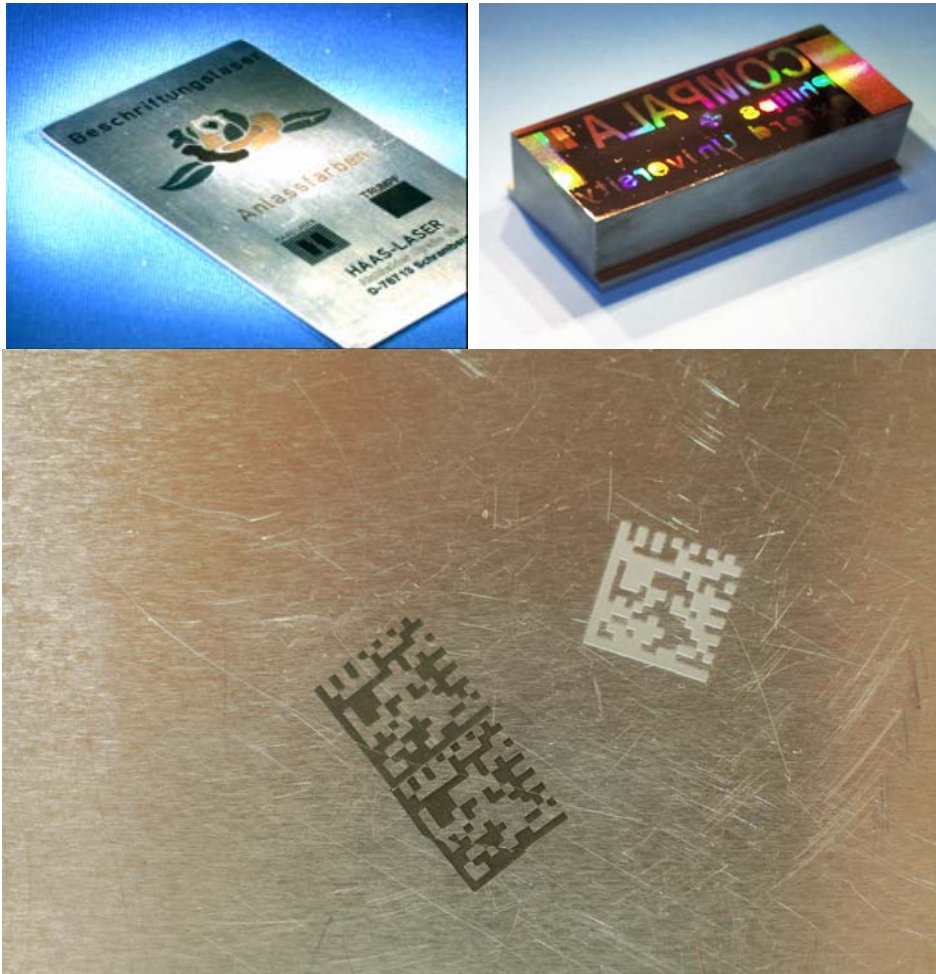
Figure 2.7: Metal oxidation
Top left: RVS coulered, source: Trumpf "Haas" [Q-switched Nd: Nd:YVO$_4$].
Top right: interference pattern marking, source:
Brite Euram Compala project (BE95 –122) [Copper vapour laser].
Bottom: oxidation of aluminium in argon (black) and normal atmosphere (white)
[3rd Q-switched Nd:YAG, 355 nm].

Laser beam

Beam splitter
binary phase grating

Compressor

Lens

Focal point
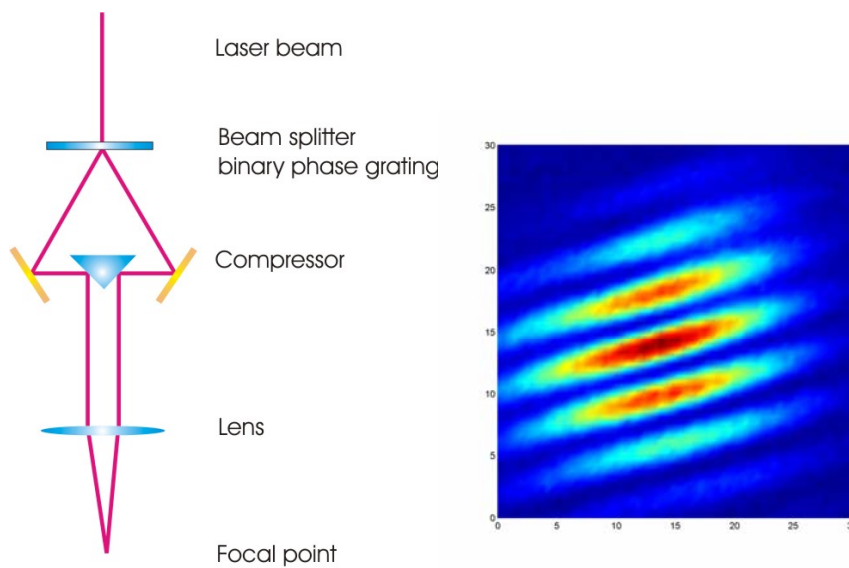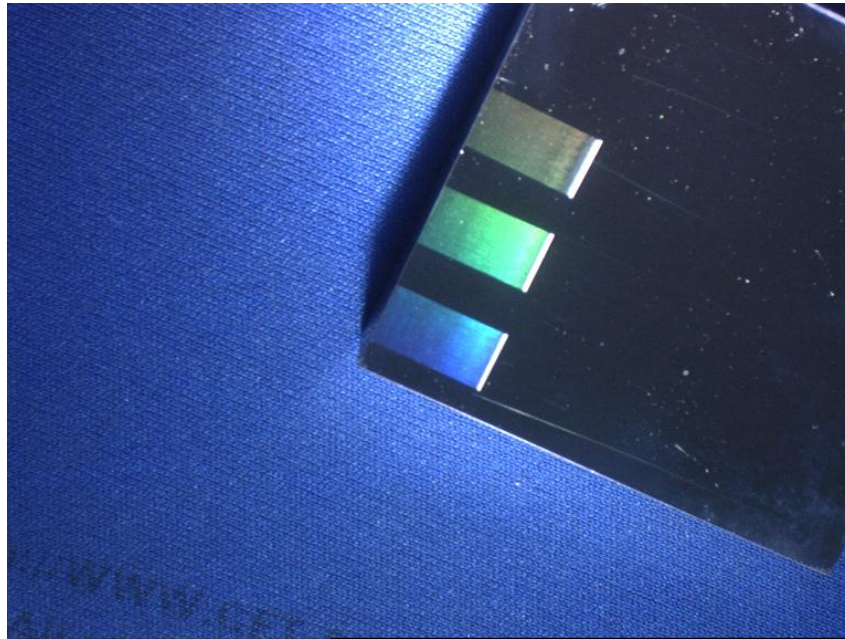
Figure 2.8: Top, marking of Stavax steel with galvanometric scanner setup (30 mm aperture) at
1064 nm [Q-switched Nd: Nd:YVO$_4$, Pulse time 10 ns].
Bottom left, interference setup using binary phase grating beam splitter
(higher orders are not displayed).
Bottom right, energy distribution in the spot in μm 80 mm lens interference period 4 μm
(x-axis y-axis in μm).

The setup shown in Figure 2.8 is the use of two beam interference together with a scanner movement. The laser is split by a binary phase grating into two laser beams (-1st, +1st order). The design of the binary grating is optimised to suppress the zeroth order completely and to reduce the higher orders as much as possible. These gratings are used also for two spot laser welding. The benefit of using this setup is that the 50% splitting is designed in the grating. The two laser beams are put together using a reflection coated prism after being aligned using two mirrors.

This optical setup is easily put in front of laser scanner with a large aperture. The scanner lens put the perpendicular laser beams together resulting in the interference pattern shown in Figure 2.8 bottom right.

2.5.3   Metal melting

Metal melting without oxidation requires an inert atmosphere. These marks will be visible only by a difference in specula reflection. The re-solidified material has not only changed its shape, but can also have a different surface morphology, texture or in case of steel can be transformed to martensite. At high power a keyhole or deep penetration can be made. The material will re-solidify as a trench with side bumps, see Figure 2.9. These markings are difficult to remove because the heat-affected-zone (HAZ) remains visible even after a complete removal of the top layer. At high power levels, the process tends to a drilling process (Michl 1992) (Weinfurtner 1995).
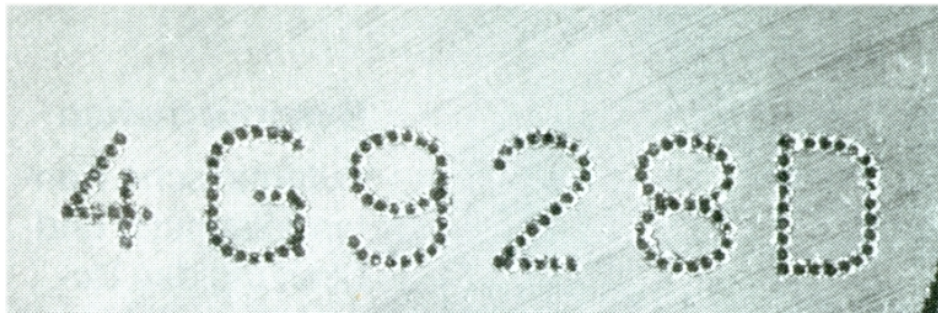
Figure 2.9: Deep engraving the penetration depth is about 1mm,
source: Rofin-Baasel [150W pulsed Nd:YAG].

2.5.4   Metal alloying/doping

Alloying is used to modify the surface of a metal object by incorporation of foreign elements into the surface layer of the material by melting or diffusion. The bulk properties remain unchanged. Next to the well-known use of alloying for functional applications, alloying can also be used to generate colours locally. Marking through alloying/doping the base material with a laser is not

very common. It is used mainly in situations the product has already a metal coating. Alloying can also be used to change the absorptivity and the melting point of a material. This makes the surface better markable e.g. Sn on Cu (Bosman and Dooren 1998)

2.5.5 Metal transfer

A metal layer (transfer layer) can be transferred from a foil or glass plate (carrier layer) to a product surface by one or more laser pulses. This process is used to produce a clear contrast (Kantor, Toth et al. 1994). There are two mechanisms: forward- and backward-transfer. The forward version transfers the metal layer by focusing through the carrier layer ablating the metal and transferring it at the underlying product surface, see Figure 2.10 left. The adhesion of the layer is important to obtain a good, homogeneous pattern. In case of backward-transfer the laser beam is focused through the product and the metal layer is transferred backwards to the laser. This is applied to depositing material locally, for example on glass, see Figure 2.10 right.

The main aspect about forward transfer of a metal layer from a carrier is to avoid vaporisation before the complete layer is molten. Otherwise if the top part of the layer is already vaporised while the bottom is still solid, a pressure is built up resulting in a poor quality (spraying) (Schultze and Wagner 1991). The gap between the foil and surface can be in the order of the width of the transferred line. Much more will result in a diffuse edge. Often no gap at all is easier to sustain especially if the used foil is thin.
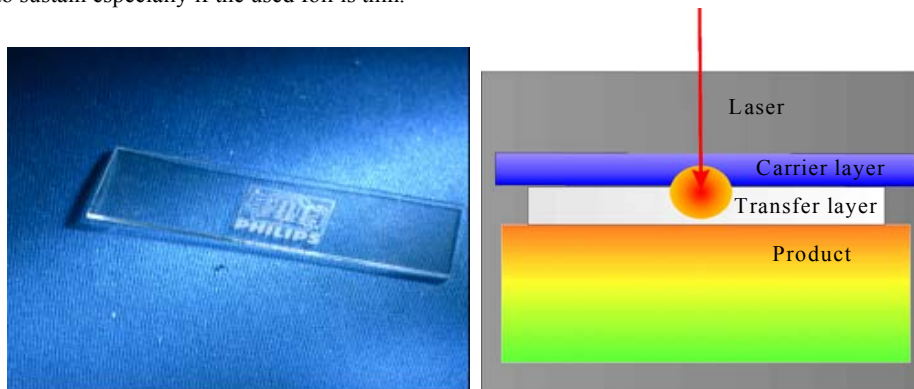
Figure 2.10: Left, forward-transfer transfer of Aluminium on glass, [Q-switched Nd:YAG]. Right, principle of laser-induced forward-transfer.

2.5.6 Metal - Ceramic dehydration of anodised Aluminium

The top layer of a dye containing anodised aluminium plate ($Al + Al_2O_3$ layer) can be dehydrated by laser irradiation and afterwards re-coloured. The principle of this method is as follows: the dehydration of the top layer of aluminium hydroxide opens-up the pores in which a dye is encapsulated. The increased volume of the aluminium hydroxide is used to block the dye

containing pores of the aluminium oxide. When the aluminium hydroxide is removed by laser irradiation the dye can be washed out of the anodised layer, see Figure 2.11 left. This method of re-colouring anodised layers was invented by P. Laakmann (1990; 1991; 1993) of the Synrad company. Synrad used a lacquer to seal the re-dyed anodised layer because the laser treatment opened the surface too much to enable a good sealing by aluminium hydroxide.

Another method is to apply a doping in the oxide layer to generate colour marks on a metallic, coloured and aluminium substrate. For example Ammonium metavanadate (NH_4VO_3) reduces to blue (VO_2). By dehydrating it to V_2O_5 a red/brown colour is obtained (Mann 1983), (Azuma and Sakaki 1987). The use of an oxide layer made by oxalic acid shows a similar behavior and is used to generate a decorative marking irons (Yeo 2004), see Figure 2.11 right.

Figure 2.11: Left, anodised aluminium re-colouring, source: Synrad [CO$_2$ laser].
Right, colour-forming in anodised aluminium, source: Philips DAP LTM(ATC)
[Q-switched Nd:Vanadate].

2.6   Glass

Glass can be marked in eight different ways. These methods are: Ablation, fragmentation, melting, alloying, reduction, optical breakdown, colour forming and glass transfer. The ablation and fragmentation of glass is used for example in marking glass substrates. Often ablation and fragmentation leads to cracking. Cracks are not accepted for high temperature or long lifetime applications. But if the glass can be melted or alloyed while heated smooth marks without cracks can be made. The marking of the UHP lamps in the Philips factory in Turnhout (Belgium) is a good example of the use of this method in production. The reduction of glass works only for a limited amount of glass under a reducing atmosphere. Glass optical breakdown is a well known application because all 3D in glass shapes are made with this process. Often the question if colours are possible is asked during 3D in glass marking demonstrations. And some doped glass show colour forming under a combination of high intensity and thermal process conditions. The process of glass transfer enables high resistance marks.

Keeping all these possibilities in mind the most effective method is ablation if fracturing the glass is permitted. The forming of cracks reduces the high stress caused by the absorption of laser energy. This absorption is limited to the far infrared and UV region of the spectrum.

An alternative to laser marking of glass is chemical etching with HF-acid. Polymeric masks are used to create the desired patterns. This is a highly toxic but cheap process and can cause severe damage to skin and tissue. Also the flexibility is limited as the masks have to be made in advance, applied and removed. This is the reason that pulsed TEA CO_2 lasers are used for many years for marking TV tube (CRT) glass, see Figure 2.12 right. Glass easily forms cracks under pressure generated by thermal expansion of the glass during the CO_2 laser pulse. The optical penetration depth of 10.6 μm (CO_2 laser) for BK7 glass is only a few μm, see Table 2.4. This energy is even after 1 μs still contained in a few μm thin layer because of the low thermal diffusion. If a 10 Hz TEA CO_2 is used with pulse energy of 500 mJ and a pulse time of 1 μs to heat up an area of 25 mm^2 the temperature will rise by more than 4000 K vaporising the glass. A small TEA laser of 5 W is capable to remove glass from a surface, partially by vaporisation and melting, but also by breaking out small particles. For marking without any cracks, short-pulse UV lasers (typical pulse width 30 ns.) are used. The short pulse and high intensity lead to surface ablation without severe thermal effects in depth.

Table 2.4: Optical penetration depth (δ_0) and thermal diffusion length (δ_h) for CO_2 lasers ($\lambda =$ 10.6 μm) as function of pulse width t_p (Bauerle 1986), (Leyen 1971), (Wood 1995), (Schott 2004)

	α^{-1} [cm^{-1}] absorption coeff.	D diffusivity [cm^2/s]	δ_0 [μm]	δ_h [μm] pulse width t_p			
				100 ns	*500 ns*	*1 μs*	*1 ms*
SiO$_2$	2.5×10^2	0.0086	40	0.6	1.3	1.9	58.7
BK7	1×10^4	0.0052	1	0.5	1.0	1.4	45.6

2.6.1   Glass ablation

Ablation of glass is done by a TEA CO_2 laser or by an excimer laser. Both wavelengths are absorbed in the first microns of the material. The ablation results in a rough surface. The contrast comes from the diffuse reflections of the rough surface. The TEA CO_2 laser is used for marking lamp bulbs, see Figure 2.12 left. The cracks generated by the marking could reduce the lifetime of the bulb by crack-propagation due to moisture.

By using an excimer laser at 193 nm the ablation depth of glass becomes less. This is used for small semi-visible marks on spectacle lenses (Daniels and Schuerle 1989). The short pulse length (30 ns) and high intensity reduces the thermal load of the glass compared to the long wavelength and longer pulse length (1 μs) of the TEA CO_2 laser.

Although the optical penetration depth of BK7 glass for 355 nm is still 30 cm it can be decreased to μm range by multi photon absorption at high laser intensities. This is the reason why a short pulse Q-switched 355 nm laser is able to ablate soda lime glass directly on the surface, see Figure 2.13 right.

Figure 2.12: Left, ablative mark laser of incandescent lamp. Right, ablative mark for laser TV tube marking, both done by [TEA CO$_2$].

Marking of glass using different kinds of removable coatings has been reported by Kvapil (1990) and Sato (1995). Sato used coloured paraffin that was ablated by a laser, and after HF-etching a mark is made. Kvapil etches the glass using an absorbing layer for plasma generation. Lenk reported that a short-pulse, high-intensity laser could generate the plasma at the glass surface. The plasma absorbs laser energy and etches the glass surface without the need for a coating. This method result in small marks (diameter <15 µm) without thermal stress (Lenk, Witke et al. 1998).

2.6.2 Glass fragmentation by particle impact

Laser ablation of Al$_2$O$_3$ generates particles with a high kinetic energy that are used to mark. The glass plate is placed in proximity of the Al$_2$O$_3$ substrate and the laser enters the substrate through the glass. These markings are 5 – 10 µm deep, see Figure 2.13 left. The use of Al$_2$O$_3$ as an intermediate considerably prevents for thermal stress in the glass (Bosman 1996). This can only be achieved by laser irradiation that is not absorbed by the glass, for example 1064 nm. To increase the absorption of the Al$_2$O$_3$ at 1064 nm an absorbing dye is used.
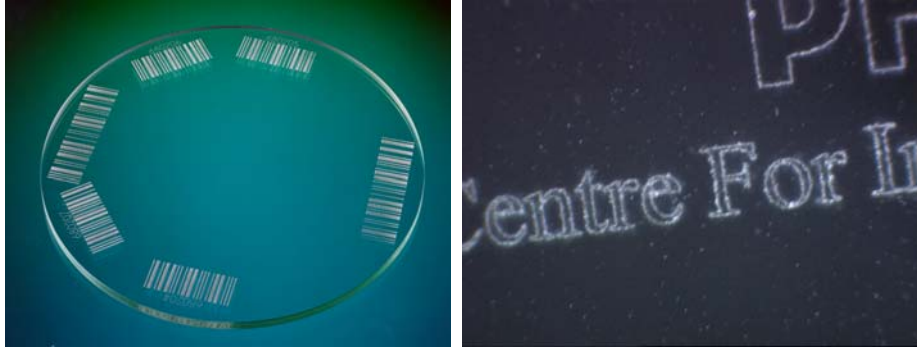
Figure 2.13: Left, abrasive glass-marking done by indirect method [Q-switched Nd:YAG]. Right, UV direct glass marking [3rd harmonic Nd:YAG laser, 355 nm].

2.6.3 Glass and Quartz melting

Melting and colouring of quartz is used to mark lighting bulbs. The low thermal expansion and high thermal resistance of the quartz prevents cracking, see Figure 2.14 left bottom. Laser induced melting of normal glass is also possible but generates cracks (Staupendahl and Gerling 1997) due to the internal stress caused by the thermal expansion specially during the cooling of the glass. Using preheated glass is a way to prevent cracks. A slow cooling phase is used to ensure that the internal stresses are reduced, see Figure 2.14 top.

The melting method can be applied for marking glass with colours. The laser generates a melt pool into which pre-heated powder is blown through a nozzle (Boden, Richter et al. 1983). The used air, glass surface and powder are pre-heated to about 400 °C to prevent crack-formation. The melt pool is made by a 200 W CO_2 laser. Boden also reported coloured laser marking of glass using a two step process without powder spraying. The molten glass solidifies into a concave form and can be filled with a coloured glass frit. A subsequent heating step (500 – 550 °C) will re-melt the frit and forms a coloured mark in the glass surface.
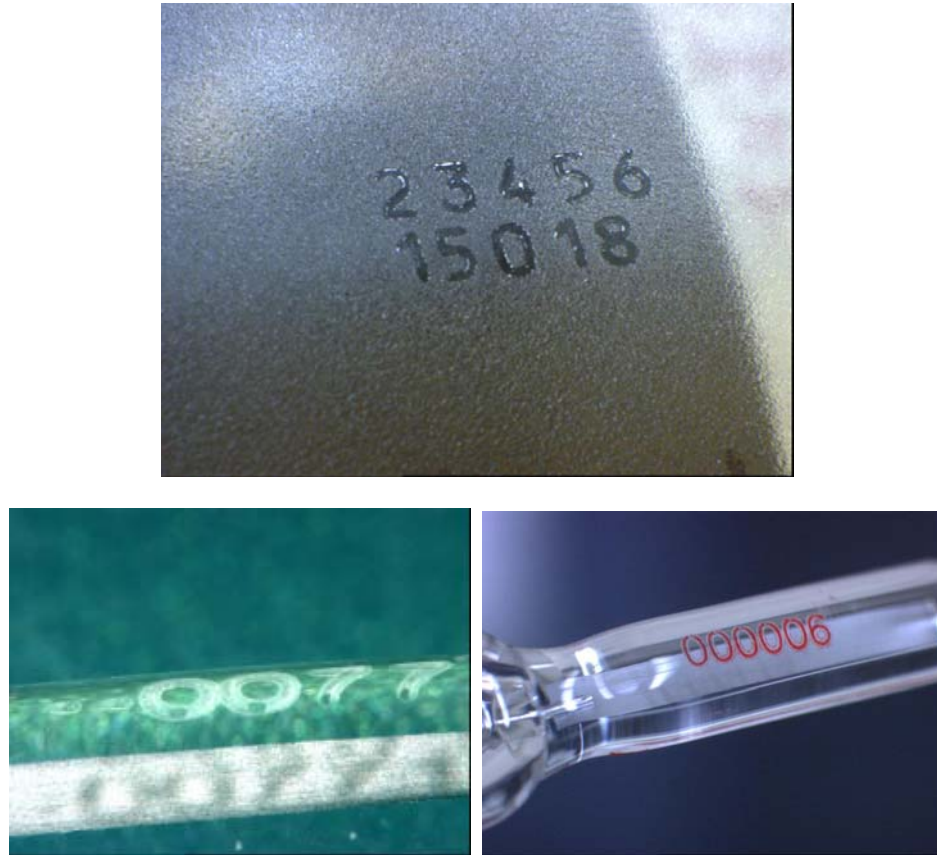
Figure 2.14: Top, surface melting of preheated glass [CO$_2$ laser].
Bottom, quartz melting by CO$_2$ laser and subsequent filling by coloured glass frit (right).

2.6.4   Glass alloying/doping

Carbon layers are used to enhance the laser absorption for metals but can also be used to mark glass. The fusion of the carbon layer with top layer of the glass leaves a permanent mark (Guskov 1984). This phenomenon was also observed when a mark was made through a glass plate onto a polymeric material. A Q-switched Nd:YAG laser (20 J/cm^2) was able to mark the glass while carbonising the polymer. Lucchesi (1996) marked glasses with diffusing materials like CuSO$_4$ and Ag$_2$O into glass, see Figure 2.15 left.

The Thermark patent by Harrison (2000) uses a low temperature glass frit or metal oxide applied as a layer and subsequent melting by the laser. Already in 1981 Boden (1983) blows the glass frit directly in the melt pool generated by a 20 – 200 Watt CO$_2$ laser. Boden claims that his application is better than a method described in the Japanese patent IA 49 – 4352. This Japanese patent describes the applying of a colour coating to a glass or ceramic substrate and the

subsequent laser melting of this layer. The new aspect of the Thermark patent is the use of absorbance enhancers, see Figure 2.15 right.

Glass frit or enamels can be marked when an opaque pigment is diluted by laser irradiation. This gives a transparent mark with a background-dependable contrast (Schumacher 1985).
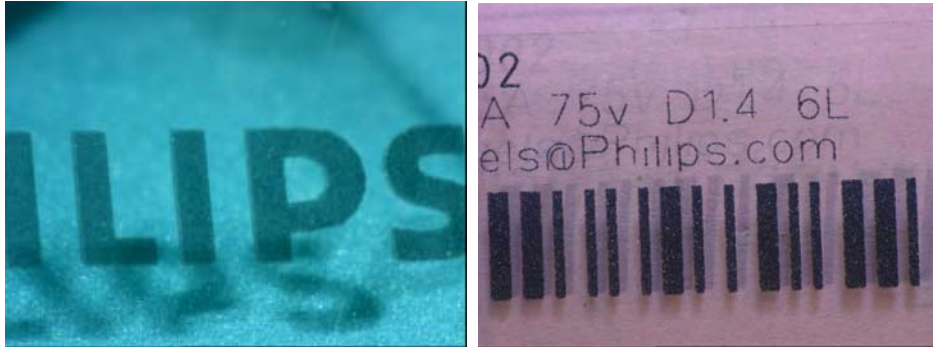
Figure 2.15: Left, carbon fusion at the glass,[[Q-switched Nd:YAG].
Right, Thermark glass mark [cw Nd:YAG].

2.6.5 Glass reduction

Glass is often used with a coating, for example to reflect sunlight (Gold) or to get a self-cleaning surface (TiO_2). For example a thin layer of TiO_2 can be reduced without destroying the layer. Hofmann (1989) of Ciba Geigy reported this method while using thin TiO_2 layers on ceramics and glass (Coating thickness: 10 nm to 1 μm). He used a third harmonic Nd:YAG laser and an Ar-ion laser to get sufficient absorption in the TiO_2 layer. This generates a dark mark on the glass surface.

2.6.6 Glass optical breakdown, in-glass marking

A high intensity laser beam induces nonlinear absorption in transparent media through two photon ionisation and avalanche ionisation (Dickmann and Dik 1995; Lenk, Witke et al. 1998).

This intensity dependent absorption enables the heating of a localised volume inside a glass sample. This area has a high pressure build up through the thermal expansion. If the heated volume is cooled through diffusion to the surrounding volume a crack is formed. Measurements of the stress inside the glass showed a high level of internal pressure. The amount of energy needed to generate an inside crack is thermal expansion dependent. A low expanding material has a higher crack threshold than a high expanding material. Using multiple pulses with intensities below the crack threshold at the same position will result in the same kind of fracture in the glass, see Figure 2.16 left. Agadjanov described this decorative use of thermally induced cracks inside glass already in 1971 (Agadjanov 1971). A well known application of this principle is the making

of 3D engravings in glass cubes. The focus plane starts at the bottom of the model and it moves upwards for every new 2D slice from the 3D model, see Figure 2.16 right.

Clements et all (Clement, Ledger et al. 1993) patented the idea again in 1990 but excluding all thermal effects of the process during the appeal of LPKF and Fraunhofer-Gesellschaft (Moser 2002). From our own experiments with soda lime glass we learned that cracks are already possible below the reported value of Clement at 355 nm. The use of multiple pulses at one spot lowers the necessary energy level even further and makes the patent obsolete. Erokhin has patented the use of a different intensity distribution (TEM01) which also causes cracks inside glass without a violation of the Clement patent (Erokhin 1993).

For highly doped glasses, such as used in CRT tubes and lead glasses, the method of inside marking is limited to small depth because the optical penetration depth is small (Kichelhain, Kusnezow et al. 1998; Dmitriev, Oshemkov et al. 2000). If the laser is focused too deep in the material the laser intensity is not sufficient anymore due to the scattering and absorption of the laser irradiation along its path. With a 100 mm lens we were able to mark inside a volume CRT tube glass at a maximum depth of 1 mm.

Figure 2.16: Left, in-glass marking set 2 mm below the glass surface, glass plate thickness 6mm,
fΘ 160 mm, P ~0.5 W , Q 10 kHz, 10 pulses at one spot,
Picture dimensions 4*3 mm, [3rd harmonic Nd:YVO$_4$].
Right, 3D picture in glass, cube dimension 40x40x80 mm [3rd harmonic Nd:YAG].

The small cracks made with 355 nm enables the use of filled patterns. The structure can be completely filled with cracks without destroying the glass object. This enables a much higher scattering causing the object in the glass to become completely white. This effect was used in the first Philips Blu-Ray recorder, see Figure 2.17.

Figure 2.17: Blu-Ray recorder Philips, top backside full in glass marking with blue led illumination [3rd harmonic Nd:YAG].

2.6.7   **Glass Colour-forming, in-glass marking**

Troiski (Troitski 2002) describes three different ways to generate coloured laser-induced images. First the use of colour centres which are defects (vacancies) in the regular spacing of atoms. A 3rd harmonic laser (355 nm) with a pulse energy of 0.05 mJ with a pulse width 10 ns already generates colour centres in soda lime glass. A second method is the use of space shapes inside the glass having a colour. The third method Troiski describes is the use of latent images in photosensitive glass and subsequent thermal processing either by a laser or full thermal processing of the glass volume. Troitski states that the use of photosensitive glass (for example doped with gold or silver particles) is of limited use because it is restricted to a relative shallow surface layer due to the dose dependant generation. Using an infra-red laser induced plasma inside the glass a broad spectrum of radiation is generated at the position of the focus. This radiation includes also the short ultraviolet wavelengths needed for the generation of the latent images. The infra-red wavelength is not able to colour the glass. Troitski mentions also the use of a short pulse (femto to pico seconds) to form the latent image. The crack caused by the shockwave of the plasma is sufficiently small to go unnoticed but the latent image is generated by the radiation of the plasma.

Gaissinsky also proposes three strategies to write colours inside glass: 1. Writing a latent image using multiple pulses at the same spot and subsequent heating by laser or volume heating. 2. Writing the latent image under exposure from a second laser or light source (UV) and subsequent heating. 3. Writing in a preheated glass volume (150 °C to 500 °C (Gaissinsky 2003). The higher

temperature of the last of Gaissinsky methods uses the extra mobility in the glass to develop the exposed areas during the laser treatment.
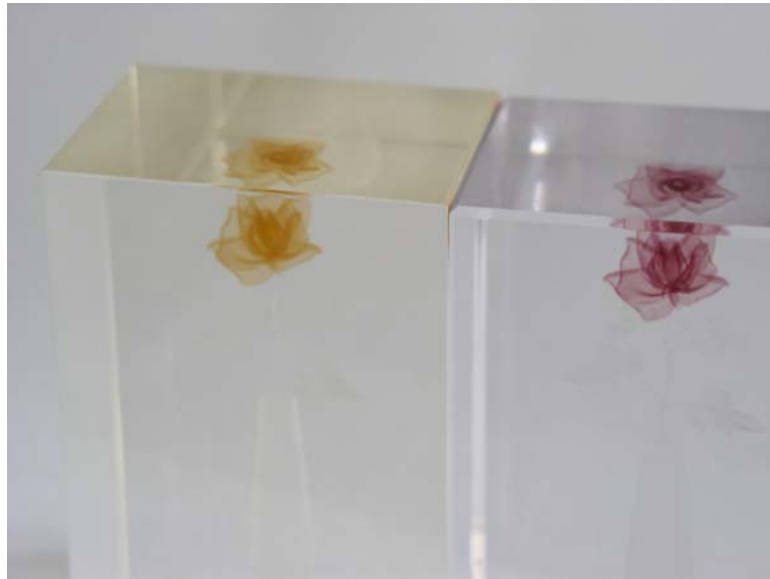
Figure 2.18: in-glass coloured marks (source: Laser Glass Ltd, Crystal impressions).

The use of different development strategies can yield different colours for the same photosensitive glass and make at least two colours possible in the same glass. A drawback of photosensitive glass could be the slight volume colouring, see Figure 2.18.

2.6.8   Glass transfer

Back-transfer of quartz onto a silicon wafer was shown by Veiko (1996). The principle is the use of a wavelength transparent substrate and an absorbing material as transfer medium. The transfer medium is evaporated by the laser energy focused through the substrate.

To transfer quartz to a silicon-wafer Veiko used a CO_2 laser. The wavelength (10.6 μm) of the CO_2 laser is transmitted through the silicon wafer onto the quartz target. Due to the high absorption the quartz evaporates onto the silicon surface. The pattern made had a layer thickness of 100 – 150 μm. This method is a forward transfer because the transfer medium is transferred away from the laser source. Backward transfer (transfer to the laser) of ceramic particles was reported by Weisser and Müller (Weisser and Mueller 1996). The laser is focused through the glass onto the layer containing the ceramic particles and binder. The ablation and subsequent deposition of the particles is caused by the evaporation of the polymeric binder. The particles are bonded to the glass by heating the particles by the same laser source, see Figure 2.19. The deposited particles not heated by the laser can be easily removed after wards.

Figure 2.19: Deposited ceramics on glass [Q-switched Nd:YAG] [source: Institut für Fügetechnik und Werkstoffprüfung (IFW)]

2.7 Silicon

Marking of silicon wafers is the preferred first step in processing a wafer, because the following processing steps change the absorption of the wafer locally. This will make uniform marking more difficult. In the early years of silicon marking, the feature size of the devices was still relatively large and some debris and splatter due to the laser marking was acceptable. The decrease of feature size resulted in more stringent specifications for mark depth, splatter, and debris. Marking Silicon without any splatter or debris is called "soft-mark". The company Lumonics introduced this term to differentiate from the former "hard" marking which included removal of molten material (McKee and Scaroni 1997).

2.7.1 Silicon ablation

Hard laser marking creates a visible mark by a change in surface texture and removal of a part of the silicon surface. The optical penetration depth of Silicon is relative large for 1064 nm, at room temperatures about 200 μm. But it decreases to 36μm at 300 °C. At 800 °C this is reduced to 5 μm (G.E.Jellison 1984). The use of a solid-state Q-switched Nd:YAG laser creates 5 - 20 μm deep marks with splatter and debris round. The molten material partly solidifies in a rim of beads around a dot-like imprint. The vapour fraction condenses, as sub-micron-sized powder. A green

laser (532 nm) reduces the amount of debris because the optical penetration depth at room temperature is only 1.1 μm. This results in a more direct ablation and a smaller volume.

2.7.2   **Silicon melting**

The high temperature dependency of absorption of Silicon can be used to reduce the depth by a predetermined pulse shape. A constant heating-rate is maintained by dosing the pulse energy in such a way that the decrease in optical penetration depth is compensated by a decrease in pulse energy. This results in a melt depth $\cong$ 2 μm. After solidification a shaped surface is visible (Kaufmann and Otto 1999). The volume of the molten silicon is smaller than the solidified volume. The centre is pushed upwards by the cooling at the edge of the molten pool. The edge of the mark is lower than the original surface because the molten pool has a smaller volume, see Figure 2.20. If the energy input is dosed properly no evaporation takes place, and no debris is formed. The pulse instability of a lamp-pumped solid-state laser is not good enough for a stable process. But diode-pumped solid-state lasers enabled a better process performance (McKee and Scaroni 1997). To eliminate the splatter and random deformities, a larger surface segment can be irradiated than the desired feature size. A Gaussian-shaped intensity profile will result in melting and partial vaporisation of the centre of the irradiated surface segment. The irradiated segment can be six times the desired marking area. The hotter area around the laser spot prevents the condensation of the Silion vapour (F.Kuhn-Kuhnenfeld, Kramler et al. 1984)..

Another method to reduce the debris is described by Kuwahara (1997). By pre-heating the complete wafer Kuwahara decreases the high absorptivity gradient and increases the absorption at the surface for 1064 nm, with the same marking quality as a 532 nm laser would have made.
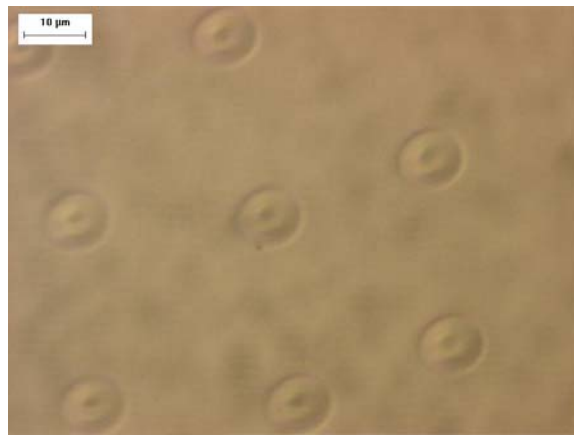
Figure 2.20: Soft mark in silicon [3rd harmonic Q-switched Nd:YVO$_4$].

2.8   Ceramics

Marking of ceramic materials became important with the introduction of ceramic IC packages in the late eighties. The use of Q-switching, which generated a short pulse ($t_p \approx 1 - 200$ ns), made it possible to consistently mark ceramic packages. (Seth and Scaroni 1986), (Lumonics 1992).

2.8.1   Ceramics ablation

Ceramic can also be marked using ablation. But the contrast is poor as the mark has the same colour as its background, and the diffuse nature of the ceramic itself hides the mark. Black ceramics show some contrast. To get enough contrast in a light ceramic like Al_2O_3 the depth of the marks can be increased to about a 100 μm, see Figure 2.21.
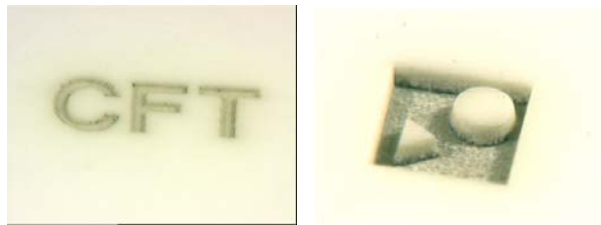
Figure 2.21: Left, Al₂O₃ ablation at 355 nm with pulse width of 10 ns.
Right, dimension 2 x 2 mm, depth 0.5 mm. [Q-switched Nd:YVO₄].

2.8.2   Ceramics melting

Melting of a ceramic with a CO_2 laser will introduce cracks and changes the surface roughness of the ceramic, see Figure 2.22. This micro-fracturing is due to the stresses by the rapidly cooling from a molten to an amorphous solid state (Perry and Huffines 1986).

Figure 2.22: Al₂O₃ melting, photo taking in reflection, melted surface reflects the light to the camera. The area around the figure scatters the light [10 W CO₂ laser].

The surface of the ceramic becomes smooth if the laser is used below the ablation threshold. Tokarev (1994) showed that melting is feasible as a method of smoothing and polishing ceramics (KrF, 248 nm, $t_p \approx 30$ ns).

2.8.3   Ceramics alloying/doping

Adding colour to uncoloured marble increases the value. Simoes (1996) introduced a method using a CO_2 laser to decorate marble and other kinds of rock. A dye is diffused into the rock using a 140 W CO_2 laser. He reported the use of a 8 mm diameter spot at a speed of 2 cm/s covering 1.7 m^2/h.

2.8.4   Ceramics reduction

An example of the reduction of a ceramic is AlN. This reduces by laser-irradiation, even in air, to Al. The metallic mark is both visible and electrically conductive, see Figure 2.23 bottom. The use of the reduction of TiO_2 to Ti gives a dark mark in ceramics, Figure 2.23 top.
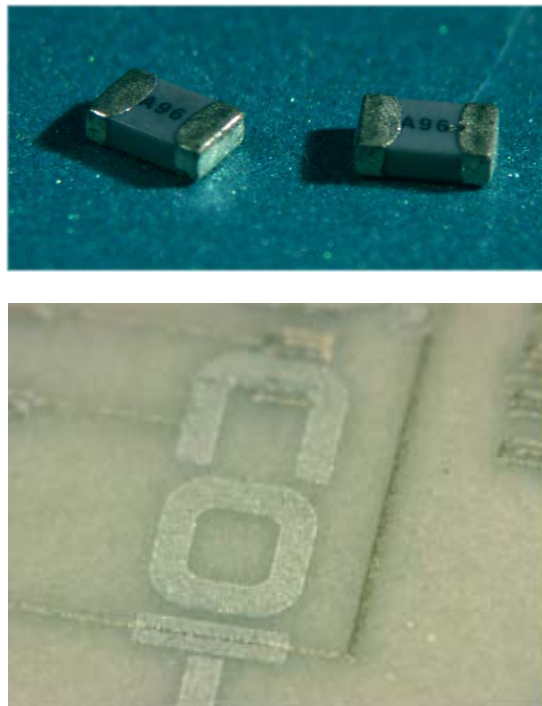
Figure 2.23: Top, Ceramic SMD component marking,[Excimer 193 nm].
Bottom, AlN reduction to Al, pulse width $\approx$ 10 ns, wavelength 355 nm,
[3rd harmonic Q-switched Nd:YVO4].

2.8.5 Ceramics transfer

Pique showed in 1999 the transfer of a wide range of powders using a matrix-assisted pulsed-laser evaporation process. The evaporation of the polymeric matrix is used to transfer the powder materials like metals, ceramics and phosphors. A subsequent step of laser sintering/heating can be applied to increase the adhesion to the surface and reduce the fraction of air gaps (Pique, Fitz-Gerald et al. 1999). This forward transfer process is called MAPLE (Matrix Assisted Pulsed Laser Evaporation) and was developed in the DARPA-MICE project. The main advantage compared to the standard laser induced foil transfer is that no evaporation of the transfer material is necessary. This increases the transfer rate and also enables the transfer of heat sensitive materials. It additionally enables the transfer to sensitive substrates as is shown by the transfer of a phosphor Zn_2SiO_4Mn powder to a dragonfly wing. The height of the text was 250 μm (Pique, Fitz-Gerald et al. 2000).

The standard foil transfer is a good alternative to mark ceramic substrates because the melting creates a layer with sufficient adhesion to its base material. Normal "green" ceramic sheet with binder can be used for this application. An important aspect to this is a slow evaporation of the binder and melting of the ceramic particles. The gasses caused by the evaporation of the binder can remove the ceramic. The versatility of laser mass transfer is shown in the application of marking fluorescent lamps by adding a phosphor at the inside of the tube. The original phosphor is removed by laser ablation prior to the application of a phosphor containing foil mounted on a pressure support.

Figure 2.24: Blue and red phosphor transfer inside a fluorescent lamp.
Left, principle setup. Right, fluorescent lamp with transferred blue and red circles.
The third and most right circle is only cleaned using laser ablation.

2.9 Polymers

Marking of polymers by radiation energy was already reported in 1956 by Pinner (1956) four year before the invention of the laser. X-ray, alpha particles, gamma rays, and high-energy electrons were used to irradiate the material causing burning and chemical changes in the materials. This process enabled coloured markings. An application for cable-coverings marking was already mentioned. Today all polymers can be marked in one way or another by laser

processes. The wide range of industrial use shows the importance of the invention of the laser and its use for marking.

2.9.1   Laser markability

A test to see if a material is laser markable is the parameter scan using small squares, see Figure 2.25. All laser machine parameters can be varied and shown in one pattern. It is a fast and effective way to see if a combination of laser and material yields good markings. It gives also an indication of the optimum settings. However an optimisation with regard to speed and contrast or colour is still necessary. Only the results of the optimisation can be used to compare different laser systems and only if the machine settings are translated into real physical parameters like intensity, pulse energy, speed and frequency.
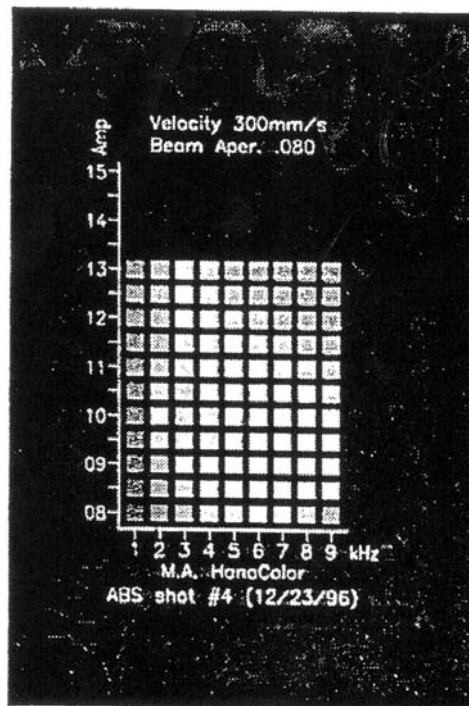
Figure 2.25: Test pattern for laser mark-ability of a plastic material as function of lamp current "Amp" and Q-switched frequency "kHz" of the laser (Feng 1997).

There are some practical problems related to the use of the square test pattern. Another laser system requires a new scan of all samples. To cover all possible parameter combinations multiple scans are necessary. For example Figure 2.25 is done at a speed 300 mm/s and doesn't show the distances between the lines filling the squares. The variation of lamp/diode current and frequency not only results in a change in pulse energy but also in pulse width. This relation between pulse

width and pulse energy is specific for a laser resonator design. Further it is impossible to obtain information about the importance of a single parameter. A more fundamental approach to the optimisation of laser marking is shown in Chapter 5.

Another source of problems can be the term: "laser-markability". It is used to indicate that the material is laser-engravable. If the customer is lucky, the polymer supplier has an identical marking laser for testing the material. But if this system is different, the term "laser-markable" is not enough. In one of Philips' production sites the contrast colour changed from grey to dark brown only because the supplier used a different flame retardant. In this case grey is vital as the marking is an integral part of the product design. The laser marking colour specification should have been added to the material specifications. There have been many other problems in laser-engraving which from the material suppliers' point of view are clearly a laser-initiated problem, and from the laser-manufacturer's point of view a common material problem. These kinds of disputes are difficult to solve, especially for the production facility that has to mark these material with the lasers available. The marking results depend on wavelength, power density and interaction time. The relation between these "real" parameters and the settings on different lasers is not known. But a good understanding of laser process parameters is essential in such situations.

2.9.2 Polymer marking and additives

Additives are important in laser marking. They make the process more or less independent of the polymer. The mica-based pigments of the companies Merck and Mearl are an example of these additives (Edler 1989), but also additives used for other purposes influence the laser-markability of polymers. Carbon black and TiO_2 are examples of such additives used to enhance laser-marking (Herkt-Maetzky 1994). The carbon black hides other colours, and the hidden colour will be visible after removal of the carbon black. TiO_2 has an increasing effect on the contrast due to scattering of the laser energy, which increases the absorption. TiO_2 is considered the future for polymer laser-marking by Coherent, a manufacturer of solid-state UV-lasers. TiO_2 reduces to black or grey by UV irradiation. Next to TiO_2 also other whiteners like Ba_2SO_4 , Al_2O_3 and ZnO are used. It is therefore often necessary to test the material with the UV laser to see if the material contains TiO_2.

2.9.3 Polymer ablation

Laser-ablation of polymers is evaporation of material during or after the absorption of a high-intensity laser pulse. The evaporation can be at or below the surface.

Evaporation below the surface result in a material rupture, due to the internal gas pressure, and escaping degradation products (Lippert 1997). This is activated by thermal or photo-chemical processes. For short wavelengths the breaking of the bonds in the polymer starts the pressure build-up. This pressure is converted to kinetic energy.

Figure 2.26: Left, ablation of three-layer foil:
black top-layer , yellow middle layer and base layer red, [Q-switched Nd:YAG].
Right, day and night technique, [Q-switched Nd:YAG].

A double layer material is used for the technique called "day and night", see Figure 2.26 right. This difference in absorption causes the laser ablation to stop at a predefined layer. A white layer with a black top-coat is often used in car radio applications. The black material is not transparent for visible light, but the white layer is. This is used to illuminate characters and logos from behind to see them at night. In daylight the white mark is seen on a black button. While at night a light illuminates the mark from behind. This concept can also be used for labels. A multi-layer label can be marked in a similar way. Different pulse intensities or wavelengths are used to remove one or more layers to obtain marks in different colours. To achieve a special effect only the backside can be removed creating a hidden display.

2.9.4   Polymer oxidation

Oxidation of polymers increases the adhesion of ink and paints on the surface. UV exposure of Polypropylene (PP) generates chemical groups that react with inks to get a strong adhesion. There is no colour contrast, only a slight change in reflection. But a visible morphology change was noticed while processing it in an Oxygen atmosphere at 193 nm (Breuer 1995).

2.9.5   Polymer melting

Melting gives no colour contrast, but can be used for a mark where only the surface reflection or the surface structure is changed. This is sometimes used for labelling of consumer products. The mark is readable but slightly visible under normal conditions, see Figure 2.27. Absorbing fillers can enhance the quality of such marks. It reduces the amount of molten material because the heated material is directly converted into gas due to the local higher temperature. So a deeper engraving can be made without much solidified material around the mark. Under these conditions polymers can start to inflame (Kern 1997).

Figure 2.27: CO$_2$ laser mark in ABS.

2.9.6 Polymer alloying/doping

Dyes can diffuse into solid polymers. This enables polymers to be tailored for functional properties. Diffusion does not need necessarily needs a laser, but the local increase in temperature caused by the laser accelerates the process. Such diffusion is known as dye diffusion, thermal transfer, or LIFT laser-induced foil transfer.

Siemens uses selective absorption in their multi-colour laser-printer based on foil transfer. The foil consists of encapsulated dyes that can be transferred by three wavelengths. These three wavelengths are arranged in a laser print-head (Kleinschmidt, Mader et al. 1987). As laser only accelerates the diffusion rate, the process will not stop after the laser has stopped. The dye migrates further in and out of the material. A second surface melting is used to stop the "bleeding", see Figure 2.28.

Figure 2.28: Top, laser-induced dye transfer, diffusion from foil into polymers, [CO₂, laser].
Bottom, LIFT, multi colour marking by laser-induced foil transfer, source: Siemens [CO₂, laser].

2.9.7 Polymer reduction

Reduction of oxides is used for marking white objects that have TiO_2 as pigment. The TiO_2 is reduced by UV light to the non-stoichiometric form, which has a characteristic blue-black colouration. This form has a reduced amount of oxygen. The resulting colour in a polymer matrix is grey because still some TiO_2 is visible (Dance 1990; Lau 1997), see Figure 2.29. The excimer laser used for marking wires has a big advantage because of the short pulse-time of this laser type. By mask projection a wire can be marked while moving at high speed (100 m/min) through.

The speed is only limited by the cable-handling equipment (Dickinson, Williams et al. 1988). The short pulse of the excimer laser (pulse width of 28 ns) enables speeds over 1000 m/min.

The penetration depth of the UV laser marks depends on the type of cable. Cornish reported for a Boeing BMS 13-48 Revision G (ETFE) cable a marking depth of 18.5 ±1 μm and for a Boeing BMS 13-60 Revision D (PTFE) cable a marking depth of 7.5 ±1 μm. These depths were independent of two types of lasers used (Excimer at 308 nm, 3rd harmonic Nd:YAG). (Cornish 1997).

Figure 2.29: TiO$_2$ reduction marking of polymers, [Excimer 308 nm].

2.9.8   Polymer carbonisation

Carbonisation is used at transparent or light-coloured polymers, see Figure 2.30. It results in a grey/black contrast due to the degradation of the polymer. The base colour of the polymer is mixed with the colour of the degradation products, and creates a dark mark. The ability of carbonisation depends on the chemical structure (Butenin and Kogan 1976). This relationship between structure and ability of carbonisation is shown in Section 3.6.

Figure 2.30: Left, PS carbonisation
[Nd:YVO$_4$, pulse width ≈ 8 ns, 1064 nm], source: Rofin Sinar.
Right, high speed component marking, PBT + glass fibre,[Nd:YAG laser].

Carbonisation is often observed together with ablation. But ablation removes some black coloured degraded polymer reducing the contrast. A transparent layer prevents the ablation. Then the actual mark is below the surface and is used for security marks, see Figure 2.30 left.

An application of avoiding carbonisation is the marking of components attached to a support foil at the foil-component interface. The first pulse is not completely absorbed by a transparent PET foil and is able to mark the underlying component. The second pulse at the same place has to travel through an already carbonised foil. If the laser pulse energy is not too high the component is only marked but not released (Bosman 2003), see Figure 2.31.
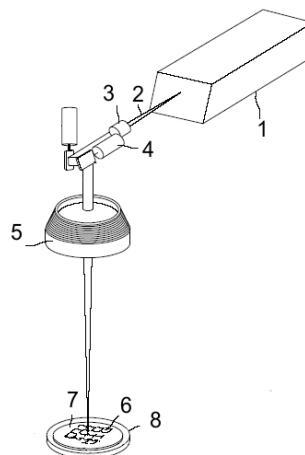
Figure 2.31: Component marking through a transparent polymer carrier layer.
1.laser, 2 laserbeam, 3 beam expander, 4 galvanometric, 5 fΘ lens, 6 component,7 foil, 8 ring.

2.9.9 Polymer foaming

Foaming is a partial degradation creating gas-bubbles. These bubbles become visible over of a distinct size. The differences of the refractive indices of the bubbles interior and walls appear white, due to scattering. The surface of these bubbles could be the original polymer or a changed structure. The interior of these gas bubbles is air or gaseous monomers. These bubbles are not sealed because the polymer structure is not rigid. Air can pass through these structures.

With the original light coloured polymers these gas phases creates only a low contrast, see Figure 2.32 left, but if carbon black (graphite) is used in a polymer that can be foamed, the carbon black is removed by ablation and oxidation (Edginger and Kohler 1980) resulting in a high contrast, Figure 2.32 right. If additionally a stable, coloured pigment or dye is added, this results in a coloured mark on black (Parts, Pinsky et al. 1971; Herkt-Maetzky 1994). Bayer (1994) found that by a combination of organic and inorganic pigments of the same colour a very bright colour is obtained. Addition of carbon black results in a coloured mark on a black background.
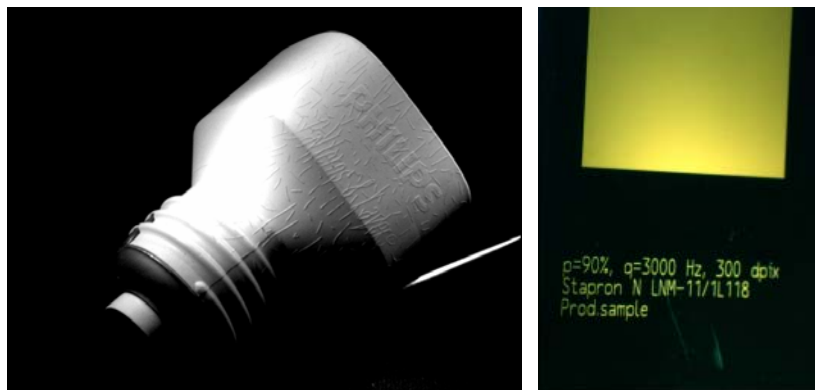
Figure 2.32: Left, foaming without colour change of Polybutylene terephthalate (PBT)[Q-switched Nd:YVO$_4$, pulse-width 10 ns]. Right, foaming & removal of carbon-black , ABS [2nd harmonic Nd:YAG (532 nm)].

2.9.10 Polymer bleaching

Bleaching is the loss of colour due to pigment degradation (crystal break-up/change, oxidation). When bleached with a short-pulsed, visible laser, the polymer matrix is not affected. A longer pulse would not only effects the pigment particles but also heat the polymer. Because of the visible wavelength the laser light penetrates deep into the polymer and is only absorbed by the pigments. Such sub-surface engraving is ideal for security applications, because it cannot be removed without destroying the surface. A major drawback is the limited colour range, which is directly related to the base colour. The desired colours are hidden in the surface masked by other pigments. The idea is to bleach hiding pigments without destroying the others. A moderate shift in colour was shown but not the desired bright marking. This technique can be used to make counterfeit resistant flexible coloured marking. The work done in the Brite euram project Licopal

and Syladec is discussed in more detail in Chapter 6 (LICOPAL BE90-4441, SYLADEC BE96-3503).

Figure 2.33: Thermal selective bleaching [2nd harmonic Nd:YAG, 532 nm, pulse width 120 ns].

The use of one wavelength only also enables multiple colours but then the pigments should have a distinct and different thermal-degradation temperature, see Figure 2.33. By modifying the laser energy all colours except the stable ones will disappear. Bleaching does not mean that the colour is lost entirely. Even, a slight change in colour appearance could be used for marking polymers. In 1973 the Kansai Paint company filed a patent describing the use of metallic compounds that change their colour under laser exposure (Kanzaki 1973). The laser used was a 30 mW He-Ne (632.8 nm) and a 60-300 mW Ar-ion laser system (457.9 nm, 488 nm, 514.5 nm). Also Philips used this technology to mark capacitors, using a TEA laser, see Figure 2.34. The contrast of the mark is achieved by the thermal decomposition of a silicon comprising dye or a dye and a silicon containing inorganic compound (Vorst 1980).
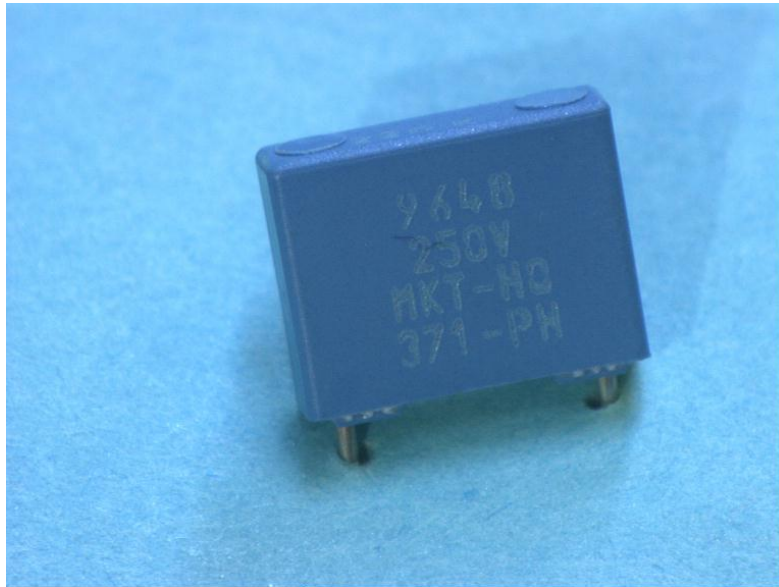
Figure 2.34: Component marking using a mask projection and Ultramarine blue glass filled PBT,
[TEA CO$_2$ laser marking].

2.9.11   Polymer colour forming

Colour-forming from a colourless chemical compound is a technique that is still in its feasibility phase. There are two mechanisms of colour-forming. The first is a thermal process which has a wide colour range, but is thermally and UV unstable (Wielstra 1994), see Figure 2.35 left. The second method uses UV for colour-generation and is a laser-driven, in-situ, chemical reaction, see Figure 2.35 right. The stability (both thermal and UV stability) is still limited, but is expected to be improved in the future. Colour-forming encounters the same problems as bleaching because the formed colour is mixed with the base colour. A combination of bleaching and colour-forming is patented by DSM. The use of UV colour-formers that can be bleached in its coloured form by a visible laser, would generate a coloured mark on a light background (Elshout and Aagaard 1996). But because of the low current efficiency of bleaching and the unstable colour-formers further development is still needed. A feasible way of using colour forming could be a two step process where both UV and thermal activation is used. During moulding UV will not be present and during normal use heat will not be available. This would solve the stability problem of both UV and thermal systems.

Colour formers are used already in stereo lithography, Zeneca has developed a UV curable resin with colour formers. Depending on the UV dose the colour former will form a red marking. The resin cures at a lower dose creating the ability to colour a 3D lithography shape only in certain areas (Popat and Edwards 1996).

Figure 2.35: Left, thermal colour-formers in lacquer [CO_2 laser].
Right, UV colour-former,[excimer, 351 nm].

2.9.12   Polymer transfer

Transfer of polymers is anemerging technology for coloured decorations. In this case the polymer
is transferred without any solvent, see Figure 2.36 right. The laser generates a kinetic transfer of
the polymer from a carrier that can be post-processed to obtain certain properties. The transfer of
a polymeric layer to an IC package by a CO_2 laser is used by the Markem corporation for the
labelling of high-end IC packages (Meneghini 1995), see Figure 2.34 left. The transferred layer is
either cured thermally or by UV irradiation. There are several methods for the polymer transfer. It
can be transferred by ablation, melting, or change in adhesion. The energy needed for the transfer
can be generated by absorption of the laser wavelength in the carrier foil, the base material
(acceptor), the functional layer (transfer material), or in a layer specially-added only for the
energy conversion called LHTC Light To Heat Conversion (Hare and Dlott 1997). This LTHC
layer will remain at the carrier and is not transferred.

Figure 2.36: Left, polymer transfer [CO_2 laser].
Right, 3 colour ablation transfer by [2nd Q-switched Nd:YAG laser, 532 nm].
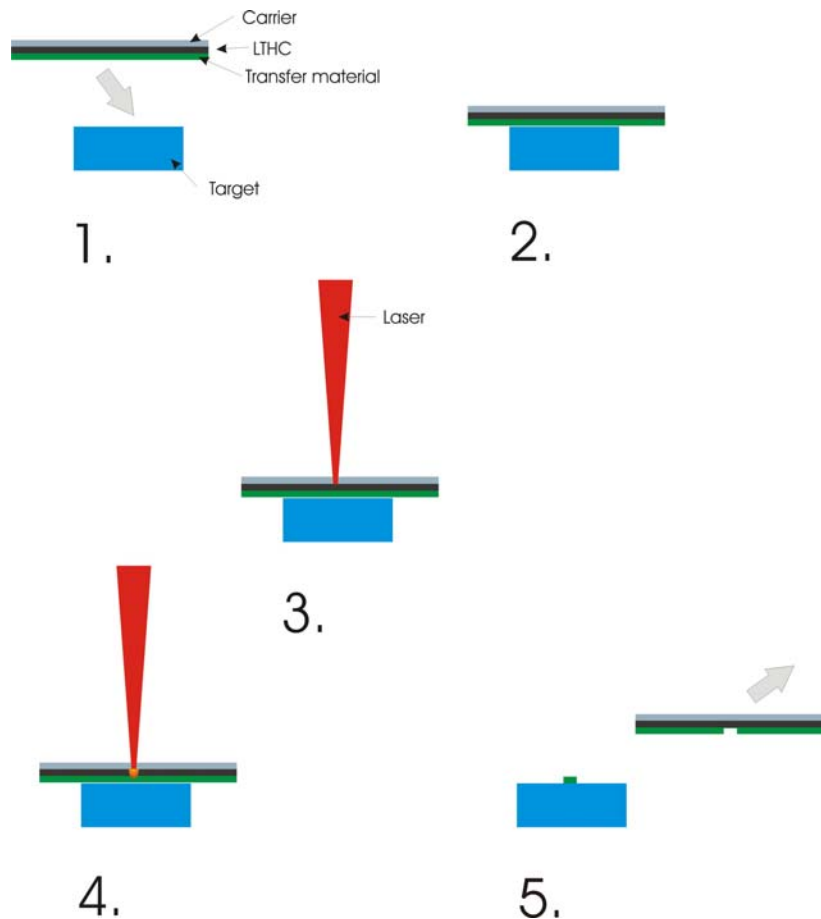
Figure 2.37: Schematic view of laser mass transfer using a light to heat conversion layer.
1. Application of foil to target
2. Foil at target
3. Start laser
4. Heat diffusion into transfer layer
5. Removal of foil

2.9.13   Polymer optical breakdown below the surface

The absorption of most materials depends on the laser intensity. When the intensity exceeds a certain level the absorption is increased due to the higher temperature. This positive feedback leads to local degradation of the material. The local high pressure due to the fast evaporation can also induce a sub-surface deformation of the material (Heumann, Kleinschmidt et al. 1985). The process is used for example to make security marks in polymers.

The sub-surface degradation of the material can also be used to write 3D structures inside the polymer. This is done by engraving sliced patterns at decreasing depth, see Figure 2.38. These 3D structures inside a polymer volume can also be used to block light from passing through. This can be used to restrict the viewing angle of a monitor like the louvre films used in ATM machines, see Figure 2.39.
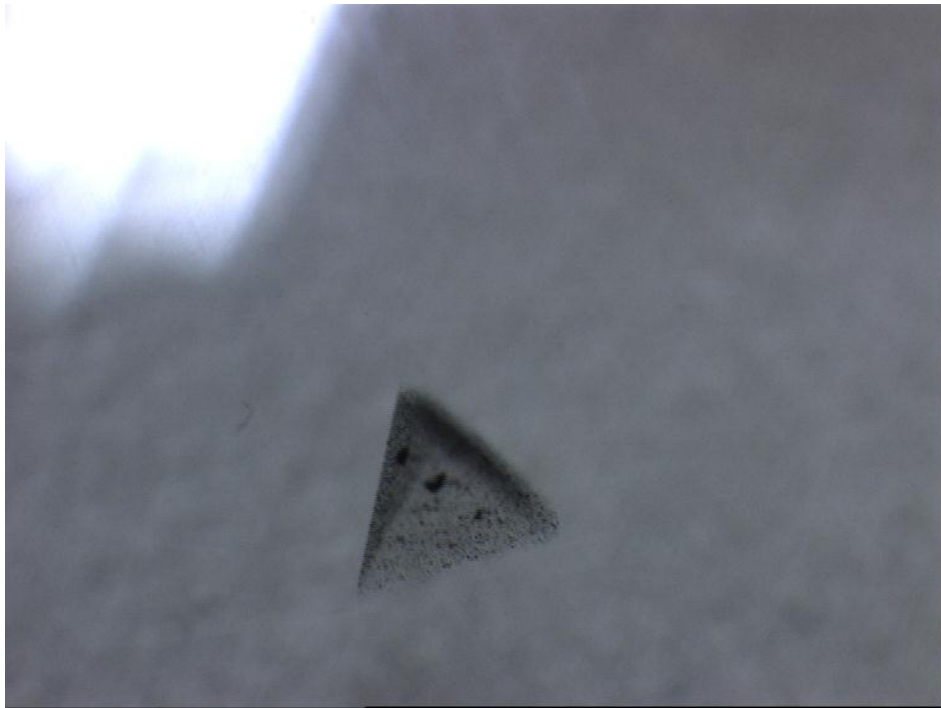
Figure 2.38: Optical breakdown in polycarbonate [Q-switched Nd:Vanadate laser, (1064 nm)].

Figure 2.39: Louvre film in 3 mm thick polycarbonate [Q-switched Nd:YAG laser].

2.9.14 Polymer unzipping

By "unzipping" the weakest bond that links one monomer to the other is broken effectively by heat generated by the absorption of laser energy. The free radical formed by the bond breaking can lead to unzipping to a monomer or the free radical transfer with the abstraction of hydrogen from the polymer chain. The weakest bond for PMMA is the bond that links one monomer MMA to another. This is the reason why PMMA degrades by unzipping. *(Blanchet 1996),* see Figure 2.38. Butenin showed using a Q-switched Nd:YAG that multiple pulses were necessary to achieve a change in material properties for PMMA, while Hopp needed only one pulse from an excimer laser at 193 nm to change the material properties (Butenin and Kogan 1976), (Hopp, Marton et al. 1998). Hopp showed also that this change in material properties starts during the excimer pulse. The photon energy of 193 nm can release all bonds with lower bond energies. For the chemical bond energy the maximum wavelength can be described using Equation 2.1.

$$\lambda_{max} = \frac{h \cdot c}{E} \qquad (2.1)$$

In which *h* is Planck's constant, c the speed of light in vacuum and E the photon energy.

*Table 2.5: Photon energies from different laser sources and required dissociation energies from several chemical bonds (*1 eV=1.6020 10^{-19} J) *(Meijer 2002).*

Laser	Wavelength λ (nm)	Photon energy E (eV)	Chemical bond	Bond energy E (eV)
CO_2	10600	0.12		
Nd:YAG	1064	1.16		
Nd:YAG 2nd	532	2.33	Si-Si	1.8
Nd:YAG 3rd	355	3.49	C-N	3.16
XeF	351	3.53	C-C,C-Cl	3.6 – 3.51
XeCl	308	4.02	C-O	3.71
Nd:YAG 4th	266	4.66	C-H	4.28
KrF	248	5.00	O-H	4.80
KrCl	222	5.58		
ArF	193	6.42		
F_2	157	7.89	C=C	6.32
			C=O (carbon dioxide)	8.32

The beam intensity distribution of a CO_2 laser is often checked by exposing a slab of PMMA, see Figure 2.41. The form of the hole corresponds directly to the laser intensity distribution. The high absorption of the CO_2 laser wavelength causes this rapid degradation of the PMMA. The monomers that are formed quickly evaporate resulting in the typical PMMA smell.
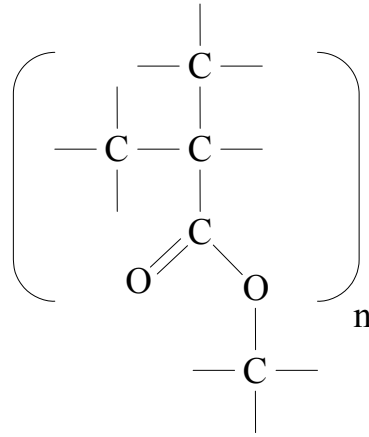
Figure 2.40: PolyMethylMethAcrylate, PMMA monomer.
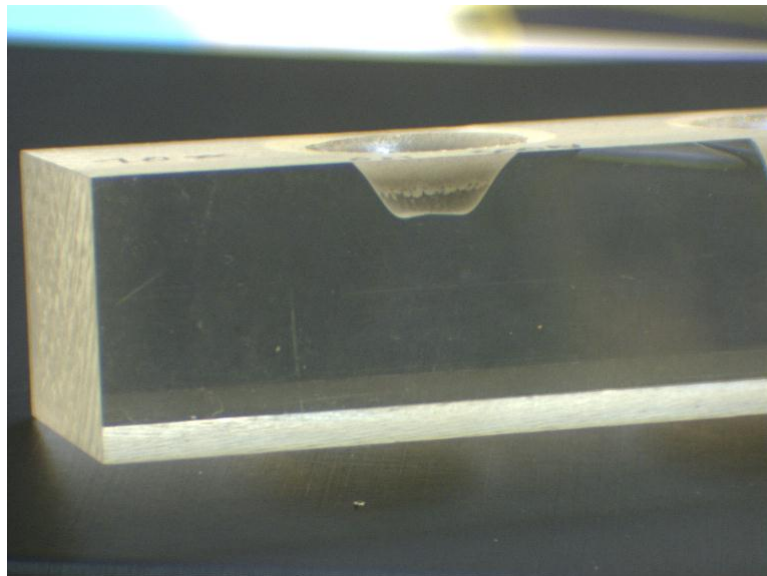
Figure 2.41: Mode pattern in PMMA of a CO_2 laser.

Air bubbles or some other impurities induce local degradation. If close to the surface the increased internal pressure is released by rupture of the material. Otherwise the surface remains intact and a local change in refractive index in the PMMA can be observed, see Figure 2.42. These sub-surface changes in refractive index have been made by a 355 nm laser.
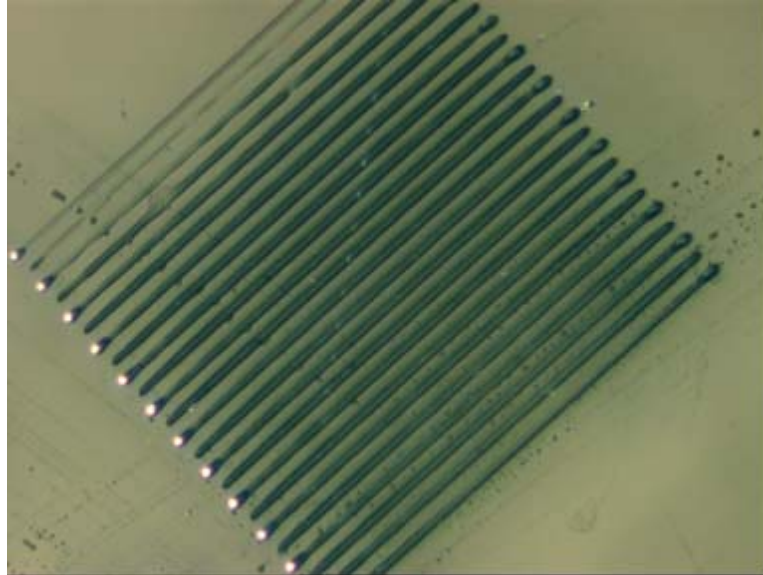
Figure 2.42: Refractive index change inside PMMA by unzipping,
[3rd harmonic Nd:YVO$_4$,355 nm].

2.9.15 Polymer dehydration

To get an irreversible or semi-irreversible colour the structure of a pigment can be changed in two ways, one being the discharge of H_2O and CO_2 by heating above 200 °C. The second is the change of crystalline structure of the pigment.

Preferred materials release their water at a temperature range of 300 °C to 600 °C because they are not restricted to lacquers. Even multi-colour changes are reported by using the differences in decomposition temperatures but the low water release temperature of these materials limits the use of this effect considerable to materials like lacquers. (Kato 1994). A colour-change from pink to blue is reported by the thermal effect generated by a TEA CO_2 laser. ($Co_3(PO_4)_2$ $8H_2O$ (pink) $\rightarrow Co_3(PO_4)_2$ xH_2O (blue) + (8-x) H_2O) (Azuma and Sakaki 1987).

2.10 Natural materials

This overview wouldn't be complete if materials like paper, fruits and meat are left out. They form a substantial part of laser marking applications which will increase in the future as cheaper and more efficient lasers will be available. A non additive method for marking produce could replace the adhesive labels and inkjet used to identify the product.

2.11 Marking of paper

Although paper is easily printable there are some limitations where lasers can help. For example printing in 3 dimensions (beverage packaging) or printing and removing features at an existing print (uniform packages).

The question if laser based printing could outperform conventional printing on large scale paper printing is not easily answered. The development of laser diodes with high beam qualities at low prices would enable large scale applications at reasonable prices. Together with energy and wavelength selective colour formers laser will be used for on demand flexible printing in the future. The principle of both heat and UV sensitivity would act as a 'child lock'. Exposed to both UV and heat a colour is formed. But only UV or heat would do nothing (Heller 1995) .

2.11.1   Paper ablation

In 1976 laser marking was introduced in the package coding industry. Roughly 15% of the laser coding systems are used by the packaging industry (Bruton 1997). The TEA CO_2 lasers (Transverse Excited Atmospheric CO_2 laser) are reliable and some of the systems form the eighties are still in use due to their high reliability and simple operation. The TEA CO_2 lasers used for marking have typical pulse energies of 5 Joule with pulse widths of 1 μs. Using a mask this enables a marking speed of 1200 bottles per minute. By using a spinning mask wheel flexible texts and codes can be written.

Figure 2.43: Beer bottle label [TEA CO_2].

Cutting a shape out of paper is a reliable way of marking. And cutting paper doesn't need high energy. A 10 W sealed tube CO_2 can already cut through paper. If the quality of the cut is important and the size of the mark is small (< 100 μm) a 3rd harmonic YAG at 355 nm is a good but more expensive alternative. For example Figure 2.44 shows a picture cut in paper using a 3rd harmonic YAG. The size of the squares is related to the intensity of the pixels. Another example of marking paper by ablation is the printing of the passport number in the Dutch passport. The holes are drilled using a CO_2 laser into the whole stack of paper.

Figure 2.44: Picture with low resolution but large grey scale range cut in paper width of picture 20 mm. With backlight (right) and without backlight illumination (left).
[3rd harmonic Q-switched YAG].
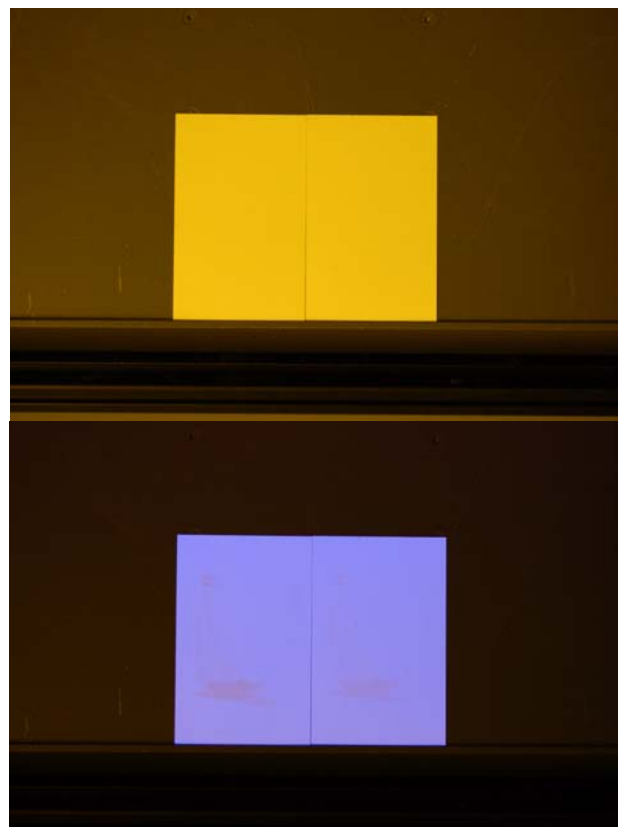
Figure 2.45: Marking of white paper with invisible mark
(Top with D65 illumination and bottom with UV illumination, see appendix E).

2.11.2   Paper reduction

The anatase form of TiO_2 is often used in paper as a whitener (Murphy 1996). Using a 3rd harmonic YAG invisible marks can be written. These marks can be made visible using UV light because the anatase form is fluorescent. The laser marking reduces this, see Figure 2.45.

2.11.3   Paper carbonisation

The carbonisation of paper is a simple but effective way to laser mark. A CO_2 laser leaves a brown marking (Fluence 100 mJ/mm^2) due to burning. The paper can also be set on fire when too much energy is applied. Heat sensitive paper shows already a dark mark at low intensities without any burning.
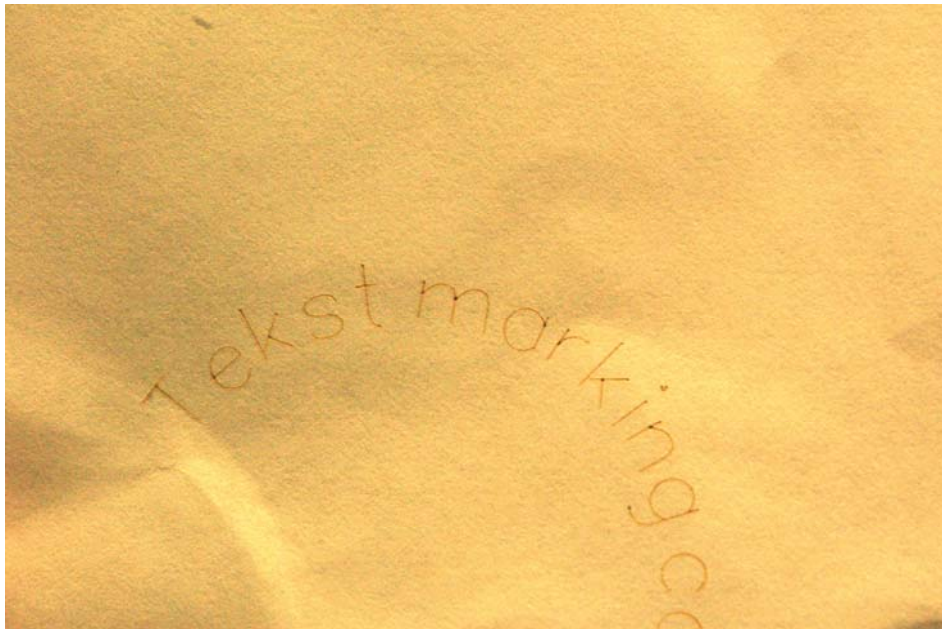
Figure 2.46: Burns on paper [CO$_2$ laser].

2.12 Marking of Produce

2.12.1   Ablation of skin

Vegetables and fruits can be marked by ablation of part of the skin. The 3 dimensional shape of fruits and vegetables makes it difficult to attach adhesive labels. A yield of the success rate of the label adhering is reported to be 80-85% (Drouillard and Kanner 1999). Figure 2.47 shows an apple marked by a third harmonic Nd:YAG. The marking creates small holes in the skin of the

apple. This increases the release of moisture. The marking will grow brown already after a few hours. This type of marking is used for fruits with a thicker skin. Oranges and citrons have a better suited skin for laser ablation.

Figure 2.47: Marking of apples by skin ablation [3rd Nd:YAG laser, 355 nm].

2.12.2 Colour forming and dehydration

Marking edible products demands non-toxic materials. The initial components and the reaction product should be physiologically acceptable. For example sucrose will char when heated by laser energy in the presence of MgO or FeO (Kahn 2002). The coating containing sucrose and a stable metal salt is applied before the laser marking. This can be done for example by spraying. The application is not limited to vegetables and fruits but is also used on candy and pharmaceutical products. Also dehydration (elimination of water) can be used to form a mark. Polyvinyl alcohol (PVA) in presence of ZnO would yield a mark. PVA is often used in hair products and can be applied by spraying.

Figure 2.48: Edible laser markings produced by Sherwood Technology, source: Sherwood technology, [CO$_2$ laser, 10.6 μm].

2.12.3 Bleaching

A major drawback of laser marking apples with the ablation method is the loss of moisture through the perforated skin. A solution for this to use the pigment in the skin to enable the marking as shown by mr. Lühs and leave the skin intact (Luehs 2005). This application makes every apple unique, see Figure 2.50.

Figure 2.50: Bleaching of apples, source: Trumpf [3rd Q-switched Nd:YAG laser, (355 nm)].

2.13 Wood

2.13.1 Burning

The CO_2 laser is an excellent tool to write on wood. The burning of the surface yields a high contrast mark. Lacquers and impregnations also react due to the laser energy.
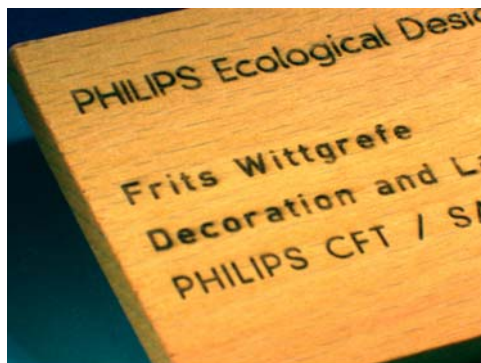
Figure 2.51: Laser marking of impregnated wood [Nd:YAG].

2.13.2 Ablation

The high intensity pulse of a tripled YAG easily removes part of the wood surface. The removal rate is not constant but depends on the wood structure. Multiple scans enhance this structure and a surface is made which looks very natural. By changing the scanned patterns according to a sliced 3D structure enables the 3D carving of wood by laser.

Figure 2.52: Sample of wood engraving [3rd Nd:YAG, 355 nm].

2.14 Marking of eggs and skin

2.14.1 Ablation of eggshell

The shell of an egg is an ideal material to ablate. The resulting mark could reduce the strength of the egg if too much material is removed. With a low average power this can be avoided enabling a colour change without much ablation.

Figure 2.53: Egg marking, ablation [3rd Nd:YAG laser, 355 nm].

2.14.2   Carbonisation of skin

A CO_2 laser burns the upper skin and normally it's better to avoid this. But marking cadavers to enable traceability during the processing is a complete different story. Making high-resolution marks would not be possible but a dot code based pattern of burns is possible and enables even machine readability. The company Bongrain patented in 1987 a machine concept for laser marking meat and cheese (Fillaud 1987). The idea of marking biological products has already been patented in 1974 by Dufour (Dufour 1974). By using different mirrors the top and the side of a cheese can be marked without handling the cheese.

2.15 Marking of textiles

2.15.1   Bleaching of jeans

CO_2 lasers are used to engrave pictures, logos and texts on denim jeans. The dye is bleached by the thermal effect of the CO_2 laser leaving a visible mark. Figure 2.54 shows an example of a marked jeans. The Italian company DS4 claims to have sold over 100 laser marking systems for textiles in China in 2005 (Graydon 2005).

Figure 2.54: Bleached jeans, source: DS4 [sealed CO_2 laser,10.6 μm].

2.15.2   Burning of textiles

A simple way of marking textiles is to burn the surface locally using a CO_2 laser. This enables a durable brown mark.

2.15.3   Cutting of textiles

Cutting of textiles is fast and easy. Sometimes it leaves a burned or reduced material but often the edges do not have to be processed any further. Next to the elimination of a wearable cutting tool this is an important advantage of laser cutting. The marks can be made by using semi-open characters (with dams) or small holes.

2.15.4   Reduction of textiles

Most textiles that are white have an additional colouring to achieve a good hiding power. Often TiO_2 is used for this. Using a third harmonic YAG a marking can be made without damaging the textile it self, see Figure 2.55.

Figure 2.55: Reduction of textiles [3rd Nd:YAG, 355 nm].

2.16 Marking of diamonds

Marking of diamonds with a mark invisible to the naked eye is reported by Smith and Cooper in 1995. The diamond reacts with oxygen in the atmosphere causing a small mark. The oxygen plays a role in the marking because a decreased oxygen percentage reduced the marking speed. In a vacuum no mark was made. The graphitisation of diamond starts can already at 700 °C under normal atmospheric conditions and is not preferred. The graphite has a much lower ablation threshold as diamond so most of the formed graphite is ablated during the marking. To avoid carbon deposits an increased oxygen percentage is used. It prevented the forming of a greyish layer leaving a clear mark (Smith and Cooper 2001).

The marking of diamonds has not only a security reason but it is also used to enable certification and branding of the diamond, see Figure 2.56. For example the Canadian company Ekati laser inscribes a polar bear on the diamond. Where a RAND diamond is marked with a unique number tying it to its birth certificated, guaranteeing the legitimate source.
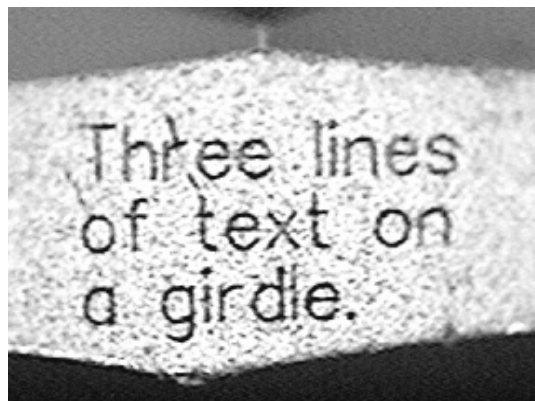
Figure 2.56: Diamond girdle mark, source: Potomac [excimer, 193 nm].

2.17 Conclusion

Laser engraving is possible by using several processes on all materials and is mainly used for labelling applications. Only in few applications a laser gives a better decorative appearance than other technologies like inkjet or pad printing. Up to now the colour possibilities are limited but laser mass transfer could overcome this limitation in the near future. If the handling and availability of the foils or other media needed are solved in an industrial acceptable way the potential high yield of the process could revolutionise production and mass customisation becomes an attractive option. A flexible appearance of the product will be a big advantage leaving the production optimised for maximum batch sizes with a minimum of variation while decoration and finishing is done at the shop.

Although laser processing of polymers is widely used there is not much information found in literature about the control of these processes. Every user has to determine and solve its own problems. The marking of polymers is an area where a lot of the different processes occur. The thermal and optical properties of the different polymers make it an interesting and challenging area for scan strategy optimisation and process control. The remaining part of the thesis is focused on the marking of polymers and its properties.

Chapter 3   Optical and thermal characteristics of polymers

3.1   Introduction

The optical and material characteristics of polymers have a characteristic effect on laser processing of polymers. These aspects should be taken into account when designing a laser process for polymers. The full surface absorption used for metals is not valid for polymers. The optical penetration and low thermal diffusion makes it necessary to understand how energy is distributed into a polymer volume. In this chapter the energy distribution during a Q-switched laser pulse is described by the optical penetration according to Lamberts law and the Gaussian energy distribution in the laser spot. Thermal diffusion during the pulse is neglected because of the short duration and slow thermal diffusivity. The temperature distribution as a result of the laser pulse energy is calculated immediately after the pulse.

3.2   Absorption of laser energy

The energy of a pulse from a Q-switch Nd:YAG laser at 1064 nm is absorbed over a large depth in the polymer material because of the low optical absorption. This is called volume absorption, in contrast to the surface absorption where due to high absorption the energy is concentrated in a thin surface layer.

The absorption as function of depth is described by Lamberts law, which defines that each layer of equal thickness absorbs an equal fraction of the light that traverses it. This can be written as:

$$\frac{dF}{dz} = -\alpha \cdot F \tag{3.1}$$

The laser fluency as a function of depth follows by integrating of Equation 3.1 as:

$$F_z = F_0 \cdot e^{-\alpha z} \tag{3.2}$$

The optical penetration depth δ_0 is defined as the depth where the laser fluency is decreased by a factor of 1/e, see Figure 3.1.

$$\delta_0 = \alpha^{-1} \tag{3.3}$$
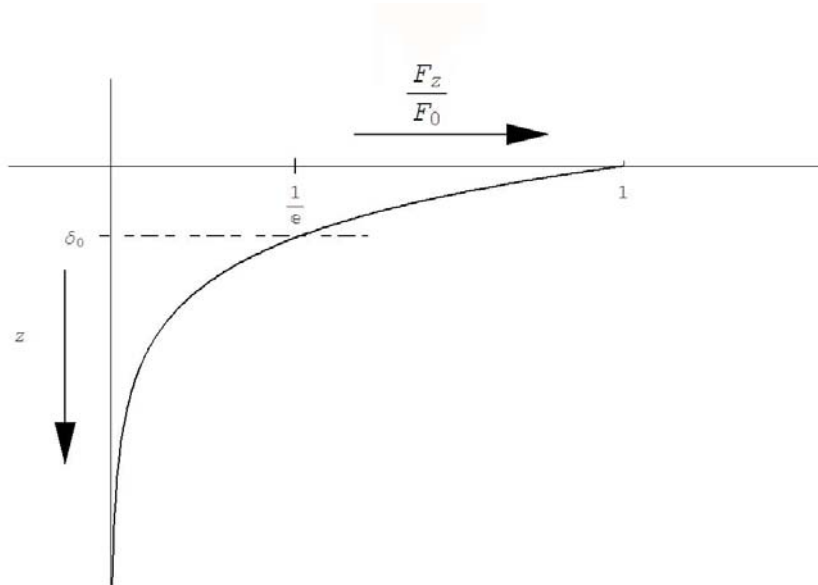
Figure 3.1: Fluency (F) vs. depth (z).

It should be considered that Lamberts law is limited to linear absorption in a homogenous material. Assuming the linear behaviour of the material we neglect the mechanisms causing non-linear behaviour. These effects are listed in Table 3.1 and discussed in more detail below:

Table 3.1: Absorption mechanisms causing non-linear behavior (see text).

Process	Description of effect
1. Size of additives	Inhomogeneous energy distribution for large additives.
2. Two photon absorption	No noticeable effect with nano second pulses
3. Slow energy to heat conversion	No noticeable effect with nano second pulses
4. Degradation of the polymer.	Change of absorption coeff. And generation of heat.
5. Temperature dependant absorption and diffusivity	Change of absorption coeff. and diffusivity.
6. scattering of laser light	Redistribution of energy

1.   When the size of the additives is large compared to the laser wavelength the additives will act as islands with different material properties in a polymer volume. In this case the volume is not homogenous. Although the additives are below the threshold of the human they will not be noticed separately. For smaller additives (same order as the wavelength) the material can be

regarded as homogenous but with different properties as the volume without additives. In these cases Lamberts law can be applied.

2. Two photon absorption is observed at high laser intensities. This non-linear absorption is for example used to enhance the absorption for in-glass marking in focus. A displacement of the focus would also mean that the marking is displaced. For normal non-ablative marking multi photon absorption is about 0.5% at 1064 nm, and can therefore be neglected.

3. Another process that introduces non-linear absorption is the time needed to convert the laser energy into heat. The excited molecules have a different absorptivity as their ground state. The lifetime of the excited states is less than 10 picoseconds normally. So the conversion into heat will have no noticeable effect on the energy conversion for pulses of 10 ns or more.

4. During pulses material parameters can change due to degradation. The increase of the absorption coefficient in this case would reduce the penetration depth and increase the heating at the surface. The speed of the material parameter change would limit the use of Lamberts law. Another effect of the degradation is the release of extra energy. The amount of this is discussed in Section 3.6.3.

5. The temperature dependant absorption and diffusivity limits the use of Lamberts law. For a small time interval the material parameters can be considered constant enabling the use of Lamberts law. But the material parameters should be known in order to describe the entire process from heating to melting and evaporation.

6. The effect of scattering distributes the laser energy in different directions. Lamberts law is used is such cases only to describe the transmitted energy in the original direction. And an additional scattering coefficient is added because scattering can be defined as: each layer of equal thickness scatters an equal fraction of the light that traverses it. This is the same definition as the one used to derive the Lamberts law of absorption. This modified Lamberts law isn't suitable to describe the temperature distribution by a laser pulse.

For a first order approximation of the absorption of a Q-switch laser the non-linear behaviour can be neglected. The use of shorter pulses like picosecond and femtosecond would change this and are an interesting field to achieve different effects in polymers.

3.3   Thermal diffusion versus optical penetration depth

Suppose the laser energy is converted to heat in an infinitive small surface layer the depth over which the energy diffuses is characterised by the thermal diffusivity and the dwell time of the laser beam. The thermal penetration depth is defined as:

$$\delta_h = \sqrt{4 \cdot a \cdot t} \tag{3.4}$$

Short laser pulses would yield a lower thermal penetration depth. The optical penetration depth δ_0 is independent on the laser pulse time. Table 3.2 displays this thermal and optical penetration depth for a set of materials as a function of the thermal diffusivity of material and the pulse or interaction time t_p for a wavelength of 1064 nm

Table 3.2: Optical penetration depth (δ_0) and thermal penetration (δ_h) at λ = 1064 nm
,pulse width t_p = 1 ns, 10 ns, 1 μs,10 μs,100 μs, 1 ms.
Data: [*](Bauerle 1986), [**] Philips PMF, G. van der Hei (Hei 1990),
(For more detailed spectra see Appendix C.3)

	Optical penetration depth δ_0 [μm]	Thermal penetration depth δ_h [μm]					
		Pulse width t_p					
		1 ns	10 ns	1 μs	10 μs	100 μs	1 ms
Metals							
Ag[*]	0.01	0.83	2.62	26.2	83.0	262	829
Al[*]	0.01	0.64	2.03	20.3	64.2	203	642
Au[*]	0.01	0.70	2.21	22.1	69.9	221	699
Cu[*]	0.01	0.68	2.14	21.4	67.5	214	675
Polymers							
ABS[**]	7020	0.03	0.08	0.83	2.62	8.29	26.2
PET	3200	0.02	0.08	0.76	2.39	7.56	23.9
PC[**]	7500	0.02	0.07	0.71	2.24	7.07	22.4
PMMA[**]	41000	0.02	0.07	0.69	2.19	6.93	21.9

For the polymers ABS, PET, PC and PMMA the optical penetration depth dominates the thermal penetration even at long interaction times. For metals this situation is the reverse. In case of polymers the temperature distribution shortly after a laser pulse can thus be described as the result of the optical penetration and the fluency distribution in the spot size.

3.4   Thermal model for absorption in polymers

If the optical penetration depth (δ_o) is large compared to the thermal diffusion length (δ_h) the average temperature rise can be estimated by an energy balance (Chan 1995). The energy absorbed by a volume of material at a certain depth results in a temperature rise of the same volume. This model does not take into account the diffusion of energy into non-irradiated regions. In literature a few models for polymer laser processing are reported, each with a different approach. The ablative models include bond breaking by UV exposure in polymers (Arnold, Bityurin et al. 1999), (Bityrin, Arnold et al. 1998). These models are focused to describe the depth of ablation rather than the thermal effect just after the pulse. This aspect of thermal

diffusion after one pulse influencing a second pulse is used by Reyna (Reyna 1994), (Reyna 1995) but only for a one dimensional multilayer structure.

Another class of models is often used to describe the laser cutting by a CO_2 laser using surface absorption because of the wavelength of 10.6 μm. (Pan and Hocheng 1997).

Although laser welding of polymers has some similarity with laser engraving the one dimensional model Potente uses is fully focused on describing the temperature profile in time at the interface of a transparent polymer (no absorption) and a fully absorbing polymer (surface absorption) (Potente, Korte et al. 1998). An alternative to an analytical model is to use factorial experiments to establish a model (Cicala, Zsivanov et al. 1998). This would lead to a wide set of experiments because the scan strategy also adds parameters to the model. As no model fulfilled our needs a new model was made using some of the aspects of the other models.

The following assumptions were made to keep the model effective for its purpose of modelling the temperature distribution of a laser engraving strategy.

- Homogeneous material.
- Thermal properties are constant (time, temperature)
- No thermal degradation or ablation, evaporation.
- No heat transfer during pulse.
- Area within Rayleigh length of the laserbeam.

3.4.1 Temporal and spatial intensity distribution

Due to the assumption of no heat transfer the temperature becomes pulse-time-independent. The laser intensity can be integrated over the pulse length yielding the laser fluency. The pulse-time is used only to verify the initial condition of no heat transfer (small thermal penetration). In case of a small thermal penetration depth compared to the optical penetration depth and spot diameter the temporal pulse form can be described as a squared pulse. Figure 3.2 shows a characteristic Q-switch pulse.
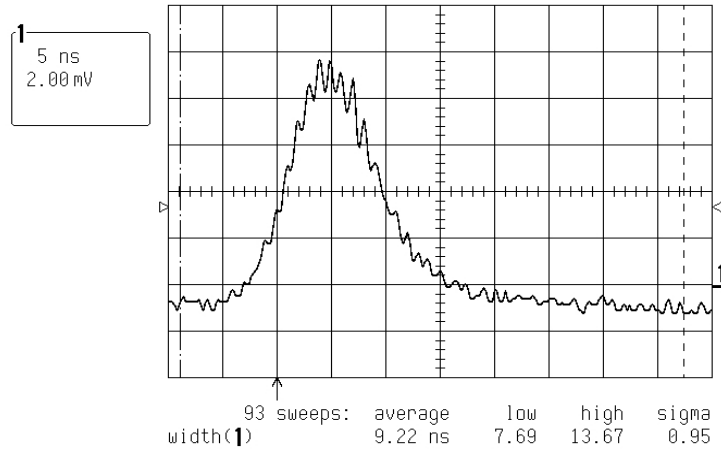
Figure 3.2: Screen dump of temporal pulse measurement of Eline 10E Rofin-Baasel
(f_Q 20 kHz, E_p 0.1 mJ, t_p 9.22 ns measured over 93 pulses at sample rate 5 G Samples/s).

To introduce focussing in the initial condition, the waist radius should be described with respect to the z position. The waist radius as function of the z position and Rayleigh length (Z_R) for a Gaussian beam is defined as:

$$w(z) = w_0 \cdot \sqrt{1 + \left(\frac{z}{z_R}\right)^2} \text{ with } \qquad z_R = \frac{w_0^2 \cdot \pi}{\lambda} = \frac{2w_0}{\theta} = \frac{4\lambda}{\pi\theta^2} \qquad (3.5)$$

Figure 3.3: Focussing of a Gaussian laser beam 1064 nm lens at -100 mm , 1 mm beam diameter
at 100 mm lens, waist 67 μm and Rayleigh length of 13.5 mm.

The properties of a Gaussian beam (w_0, Θ) describe the propagation of a Gaussian beam. The Rayleigh length position is defined as the length from minimum wave front radius to its maximum. The position of the minimum wave front radius has a waist of $w_0\sqrt{2}$. The waist changes little within the Rayleigh range and if the z position is smaller than the Rayleigh l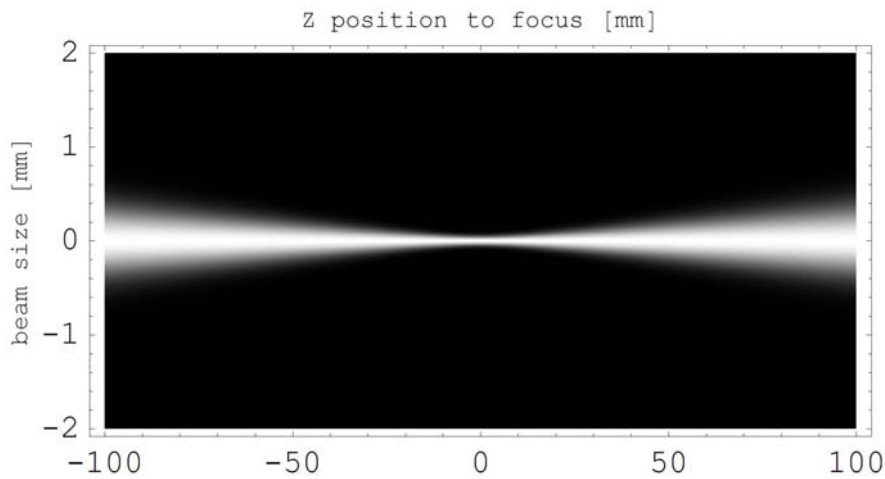ength the waist function 3.5 reduces to 3.6. If the z position equals the Rayleigh range the waist function can be replaced by Equation 3.7. Is the z position far beyond the Rayleigh range the waist is the product of the divergence of the beam times the distance to the focus, see Equation 3.8. With Θ the full divergence angle.

$$z << z_R \qquad w(z) \approx w_0 \tag{3.6}$$

$$z = z_R \qquad w(z) \approx \sqrt{2} \cdot w_0 \tag{3.7}$$

$$z >> z_R \qquad w(z) \approx w_0 \cdot \frac{z}{z_R} = \frac{1}{2} \cdot \theta \cdot z \tag{3.8}$$

If a solid state laser with a zero order Gaussian energy distribution and a wavelength of 1064 nm is focused to a diameter of 80 μm the Rayleigh length is 4.7 mm.

Normally the intensity distribution is not completely Gaussian. In practice a beam quality of M^2 of 1.4 is acceptable for an engraving laser system. The minimum spotsize is increased by the factor M^2 if the divergence of the beam and subsequent the diameter of the beam on the lens is kept constant. The spotsize increases to 112 μm. The Rayleigh length will increase than by a factor of M^2. As Table 3.3 shows the Rayleigh length can be considerable. Although the Rayleigh length describes the area where the intensity changes by a factor of $\sqrt{2}$ with respect to the z' position it should not be mistaken with the process range. The threshold intensity of the process determines the z range where the process is still possible. This could be for a low threshold process larger than the Rayleigh range. For sub surface engraving the Rayleigh length has to be reduced without loosing too much intensity. This can be done by decreasing the focal length of the lens and increasing the beam diameter at the lens.

Table 3.3: Achievable spot diameter (μm) and corresponding Rayleigh length (mm) for standard scanner apertures and available scan lenses (situation 2007).

Minimum spot diameter [μm] at wavelength 1064 nm and beamquality $M^2=1$ *(Rayleigh length [mm])*											
	Focal length [mm]										
Scanner Aperture [mm]	56	100	160	162	245	300	330	346	409	420	815
7	11 *(0.09)*	19 *(0.28)*	31 *(0.71)*	31 *(0.73)*	49 *(1.78)*	58 *(2.49)*	64 *(3.01)*	67 *(3.31)*	79 *(4.62)*	81 *(4.88)*	158 *(18.36)*
10	8 *(0.04)*	14 *(0.14)*	22 *(0.35)*	22 *(0.36)*	34 *(0.87)*	41 *(1.22)*	45 *(1.48)*	47 *(1.62)*	55 *(2.27)*	57 *(2.39)*	110 *(9.0)*
14				16 *(0.18)*	25 *(0.45)*	29 *(0.62)*	32 *(0.75)*				79 *(4.59)*
20				11 *(0.09)*	17 *(0.22)*	20 *(0.30)*					55 *(2.25)*
25					14 *(0.14)*						
30					11 *(0.10)*						
Scanfield [mm]	17x17	60x60	99x99	100x100	156x156	207x207	216x216	213x213	246x246	290x290	586x586

3.4.2   Heat balance with Gaussian intensity distribution

The heat balance is established by calculating the amount of energy absorbed in a volume at a certain depth, see appendix A.

$$T(z) = \frac{\alpha \cdot F \cdot e^{-\alpha \cdot z}}{c_p \cdot \rho} \tag{3.9}$$
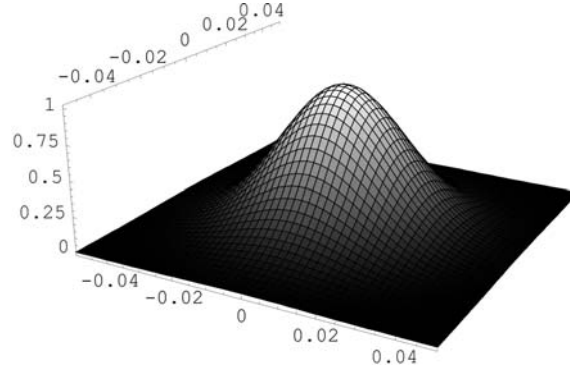
Figure 3.4: First order gaussian intensity distribution at 1064 nm, 1 mm beam diameter at 100 mm lens, spot waist 76 μm (scale in cm) and Rayleigh length of 13.5 mm.

By adding the gaussian distribution in the x and y dimension for the fluency (F) in 3.9 becomes:

$$T(x, y, z) = \frac{\alpha F_0}{\rho c_p} \cdot e^{-z\alpha - 2(x^2 + y^2)/w^2}$$

(3.10)

The fluency integrated over the spot yields the pulse energy. The pulse energy is easy to calculate because power P can be measured and frequency f_Q is known, see Equation 3.11. From the pulse energy and waist the fluency F_0 can be calculated using Equation 3.12.

$$E_p = \frac{P}{Q}$$

(3.11)

$$E_p = \int\limits_{-\infty}^{\infty} \int\limits_{-\infty}^{\infty} F_0 \cdot e^{-2(x^2 + y^2)/w^2} \, dx \, dy = F_0 \cdot \tfrac{1}{2} \cdot \pi \cdot w^2$$

(3.12)

$$F_0 = \frac{2 \cdot E_p}{\pi \cdot w^2}$$

(3.13)

3.4.3 Temperature distribution by a focused laser beam vs. absorption coefficient

Figure 3.5 shows the effect of the absorption coefficient on a focused Gaussian beam. The increase in absorption coefficient clearly reduces the penetration depth. The absorption coefficient value of 0.06 mm^{-1} is the average for transparent polymers at 1064 nm, 0.1 mm^{-1} is the average of the materials in Table 3.4 at 532 nm (green) and for the UV (355 nm) the average is 0.6 mm^{-1}.

Table 3.4: Absorption coefficients for 1064 nm, 532 nm and 355 nm.

Name	Type	Absorption coeff. [mm^{-1}]		
		1064 nm	532 nm	355 nm
Terluran 2802 TR	ABS	0.07	0.11	1.61
Durethan T40	PA	0.035	0.038	0.63
Makrolon 2405	PC	0.075	0.087	0.27
Vitrex	PES	0.05	0.13	1.0
Arnite A04	PET	0.06	0.085	0.78
Plexiglas 7H	PMMA	0.037	0.037	0.06
Polystyrol 168N	PS	0.07	0.077	0.35
Vinoflex466TBS12A	PVC (hard)	0.06	0.15	0.30
Luran 358N	SAN	0.08	0.16	0.53
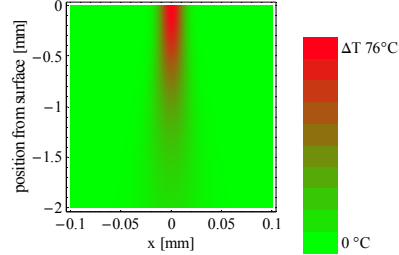
max. temp. increase 38 °C

max. temp. increase 76°C

max. temp. increase 381 °C

max. temp. increase 572°C

Figure 3.5: Temperature distribution after 1 mJ pulse
(100 mm lens, wavelength 1064 nm, Pulse energy E_p = 1 mJ, focus diameter 34 μm).

A pulse of 1 mJ focused down to 34 μm needs at least an absorption coefficient of 0.5 mm^{-1} to get to a temperature of 381 degrees. The measured values in Table 3.4 reach this level only in the UV (355 nm). By creating an overlap of pulses the material starts to degrade even if only one pulse heats up to a 75 degrees, 10 pulses could yield approximate 750 degrees (if placed within 100 μs, f_Q = 100 kHz). There is a loss due to the low diffusion and for calculation with longer pulse trains the diffusion has to be taken into the calculation.

If the laser is focused inside the material the maximum temperature becomes a function of the absorption coefficient and the focus depth. The maximum is reached before the laser is fully focused. If the absorption value increases the maximum temperature position moves toward the surface.

max. temp. increase 36 °C at 0.98 mm depth   max. temp. increase 69 °C at 0.96 mm depth

max. temp. increase 242 °C at 0.8 mm depth   max. temp. increase 301 °C at 0.7 mm depth
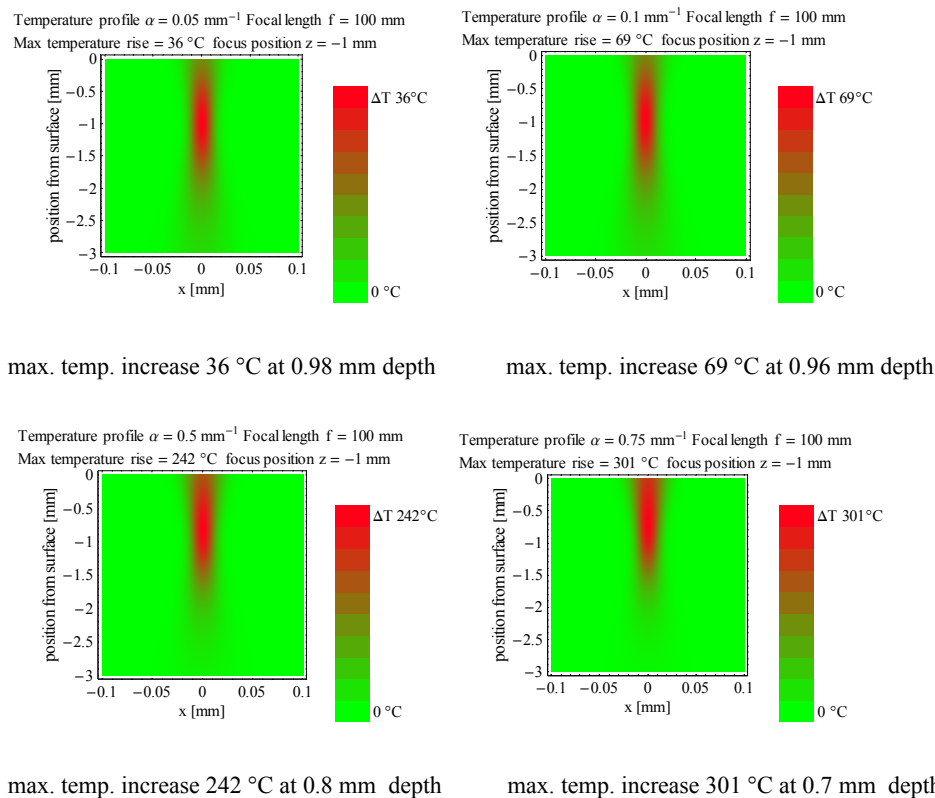
Figure 3.6: Temperature distribution after 1 mJ pulse
(100 mm lens, wavelength 1064 nm, Pulse energy E_p = 1 mJ, focus diameter 34 μm),
focus 1 mm below the surface.

This way of focusing can be used to engrave inside a polymeric volume. For example the triangles written in polycarbonate shown in Figure 2.38 are made by focusing a 1064 nm laser inside the volume.

If the laser is focused inside the material the maximum temperature is reduced and the distribution changes, see Figure 3.7.
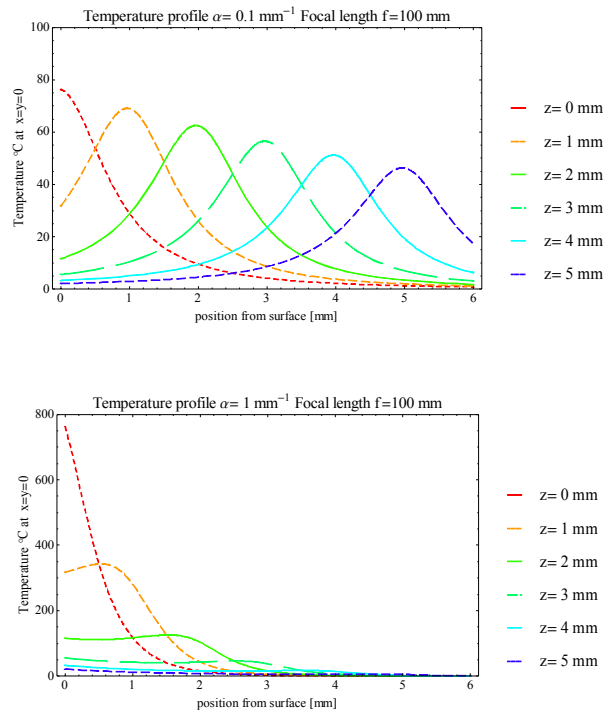
Figure 3.7: Change in temperature in °C (y'axis) at center spot (x = y = 0 mm).
With focus set in material at depth (x'axis) for absorption coefficient 0.1 mm^{-1} and 1 mm^{-1}.

If the absorption coefficient is too high it is difficult to create a local maximum temperature. The best that is achieved is a volume with the same temperature, see Figure 3.7 for absorption coefficient α = 1 mm^{-1} and focus position z = 2 mm). This uniform situation is ideal for laser welding of polymers. The uniform distribution in depth enables a butt weld of 2 mm thick material.

3.5   Optical characteristics of polymers

The optical characteristics of polymers will be described for three areas of the spectrum (UV, visual and infrared). The absorption curve of PET is an example of how polymers behave, see Figure 3.8. For other absorption curves see appendix C. Figure 3.9 shows the corresponding optical penetration depth.

In the UV polymers have a strong absorption up to a certain wavelength. The UV-absorption for ABS, PA and PVC ends at 310 nm. For SAN and PC the absorption ends at 280 nm while

PMMA stops absorbing at 240 nm. PP and PE are transparent already from 220 nm. (Rabek 1996).

In the visual area (450 - 650 nm) most polymers have a low absorption. The amorphous polymers are transparent, while the crystalline polymers appear milky to opaque, due to scattering. Co-polymers or blends have often a hazy or opaque appearance.

The near-infrared (NIR) absorption of polymers is low at 1064 nm, the absorption increases from 1000 nm to around 2500 nm. For most polymers around 1667 nm a distinctive absorption peak is observed. Only for PA (polyamide) this absorption peak is less obvious due to other absorption peaks in this area. This peak is the result of a resonant frequency of the C-H bond. The infrared area from 1667 nm to 2200 nm is an interesting wavelength range for polymer laser processing. The higher absorption enables volume absorption. Where the CO_2 laser at the wavelength of 10.6 μm shows a surface absorption a 2 μm laser could heat up a polymer volume more effectively. Through focussing the laser beam the temperature can be controlled in depth. The 2 μm laser is used for polymer welding and other polymer laser processes like polymer surface shaping and modification.
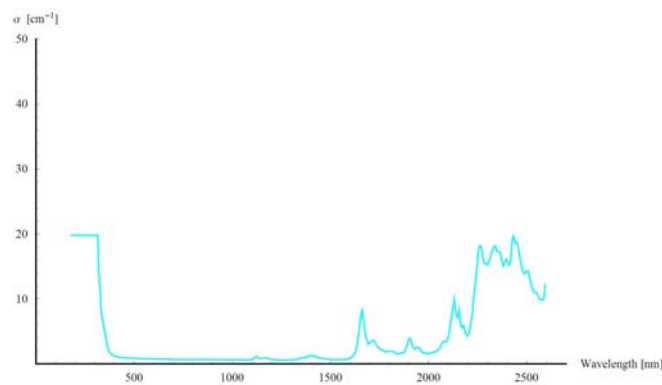

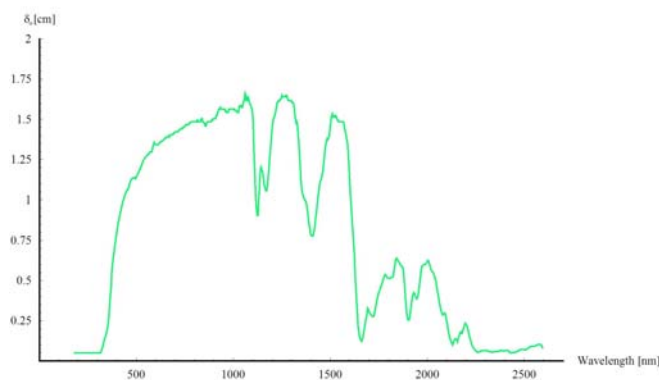*Figure 3.8: Absorption coefficient of PET (2.2 mm) Arnite A04 102 (Hei 1990).*

Figure 3.9: Optical penetration depth of PET Arnite A04 102 vs. wavelength [nm].

3.5.1   Local absorption of light

The absorption of a polymer volume is not uniform. One of the reasons for this non-uniform absorption could be a defect in the polymer chain or a polymerisation catalyst embedded in the polymer mass. These absorbing spots are called chromophores. Table 3.5 lists the schematic representation of the three different chromophore types related to a polymer chain (indicated by X). The polymer chain itself is represented by the dotted line. All these chromophores introduce a localised absorption of energy. During laser exposure this results in locally high temperatures, see Section 6.5. The first type of chromophore is incorporated into the polymer chain during the polymerisation. These internal impurities are the result of unwanted thermal or photo-oxidative processes, but can also add to change the polymer processing characteristics and remain after polymerisation. Other types of chromophores are additives like dyes and pigments. These impurities are distributed throughout the complete polymeric mass and are used to change the visual characteristic of the polymer.

Chromophores can also be an intrinsic part of the polymeric structure, for example, polycarbonate and polystyrene. Chromophores are one of the reasons why sometimes the same type of polymer behaves differently.

Table 3.5: Types of chromophores.

Type of chromophores	Schematic polymer structure (X = chromophores , ----- polymer chain)
Internal	in-chain -----------X------------- end-chain ----------------X
External For example: dyes and pigments	X X ------------------- X X X
Structural part of the polymer structure	---X---X---X---X---X---X---

3.5.2   Scattering of light in polymers

For amorphous polymers, the Lamberts law of absorption is sufficient to describe the intensity distribution in the volume. This is due to a homogeneous refractive index. Refractive index differences introduce reflection and phase changes due to refraction at the sections of index change. The light is transmitted in different directions. For crystalline polymers, the Lamberts law equation is modified by the introduction of a scattering coefficient. This coefficient (α_s) only describes the energy loss due to scattering and does not describe the distribution of this energy into the polymer volume. The scatter coefficient is equal to the fraction of the energy, which is deflected from its original path. From a transmission measurement only the sum of the absorption and scatter coefficient can be calculated.
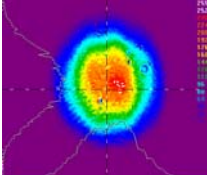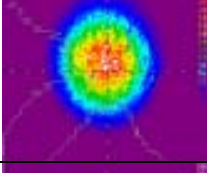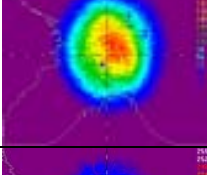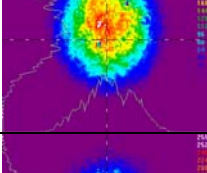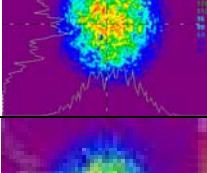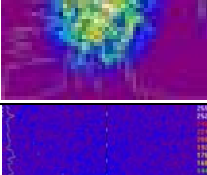
$$F(z) = F_0 \cdot e^{-(\alpha + \alpha_s)z}$$

(3.14)

Prahl and Keijzer describe the photon scattering using a Monte Carlo model (Prahl, Keijzer et al. 1989). To reduce the amount of calculation a fixed surface launch point was used. The result of this single point corresponds to the Green's function for the medium. If the irradiation source profile is not a function of depth the convolution becomes depth independent. This means that the fluency of an arbitrary radiation profile can be obtained by convolving the medium Green's function with the irradiation profile. For a Gauss distribution, the result is the original Gauss multiplied by some modulating function. Because the nature of this modulating function is monotonically decreasing the result is a "washed out" Gaussian profile (Prahl, Keijzer et al. 1989). The intensity distribution of a focused laser beam is depth dependent. A solution to measure the intensity distribution of a focused laser is to use polymer plates with different thicknesses. This approach was done by Frick of the Bayerisches laserzentrum (Frick, Polster et al. 2004). The measured profiles can be used to reconstruct the volume intensity distribution.

An illustrative way is to look at the intensity distribution after the transmission, see Table 3.6. For Poly Propylene (PP) the scattering destroys the original beam profile completely. For the other polymers the original shape of the energy distribution is more or less not affected. The ABS intensity profile showed an orientation in the disturbance of the profile along the flow-lines of the sample but the diameter of the beam remained 2 mm. The Gaussian profile is disturbed. The flow-lines in this ABS sample were caused by the injection moulding. Although ABS is a non-transparent polymer for visible light, at 1064 nm the laser beam passes the 2 mm thick ABS plate rather undisturbed when the diameter of the laser beam is considered. This means that only a weak scattering takes places. PP shows a strong scattering. In the latter case the Lamberts law cannot be used to describe the intensity distribution in the polymer matrix. If the laser spot is distorted by scattering the minimal feature size of the engraving pattern is increased and the intensity of the laser spot decreases. This can result in no marking at all because the intensity stays below the engraving threshold value.

If scattering reduces the contrast of a laser mark an increased absorption will sharpen the marking and reduces the intensity needed for marking. If this is not possible a higher intensity using a smaller focus will also increase the contrast. A high scattering polymer can also be used to stop the laser processing for example the ablation of a lacquer. After ablation the laser energy is scattered by the underlying material and acts as an energy dump. In this way even a thin metal coating (10 μm) can be removed from a polymer.

Table 3.6: Intensity profile and transmitted power for 1064 nm, 1000 Hz pulse frequency, E_p 0.55 mJ /pulse, t_p 120 ns.

	Thickness sample	Power	Diam. beam	
Beam profile	-	0.55 W	2 mm	
PC	1 mm	0.5 W	2 mm	
PET	0.1 mm	0.46 W	2 mm	
Kapton (PI)	0.1 mm	0.47 W	2 mm	
PEN	0.1 mm	0.47 W	2 mm	
ABS	2 mm	0.16 W	2 mm	
PP	1 mm	-		

3.5.3 Additives and energy absorption

Laser-engraving is used to mark all kind of polymers. These polymers are modified for specific use. The use of additives influences the result of the laser engraving process. For example, UV-stabilisers are designed to absorb the UV photons that are likely to photo-degrade the polymer. Normally all non-transparent polymers are coloured by adding pigments and dyes. Unfortunately, polymer manufacturers will not disclose these additives. This is their competitive edge. One sometimes even stumbles upon the use of different additives in different batches. A mix-up of these batches in a production will yield different marking results on the "same" product.

There are two groups of additives: Organic and Mineral. Mineral additives such as titanium dioxide (white pigment), carbon black (black pigment), $BaSO_4$ (filler/white pigment), and zinc oxide (white pigment) form a dispersion of non-agglomerated particles. The organic additives like dyes can be dissolved into the polymer provided they are compatible with it. Organic pigments can be dissolved into polymer matrices too but lose their colour due to the loss of crystal structure. Some additives are used in such excessive amounts that the additive represents an important proportion of the final mixture (Moisan 1985), see Table 3.7. Most polymers have defects like a small percentage of monomers, air bubbles, and some other form of contamination in their matrices. These "defects" act also as additives. The defects introduce a local change of absorption, and could also change the local thermal behaviour of the matrix.

Table 3.7: Polymer additives.

Type of additive	Normal concentration	Classification
Antioxidant	Low	Organic
UV absorbers	Low	Organic
Colour (dye/pigments)	Low	Organic / Mineral
Plasticicers	High	Organic
Reinforcing agents (glass-fibre, carbon-fibre)	High	Mineral
Density increasing fillers	High	Mineral
Fillers to make material cheaper	High	Mineral
Anti-static agents	Low	Organic

When additives are considered there are four major groups of polymer-additive systems, see Table 3.8.

Table 3.8: classes of doped polymers and their optical / thermal behaviours function of the ratio of their absorptions.

		MATRIX	
		Absorbing	Low-absorbing (transmissive)
Additive(s)	Absorbing	I, Volume absorption	III, Additives absorption dominates
	Low-abs.	II, Volume absorption	IV, Transparent or diffusing volume

In the first case (I) both the matrix and additive will absorb the laser energy. Both are heated, but the matrix will shield all the additives (surface absorption) below the surface. The second class (II) will be completely dominated by the matrix. The additive will only receive energy by thermal diffusion from the polymer matrix. The third class (III) will have a transfer of energy from the absorbing additives to the matrix, and the fourth (IV) could act as a non-doped polymer when the differences between other aspects like thermal capacity and refractive index are small. Lippert proposed a qualitative mechanism for the ablation of class III additive/polymer systems as described in Table 3.8 (Lippert 1997). Although it is focused on the pressure increase in the polymer and the subsequent ablation it describes the interaction between additives and the polymer matrix. When all the possible additives from Table 3.7 are considered, a lot of different interactions between polymer/additive and additive/additive are possible The Lippert scheme ends with the mechanical rupture of the polymer matrix but for laser-engraving ablation this reduces the contrast.

If the additive absorbs the laser energy it is brought in an excited state. The excited additive can relax to its ground state by either emission or by radiationless decay. This means that some of the thermal energy contained in the additive is transferred to the polymer by conduction. There is of course a chance for the photon that is produced by the emission of leaving the polymer before absorption. The excited additive could also degrade by photolysis into smaller molecules, radicals or ions. These photolysis products can either react with each other or with the thermal decomposition products of the polymer. Due to the reaction products and the photolysis products the internal pressure is increased. The excited polymer can degrade into its monomers or pyrolysis and photolysis products. These products can react with each other or with the photolysis products of the additives. The pyrolysis is an exothermal reaction and introduces an extra amount of energy in the polymer-additive system. Due to the locally high temperatures an internal pressure builds up and can be released by mechanical rupture of the polymer.
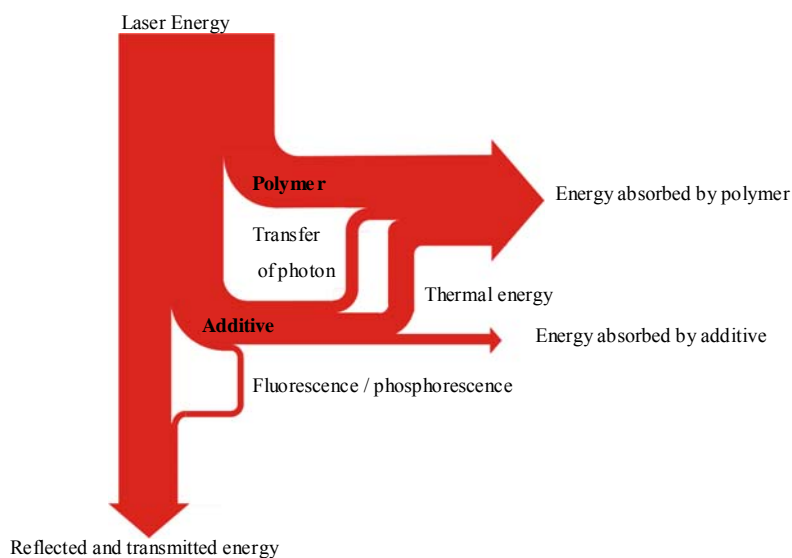
Figure 3.10: Polymer – additive laser energy flow scheme.

From this we can conclude that the absorbed energy that is not consumed by the endothermal reaction between the photolysis products or transmitted by fluorescence/phosphorescence ends up heating up the polymer. If ablation occurs some of the energy is converted into kinetic energy and is removed from the system together with heated fragments of polymer, additive and their degradation products.

3.6   Degradation of polymers

3.6.1   Structure related decomposition

According to Blanchet (1996) and van Krevelen (1976) the chemical structure of the polymer is the primary factor determining stability and decomposition characteristics. As the change in entropy is roughly the same for almost all dissociation reactions, it may be assumed that also the activation entropy will be the same. Van Krevelen states that because of this, the decomposition mechanism and phenomena may be determined by the bond dissociation energy.
In a standard pyrolytic process, once a free radical is formed by the breaking of the weakest bond two competing processes may follow:

1.   Unzipping to monomer.
2.   Free radical transfer with the abstraction of a hydrogen bond from the polymer chain.

This free radical transfer with the abstraction of a hydrogen bonds leads to the formation of random fragments (random degradation). These fragments are usually large when compared with

the monomer unit. The unzipping to monomer is in fact the reverse polymerization of the polymer (chain de-polymerization). Which of these types prevails, depend on the amount of hydrogen in the chain. For polyethylene, with the greatest amount of H on the chain, degradation occurs via random degradation. However when some of the H-atoms on the chain are replaced with methyl or other small groups, hydrogen transfer becomes restricted and some scissions result in the formation of free radicals that unzip to monomers.

3.6.2   Dissociation temperature and degradation delay

The dissociation temperature is related to slow heating when compared to laser induced temperature profiles. According to Gao (1997) the heating rate has little influence on the mechanism of PMMA degradation (monomer major pyrolysis product). But for ethylene-tetrafluorethylene (ETFE) Berman (1992) found that the heating rate in combination with high intensity (just below ablation threshold) has a distinctive effect on the decomposition route. Under slow, thermal excitation the polymer degrades to low-molecular-weight fragments (no char in flame). The fast laser heating rate induced darkening of ETFE (308 nm, 14 ns pulse length). The major chemical process occurring is the elimination of HF from the polymer chains. Leaving a dark, noncrystalline graphite material. Cross linking (also crystallinity chances) of the ETFE film reduces the rate of darkening. If a Q-switch laser pulse at 1064 nm is focused inside a PMMA volume large cracks can be made. This cracking can be seen and heard. The cracks formed have along their edges black patches indicating graphite or char forming. This effect can only be made inside the PMMA volume and not at the surface.

Considering the degradation into gas at 350 °C for PolyStyrene (PS) of 0.24 % weight loss per minute, a short period of nanoseconds couldn't have a visible effect. Therefore the time the polymer is above the degradation temperature has to be considered. This indicates that a short pulse is able to travel through a polymer volume, heating it but without absorption due to degradation during the pulse period. A second and later pulse will however be absorbed by the carbonised material if the polymer can carbonise or in case a polymer degrades to its monomers or gas scattered. This effect is used to mark components mounted on a polymer foil through the same foil (Bosman 2003). If the pulse energy is not too large the components stay attached to the foil with a mark at the component surface. Too much energy will remove the component from the foil in a random direction, because the marking is not uniform distributed with respect to the component. Marking with lower speed with overlapping pulses didn't yielded good results, the foil started to degrade hiding the component for the laser.

3.6.3   Energy generated by pyrolysis

The "van Krevelen" tests with respect to half lifetime temperatures (The temperature at which the polymer losses half its weight when heated for 30 min) were done in vacuum. If oxygen is present the combustion will generate an additional amount of energy. The combustion of PE in oxygen would generate for a volume of 20 μm depth and a diameter of 50 μm 0.9 mJ. Some of the energy is lost by the evaporation of the combustion products thus not all extra energy will diffuse into the base material. If the reaction products are prevented from leaving, for example in volume

polymer marking or when a glass or other transparent cover is used the pressure and temperature will increase causing cracking.

Table 3.9: Combustion energy of different polymers (exothermal).

	Combustion energy [J /mm^3]	Diameter 50 μm, depth 20 μm [mJ]
PMMA	23.6	0.9
PP	32.4	1.3
PET	28.1	1.1
POM	15.3	0.6
PE	22.2	0.9
PC	39.3	1.5

3.6.4 Marking capability prediction by Char Forming Tendency (CFT) index

The char forming tendency is introduced to describe the results of a set of pyrolysis experiments (Krevelen 1976). The char forming tendency (CFT) is defined as the amount of char per structural unit divided by 12 (the atomic weight of carbon), or the amount of C equivalents in the char per structural unit of polymer, see appendix C. All groups supply in their own way to the char forming tendency. Groups with enough H atoms reduce the char forming because they can supply H for the dis-proportionation reaction. This CFT index can also be used to show the tendency for a dark or carbonization mark by a laser. Although the marking is made in an oxygen atmosphere and halogen containing polymers are excluded the results are consistent with the CFT index value, see Table 3.10. For PEN the same correction was used as for PET.

The carbonization of PVC is reported by Decker to be the dehydrochlorination with the formation of polyene sequences which are responsible for the discolouration of the irradiated polymer (Decker 1980). The markings on PCTFE show the same tendency of a brown and yellow mark as the PVC marking, see Table 3.11.

The chemical structure can be used to predict if a polymer shows carbonization. A hydrogen deficit will promote the formation of char and finally graphite. Only if all hydrogen is replaced by fluor a stable situation without carbonization is reached (for example Teflon).

Table 3.10: CFT index vs. carbonisation observation.

Polymer abbreviation	Polymer name	Structure	CFT index	Carbonisation
PE	Polyethylene		0	No
POM	Polyoxymethylene		0	No
PP	Polypropylene		-1.5	No
COP	Cycloolefincop olymer		0	No
PET	Polyethylene terephthalate		1.25	Yes
PMMA	Polymethylmetha crylate		-1.5	No

PS	Polystyrene	(structure)	1	Yes
Nylon 6		(structure)	0	No
SAN	Styrene acrylonitrile copolymer	(structure)	1	Yes
ASA	Acrylic-styrene-acrylonitrile	(structure)	1	Yes
ABS	Acrylonitrile-butadiene-styrene	(structure)	1	Yes
PBT	Polybutylen eterephthalate	(structure)	1.25	Yes
PEN	Polyethylenenaphthalate	(structure)	3.25 (PET correction)	Yes
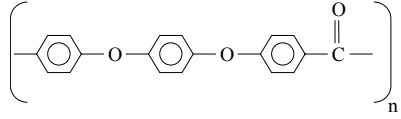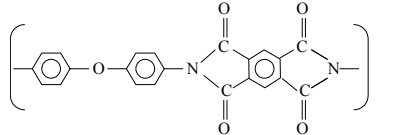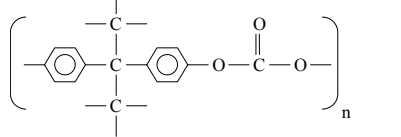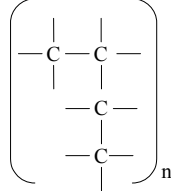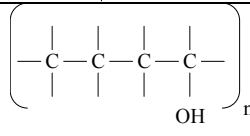
PEEK	Polyetheretherk etone		12	Yes
PI	Polyimide		20	Yes
PC	Polycarbona te		5	Yes
PB	Polybutylene		0	No
EVOH	Ethylene/Vi nylalkohol- Copolymere		0	No

Table 3.11: Halogen containing polymers and Carbonization observation.

Polymer abbreviation	Polymer name	Structure	CFT index	Carbonisation
PVC	Polyvinylchloride	$\left[-C-C- \; (Cl) \right]_n$	Halogen containing	Yes, dechlorination
PCTFE	Polychlorotrifluorethylene	$\left[-C(F)(Cl)-C(F)(F)- \right]_n$	Halogen containing	Yes, dechlorination
ETFE	Ethylene-tertafluoroethylene copolymer	$\left[-C-C-C(F)(F)-C(F)(F)- \right]_n$	Halogen containing	Yes
PTFE	Polytetrafluorethylene	$\left[-C(F)(F)-C(F)(F)- \right]_n$	Halogen containing	No

3.7 Local absorption by impurities and degradation centers.

3.7.1 Forming of small dark particles in a polymer volume.

After laser processing some types of PC small carbonized areas can be seen. These areas start forming through the whole volume that is illuminated by the laser beam. If the laser energy is increased more and larger particles are formed. These particles already form at fluencies where only a small temperature rise is expected throughout the volume of the material. After the forming of the particles the absorption of laser energy is locally increased.

Figure 3.11: Locally degraded PC (horizontal distance between the two vertical lines 0.5 mm)

A second pass would have a much higher absorption creating a complete black mark. During experiments on polycarbonate with a laser setting optimized for creating a homogenous dark mark (1064 nm) we observed that in some places the material started to show enlarged marks. During the process the increased processing was audible. Lowering the setting did solve the problem a little but still some areas behaved completely different. A cleaner PC grade didn't show this behavior.

3.7.2   Temperature estimation of small graphite areas in a polymer volume

A temperature calculation can be made for a single spherical graphite particle behaving as a blackbody radiator. The absorbed laser energy is lost in three ways: First by radiation, second by heat conduction to the surrounding polymer, third by evaporation or thermal decomposition. Assuming that we are not interested in evaporating graphite particles inside polymer matrices we get:

$$\frac{4}{3}\pi r^3 \rho \cdot c_p dT = \pi r^2 I \cdot dt - 4\pi r^2 \cdot dt(\Phi_{con} + \Phi_{rad}) \qquad (3.15)$$

With on the left side the energy needed for a temperature rise of the particle and right the laser absorption by one side of the particle and the loss factors. The conduction can be described using the temperature difference between polymer and particle.

$$\Phi_{con} = \frac{k_s(T - T_0)}{\Delta r} \tag{3.16}$$

The expansion of the heated area Δr can be described using the thermal penetration depth, see Equation 3.4.

The radiation can be calculated using the Stefan-Boltzmann constant under the assumption of black body radiation.

$$\Phi_{rad} = \sigma \cdot T^4 \tag{3.17}$$

This results in a description of the temperature caused by a laser pulse

$$\frac{dT}{dt} = \frac{3}{4} \cdot \frac{I - 4(\frac{k_s(T - T_0)}{\sqrt{4 \cdot a \cdot t_p}} + \sigma \cdot T^4)}{r \cdot \rho \cdot c_p} \tag{3.18}$$

This equation is valid from 0 to t_p and assumes a square pulse and flat intensity distribution.

Table 3.12: Temperature rise of absorbing particles in ABS.
(P=10 W, f_Q=10 kHz, r=50 μm, t_p 10 ns)

	T_{max} °C (temperature rise at end of pulse)
1 μm	59958
5 μm	13210
10 μm	6776
50 μm	1598
100 μm	949

As shown in Table 3.12 small particles heat-up very easily even at 10 W, although a real temperature of 60000 degrees is unexpected, the lower temperatures of around 7000 degrees correspond to measurements made by Zelensky of absorbing particles in an aqueous suspension (Zelensky 1999). During laser marking these small absorbing spots can be seen as white points. The local absorptions initiate degradation and are the reason why polymers already carbonize at low intensities and the irregular in depth marking. Good and even dispersed additives with sizes below 1 μm can be used to mark in a more defined way in depth and quality.

3.7.3   Carbonization in 3D applications

The low thermal conductivity results in a slow temperature relaxation after a pulse. Subsequent pulses heat up the material like one larger pulse would have done but without the high intensity of a large pulse. This explains the difference between the low absorption of polymers and the observed phenomenon of melting, carbonization and ablation for pulse laser processes of polymers at 1064 nm. The volume absorber nature of polymers limits the temperature at the surface and enables in depth processing for transparent polymers. The high absorption of the char and carbon increases the temperature of the polymer and lowers the threshold intensity. This can be used to create structures growing from the already carbonized material, see Figure 3.12.
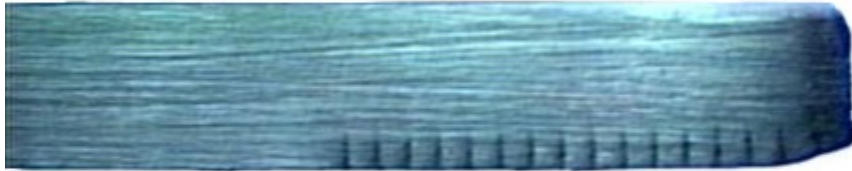

Figure 3.12: Carbonisation in depth (thickness PC 2 mm) 25 scans, Focal length lens 160 mm
[Q-switched Vanadate 1064 nm].

3.8   Conclusions

The temperature calculated using Lamberts law and a Gaussian Tem_{00} energy distribution in the laser spot show for the normal absorption coefficient of polymers relative low temperatures. By increasing the absorption coefficient temperatures of 500 degrees and higher can be achieved. Also the use of multiple pulses overlapping each other will create these high temperatures. Absorption by small particles inside the polymer initiates the degradation even better. A temperature of 6800 degrees is calculated for a particle with a diameter of 10 μm (P= 10 W, f_Q= 10 kHz, w= 50 μm, t_p = 10 ns).

The distribution of the laser can be controlled by focusing below the surface. The maximum energy is reduced and the distribution changes.

The structure of polymers is directly related to its ability to carbonize. The CFT index is used to predict the percentage of char formed during thermal degradation. A CFT index of zero indicates that a polymer doesn't form any char during thermal degradation. The laser marking results are consistent with the CFT index value, although laser marking is done in an oxygen containing atmosphere.

Chapter 4   Writing strategies

4.1   Introduction

Laser engraving of polymers is characterised by the use of multiple pulses written in a predetermined pattern. It is observed that different patterns (scan strategies) give different final results. In practice several scan patterns are tested to obtain the best marking quality. This pre-processing is necessary for all new patterns and reduces the flexibility of laser engraving. This chapter uses the specific material and optical characteristics of polymers described in Chapter 3 to establish a 3D model to calculate the thermal distribution of multiple pulses placed in different strategies. The scan strategies can be divided into two major application areas: marking of machine/human readable text/codes and marking of logos/decorations. For both fields of application speed is important. But for writing of text and codes the readability (contrast and shape) is the most important issue while for writing logos and decorations the uniformity and quality is the major issue. The first part of this chapter is focused on the fast writing of human readable text with galvano mirror systems (readability). The second part will deal with the use of laser engraving for decorative marking (uniformity).

4.2   Writing of codes

A galvano scanner system deflects the laser beam through the use of two mirrors. The position of these mirrors together with the focal length of the lens determines the position of the laser-spot.
A text can be split into the two separate movements of the mirrors. A circle scan is for the X axis a cosines signal and for the Y axis a sinus signal, see Figure 4.1. Every text can in this way be divided into two signals, see Figure 4.2. The frequency and amplitude content of this signal determines the ability of the scanner to follow this signal. Most laser scanner systems use a closed loop feedback system to control the movement of the mirrors. Depending on the tuning the speed, position or step response could be optimized. The digital control systems used in the new generation of scanners (2007) make it possible to setup the control depending on the nature of the scan movement. Although it is possible to calculate the optimum tuning parameters for each line the solution chosen by the supplier is limited to the first initiation. The limitation of adapting the control system is the extra amount of data. Not only start and stop data but also the control parameters should be sent to the scanner. Two possible ways to increase the speed are first the pre-filtering signal with respect to bandwidth and second the deformation of the curve to use bandwidth limitation. Another solution is to wait till the acousto-optic scanner of NTT comes on the market, see Section 2.4.5.
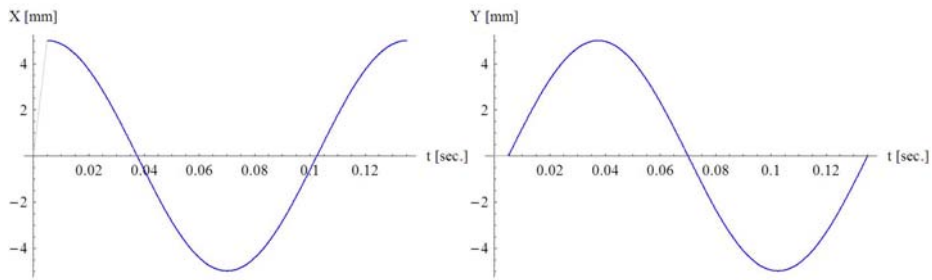
X movement [mm] vs. time [s]   *Y movement [mm] vs. time [s]*
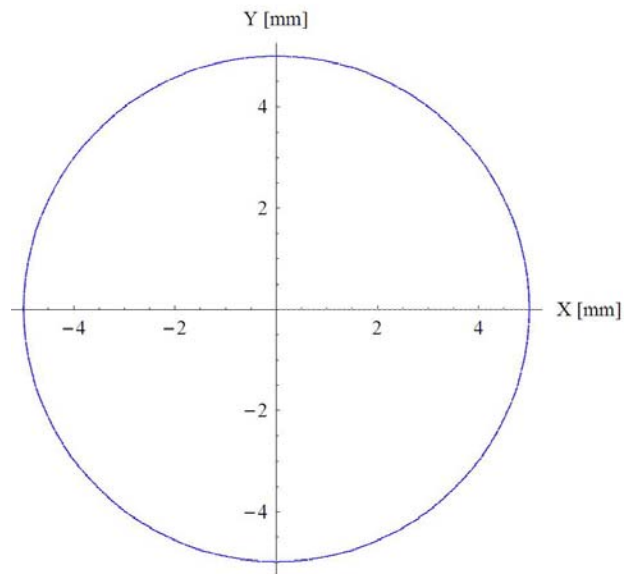
Figure 4.1: Marking of circle in XY plane (bottom) en X en Y vs. time (top).
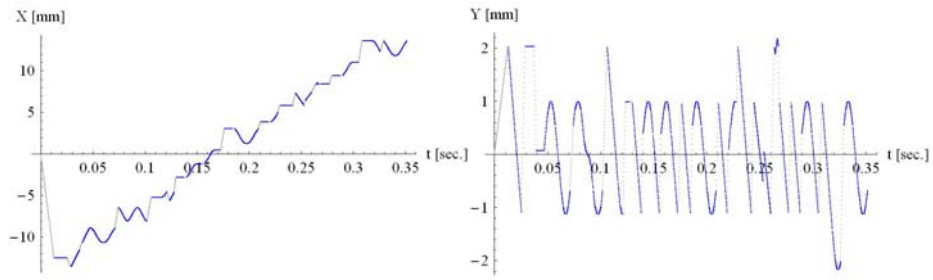
X movement [mm] vs. time [s]   *Y movement [mm] vs. time [s]*
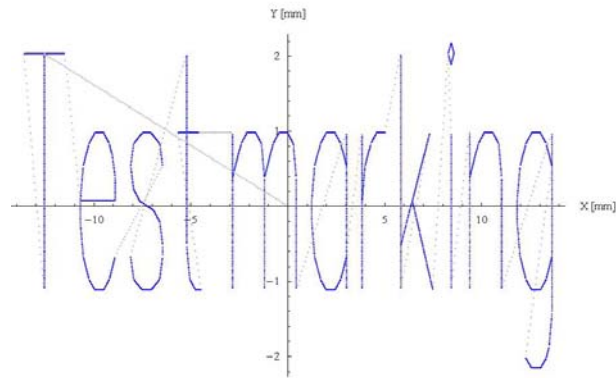
Figure 4.2: X signal (left) and Y signal (right) of test pattern shown in XY representation (bottom) laser on (blue), laser off (grey).

4.3 Human readability of fonts

The readability of a text is crucial for marking. Illegible signs or mistakes could have severe consequences. There are combinations of letters that can easily be misinterpreted, see Table 4.1.

Table 4.1: Similarity table.

Number					
1.	5	S			
2.	1	l	7	I	T
3.	0	O			
4.	U	V	W		
5.	6	b			
6.	8	B			
7.	N	M			
8.	9	g	q		
9.	0	Q			
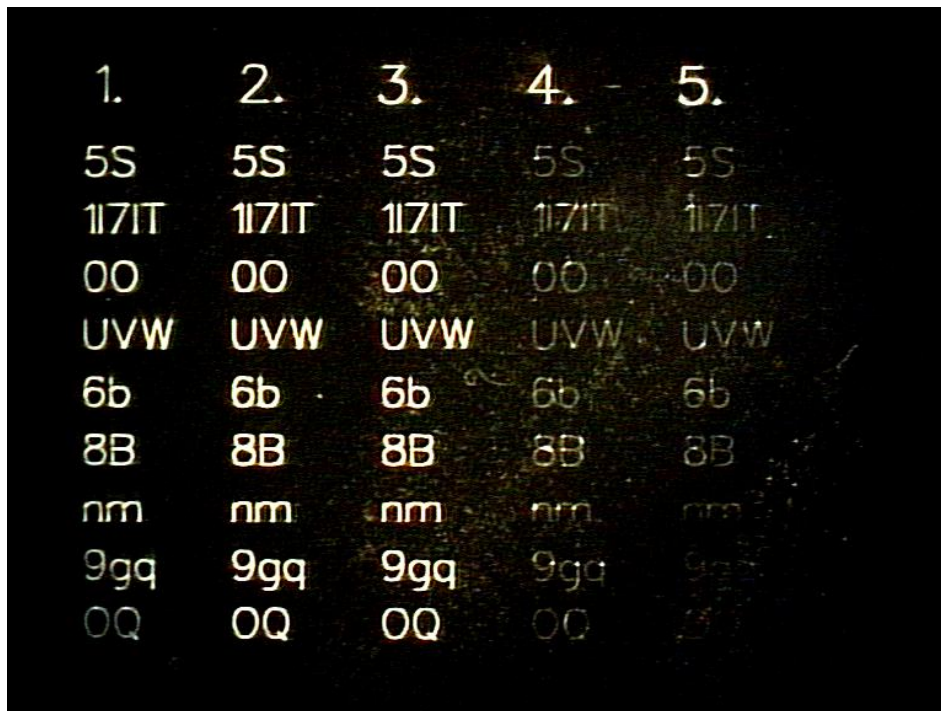
Figure 4.3: Example of test pattern for similarity test, Scanner type Intelliscan 14 mm Scanlab , wavelength 1064 nm, f_Q 20 kHz, P 1.9W,fΘ 160 mm. Font Simple Straight 2 Scaps, Letterheight 1 mm, 20 times marking on black foil layer on white background. Scanspeed 1. 100 mm/s, 2. 250 mm/s, 3. 500 mm/s, 4 1000 mm/s, 5 1500 mm/s.

Table 4.1 can be used to show how readable the text is when marked at higher speed and different intensities. For example the standard font of 1 mm height written at different speeds shown in Figure 4.3 shows the difficulties in writing codes. During the design phase of a laser marking process the most important feature is the readability. If everybody can read it without difficulties the code is accepted. Often a lower speed will make a code more robust. The experiment shown in Figure 4.3 shows for 1000 mm/s already a similar shape for the "O" and "Q" pair and for the "9" and "g" pair. The "l" and "I" pair already have a similar shape due to the design.

If the contrast is low the readability will always be a problem. In these cases an optic system is often accepted as a solution. Machine readable codes can be tested using a verifier. This device reads the code and will give the quality of the code back. This information can be used during the design phase of a process to improve the code. The use of redundancy of information in the code improves the reliability after partial code destruction or poor reading circumstances. If the code for example with a data matrix code is very repetitive this redundancy would only partially help because all parts are equally affected. Codes in which the position of the data is absolute will give problems with position errors due to scanner deviation. Codes that are encrypted relative will be more robust. There are more than 20 different 2 dimensional codes according to Russ Adams (Adams 2005). The reason of the many codes is that for every application or printing machine you can design a method of encoding information. Some of them are for public use others are proprietary. And everybody is free to design his own code so there will be more 2D codes. In the past even Philips has designed it own code, dotcode A. It is a simple dot matrix code without redundancy designed for low precision marking technologies.

The similarity table is the basis of a standard test where similar codes are written at different speeds and intensities, the test is described in more detail in appendix D.

To show if the scanner has reached its limits the total writing time can be measured. Often scanner programs report an actual marking time. To reduce the effects of start and stop times and measurement inaccuracy the marking is repeated at the same spot (for example 10 times the same letter). These times can be displayed in a graph versus the marking speed, see Figure 4.4 left. The marking time tends to go to a minimum. From the assumption that the low scan speed of 100 mm/s is actually achieved the actual speed can be calculated, see Figure 4.4 right. This Figure shows that the limit of the scanner is 800 mm/s.
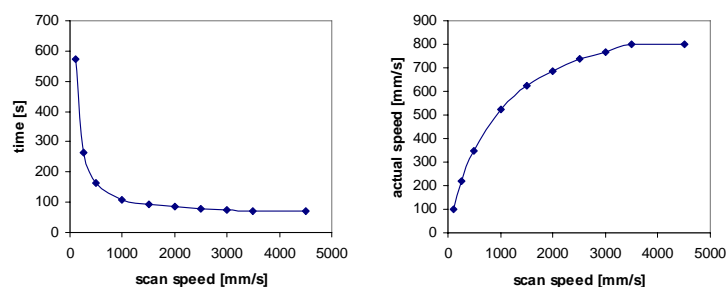

Figure 4.4: Scanner marking test result of test pattern.
Scanner type, intelliscan 14 mm Scanlab , ƒΘ 160 mm,
Font Simple Straight 2 Scaps, letterheight 2 mm, pattern "0123456789" 10 times marked to increase accuracy.

Together with a visual assessment of the marking result the minimum writing time can be set. This should be done at low intensity sensitive material. For this a black photocopy or a black foil on a white background can be used.
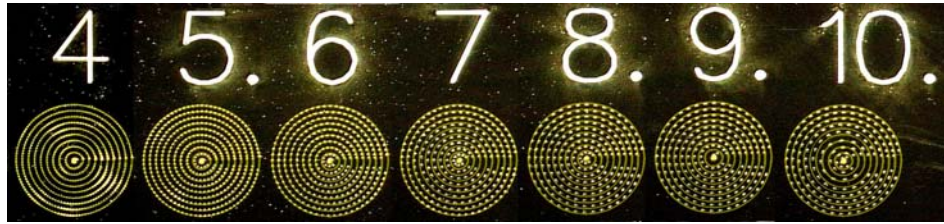

Figure 4.5: Scanner performance, Scanner type intelliscan 14 mm Scanlab , f⊖ 160 mm, f_Q 20 kHz, yellow pattern gives the programmed pattern. Programmed scan velocity : 4. 1000 mm/s, 5. 1500 mm/s, 6. 2000 mm/s, 7. 2500 mm/s, 8. 3000 mm/s, 9. 3500 mm/s, 10. 4000 mm/s.

Figure 4.5 shows the performance of an intelliscan 14 mm from Scanlab. The circle pattern that is programmed is shown in the Figure 4.5 as a yellow path to distinguish between the actual path written by the white pulses. From 2500 mm/s on the actual pattern starts to deviate from the programmed pattern. At 4000 mm/s and a diameter of 1 mm the difference becomes 0.26 mm, 10% of the total diameter. Table 4.2 shows the performance of this scanner with respect to the scanned diameter of a circle and speed.

Table 4.2: Diameter ratio and (speed ratio) of intelliscan 14 mm.
Actual / programmed for pattern of Figure 4.5.

Diameter [mm]	4. 1000 mm/s	5. 1500 mm/s	6. 2000 mm/s	7. 2500 mm/s	8. 3000 mm/s	9. 3500 mm/s	10. 4000 mm/s
2	1.00 (1.08)	1.00 (1.06)	0.99 (0.94)	0.99 (0.98)	0.97 (1.06)	0.97 (0.86)	0.97 (0.76)
1.8	0.99 (1.12)	0.98 (1.15)	0.98 (1.08)	0.98 (1.04)	0.96 (1.01)	0.97 (0.87)	0.96 (0.79)
1.6	0.98 (1.04)	0.98 (1.06)	0.98 (1.08)	0.96 (1.21)	0.94 (1.10)	0.94 (0.83)	0.94 (0.68)
1.4	0.97 (1.01)	0.97 (1.06)	0.96 (1.01)	0.95 (1.27)	0.93 (0.96)	0.92 (0.91)	0.91 (0.8)
1.2	0.96 (1.01)	0.97 (1.06)	0.95 (0.86)	0.90 (1.16)	0.91 (1.01)	0.91 (0.87)	0.86 (0.97)
1	0.94 (0.94)	0.94 (0.86)	0.90 (0.87)	0.86 (1.21)	0.86 (0.91)	0.85 (0.91)	0.74 (1.09)
0.8	0.90 (0.92)	0.88 (1.06)	0.87 (0.94)	0.81 (0.99)	0.80 (0.87)	0.80 (0.79)	0.59 (0.95)
0.6	0.84 (0.93)	0.82 (0.87)	0.77 (0.79)	0.68 (0.89)	0.70 (0.84)	0.69 (0.62)	0.42 (0.76)
0.4	0.72 (-)	0.65 (0.70)	0.56 (0.80)	0.50 (0.59)	0.50 (0.54)	-	-

4.4 Area engraving

The use of laser-engraving for decorative applications makes it necessary to mark complete areas instead of just simple lines. For some applications writing a set of lines with a certain distance between them is sufficient for an acceptable result. But in most cases a complete and uniform gray-tone has to be made. The length of the path that has to be written for a complete and uniform filling is relatively long. Therefore optimization of the strategy is necessary. The time needed to fill a contour depends on its area. When the contour length is reduced by half, the filling time is reduced by a factor of four. The reduction of the size is not always an acceptable solution, and other optimizations have to be found. The strategy chosen influences both the uniformity (quality) and the time needed for a complete marking. In the first part of this chapter the time aspect is the main focus. In the second part the uniform filling will be calculated according to the thermal model.

Some materials show more thermal effects for different strategies than others. Melting and foaming are two processes that are strong thermally dependant while carbonization will show a much lower dependency. Thermal effects cause not all differences. Some can be caused by scan errors or by the first pulse effect.

The time needed to fill an area depends on the effectiveness of the writing pattern that is chosen during the pre-processing stage. The fact that a scanning system can have different speeds, but is always linked to a certain position error, makes it possible to move slowly during writing and fast during the non-writing moves. The non-writing moves are not effective because they leave no visible mark. The number of pulses needed to fill a pattern with a surface area A can be written as:

$$n = \frac{A}{\Delta x \cdot \Delta y} \tag{4.1}$$

Where Δx is the distance between two pulses, and Δy is the distance between two parallel lines. The minimum fill time of this area written with a pulse frequency f_Q is:

$$t_{\min} = \frac{A}{f_Q \cdot \Delta x \cdot \Delta y} \tag{4.2}$$

The fill strategy will have an effect on the thermal degradation of the polymer. Due to different absorption conditions induced by different temperatures, and partially degradation of the polymer matrix, the scan sequence can be clearly visible.

4.5   Fill strategies

A writing or fill strategy is normally calculated without any attention to the effect on the polymer matrix but only with regard to the time that is needed for a specific area that is to be filled. This lack of attention has to be compensated by adjustment of the laser parameters and by lowering the scan speed. Filling an area can be done in different ways. The fill strategies can be divided into four basic categories: Line fill, contour fill, bitmap fill and sub area fills. These categories consist of different types of filling and for each filling different sequences can be chosen. Table 4.3 shows the possible combination of fillings. In the next paragraph the different basic categories are discussed with their effects on marking time. In Section 4.8 the thermal effects of strategies are discussed.

Table 4.3: Area fill strategies.

Basic element	Type	Sequence
Lines	Uni-directional fill	Normal Random Alternating
	Bi-directional fill	Normal Random Alternating
	Meander fill	-
	Sub lines	Alternating within line Sub lines two scan 1 line Alternating in two scans Alternating lines in two scans
	Tilted lines	-
Contours	Contour fill	Middle to edge Edge to middle
	Single line fill	Inside to outside Outside to inside
	Sliced fill	Inside to outside Outside to inside
	Sub line fill	
Bitmap		Normal Random
Sub areas	Cells Crystals Natural	

4.5.1 Line fills

UNI-DIRECTIONAL FILL

The uni-directional fill is used most. It is easy to implement and provides acceptable results in most applications. It is also mostly supported by scanner software.
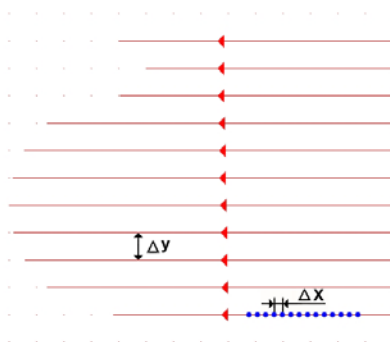

Figure 4.6: Uni-directional fill

The uni-directional scan has more non-marking length as marking length. Together with the stop and start points this filling is not the most time effective. This is shown in Equation 4.3 where for a uni-directional filling of a rectangular (x length, y height, △y distance between the lines, △x distance between the spots, V_{jump} non marking movement speed) the time is calculated.

$$t_{uni-dir} = \frac{x \cdot y}{f_Q \cdot dx \cdot dy} + \frac{(\sqrt{\Delta y^2 + x^2} - \Delta x) \cdot \dfrac{y}{\Delta y}}{V_{jump}} + \frac{y}{\Delta y} \cdot (t_{start} + t_{stop}) \qquad (4.3)$$

The time needed to get to the beginning of the line can be reduced by increasing the jump speed. This could mean that the stop time should be increased to wait for a complete stop.

BI-DIRECTIONAL FILL

The bi-directional fill strategy is faster compared to the uni-directional fill strategy. A disadvantage is the concentration of energy at the turning points. This can have an effect on the uniformity of the filling. If the length of the lines is not exactly matched with the pulse distance the start at the other side will cause a slight displacement in the scan pattern.
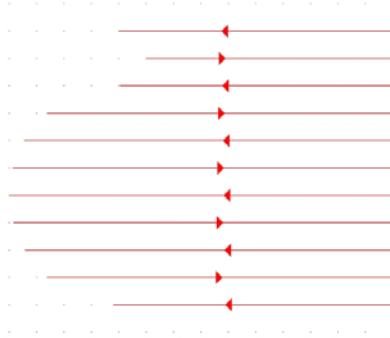
Figure 4.7: bi-directional fill

The time for marking a rectangular of height y and width x becomes:

$$t_{bi-dir} = \frac{x \cdot y}{f_Q \cdot \Delta x \cdot \Delta y} + \frac{(\Delta y - \Delta x) \cdot \dfrac{y}{\Delta y}}{V_{jump}} + \frac{y}{\Delta y} \cdot (t_{start} + t_{stop}) \qquad (4.4)$$

The bi-directional fill will always be faster than the uni-directional filling because the distance between the lines ($\triangle$y) is always smaller than the combined movement in x and y direction.

MEANDER FILL

The meander fill is in principle equal to the bi-directional fill but without any jumps. The pattern is written as one single path without modulating the laser. This has no negative effect on the speed if the jump between the lines is small. If $\triangle$x = $\triangle$y the meander fill will generate the same pattern as the bi-directional fill but without the start and stop times.
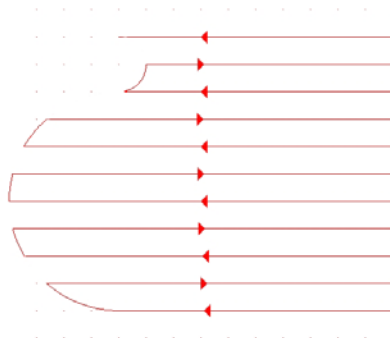

Figure 4.8: Meander fill.

$$t_{meander} = \frac{x \cdot y}{f_Q \cdot \Delta x \cdot \Delta y} + \frac{(\Delta y - \Delta x) \cdot \dfrac{y}{\Delta y}}{f_Q \cdot \Delta y} \quad (\triangle x \leq \triangle y)$$ (4.5)

The meander time becomes the minimum time as defined in Equation 4.2 if $\triangle y = \triangle x$. The meander fill could even be the slowest compared to uni-directionair and bi-directional fill, if V_{jump} is large and t_{start} and t_{stop} are near to zero.

SUB LINES

Sub lines is a fill strategy that uses a subdivision of the original lines into smaller lines with different directions. The sequence of these sub lines can be chosen. For example an alteration of the directions in one line. Another solution is to scan first one direction sub-lines and after that on the way back the other direction.
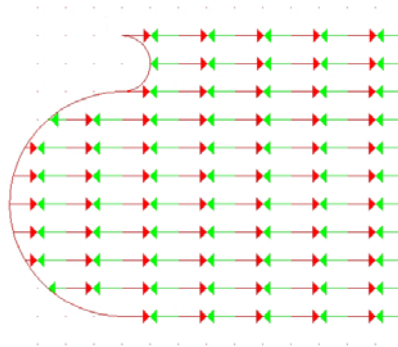
Figure 4.9: Sub lines fill.

Sub lines fill are not supported by standard software but they give good results when used on polymers. If the sequence of the sub lines is carefully chosen the amount of writing time could be kept in the normal range.

TILTED LINES

Tilted lines can be used to compensate the concentration of energy at the turning points of the meander and bi-directional fill, see Figure 4.10 right. Due to the slight tilting the concentration of energy is lowered. Tilted lines can also be used to increase the writing speed, see Figure 4.10 left.
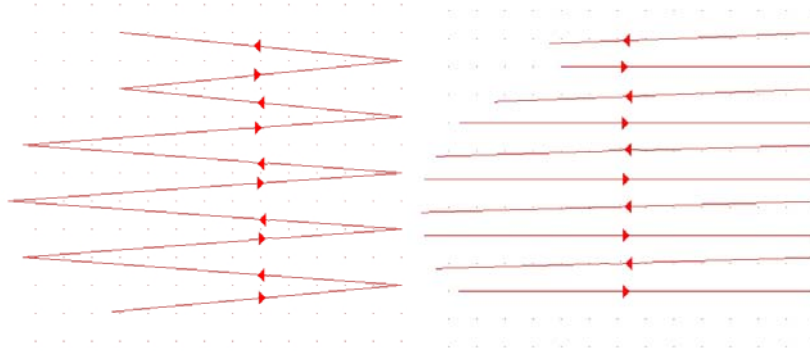
Figure 4.10: Tilted lines fill, Left increased speed, Right, change energy concentration.

4.5.2 Contours

CONTOUR OFFSET

Filling along a decreasing contour is a method developed for milling applications. It is easy to use because it is incorporated in standard processing software. The result is not uniform because at the edges the distance between the edge points is larger than the distance between the lines.

Figure 4.11: Contour fill.

The laser has to write first the outline, and with steps of the distance of the lines, increasing patterns generated from the previous written pattern. The inverse contour fill does not have the problem of the concentration of all energy in the centre. The filling from the inside has a much better thermal behavior than the contour filling. The engraving time will be the same.

SINGLE-LINE FILL

The optimum filling is a single-line filling. There are no jumps necessary which will take time to complete. This optimum cannot be achieved for a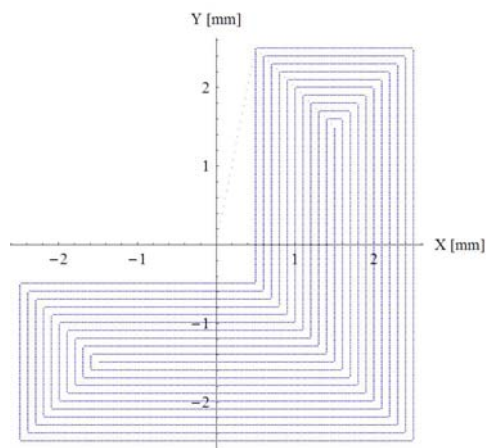ll contours, and a small change in line distance can destroy the complete fill strategy. Because single line fill wasn't available, an algorithm has been made in order to study this fill method. Section 4.7 describes the basic elements of the algorithm that generates a line fill with a minimum of lines.

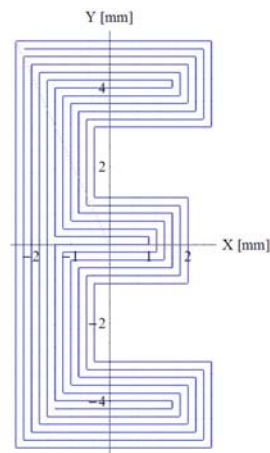*Figure 4.12: Single line fill of the letter E.*

SLICED FILL

A sliced fill is used to create a more natural way of marking. The pattern is first used as a base to setup a 3D shape. This shape is then sliced to create a set of fillings with different distances between the lines.
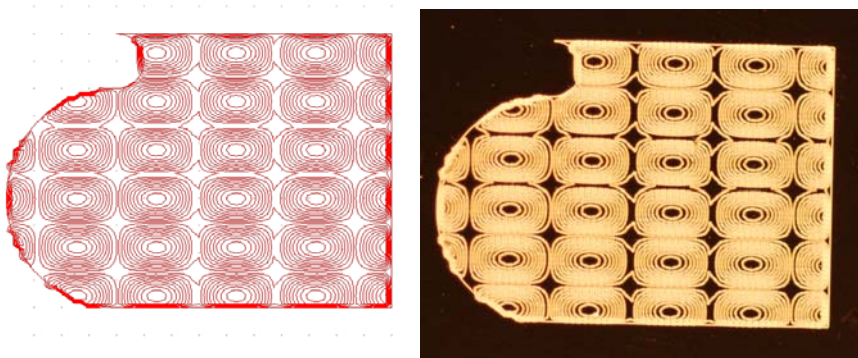

Figure 4.13: Sliced fill and marking result on
POM (Hostaform C27021), dimensions pattern (width x height, 14 mm x 10 mm).

4.5.3   **Bit-map filling**

The bit-map can be used to describe areas that are filled with a certain pattern. This approach opens up the possibility to add intensity information for every pulse to a pattern, or use-dithering, as a technique to simulate these intensities by changing the dot density, see Figure 4.14. For example, a filling can be made to simulate a stone structure. By using a rather small dot distance compared to the spot-size, the intensity of the print can even be changed without showing the actual dots.
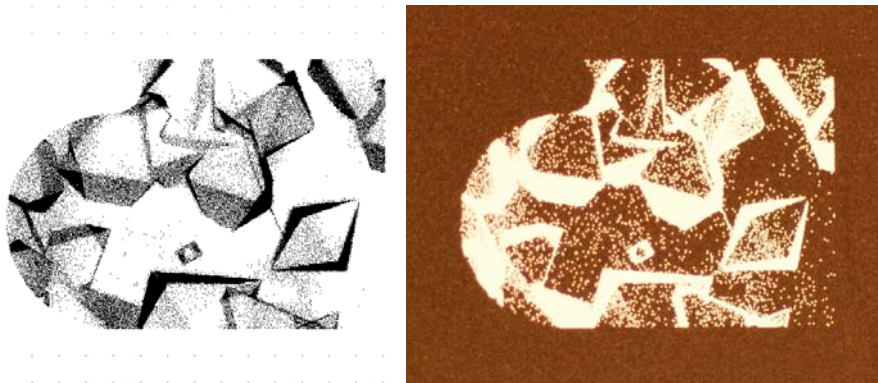

Figure 4.14: Bit-map filling with dithered gray-scale structure and marking result on POM (Hostaform C27021), pattern (width x height, 14 mm x 10 mm).

By using an external modulator, or the technique of inversion modulation, the gray scale can be translated into pulse energies. This enables a fast and controllable marking of complex patterns like pictures with a higher resolution than is possible with the dither technique. The reason why dithering cannot achieve the same resolution of the modulation is that by using dithering one spot is divided into an array of spots that has only two colour levels (black – white), see Figure 4.15. And these spots have the same dimensions as the original spot when laser-marked. By adjusting the distribution of the spots, the introduced errors are to a certain extent leveled. This error diffusion algorithm (floyd-Steinberg) is a standard option in most of the graphics software. The use of dithering can introduce artifacts into the picture. For example, large areas of light gray will be translated to only a few spots which look rather odd. An array of n x n can simulate $n^2 + 1$ different gray levels, see Figure 4.16. This means that if a 256-level gray tone filling has to be simulated, a 16 x 16 array is needed. If this picture had a resolution of 300 dpi, the laser spot-size should be around 5 μm. When the pulse is modulated this would be only 85 μm, which is a more realistic value. This is the reason that a dithering of 3 x 3 is a more realistic figure, and therefore the picture has to be leveled to ten gray tones.

Figure 4.15: Written by inversion modulation with a second harmonic Nd:YAG on ABS, source: PHILIPS DAP-LTM, Martijn de Keijzer.
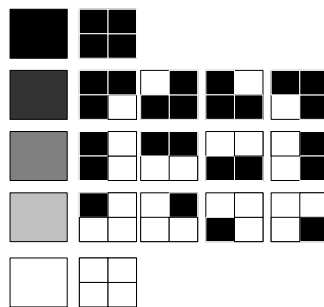
Figure 4.16: Principle of dithering. (a 2x2 array can simulate five different gray tones).

4.5.4   Sub area fill

CELLS

Dividing the contour into a pattern gives a different appearance. Every cell is filled before starting the next one. And each cell can have its own filling. In this way large fills can be made without having to take too long cooling times. The time to create such a filling is larger because of the large number of start and stop points. If however the cells are filled with a meander fill the total time is not that much longer. Only the movements between the cells are extra in this type of filling.
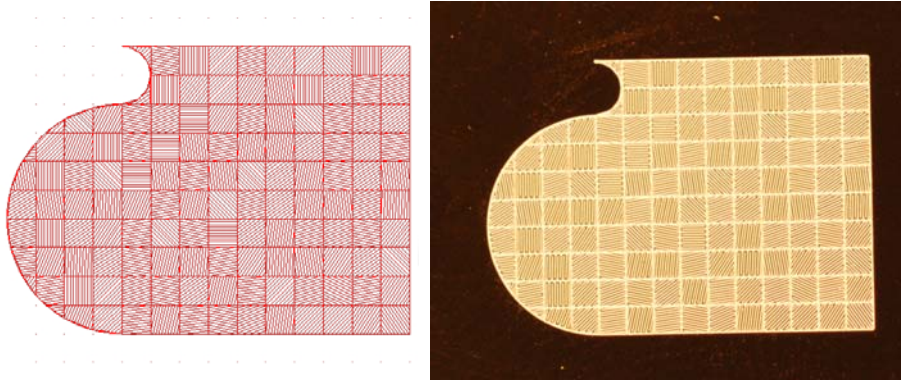
*Figure 4.17: Cells pattern and marking result on
POM (Hostaform C27021), pattern (width x height, 14 mm x 10 mm).*

CRYSTALS

Although the crystal type of filling is slightly different than the cell fills it could hide fill defects more effective. As all crystals have a different thermal behavior the total effect becomes more natural. The total writing time depends on the structure and the size of the crystals.
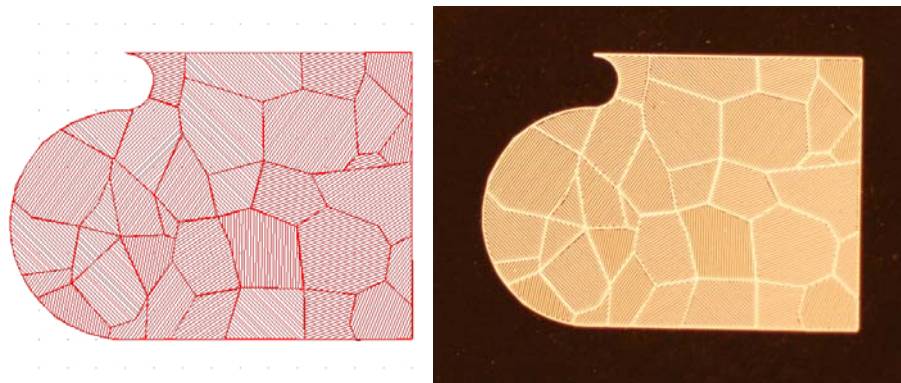
*Figure 4.18: crystal filling and marking result on
POM (Hostaform C27021), pattern (width x height, 14 mm x 10 mm).*

A design fill doesn't have to be a complete filling. The pattern could be either a fill oriented sequence of shapes or a filling caused by lines or dots. The time aspects are rather challenging because a lot of time can be lost if for example the line filling isn't optimized.
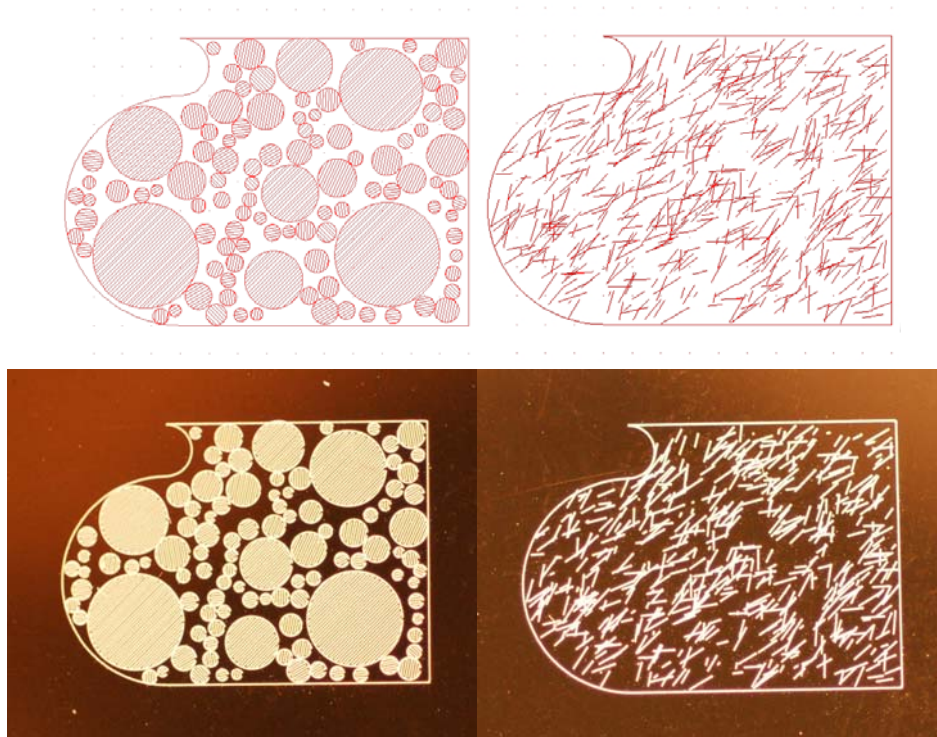
Figure 4.19: Design fillings with marking result on
POM (Hostaform C27021),, pattern (width x height, 14 mm x 10 mm).

4.6 Implementation of single line optimization.

The idea behind the multi directional filling is to use only a single line to fill a contour. The writing of one continuous line is the fastest way to fill a contour. No extra time is needed for non-marking lines and jump/start/stop delays.

The filling with one continuous line is not always possible but a filling can be optimized in order to come to a minimum number of continuous lines. A computer algorithm has been developed to test the idea and the usefulness of this multi-directional filling. An example of the result of the algorithm is shown in Figure 4.24.

4.6.1 Basics of multi directional fill method.

The basic idea is to calculate a starting point and to start from this point with a filling. The starting point can be any point within the logo at the filling distance to the logo. The filling is calculated as far as possible. The remaining gaps are detected and treated similar as the original contour. The algorithm detects also contours in logos that should remain open spaces. For this a

flexible data structure is necessary in order to hold the calculated lines. The open contours have no links to line sequences.
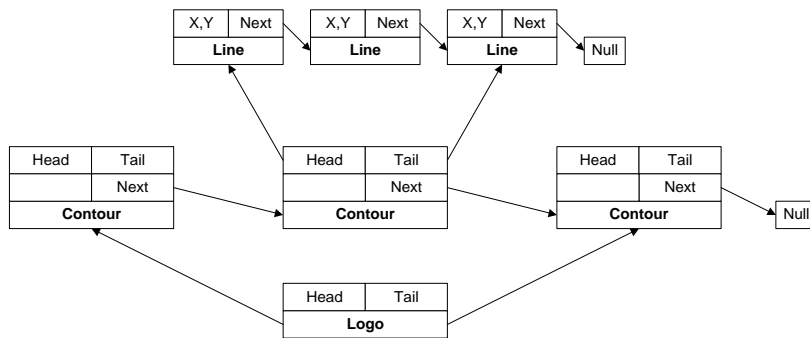
Figure 4.20: Data structure used for fill algorithm.

For the calculation of the filling of a contour the following steps are implemented:
1. Single contour testing and splitting, see Figure 4.21.
2. Merging overlapping contours, see Figure 4.22.
3. Inclusion of contours, see Figure 4.23.
4. Startpoint calculation
5. Testing of filling lines
6. Detecting of open spaces
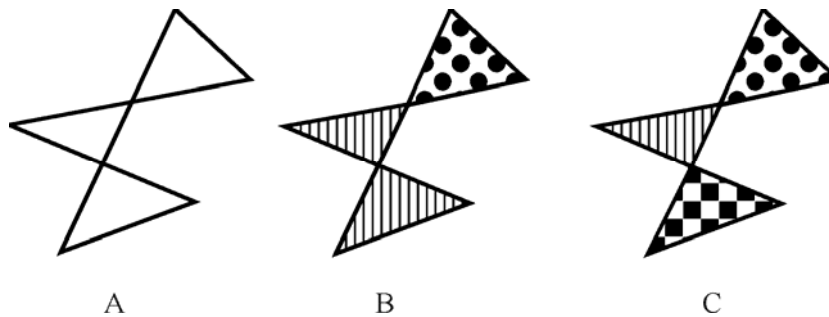
Figure 4.21: Splitting of a single contour in three separated contours using the single point crossings.
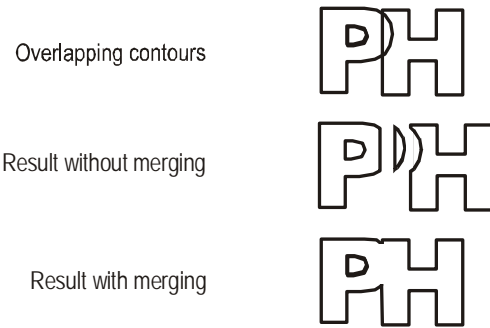
Figure 4.22: Merging contours to create one new contour.
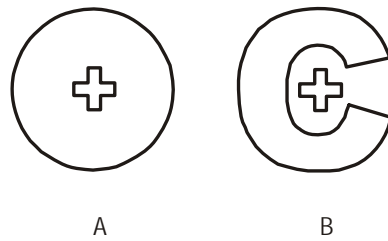
Figure 4.23: Two types of contour inclusions A. complete, B embraced.
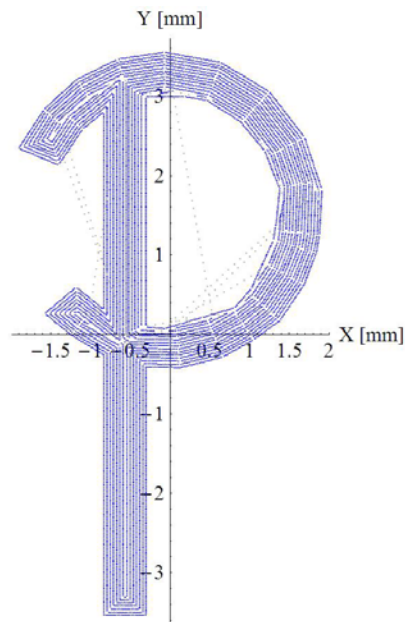
Figure 4.24: P calculated using the multi directional fill algorithm.

4.6.2   **Marking results with multidirectional fill algorithm**

This way of writing fill patterns was introduced in the PHILIPS factory in Terneuzen (the Netherlands) to be able to decorate lamp caps within the production time available without reducing the print. Table 4.4 shows the marking times for a PHILIPS logo, the marking results are shown in Figure 4.23.

Table 4.4: Marking times of Philips logo (30.67 mm x 6.07 mm) with 0.1 mm fill.

	Angle	Marking Time
Single line fill	-	1.31 sec.
Bi-dir. fill	0 degrees	2.374 sec.
	90 degrees	1.578 sec.
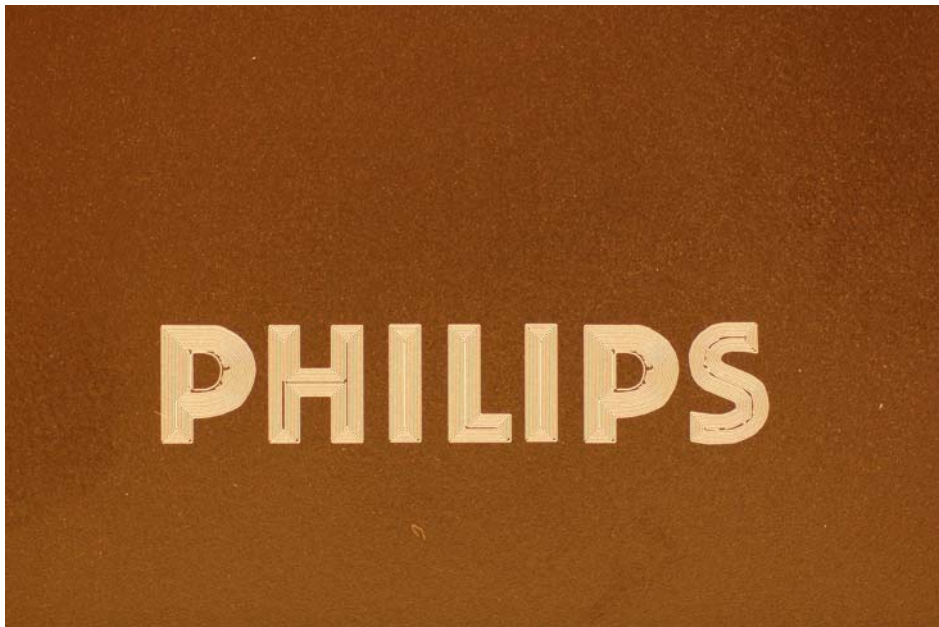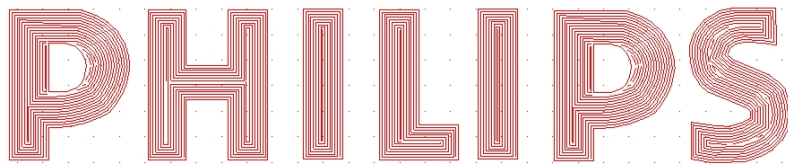
Figure 4.25: Top, Philips logo, multi directional fill pattern 0.1 mm distance. Bottom, marking result on POM (Hostaform C27021) (width x height 30.67 mm x 6.07 mm).

4.7   3D thermal model of laser engraving

The temperature field is used as the initial condition for a three dimensional diffusion model. From this model a surface model for irradiation can be derived. This model is used to describe the effect of different fill strategies for laser engraving of polymers.

4.7.1   Basic 3D model

With a three-dimensional model the diffusion of the energy after the laser pulse can be modelled. As the pulse of a Q-switch Nd:YAG is relatively short the heat generation has completed 20 ns after the pulse, even with a relatively long half-lifetime of 5 ns. The relative low heat diffusion during this short laser pulse compared to the pulse diameter and optical penetration depth enables the exclusion of the diffusion during the pulse. The temperature distribution is calculated with the heat balance at the end of the laser pulse (t=0). The initial temperature distribution T(x,y,z) is calculated using Equation 3.10.

The thermal diffusion equation has no source term as t = 0 is defined just after the laser pulse for an infinite space:

$$\frac{\partial^2 T}{\partial x^2} + \frac{\partial^2 T}{\partial y^2} + \frac{\partial^2 T}{\partial z^2} = a^{-1} \frac{\partial T}{\partial t} \quad -\infty < x < \infty; -\infty < y < \infty; -\infty < z < \infty \quad (4.6)$$

The initial condition (Gaussian distribution, within Rayleigh length Z_R, $z << Z_R$) is given by the thermal balance just after the laser pulse. For materials with a penetration depth smaller than the Rayleigh length and the material thicknesses the assumption of infinite material and constant beam diameter are valid (most coloured materials). Transparent materials have a penetration depth larger than the Rayleigh length and thickness. In these cases the assumptions are only valid close to the surface.
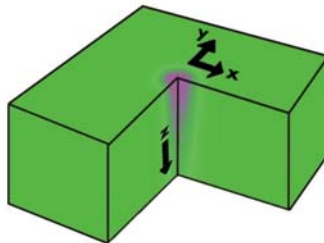
Figure 4.26: 3D view of temperature distribution as described by Equation 4.7.

Because the Fourier solution route demands a continuous field the negative part of z has to be defined. Adding a temperature field preventing energy to flow across the z=0 plane is often used. This is done by applying the same temperature field at the negative part mirrored at z=0. The complete temperature field and the initial condition become:

$$T(x,y,z,0) = \frac{\alpha \cdot F_0}{\rho \cdot c_p} \cdot e^{-|z|\alpha - \frac{2(x^2+y^2)}{w^2}} \quad -\infty < x < \infty; -\infty < y < \infty; -\infty < z < \infty \quad (4.7)$$

Appendix F describes the route used to solve the thermal diffusion equation for the initial condition 4.7 yielding Equation 4.8.

$$T(x,y,z,t) = \frac{\alpha w^2 F_0}{\rho c_p} \frac{-1}{2(8at+w^2)} \cdot e^{-z\alpha + at\alpha^2 - 2(x^2+y^2)/(8at+w^2)}$$

$$\left(-2 + erfc\left(\tfrac{1}{2}\sqrt{\frac{1}{at}}(z - 2at\alpha) \right) - e^{2z\alpha} erfc\left(\tfrac{1}{2}\sqrt{\frac{1}{at}}(z + 2at\alpha) \right) \right)$$

$$-\infty < x < \infty; -\infty < y < \infty; 0 < z$$

(4.8)

With z=0 the representation for the surface is reduced to:

$$T_{z=0}(x,y,t) = \frac{\alpha w^2 F_0}{\rho c_p} \frac{e^{at\alpha^2 - 2(x^2+y^2)/(8at+w^2)} erfc\left(\frac{\alpha}{\sqrt{\frac{1}{at}}} \right)}{8at + w^2}$$

(4.9)

The surface form gives sufficient information to calculate thermal patterns caused by scanning a pulsed laser beam, see Equation 4.9.

4.7.2　　Multiple pulses, same position

The temperature level stays relative long at a high value and the second pulse would increase the temperature even further.

By overlapping the pulses a relative low absorber as ABS can be heated to its thermal degradation temperature. Normally laser marking is a move of a pulsed laser beam across a surface. The velocity of the scan and the pulse frequency determines the distance between two pulses. If the distance is zero, the temperature distribution directly after (n+1) pulses of the same energy will be:

$$T_n(x,y,z) = \sum_{m=0}^{n} T(x,y,z,\frac{n-m}{f_Q}) \tag{4.10}$$

Where T *(x,y,z,(n-m)/f_Q)* is the temperature contribution from the mth pulse in a row of (n+1) pulses. The first pulse written in a row is pulse m=0. This can be simplified if the pulse frequency f_Q is high. For example a pulse train of 10 pulses at 100 kHz would result in a thermal diffusion length of the first pulse of 8 μm. The time between the pulses is for a 100 kHz 10 μs, see Table 3.2. The temperature caused by a train of n pulses can be written as:

$$T_n(x,y,z,t) = n \cdot T(x,y,z,t) \tag{4.11}$$

Which means for a limited quantity of pulses the temperature distribution is the sum of all different temperature distributions. This super position principle explains why a low absorber for example the ABS polymer can be marked using multiple pulses. A limited temperature rise of for example 15 degrees for a specific pulse will increase to 150 degrees for 10 of these pulses. At a frequency of 100 kHz this will only take 100 μs.

Important to note is that most polymers used for marking have additives. At higher intensities these additives can obtain very high temperatures resulting in local degradation and thus a chance in absorption. If the intensity is below this level a high pulse frequency (> 50 kHz) can be used to process polymers like a continuous laser beam. The sample shown in Figure 2.32 left is made with a pulse frequency of 50 kHz, 10 ns pulse width resulting in a foaming of the glass fiber filled PBT. In this case the pulse intensity was below the carbonization and ablation threshold of the material resulting in a foaming of the material.

4.7.3 Multiple pulses, distribution in xy plane, with diffusion between pulses

As larger patterns are marked some pulses have a considerable period in between. The assumption of no diffusion is in these cases not valid. The initial temperature distribution of the first pulse results in a diffused distribution just before the second pulse and forms together with the second pulse a new initial distribution. Because the heat equation is linear the principle of superposition of solutions can be used to describe the temperature just after the nth pulse where t=0 sec. :

$$T_n(x,y,z,t) = \sum_{m=0}^{n} T(x-x_m, y-y_m, z, t + \frac{n-m}{f_Q}) \tag{4.12}$$

Where the nth pulse is placed at position (x_m, y_m).
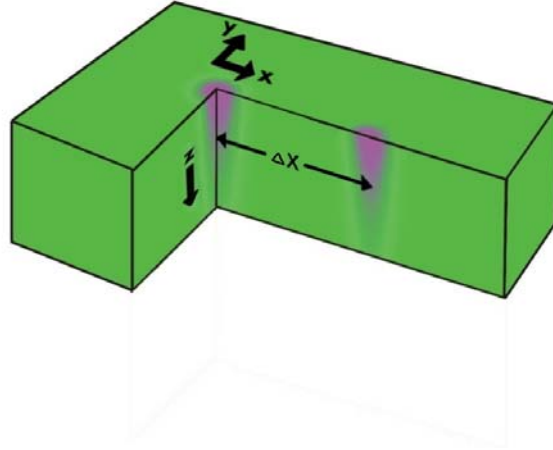
Figure 4.27: 3D view of temperature distribution for two pulses at (0,0) and (Δx,0).

Combined with 4.8 this result in the following solution:

$$
T(x,y,z,t) = \frac{\alpha w^2 F_0}{\rho c_p} \sum_{m=0}^{n} \frac{-1}{2(8a(t+\frac{n-m}{f_Q})+w^2)} \cdot e^{-z\alpha+a(t+\frac{n-m}{f_Q})\alpha^2 - 2((x-x_m)^2+(y-y_m)^2)/(8a(t+\frac{n-m}{f_Q})+w^2)}
$$

$$
\left(-2 + erfc\left(\frac{1}{2}\sqrt{\frac{1}{a(t+\frac{n-m}{f_Q})}}(z-2a(t+\frac{n-m}{f_Q})\alpha) \right) - e^{2z\alpha} erfc\left(\frac{1}{2}\sqrt{\frac{1}{a(t+\frac{n-m}{f_Q})}}(z+2a(t+\frac{n-m}{f_Q})\alpha) \right) \right)
$$

(4.13)

For polymers (low thermal diffusivity) the complementary error functions will tend to go to zero and can be disregarded introducing a small error, this will result in Equation 4.14.

$$
T(x,y,z,t) = \frac{\alpha w^2 F_0}{\rho c_p} \sum_{m=0}^{n} \frac{1}{8a\left(t+\frac{n-m}{f_Q}\right)+w^2} \cdot e^{-|z|\alpha + a\left(t+\frac{n-m}{f_Q}\right)\alpha^2 - \frac{2\left((x-x_m)^2+(y-y_m)^2\right)}{8a\left(t+\frac{n-m}{f_Q}\right)+w^2}}
$$

(4.14)

4.8 Cooling ratio between consecutive pulses

An important aspect of multiple pulses is the influence of the frequency and the distance between the first and second pulse. This can be made visible using the ratio between the temperature just after the first pulse (T_0) and the temperature after $1/f_Q$ seconds just before the second pulse (T_1). If the time between two pulses is short enough no energy is diffused into the bulk. The second pulse starts at a higher temperature and will end also at a higher temperature. This cumulative effect causes degradation of polymers even at low intensities.

The ratio can be calculated for the centre and surface of the pulse (x=y=z=0) using Equation 4.7 and Equation 4.8, see Equation 4.15.

$$\frac{T_1}{T_0} = \frac{e^{\frac{a\alpha^2}{f_Q}} f_Q w^2 erfc\left(\frac{\alpha}{\sqrt{\frac{f_Q}{a}}}\right)}{8a + f_Q w^2} \tag{4.15}$$

The ratio approaches one if f_Q becomes large. Figure 4.28 shows the cooling ratio for a 1064 nm pulse with a waist of 0.1 mm on ABS.
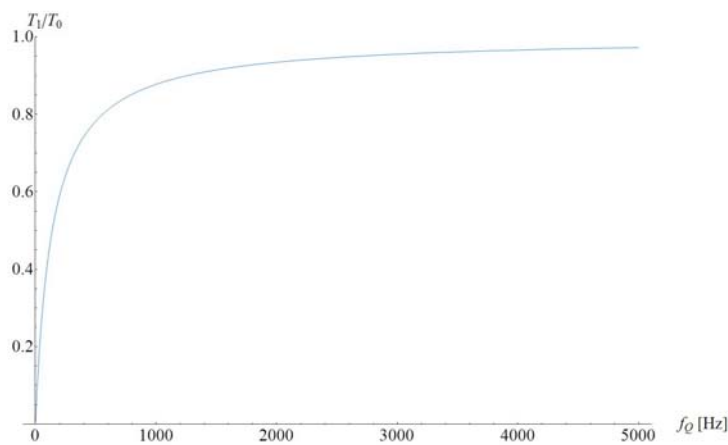
Figure 4.28: Cooling ratio between first and second pulse for ABS.

4.9 Thermal effects of scan strategies

Looking at laser marking results of filled areas the first thing that is noticed is the irregularity of the fillings. The different scan strategies yield different patterns. The pulses create a thermal distribution in the material which leads to a non-uniform heating. To make these temperature

differences visible the temperature just before the laser pulse is calculated. As the number of possible strategies is very large we limit the calculations to a few standard strategies using Equation 4.5 to calculate the temperature caused by a prior pulse placed at a known distance and time. Although the complete distribution is not calculated, the amount of calculation time is still considerable and to reduce the calculation time the structure is kept small. A 1mm square is filled with different strategies with a filling distance of 0.1 mm , marking speed 25 mm/s, jump speed 1000 mm/s, pulse frequency 10 kHz, pulse energy 0.1 mJ, spot size 100 μm, Fluency 0.0160 J/mm^2 and an absorption coefficient of 0.142 mm^{-1}. Figure 4.29, 4.31, 4.33 and 4.35 shows the result of the calculation whereas Figures 4.30, 4.32, 4.34 and 4.36 shows the marking results on PC. The carbonization of the PC adds a lot of extra energy. This is the reason why the temperature doesn't correspond to the degradation temperature of 300 °C. But the tendency shown by the calculation is visible. The contour filling from outside to inside shows the highest temperature in the calculation and also the widest line in the centre, see Figure 4.35 and 4.36.
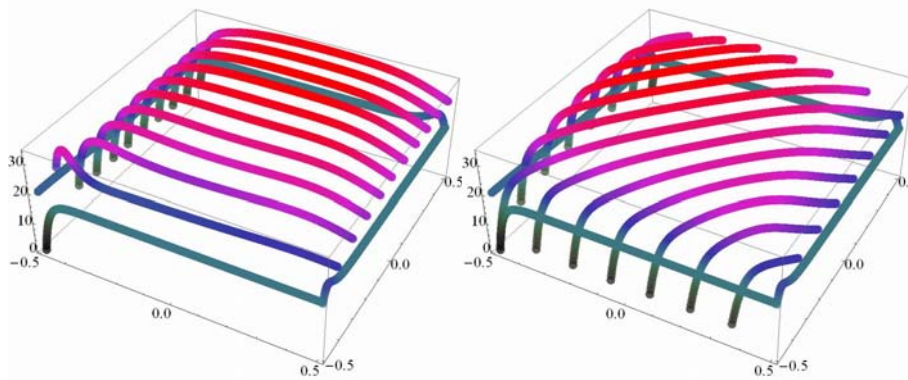
Figure 4.29: Unidirectional filling, material temperature change prior to laser spot at position. Left, 0 degrees (x direction). Right, 45 degrees.
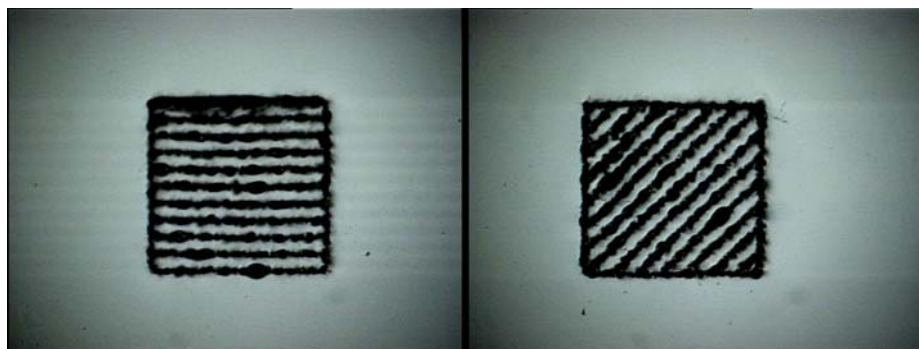
Figure 4.30: Unidirectional filling, PC (poly carbonate) marking results of filling to 1 mm square.
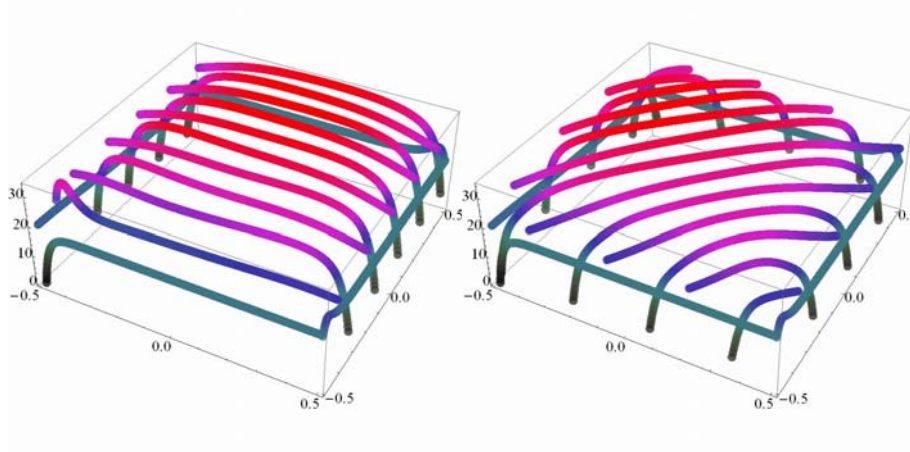
Figure 4.31: Bidirectional filling, material temperature change prior to laser spot at position. Left, 0 degrees (x direction). Right, 45 degrees.
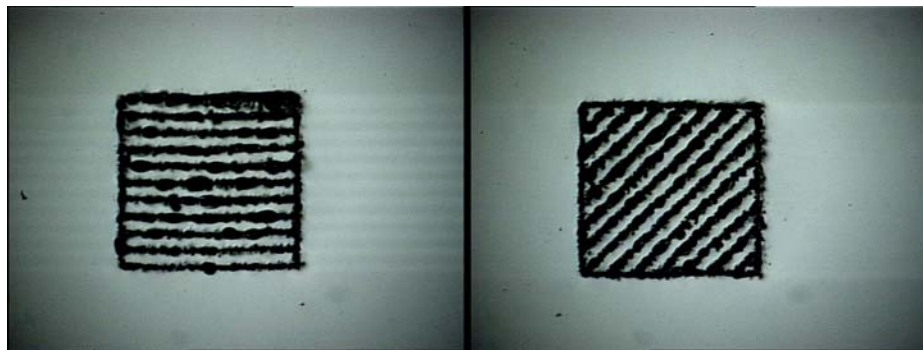
Figure 4.32: Bidirectional filling, PC (poly carbonate) marking results of filling to 1 mm square.
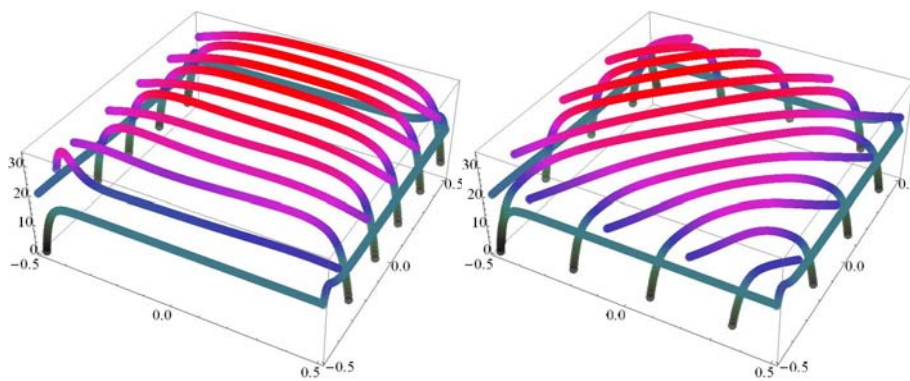
Figure 4.33: Meander filling, material temperature change prior to laser spot at position. Left, 0 degrees (x direction), Right, 45 degrees.
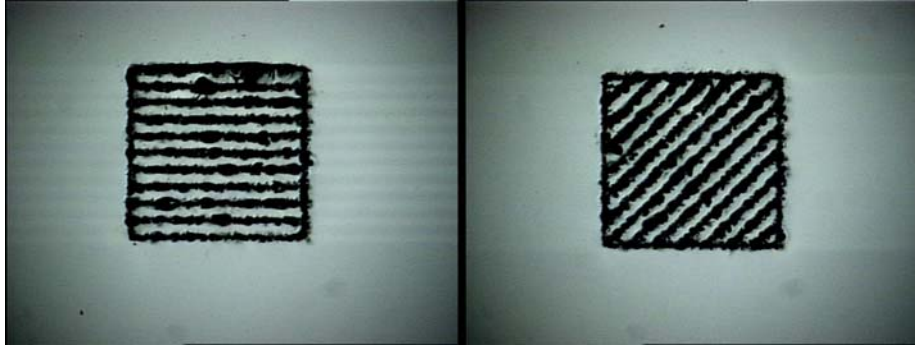
Figure 4.34: Meander filling, PC (poly carbonate) marking results of filling to 1 mm square.
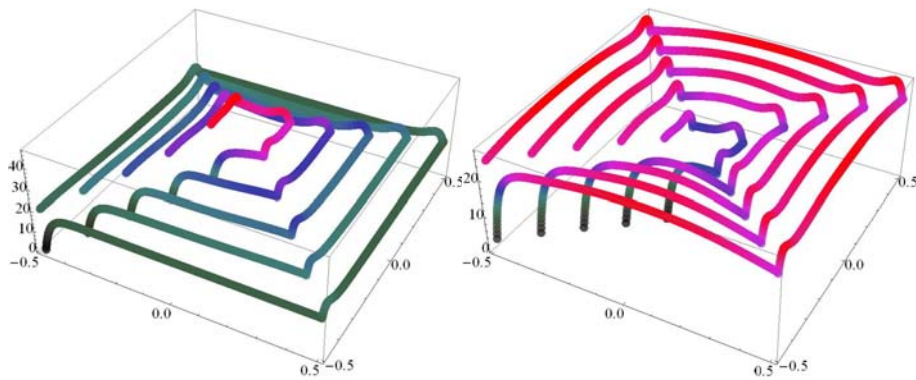
Figure 4.35: Contour filling, material temperature change prior to laser spot at position.
Left, from outside to inside, Right, from inside to outside.
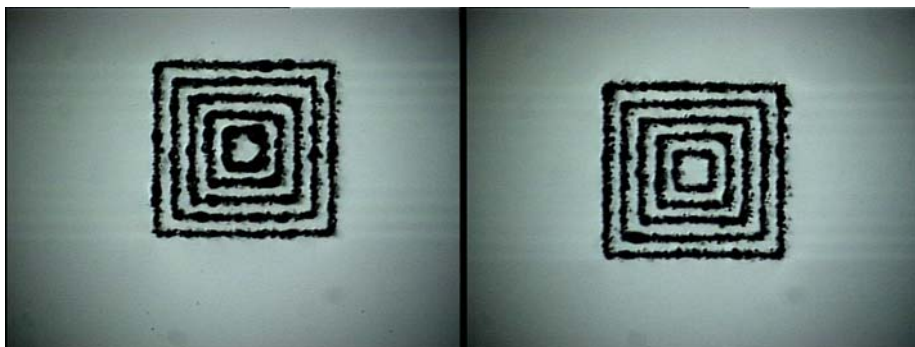
Figure 4.36: Contour filling, PC (poly carbonate) marking results of filling to 1 mm square.

4.10 Conclusions

Writing and fill strategies add extra dimensions to the polymer-marking process. In practice not all these strategies are used because of the lack of software that is able to analyze the complex patterns at a sufficient speed. And if there is enough time for this analysis, the different behavior of the polymers will sometimes be unpredictable because the chemical structure and additive packages are not revealed. All these things make it difficult to predict the exact result. This pre-processing is an extra tool to see how the strategy influences the marking. Being especially important for decoration applications. Filling a closed surface should also be done in one direction or from the inside to the outside. The energy has to be spread out, instead of concentrated with respect to time and position as it is done at the contour filling from the outside to the inside.

Chapter 5   Selection and experimental setups

5.1   Introduction

This chapter starts with the description of the basic elements of an engraving system. All experiments except the OPO experiments of Chapter 6 were carried out using standard engraving systems. Also a quick scan method for laser system evaluation is introduced based on the characteristics of Q-switching of solid state lasers.

5.2   Basic elements of a laser engraving system

All engraving systems used in industry consist of a laser combined with a beam expander, scanner, focussing optics and a control box with software. Some of the optical, mechanical and electrical interfaces of these elements are standardised. This makes it possible to change some of the elements without any structural change of the system. For example a scanner can be replaced from a different supplier if a bigger aperture or a faster scan speed is needed. Also the beam expander can be changed without problems, with the restriction that the beam diameter should fit the scanner aperture. A system supplier tries to optimize the components in such a way that a better performance is reached. Specific software and scanner cards are the result of this achievement. In a production environment multiple scanner software and scanners are not wanted. In a development situation different scanner software is also not ideal. A way out of this problem is the standardisation of the interfaces.

5.2.1   Scanner system, interfaces

The interface of the scanner to the PC card is described in the XY2-100 protocol. GSI-Lumonics has introduced it as an industry standard. When Scanlab started with their first system they adopted this scanner interface. That wasn't a major problem because some of the people came from General Scanning now GSI - Lumonics. For practical reasons also the lens diameter was copied. This enabled customers of General Scanning a smooth transition to Scanlab systems. Other scanner suppliers also use this XY2-100 protocol and even adopted the mechanical interface of Scanlab. The protocol is not an open standard but a Belgian company Rhothor published a complete technical datasheet (Rhothor 2007). The development regarding digital controlled scanners demand for a more advanced protocol. Some scanner companies like Arges and Scanlab already have it. These protocols are supplier specific and will not be published as an

open standard. For users an open standard will enable a more transparent integration and a faster development of new features because more suppliers can enter the market.
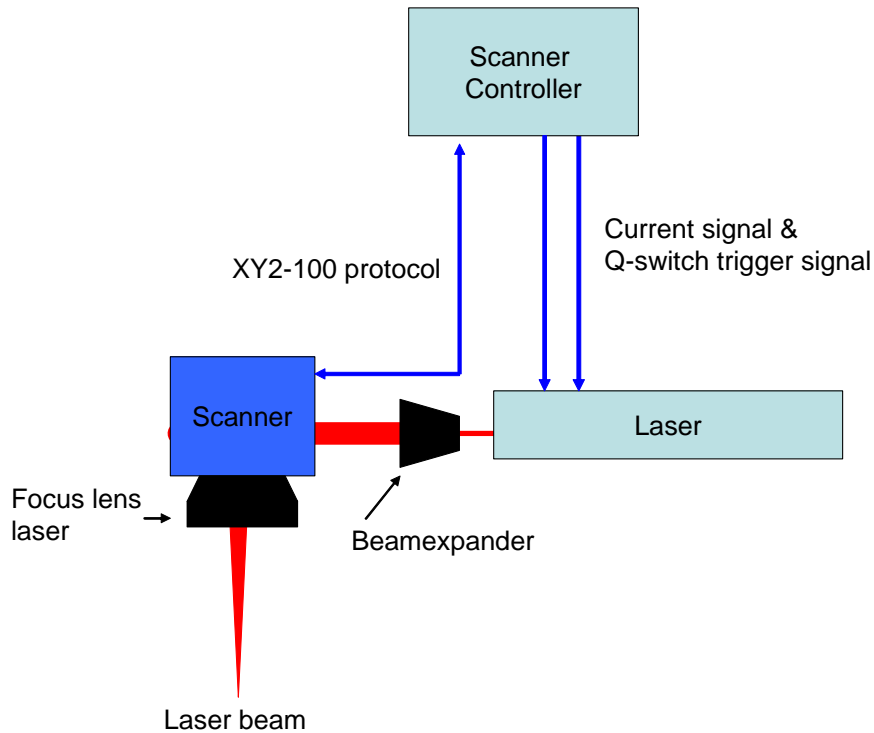
Figure 5.1: Standard elements of laser engraving system.

The mounting plate of the scanner is supplier dependent. An interface plate can be used to solve the differences. The mounting of the lens is for the standard 100, 160 and 256 mm the same and use a M85x1 thread. Smaller focal lengths use an adapter to be able to use the standard thread. Larger focal lengths can give problems with large mirrors inside the scanner. Every lens type should not only be calibrated for the scan dimensions but also for the distortion they introduce. Scanlab uses a 9 x 9 grid as a base to interpolate the compensation values. The deformation is caused by the lens design. A single mirror two axis scanner would make the lens design better adapted to the angle distribution of the laser scanner. In that case the laser comes from a single point and has a linear relation between displacement and angle of the mirror.

5.2.2   Beamexpander, interfaces

The beamexpander comes in different sizes and is used to match the laser beam diameter with the scanner aperture and reduce the divergence. It should be noted that also the lenses have their optimum optical aperture. A large aperture would result in large scanner mirrors and subsequently in a lower speed. But that could be compensated by a larger focal length resulting in a larger spot and lower accuracy. A larger spot could be effective if the laser has enough power. The best

approach is often to look at the application and determine the minimum and maximum acceptable spot size. From this a setup can be calculated choosing the right aperture for the scanner and optics. This beam diameter can be reached using a beamexpander. It should be checked if the laser can still deliver the threshold intensity at the maximum spot size.

5.2.3 Laser, interfaces

Solid state Q-switch laser have different supplier based interfaces. But often a simple opto-coupler circuit is enough to interface the laser with a TTL signal. The lamp or diode current is often voltage based. It becomes more complicated with systems that are free running. A free running Q-switch laser has its own internal clock. In these cases it is difficult to synchronise the scanner and the laser. A simple way is to accept the fact that the laser runs its own cause. Another more complex way is to let the scanner wait for a second start pulse from the laser clock. This will result in a constant time between laser pulse and scanner start.

5.3 Determination of basic laser/material interaction

First the effect of just one laser pulse has to be determined to get some idea of the basic laser/material interactions. These interactions are the combined result of wavelength and pulse characteristics of the laser.

In practice it is difficult to use a single pulse. Solid-state lasers have a first pulse with a different characteristic than the other pulses. The pulse energy of a pulse is directly related to the inversion prior to the pulse build-up. If the inversion of the first pulse is higher than the inversion of the second pulse a higher first pulse will be generated. This difference in inversion is caused by the different time available for the inversion build-up. If the inversion reaches its maximum between two pulses there is no first pulse problem. One way to eliminate the first pulse effect is to limit the pulse with a reduced Q-switch open time. This first pulse suppression is often standard in commercial Q-switch laser systems. Another less used system is to keep the laser running and to use a second Q-switch to modulate the laser outside the resonator. The latter system is used in lasers that have the tendency to destroy themselves with a high first pulse. These systems have extra possibilities like the selection of single pulses and the modulation of pulse energy without changing the system thermal load.

The second step is to use multiple pulses written in a line to see how the pulses interact with each other. After this depending on the application a third step determining the effect of a 2D array of pulses can be made. Step two and step three involve next to the laser characteristics also the effect of beam manipulation and the strategy of writing.

The main parameters of a laser pulse are the pulse-energy and the pulse-width. These two parameters can be measured for every pulsed-laser system. For solid-laser systems, and to a certain extent also for gas lasers, a dependence of the pulse form and its width exists. For every laser system the pulse has a distinct form that is determined by the gain and by the inversion prior to the pulse. The inversion is determined by the amount of optical pumping and the optical pumping time. This explains why a pulsed-laser operating at low frequencies and low diode or lamp current has the same pulse characteristics as the high-frequency pulse operating with a high diode or lamp current. The same amount of inversion is available prior to the pulse.

The pulse-energy, pulse-width curve can be used to display different types of pulsed systems in one graph. This overview can be used in the design of the laser experiments and choice of the best laser system.

Although the inversion prior to a pulse is the same, the total power needed to maintain this inversion for every pulse is different for every system. This power, or more the power lost during the conversion build-up, has to be removed. If the heat conduction is not effective thermal-lensing will start. The thermal-lensing changes the divergence of the laser beam through the non-uniform heating of the laser rod, resulting in a focus shift and an increase or decrease in spot intensity. The phenomenon will give different results for the same pulse-width, pulse-energy combination at different frequencies. The modern diode-pumped solid-state lasers are very efficient with their optical pumping, and the effect of thermal lensing is reduced to a minimum. The latter is due to the emission spectra of the diodes being closely matched to the absorption spectrum of the Neodynium. No additional thermal energy is generated in laser rod. This doesn't mean that a diode pumped solid state laser have no thermal problems. The heat generation is localised in the diodes. A cooling of the diodes is sufficient to keep the heat from the laser rod. The optical coupling with a fibre establishes an even better separation of the heat source and rod.

5.4   Selecting lasers

The selection of the best laser-engraving system for a process is time and money consuming if all available laser systems should be evaluated and tested. If systems become available at a later moment new tests are needed. In practice a pre-selection is made on the basis of service ability, past experience and reputation of the supplier. For this limited set of systems a more thorough evaluation is made. A method of classifying the laser systems prior to the laser design can be used to reduce the effort even further. If a process will run in different factories the need for a more uniform evaluation could reduces the total work. From experience the high priority for fast service and integration into the existing production environment will often result in different suppliers for different factories.

5.4.1   Pulse-energy vs. Pulse-width

Schildbach showed that for each Q-switch laser system there is a relation between pulse width (FWHH) and pulse energy (Schildbach 1990), see appendix B. More energy will result in a shorter pulse because the chance of hitting an excited state is larger when the inversion is high. This results in a fast build-up of the pulse, with a subsequence reduction of the pulse.

$$t_p = C_{laser} \cdot \frac{1}{E_p} \hspace{6cm} 5.1$$

With C_{laser} defined as:

$$C_{laser} = (\frac{1-R}{1-R+R_{loss}}) \cdot \frac{8h}{\lambda \cdot \sigma} \cdot A \cdot L \hspace{4cm} 5.2$$

where:

R *reflection out-coupling mirror*

R_{loss} *resonator losses.*

h *Planck's constant*

λ *wavelength*

σ *cross-section for radiative transition*

A *Transversal area in resonator*

L *optical length of the resonator*

The value of C_{laser} depends only weakly on the mirror transmission (1-R) as long as (1-R)$\gg R_{loss}$. Heating up the laser setup changes the resonator length L and a heating of the laser rod (thermal lensing) changes the transition area A. Both effects are often caused by a non optimal laser design and can be made visible using the laser constant C_{laser}. The change in C_{laser} can be used as an indicator of the thermal stability of the laser system.

5.4.2   Pulse energy – pulse width graph

The inverse pulse energy vs. pulse width graph can be used to select a limit set of combinations. As the graph shows ideally a line only a few experiments are necessary to show the laser capabilities. Some areas in the graph are not available because no laser system gives the desired combination.

The combination of pulse-width and pulse energy can be used to determine if a new laser system should be tested for new applications or if older systems already deliver the same combinations.

In order to show how well a laser behaves according to Equation 5.1 the x axis is set to $1/E_p$. This should result in a straight line. The Rofin 50D with the 2 mm aperture behaves well according to the Equation 5.1. The laser shows a completely different behaviour for the 1 mm aperture. The distribution is scattered showing a wider distribution, see Figure 5.2. The same resonator is used but with a different aperture. The resonator has been original designed for a larger aperture. The 1.0 mm aperture reduces the amount of possible modes. This changes the laser constant due to laser resonator losses caused by temperature changes in the laser rod.

The Vector mark is an end pumped system and shows over its power range less change in pulse length. The same system is also measured in the second harmonic version (532 nm). Figure 5.3 show the result of both versions. The reduction in pulse length is clearly visible in this graph. The conversion is done outside the cavity and the conversion efficiency depends on high intensities. Longer pulses are converted less efficient or not at all.
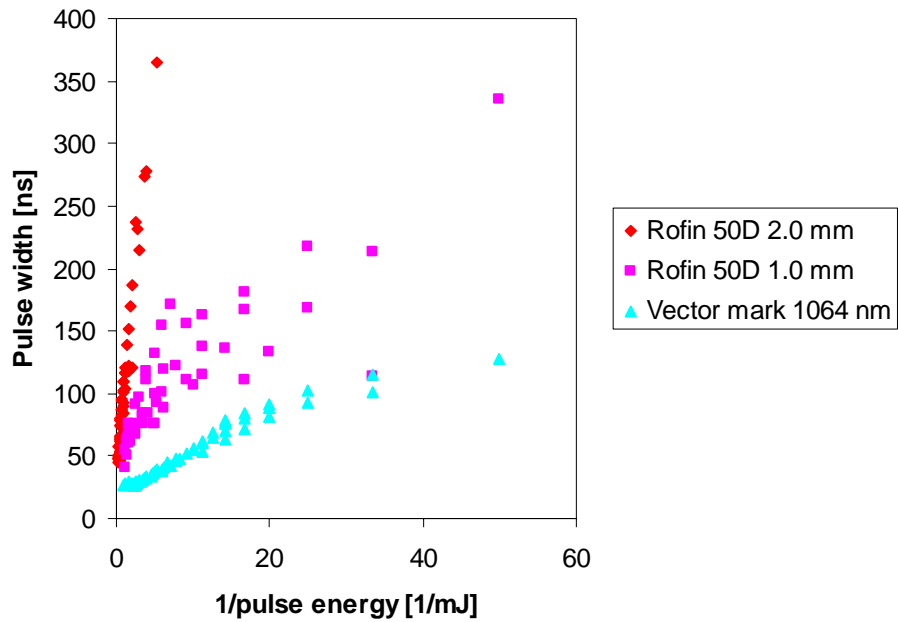
Figure 5.2: Laser pulse width vs. 1 / pulse length graph.
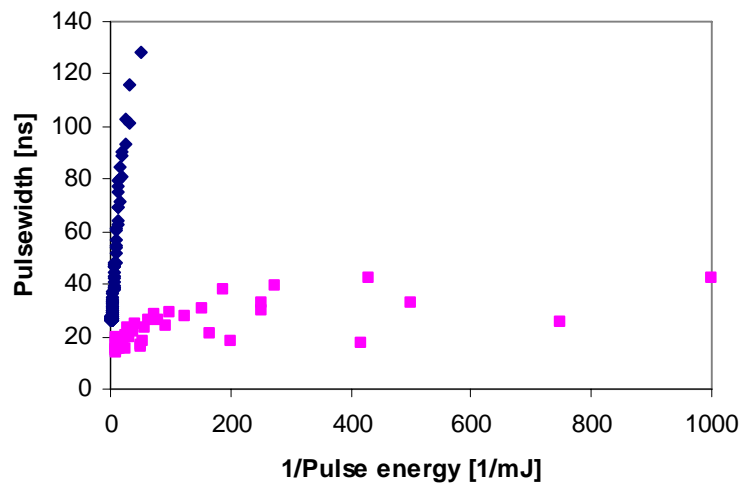
Figure 5.3: Laser pulse width vs. 1 / pulse length graph
Vectormark 1064 nm and 532 nm.

5.5   Standard test, process parameters

The best way to look for process thresholds is to use an attenuator. For linear polarised lasers this can easily be done by rotating the polarisation plane with a half lambda or half wave plate. A polarizing cube beam-splitter rejects one polarisation plane and this plane exits the cube at a different angle. The non rejected plane is passed though the prism. The rotation with the half wave plate changes the attenuation without changing the stability and beam quality. After this the linear polarised beam is changed to circularly polarise with a quarter wave plate.

Often a matrix of Q-switch frequencies and diode/lamp currents is made to search for process settings. From this a suitable setting is chosen and used for production. The boundaries of the process or process window are still unknown. This could result in production failure or yield problems. In order to get the boundaries more visible a standard setup should be made on process parameters instead of machine parameters. From the pulse energy and pulse width measurements pairs can be chosen and used to see how much power is necessary $((e_p, t_p) \rightarrow (I, Q))$. Some processes are governed by the intensity (ablation) others by average power (melting). In the latter case a setup with respect to Q-switch time and scan speed should be made where for the ablation case only intensity is sufficient. By searching for the lower and upper threshold of a process the process window becomes clear, see Figure 5.4. From this also an estimation of the production window can be made because production has always a time constraint. This results in a process capability for the tested system for the production process. If this is done for different systems, a ranking can be made.

It should be mentioned that from a production point of view, aspects as service ability, cost of ownership, maintenance time, initial investment and service organisation are also important.
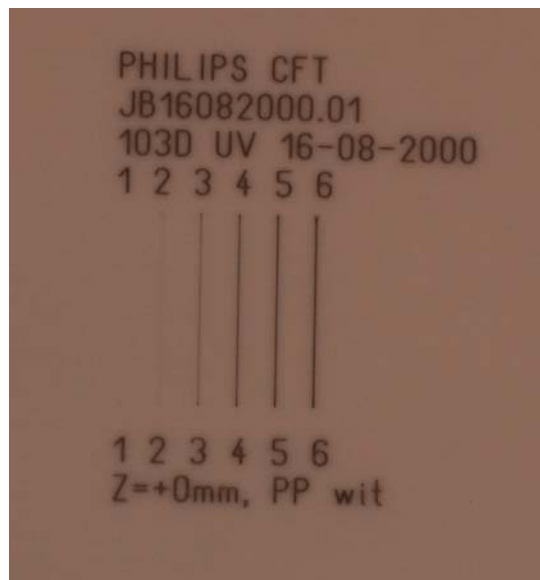
Figure 5.4: Standard test for process parameter threshold based on prior measurements of laser system, f_Q 10 kHz.
1. 5 μJ, 2. 14.5 μJ, 3. 22.5 μJ, 4. 31 μJ, 5. 38.5 μJ, 6. 46.7 μJ.

5.6   Experimental setups

The bleaching experiments of Chapter 6 were carried out using a Spectra Physics MOPO 700 system. This is the only non-industrial laser system that was used during this thesis. The other experiments in this thesis were done with industrial systems. Industrial means that the systems are stable and have predictable and low service needs under industrial conditions.

5.6.1   Optical Parametric Oscillator system

MOPO 700 BROAD BAND OPO SYSTEM

The MOPO 700 is a Master Oscillator Parametric Oscillator. The Master oscillator is designed to oscillate mainly the signal wavelength. The MOPO is pumped by a 3rd harmonic GCR-100-30 Hz pump laser. This system is seeded to avoid unnecessary damage due to the longitude mode structure. The MOPO generates two wavelengths one the idler wavelength and a second the signal wavelength. By generating a photon with a lower level of energy (higher wavelength) by dividing the original photon, the difference is used to generate the second wavelength. This is also a longer wavelength because of energy conversion. For example at an idler wavelength of 735 nm the signal wavelength is 690 nm. If the signal is 423 nm the idler should be 2200 nm. The OPO system has a relative low fixed frequency of 30 Hz. This makes a XY axis setup with the lens and the Z axis fast and flexible enough.

Table 5.1: Spectra Physics MOPO700.

MOPO-700	Specs.
Signal range	410 nm – 960 nm
Idler range	735 nm – 2200 nm
Pump laser	Nd:YAG
Pump wavelength	355 nm
Pulse frequency	30 Hz
Pulse width pump	10 ns
Pulse width OPO	8 ns

5.6.2   Diode pumped Q-switch solid state lasers

Although a lot of systems were tested in the past years only a few were purchased or used for marking projects. We used mainly Rofin-Baasel systems. During the development of the diode pumped laser systems we were able to have the newest developments. While others were still under development and not available.

Table 5.2: Diode pumped Q-switch solid state laser Rofin-Baasel.

	103D	103D UV	50D	Eline 10E
type	Nd:Vanadate	Nd:Vanadate	Nd:YAG	Nd:Vanadate
Wavelength	1064 nm	355 nm	1064 nm	1064 nm
M^2	1.2	1.2	$1.1 - 2$	1.1
Power	3 W	1 W	50W	7W
Pulse length	9 ns	8 ns	70-90 ns	10 ns
Max. pulse power		48 µJ		
Frequency	10-100 kHz	10-100 kHz	1-80 kHz	10-100 kHz

5.6.3　　Passive Q-switch solid state

The dual chip laser from nanolase only produced 50 mW in the UV (355 nm). But if focused to a small focus the intensity was enough for marking TiO_2, see Chapter 7. The frequency was fixed due to a saturable absorber Q-switch.

Table 5.3: Nanolase, laser specifications.

Laser	Wavelength [nm]	Average power [W]	Pulse length [ns]	Pulse energy [µJ]	Q Frequencies [Hz]
dual chip	351 nm	50 mW	1 ns	0.8 µJ	63 kHz

5.7　Conclusion

Although the inverse pulse width - pulse length graph is a simplification it has been effectively used to get an overview of multiple laser systems.

The main advantage of the use of the inverse pulse width / pulse length graph is that experiments done with one laser type can be used to estimate in what kind of way another and similar laser (with respect to pulse energy and pulse width) will perform. Some lasers will be considered promising and should be added to the chart. This enables the use of former collected data for new process designs. With respect to the standard relation of inversion and pulse characteristics for a Q-switched system, each new laser can be categorised easily.

Chapter 6 Multi colour laser marking by selective bleaching of pigments

6.1 Introduction to multi colour laser marking

In 1987 Hofmann of Ciba Geigy (now Novartis) showed the possibility of a high contrast and intact surface for laser marking of plastics. By changing the laser wavelength different markings were made introducing the first multi colour laser marking (Hofmann, Sykes et al. 1987).

The change of wavelength and the short pulse width of less than 10 ns resulted during the Brite Euram projects Licopal (BE90-4441) and Syladec (BE96-3503) in the first multi colour mark using three contact masks to bleach the three different pigments in the lacquer, see Figure 6.1.

Figure 6.1: First multi colour laser mark three-wavelength bleaching
[3rd harmonic pumped OPO].

The ideal state is that the pigment not only loses its colour but also has the same refractive index as the polymer matrix. Otherwise the pigment starts to act as a diffuser.

An alternative to selective bleaching is selective thermal degradation. The process of heat generated laser polymer colour-marking was used by Azuma. He used pigments with crystal water and a TEA CO_2 laser for colour-marking (Azuma and Sakaki 1987). Due to the heating

induced by the TEA CO_2, the crystal water is removed from the crystal structure. This changes the colour of the inorganic compound. In some combinations this is irreversible. The thermal load on the pigment during laser processing can be used to evaporate and degrade it. Pigments have their own specific thermal breakdown temperatures. The difference in thermal resistance of the pigments can be used to create multiple colours. A sample of a multiple colour mark made using selective thermal stability is the sample shown in Figure 2.33.

6.2   Selective laser bleaching of pigments

Hofmann identified a short pulse length as an important parameter. All successful markings he made were with lasers with a pulse length of less than 10 ns. Hofmann also showed that the matrices containing the pigments to be bleached have an influence on the effectiveness of the laser bleaching. The term bleaching describes the loss of colour due to exposure to light, but bleaching is not the only process resulting from light exposure. Also fragmentation and colour shift were observed during laser exposure. Fragmentation first increases the colour strength to a maximum. If the particle size is further reduced, the colour strength will be reduced or completely lost when the size becomes less than the visible wavelength area. Laser exposure can also promote chemical processes like photo-oxidation altering the colour and colour strength of a pigment.

The high intensity of a pulsed laser combined with the low average power limits the effect of the exposure to the absorbing pigment particles leaving the matrix unaffected. If the intensity becomes too high gas forming would result in an ablation of the matrix. If the average power is increased or too much energy is accumulated in a limited volume degradation of the matrix is initiated resulting in a dark mark or foaming of the matrix. Degradation, ablation and foaming are unwanted processes during multi-colour laser marking because the surface is destroyed. The destruction of the surface would reduce the chemical and abrasion resistance.

All these unwanted processes define the boundaries of the process area of laser bleaching. The different chemical and crystal structures of the pigments result in different process windows. This opens the way to selective laser bleaching. If there are wavelength and intensity combinations where only one pigment is bleached and others are unaffected, multi laser marking would be possible. This chapter will not go further into the depth of the chemical aspects of bleaching, but will deal with the aspects and usefulness of multi laser colour marking.

6.3   Creating colours

There are two different systems to make colours: subtractive and additive (see appendix D). The additive system can be demonstrated by three light sources. One is green, the others are blue and red. These colour sources when mixed together give the perception of white. White can also be made by mixing yellow and blue as used in white leds. This colour system is used in displays and led based lighting systems. The different sources of radiation are mixed to form one new source. If a red, a green, and a blue pigment are added into a polymer matrix it does not look white at all. A dark brown, purple or grey will be the result. The reason why this is not white, although a pigment can be seen, as a source of red, green, or blue light is that pigments absorb light. They

are not independent light-sources. The pigment absorbs one part of the visible spectrum and reflects, transmits and scatters another part. This is the reason why a mix of red, green and blue pigments doesn't look white. At least some 2/3rd is absorbed, resulting in a darker colour. By adding pigments to a polymer part of the spectrum is subtracted. Another example of the subtractive system is inkjet. It starts with a white paper and the inks are used as filters, they absorb a small part of the visible spectrum. The light passes twice through these filters and the spectrum is altered according the combination of filters. If these filters are constructed as Cyan, Magenta, and Yellow, all visible light can be filtered out creating black. It is difficult to get complete black because inks are usually not exactly Cyan, Magenta, or Yellow. Small colour deviations and scattering make the black turn into brown. This is next to speed consideration the reason why ink-jet systems often use black as a fourth colour. The use of pigments restricts the filter effect considerable. Filters are normally constructed using dye molecules having a much higher transmission than pigments.

6.4 Absorption and scattering, pigments in a polymer matrix

The absorption and scattering of an incident wave by a particle depends on its size. In case of particles much bigger than the wavelength, geometric optics would be sufficient to describe the scattering and absorption. If the particles are much smaller compared to the wavelength the much simpler Rayleigh approximation can be used. The intermediate area where the particle size is of the same order as the wavelength the Maxwell equations have to be solved for the geometry, electrical and magnetic properties of the particle and suspending matrix. Mie introduced in 1908 his solution of the Maxwell equations for an isotropic-homogenous sphere. The Mie theory describes both the scattering and absorption of pigments suspended in a polymeric medium. The diameter of commercial pigments ranges from 0.1 μm to 0.5 μm. It should be noted that not all pigments are sphere like and isotropic. To determine if the Mie solution should be used the Mie parameter, ξ (6.1) is introduced. For pigments this Mie parameter ranges from 0.09 to 1.1 for the wavelength range of 450 nm to 1064 nm. For situations where the Mie parameter is much smaller than 1 the Rayleigh approximation can be used (Hulst 1957).

$$\xi = \frac{2\pi r}{\lambda} \tag{6.1}$$

Using the Mie scattering solution with respect to the far field, the scatter and absorption cross sections of a pigment can be calculated as a function of the wavelength, using the particle size and the complex refractive index of both pigment and polymer. In Section 6.5 Mie absorption is used to show how a pigment particle absorbs light.

To come from the individual scattering properties of a pigment particle to a bulk value a multiple scattering model is used. Kulbelka-Munk is one of the simplest models but there are many other each with a specific application field.

6.5   Internal absorption of laser light by pigments in a polymer matrix

While the absorption cross section is used to describe the amount of energy absorbed by the particle the remaining unknown is the energy distribution inside the particle. Figure 6.3 shows the internal absorption intensity calculated using the MIE absorption algorithm of August Miller (Miller 2006) for a 0.4 µm pigment particle using the pigment data as supplied by Hofmann for irgazin yellow embedded in PC. The laser is not only absorbed at the laser illuminated side but also at the backside. The light wraps around the particle. The middle of the particle has the lowest intensity.
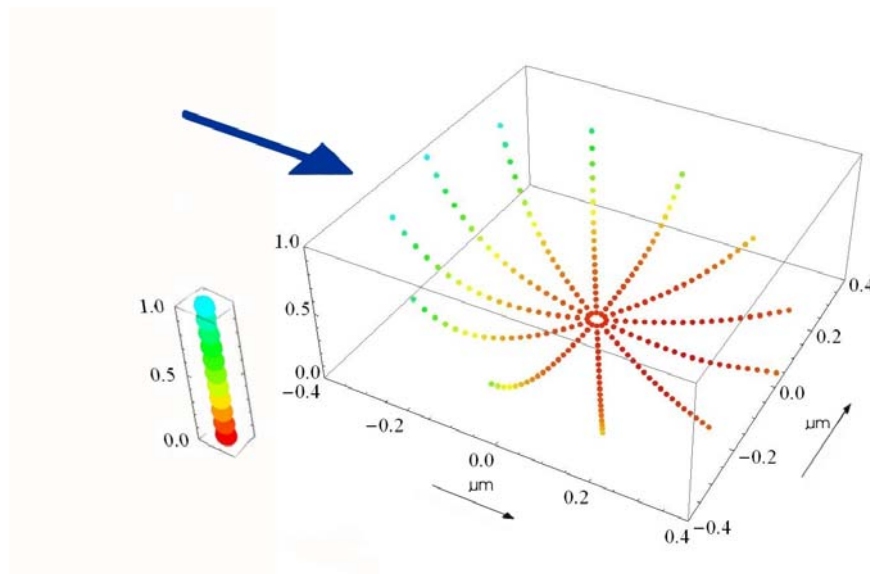
Figure 6.2: Internal absorption graph, normalised intensity (z-axis) vs. x,y with respect to centre and light direction (blue arrow) (0.8 µm diameter spherical particle with refractive index of irgazin Yellow at 1064 nm in PC (calculated with MIE Tab, (Miller 2006)). Intensity is normalised to the incident intensity of the incoming field.

Hofmann (Ciba) used a heat balance to show the high temperatures generated by the absorption of laser light by small particles embedded in a polymer matrix with the assumptions: isolated cubic particle, 100% surface absorption and thermal conductivity of the particle larger than the thermal conductivity of the matrix. (Hofmann, Sykes et al. 1987). The model of Hofmann predicted high temperatures for small particles and low temperatures for larger particles and use Lamberts law to calculate the energy directly after the laser pulse. The model predicted high temperatures for small particles and low temperatures for larger particles.

The time needed to diffuse into the particle can be expressed as $\tau = r^2/4a$. For a 0.1 µm particle this will take about 3.8 ns and for a 0.5 µm 91 ns (ABS thermal diffusivity). In case of a 10 ns pulse width diffusion during the pulse should be included in the model, see Table 6.1.

Table 6.1: Thermal diffusion time with respect to particle size.

	Thermal diffusivity a [m²/s]	Particle diam. [μm]	Thermal diffusion time
ABS	$171.9 \ 10^{-9}$	0.1	3.8 ns
		0.5	91 ns
Aluminium	$9.75 \ 10^{-5}$	0.1	0.007 ns
		0.5	0.15 ns
Carbon (graphite)	$1.0 \ 10^{-6}$	0.1	0.6 ns
		0.5	15.6 ns

This means that the assumption made in Section 3.7.2 is also valid for a pigment particle.

6.6 Qualitative colour balance model of multi-colour laser-marking

If a mixture of three pigments in a matrix is bleached by a laser with a wavelength λ_1 the result will be a change in pigment concentrations. If we assume that in the ideal case a laser bleached pigment becomes completely transparent the bleaching would change the balance between the pigments. Bleaching one would increase the visibility of the other pigments. This means that the bleaching stops when the non-bleached pigments hide the bleachable ones. This would open up a route to multi-colour laser marking. After sufficient exposure the desired colour would become visible, see Figure 6.3.
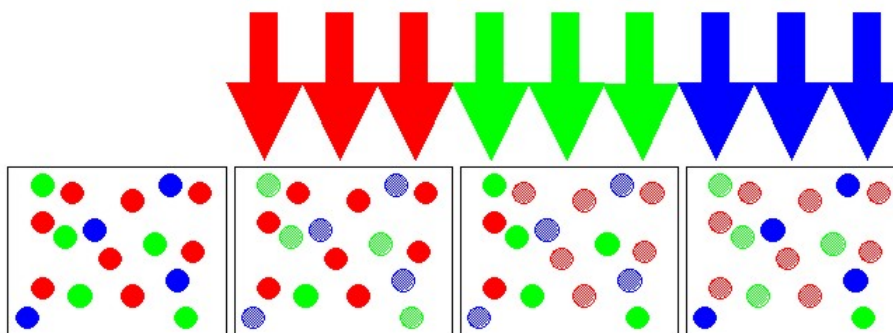
Figure 6.3: Bleaching for multi-colour laser marking using a red, green and blue laser light, red laser light bleaching all but the red pigments (three pigments semi-transparent is bleached).

Even in this ideal case some bleachable pigments remain intact because they are blocked by a non bleachable pigment. These pigments do have an effect on the final colour. Each pigment particle has a chance of surviving the bleaching while hidden by a non-bleachable pigment. This chance

increases with depth, concentration of the non-bleachable pigments and the relative size of the pigments. But decreases with bleachable pigment size and concentration.

In case the pigments are not ideal, meaning the refractive index changes or the colour loss is not complete, pure colours won't be possible. This means that part of the original pigments is chanced into a new pigment. The total colour will be the result of the original remaining pigments (reduced concentration) and the bleached pigments (increased concentration).

6.7   Monte-Carlo modelling of multi-colour laser-marking

In the model, a slice of the product is divided in an area consisting of cube cells with equal volume. Each cube is assumed to contain one pigment. In order to limit the number of calculations and the total size of the data the calculation is performed with a 50 by 50 array of such cubes. In order to make the calculation relevant for an infinite area the assumption was made that the area is periodically extended. The colour pigments are assumed to be of three types Cyan Magenta and Yellow. The cyan pigment absorbs red light, the magenta pigment absorbs green light and a yellow pigment absorbs the blue wavelengths. The pigments are randomly distributed over the cells (see Figure 6.4). To be able to say something about the penetration depth the 50 x 50 x 1 cell structure was also extended into depth by 19 extra layers. To extend the model a non-absorbing scattering white pigment is introduced. To calculate the scattering different distributions can be assumed. Given the cell structure of the model a photon can be reflected into 26 neighbouring cells, assuming a hit rate of 100%. It is possible to reduce or increase this hit rate for a specific wavelength to test the effect of the pigment absorption cross-section and side band absorption. To avoid too much complexity the hitting probability is set equal for the absorption and scattering. The volume is assumed to be an infinite slab of material. The bleaching model used assumes a full bleaching after absorption without refractive index change.
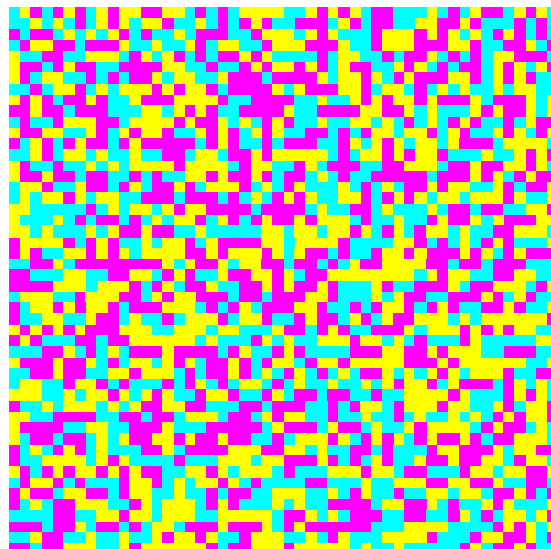

Figure 6.4: Cyan magenta and yellow pigment mix in 50 x 50 x 1 cell array (1:1:1).

The scattering is modelled using a probability function for direction i (6.8). With α_{inout} the angle between the incoming ray and the outgoing ray. The rays are used only as directions and have the same origin (centre of the cell).

$$Cos(\alpha_{inout}) = \frac{d_{in} \bullet d_{out}}{|d_{in}| \cdot |d_{out}|} \tag{6.2}$$

$$P_{chance} = \frac{1 + \beta \cdot Cos(\alpha_{inout})}{\sum_{26} (1 + \beta \cdot Cos(\alpha_{inout}))} \tag{6.3}$$

The chance of a direction is calculated using Equation 6.3. There are three standard situations: first, isotropic, every direction has the same chance ($\beta = 0$) second, backward scattering, angles larger than ½π have a higher chance because the $Cos(\alpha_{inout})$ for these angles is negative ($\beta = -1$) and third forward scattering, angles smaller than ½π have a higher chance because of $\beta = 1$. In case of the simulation only 26 directions are possible (n=26). This sum is two times 9 directions and 8 directions in the cell plane.

The area of cells is probed by multiple non bleaching beams in order to calculate the reflection percentage at different wavelengths. This can be done after each laser bleaching. The complete 50 x 50 surface area is hit by a laser beam.

6.7.1 Single pigment case

The calculated volume is 50 x 50 x 20 cells. Five different situations before bleaching were calculated (see Table 6.2). The complete backward scattering causes only reflection and no transmission. Penetration depth in this case becomes 0.5 cells. The isotropic scattering still has a transmission after 20 cells of 5%.

Table 6.2: Reflection of Magenta pigment before laser bleaching for blue and red wavelength.

	Reflection	Transmission (20 cells)	Average cell penetration depth
Only backward scattering	100%	0%	0.5
Backward scattering ($\beta = -1$)	98%	2%	1.8
Isotropic scattering ($\beta = 0$)	95%	5%	2.9
Forward scattering ($\beta = 1$)	90%	10%	5.1
No scattering	0%	100%	-

If side band absorption of 10% is assumed the reflection and transmission reduces significantly. Side band absorption is the absorption of a pigment at it highest peak of reflection. All industrial pigments have side band absorption. This means that even when a red pigment should reflect red light 10% of the incoming red light is still lost due to absorption. This has such an effect that only the "no scattering" case has some transmission after 20 cells.

Table 6.3: Reflection of Magenta pigment before laser bleaching with 10% side band absorption
in the blue and red wavelength.

	Reflection	Transmission (20 cells)	Average cell penetration depth
Only backward scattering	90%	0%	0.5
Backward scattering (β = -1)	70%	0%	0.9
Isotropic scattering (β =0)	57%	0%	1.5
Forward scattering (β = 1)	41%	0%	2.3
No scattering	0%	12.6%	8.3

The bleaching in the single pigment case causes for this model an increase in average cell penetration depth and transmission. Also the total reflection is decreased. If the volume is infinite in depth the reflection (with no side band absorption) would be the same as in the non bleached case. Thus to see bleaching a contrast pigment is needed.

6.7.2　　　　Three pigment case

The case without side-band absorption and backward scattering resulted after 5 green laser pulses with a full hitting chance in a 98% reflection for the green wavelength. For the blue and red wavelength this resulted in a 52% reflection.

For isotropic (β=0) the result after 5 green pulses was 73% reflection at the green wavelength and 18% for the blue and red wavelengths.

Adding white to the mixture at a ratio of 1:1:1:0.1 the reflection after 5 pulses increased to 78% at the green and to 29% in the red and blue wavelength. So the colour contrast does not increase because the background also increases the reflection from 33% to 39%. The contrast decreases slightly because of the white pigment.

If sideband absorption is introduced without white pigment the reflection at the green wavelength is reduced to 43% (isotropic, 10% bleach chance of cyan and yellow pigments, 5 green laser pulses). The reflection in red and blue reduces to 17%.

Table 6.4: Reflection after 5 green laser pulses.

	Backward scattering	Isotropic (β=0)	White pigment (C:M:Y:White =1:1:1:0.1)	Sideband 10%
Green Initial	66%	33%	39%	27%
After 5 laser pulses	98%	73%	78%	43%
Blue/red Initial	66%	33%	39%	31%
After 5 laser pulses	52%	18%	29%	17%
Change in reflection % green - red/blue	46%	55%	49%	26%

The model calculations showed that a maximum change in reflection after 5 pulses of 55% can be obtained if the bleaching is assumed to be optimal and isotropic. This means no absorption, scattering and sideband absorption. If a realistic value of 10% is assumed the change in reflection reduces to 26% for optimal bleaching. Addition of a white pigment gives a change in reflection of 49%.

6.8 Multi-colour laser- marking on ABS

6.8.1 Process Sheet

The aim of the process sheet is to show the process area with regard to wavelength and pulse intensity. The energy distribution of the MOPO 700 is not exactly known because of the optical parametric oscillator that was used to generate the different wavelengths, see Section 5.6.1. The distribution of the laser beam has a Gaussian shape. Due to the subsequent non-linear processes the laser beam is not circular anymore. By introducing an aperture into the beam the size is clipped to a circular shape. After this aperture a top-hat distribution is assumed to calculate the average intensity. Because of the large range of the fluency from a focused to a defocused beam, a logarithmic scale was introduced for the process sheet. The average laser energy was measured before and after the experiments.

6.8.2 ABS

The process sheet of normal ABS (ABS FG-50, DSM) is a simple one. Only carbonisation was observed. Because no overlap was used also no melting or foaming was observed. The reason why overlap wasn't used is that the absorption of the polymer changes after one laser pulse, the process initiated by a second overlapping pulse differs from the first. Because of this the laser effect will be accelerated using an overlap in pulses. This acceleration can also be observed during long pulse laser processing (120 ns). In the process sheet shown in Figure 6.4, carbonisation is indicated as a grey area. The crosses and dots correspond with the focal positions of the lens (KBX 064 BK7 glass focal length 100 mm @ 632.8 nm). The fluencies for the different focal position are compensated with respect to the wavelength using the refractive index of BK7.
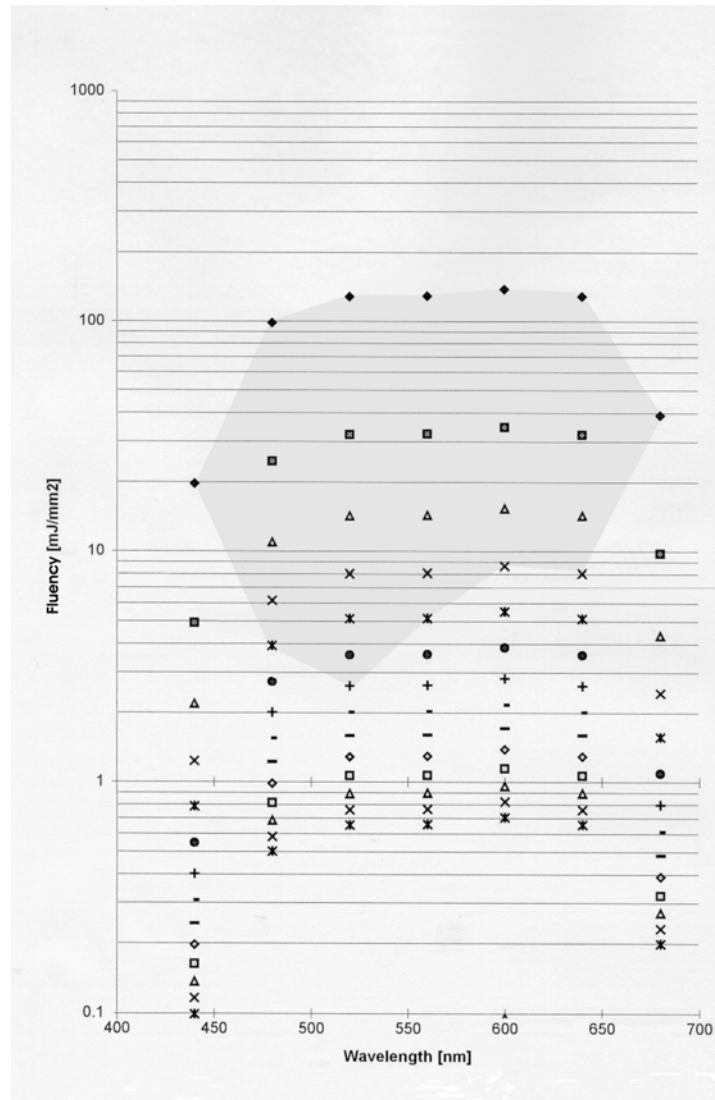
Figure 6.5: Process sheet ABS.
grey area = carbonisation (MOPO 700, t_p 4 – 5 ns / pulse, single pulse and no overlap).

6.8.3 ABS with one pigment

The pigment changes the absorption of the ABS. If a bleachable pigment is used there is an area in the process sheet that shows a loss of colour, so the colour of the matrix becomes more visible. Carbonisation can also be found, but at lower intensities than for non pigmented ABS (FG-50, DSM). The cinquasia magenta RT-235 D pigment does not bleach at all but changes it colours to dark blue. This colour change occurs only at wavelengths from 520nm to 600nm. A small area

shows carbonisation (middle) and bleaching in the same pulse. The intensity in the centre of the laser spot is higher than at the edges of the spot.
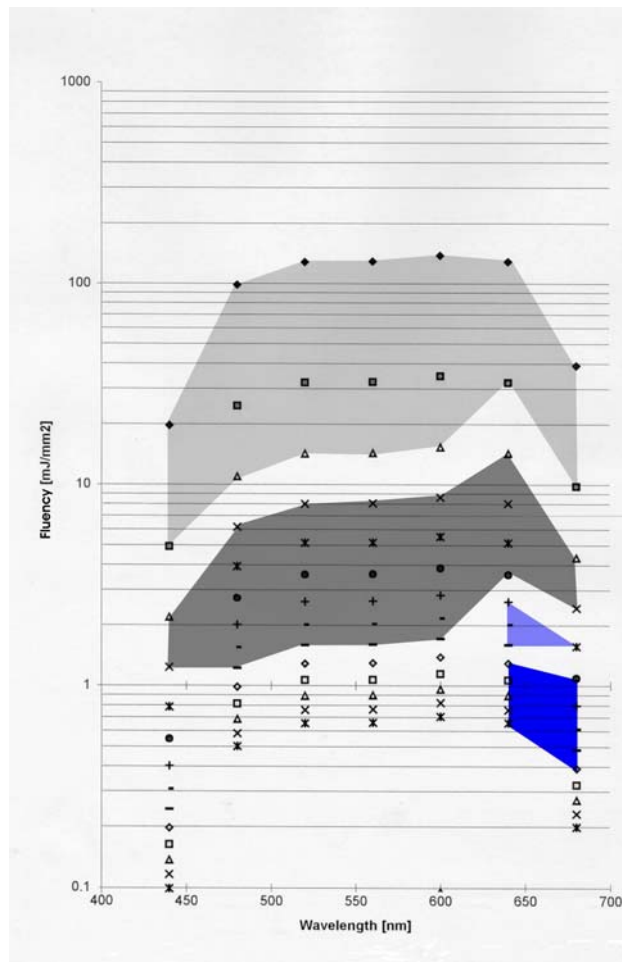

Figure 6.6: Process sheet ABS + cromophtal blue 4GNP.
Light grey white appearance (foaming)   Dark grey=carbonisation
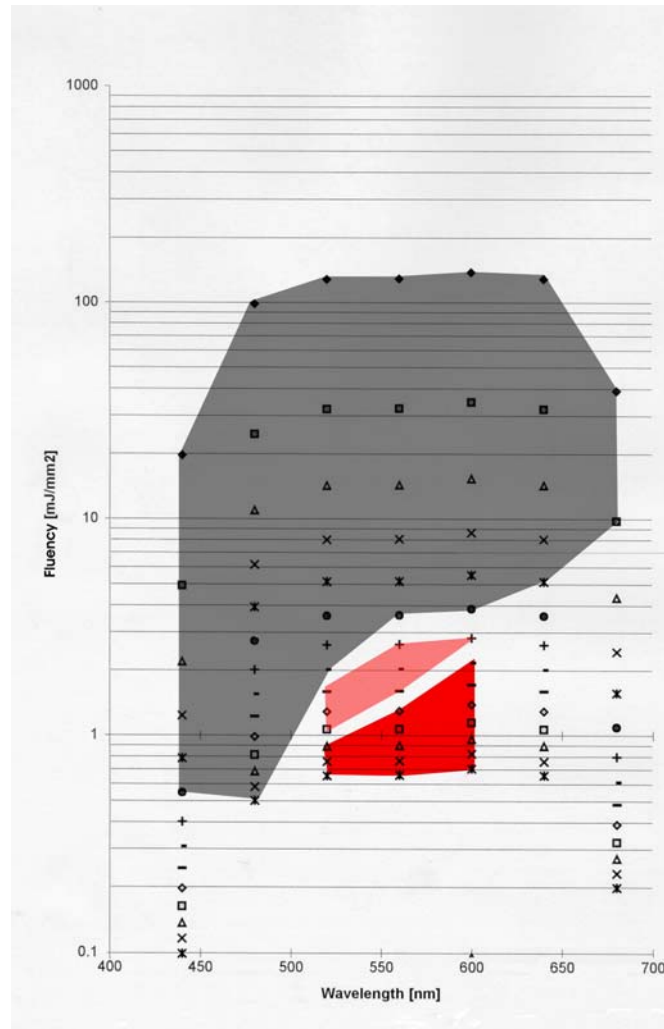*Blue=bleaching   Light blue=bleaching + carbonisation*

Figure 6.7: Process sheet ABS + cinquasia magentaRT235D.
Dark grey=carbonisation   Red=colour change
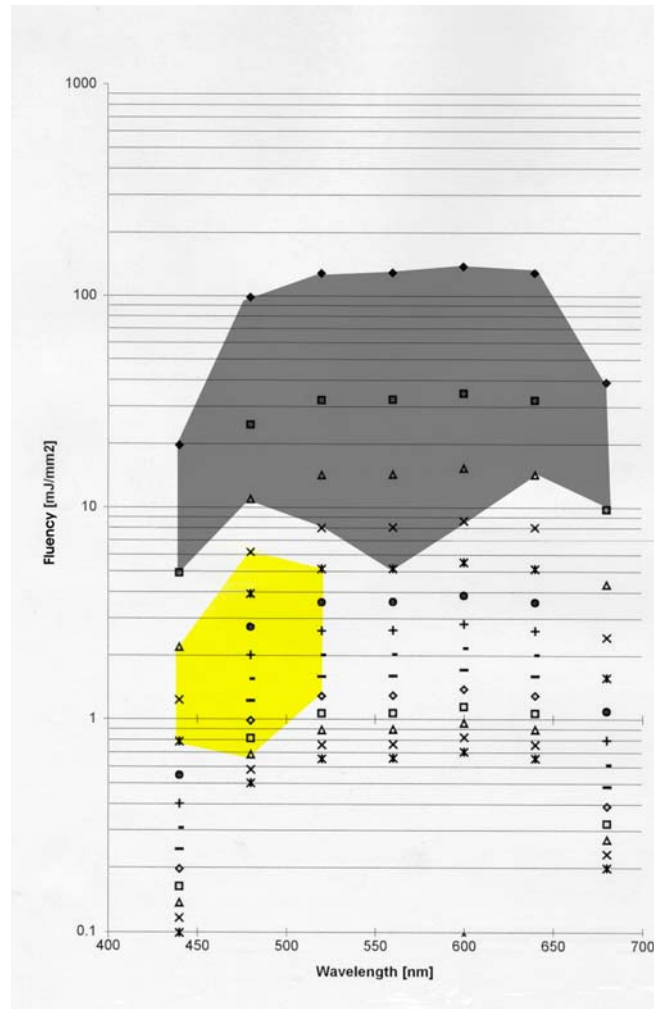*Light red=colour change + carbonisation*

Figure 6.8 Process sheet ABS + Yellow HRP.
Dark grey= carbonisation   Yellow=bleaching

From the process windows we can see that the blue pigment (cromophtal blue 4GNP) can be bleached from 630 nm to 680 nm. In this area the other two colours remain unaffected. The red pigment (cinquasia magenta RT235D) can be bleached using a wavelength from 530 nm to 600 nm. But with the restriction introduced by the blue pigment of a maximum intensity of 1.5 mJ/mm^2. And the yellow pigment (yellow HRP) already show some effect for 1.5 mJ/mm^2 and 530 nm. The yellow pigment can only be processed using the wavelength range from 440 nm to 530 nm and with intensities above the carbonisation intensity of 0.5 mJ/mm^2 introduced by the red pigment. Under the assumption that the interaction of the three pigments doesn't decrease the process areas, the combination of the three pigments as shown in Figures 6.6, 6.7 and 6.8 doesn't have a complete selectivity, see Figure 6.9. The red pigment hides almost completely the area

where the yellow pigment is bleachable. Selectivity is defined as the ability to have three different wavelengths in order to select the three pigments for bleaching separately.
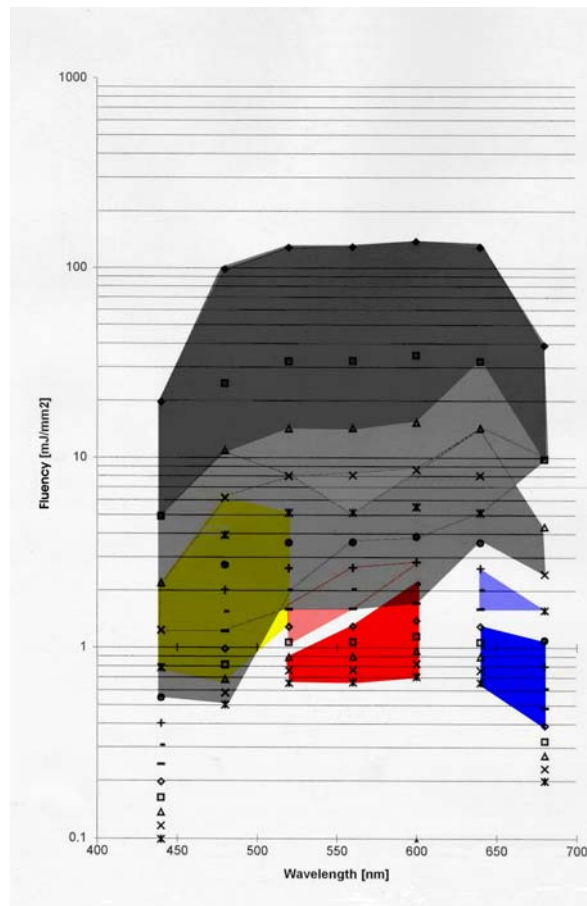
Figure 6.9: Combination of Figures 6.5 6.6 and 6.7 in order to emphasize the selectivity.

6.8.4   ABS with a whitener and a pigment

A whitener changes the base colour because the reflection increases. The absorption is limited to a thinner layer than without the whitener. In the process sheets a decrease of the carbonisation threshold is clearly visible. This change can be observed at all wavelengths. For cromophtal blue 4GNP the bleaching area extends towards $560 - 600$ nm both for TiO_2 and lithopoon. The foaming for cromophtal blue 4GNP shown in Figure 6.5 disappears, see Figure 6.10.
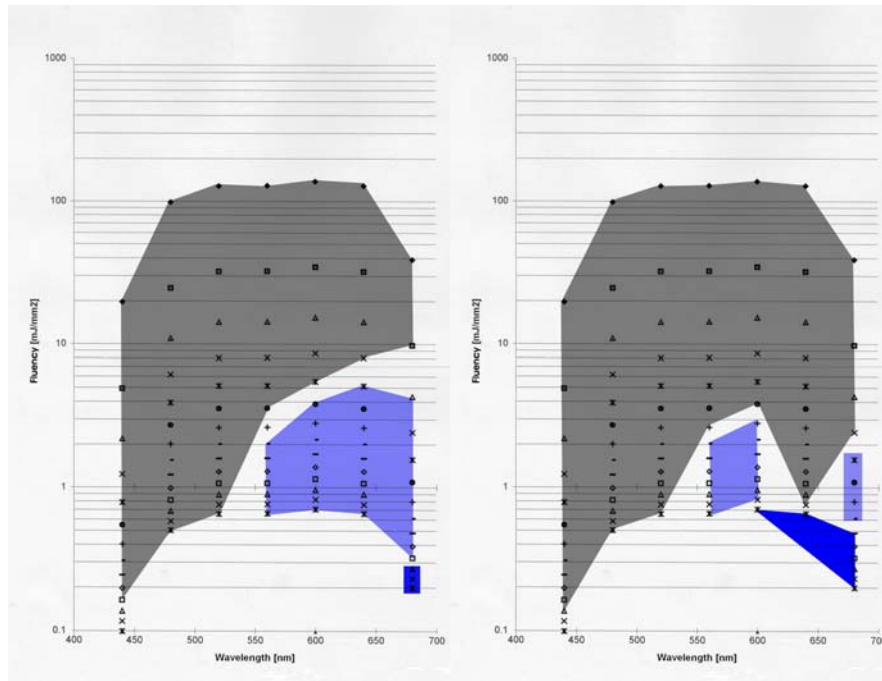
Figure 6.10: Left, Process sheet ABS + crom. blue 4GNP + TiO2.
Right, ABS + crom. blue 4 GNP + lithopoon D-S.
Dark grey=carbonisation; Blue = bleaching; Light blue = bleaching + carbonisation.

Cinquasia magenta RT-235 D is not a bleachable pigment. Under laser conditions the colour changes from magenta to dark blue. The material without whitener shows an area of colour change from 530 nm to 600 nm. The colour is very faint, but is visible. By adding whitener to the material, the colour-change area extends towards 680 nm. The carbonisation threshold decreases by a factor of two for the wavelength without colour change, see Figure 6.7 and Figure 6.11. If cromophtal yellow HRP is used with TiO_2 or lithopoon, the carbonisation threshold decreases even more also at bleachable wavelengths. The bleaching (b) area does not extend towards longer wavelengths but is shifted towards lower intensity. Only with TiO_2 a bleaching area appears at 680 nm, see Figure 6.12.

Figure 6.11: Left, Process sheet ABS + cinq. mag. RT-235 D+TiO$_2$.
Right, ABS + cinq. mag. RT-235 D+lithopoon D-S.
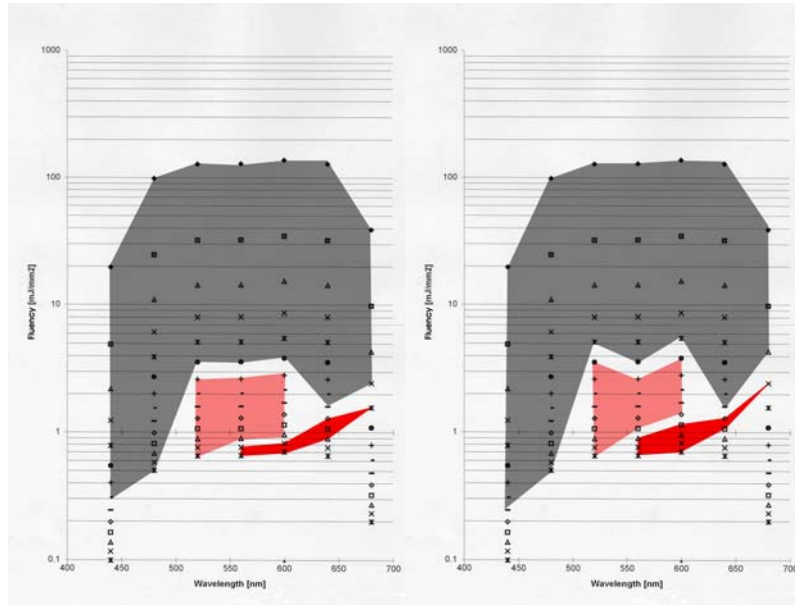*Dark grey=carbonisation, Red=colour change, Light red=colour change + carbonisation*
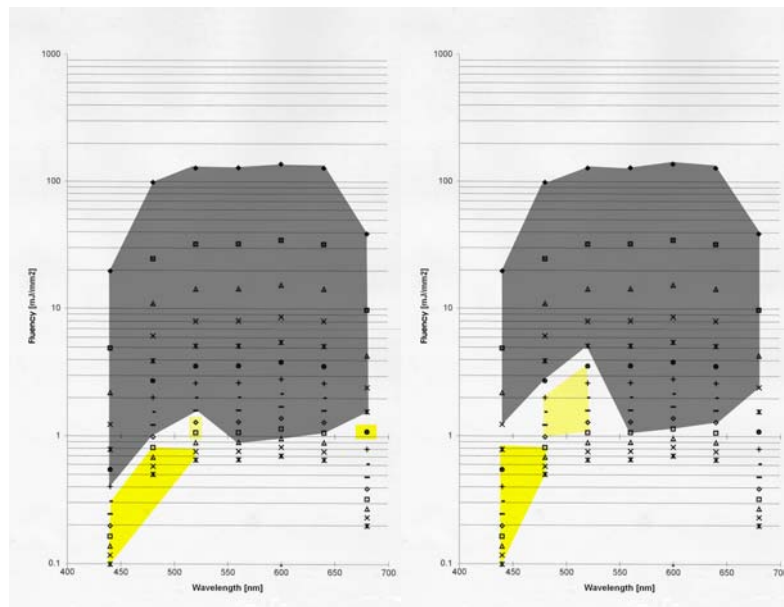

Figure 6.12: Left, ABS + cCrom. yellow HRP + TiO$_2$.
Right, ABS + crom. yellow HRP +lithopoon D-S.
Dark grey=carbonisation, Yellow=bleaching, Light yellow=bleaching + carbonisation.

6.8.5   **ABS with a combination of three pigments**

ABS with 3 pigments foams at the intensities where only carbonisation was observed for the virgin ABS. Because of the colour appearance of the combination of three pigments (dark) the carbonisation is difficult to distinguish. The foam area extends over the complete visible spectrum. The possibilities for selective bleaching are limited. If only one wavelength is used to get selectivity, the possibility for selectivity decreases even more. The colours obtained are mixed colours, and their brightness is not very high. The maximum measured contrast or DE^* value is 17.7. Under normal conditions a DE^* of 0.5 is not visible. A DE^* of 80 enables a high quality decoration (for example a red mark on a green substrate). The complexity of the process sheets of the mixed pigment ABS plates, ABS 13 - 21 is high, see appendix C for plate material specification. A lot of different areas with colours, foaming, carbonisation, and combinations of these, were found. For example, ABS plate 19 (equal combination of cromophtal yellow HRP, cinquasia mag. RT-235 D, and cromophtal blue 4GNP) should be able to be marked with a yellow, a blue, and a magenta mark, see Figure 4.14. The colours expected in an optimum situation of bleaching are listed in Table 6.4 and shown in Figure 6.15 (cromophtal yellow HRP, cinquasia mag. RT-235 D, cromophtal blue 4GNP).

Table 6.4: Theoretical DE^* values for coloured mark in ABS plate 19.

Theoretical marks	DE^* (D65, 10°)	L^*	a^*	b^*
Colour plate 19	-	34.56	-0.14	-7.72
Yellow mark (all but yellow removed)	60.65	81.52	1.91	30.06
Magenta mark (all but magenta removed)	37.96	55.12	31.73	-15.89
Blue mark (all but blue removed)	30.41	49.91	-20.12	-24.75

This can be related to the actual values, see Table 6.5. The real DE values do not come even close to the theoretical values.

Table 6.5 Real DE^* values for coloured mark in ABS plate 19

Marking wavelength [nm]	DE^* (D65, 10°)	L^*	a^*	b^*
680	2.37	34.87	0.31	-5.58
532	1.02	33.76	-0.55	-8.44
480	2.24	32.97	0.06	-9.42

Reflection curves
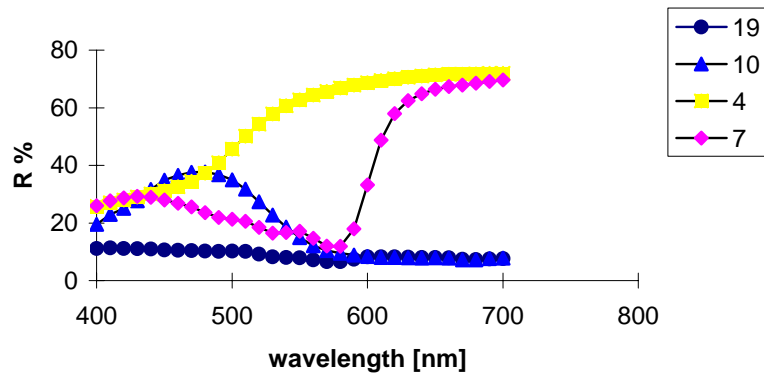
Figure 6.13 Reflection of coloured ABS plates;
4, cromophtal yellow HRP; 7, cinquasia mag. RT-235 D; 10,cromophtal blue 4GNP
19, cromophtal yellow HRP, cinquasia mag. RT-235 D, cromophtal blue 4GNP
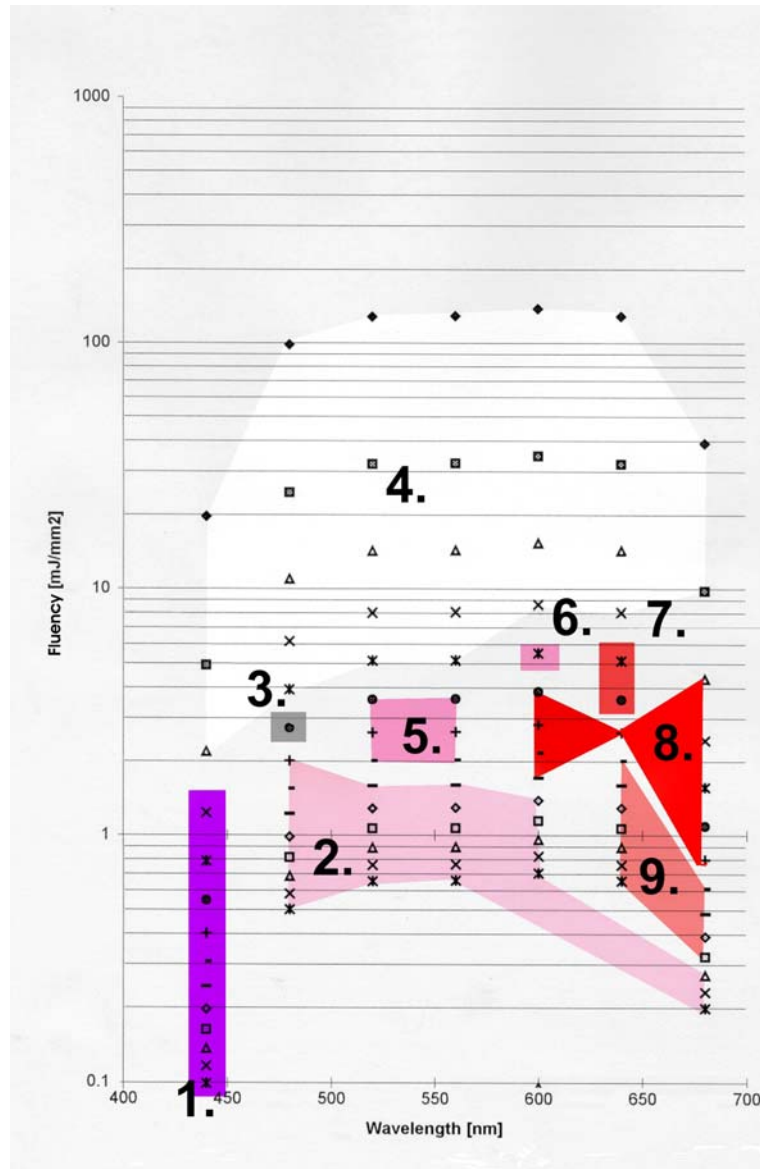
Figure 6.14: Process sheet ABS FG50 + cromophtal yellow HRP + cinq. mag. RT-235 D
+cromophtal blue 4GNP, weight ratios 1997:1:1:1, plate 19.
1. Purple=purple 2. lilac=colour change 3. Dark grey=carbonisation 4. White=foaming
5. Dark lilac =colour change + carbonisation 6.Lilac=red + foaming 7. Red= red +
carbonisation 8. Red=red 9. red + colour change.

Figure 6.15: Top left, plate 4, ABS + cromophtal yellow HRP.
Top right, plate 10, ABS + cromophtal blue 4GNP.
Down left, plate 7,ABS + cinquasia mag. RT-235 D.
Down right, plate 19, ABS + cromophtal yellow HRP+ cinquasia yag. RT-235 D
+ cromophtal blue 4GNP

6.8.6   ABS with three pigments and a whitener

The theoretical colour difference (DE*) that should be achievable by optimum bleaching for ABS with a whitener is a little lower than for the same combination without the whitener, see Table 6.6 and 6.5. The colour differences achieved are higher than in the same system without the whitener. The DE* at 680 nm is 12.15. This indicates a visible mark; it does not contain any information about the colour change that took place.

Table 6.6:.Theoretical DE* values for coloured mark in ABS plate 13.

Theoretical marks	DE* (D65, 10°)	L*	a*	b*
Colour plate 13	-	60.56	-13.16	-10.64
Yellow mark (all but yellow removed)	46.62	92.36	0.24	20.71
Magenta mark (all but magenta removed)	36.00	74.65	19.97	-10.15
Blue mark (all but blue removed)	20.17	72.21	-22.98	-23.87

Particular the mark at 680 nm shows compared to the mark of the undoped material a good contrast. A colour difference of 12.15 is not close to 46.62 but better than the DE^* 2 made at 680 nm without TiO_2.

Table 6.7: Real DE^* values for coloured mark in ABS plate13.

Marking wavelength [nm]	DE^* (D65, 10°)	L^*	a^*	b^*
680	12.15	61.87	-4.53	-2.58
532	2.19	60.18	-12.54	-9.07
480	3.55	61.13	-11.71	-14.22

Reflection curves
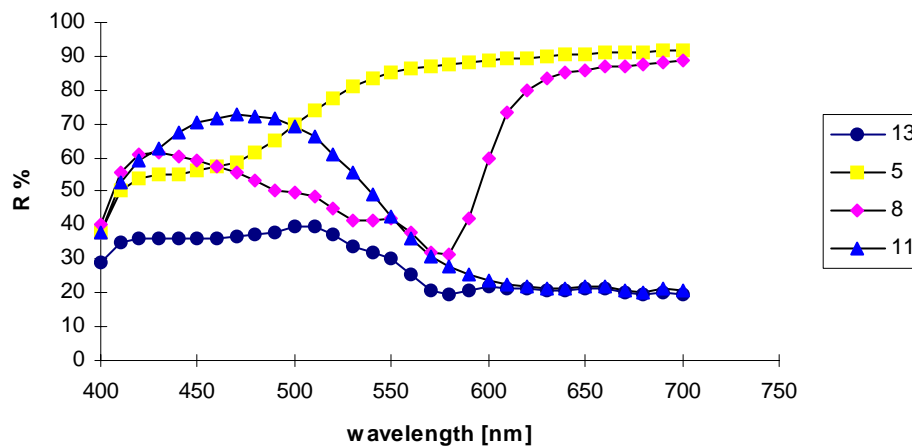
Figure 6.16: Reflection curves of coloured ABS plates 13,5,8 and 11.
Plate 5,ABS + cromophtal yellow HRP + TiO_2
Plate 8,ABS+ cinquasia mag. RT-235 D + TiO_2
Plate 11, ABS + cromophtal blue 4GNP + TiO_2
Plate 13, ABS + cromophtal yellow HRP +cinquasia mag. RT-235 D
+ cromophtal blue 4GNP + TiO_2.
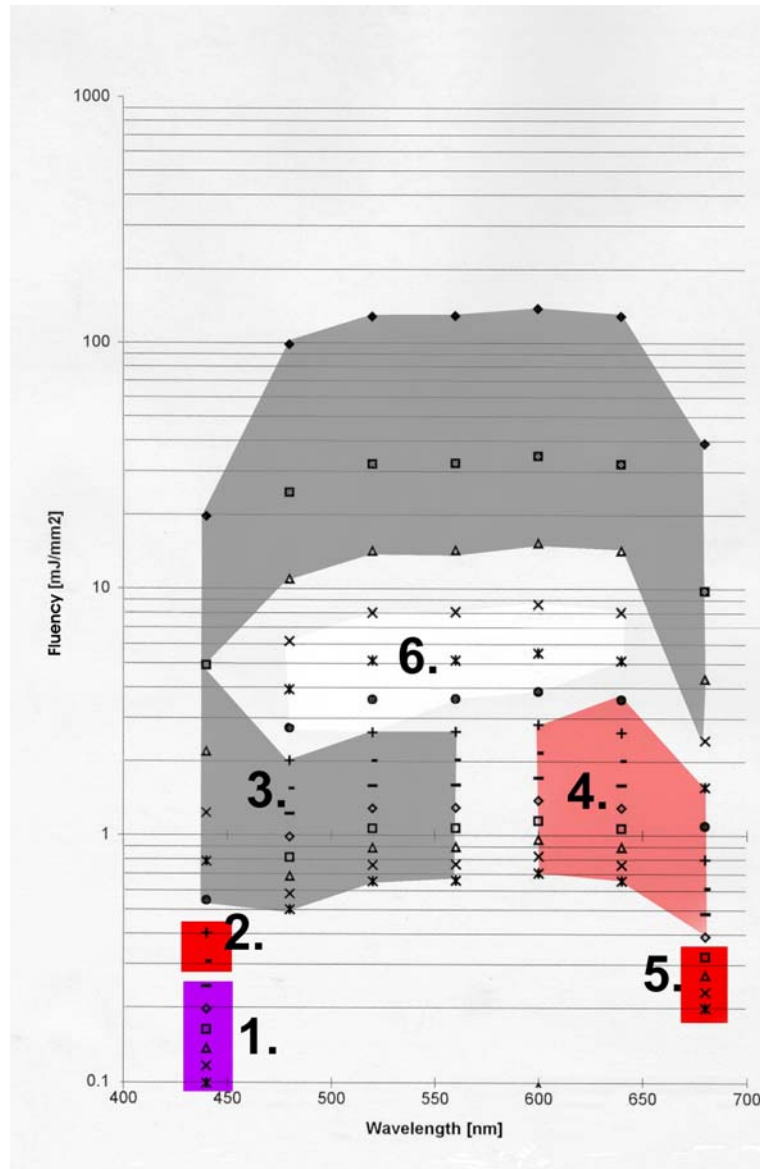
Figure 6.17: ABS, cromophtal yellow HRP: cinq. mag. RT-235 D: cromophtal blue 4GNP:TiO₂ ,ABS FG50 1:1:1:50:1925 weight ratios.
1. colour change 2. red 3.carbonisation 4. bleaching + carbonisation 5. bleaching 6. foaming.

The process areas of the three used pigments limit the selectivity. Selectivity can be reached if the pigments can be bleached without affecting the other pigments. Only in that case a set of three wavelengths is possible to select between the three colours. The process windows of the single pigments in ABS with a whitener show a larger area of bleaching than the process sheets of the

pigments without a white. Considering the goal of selectivity it is not feasible to reach three colour marking for this combination of pigments with MOPO 700.

6.9   Multi-colour laser-marking of acrylic lacquers

The higher pigment load, less carbonisation and the wider pigment choice make a lacquer system ideal to test bleaching. The industrial lacquers used for these experiments are based on a 2K acrylic system. The weight percentage for the mono-coloured lacquers is 5%. For the two whites this is 30%.

6.9.1   Industrial Lacquers with one pigment.

The group of yellow-coloured pigments show a similar behaviour. In the blue region (450nm) moderate intensity levels are sufficient for a structured or ablated surface. The same intensity at 550 nm to 650 nm could not influence the lacquer at all. Even at 680 nm with a 10 times higher intensity no structure change has been found. In the red region 600 nm – 680 nm ablation or structuring would be expected at lower levels. For the bleaching a clear relationship has been observed for 440 nm – 570 nm. A decrease in absorption can be compensated by an increase in pulse intensity, see Figure 6.17.

The red group is somewhat different. Two of them (crom. Red BN and fast Red HF 4B) show a bleached area. The other two (cinq. Red B-RT-195 D and cinq. magenta RT-235 D) have a different behaviour. The colour is darkened over a long wavelength range. No bleaching was observed not even at edges of the colour change area. Fast red HF 4B and cromophtal blue A3R show a small area of carbonisation see Figures 6.19 and 6.21.
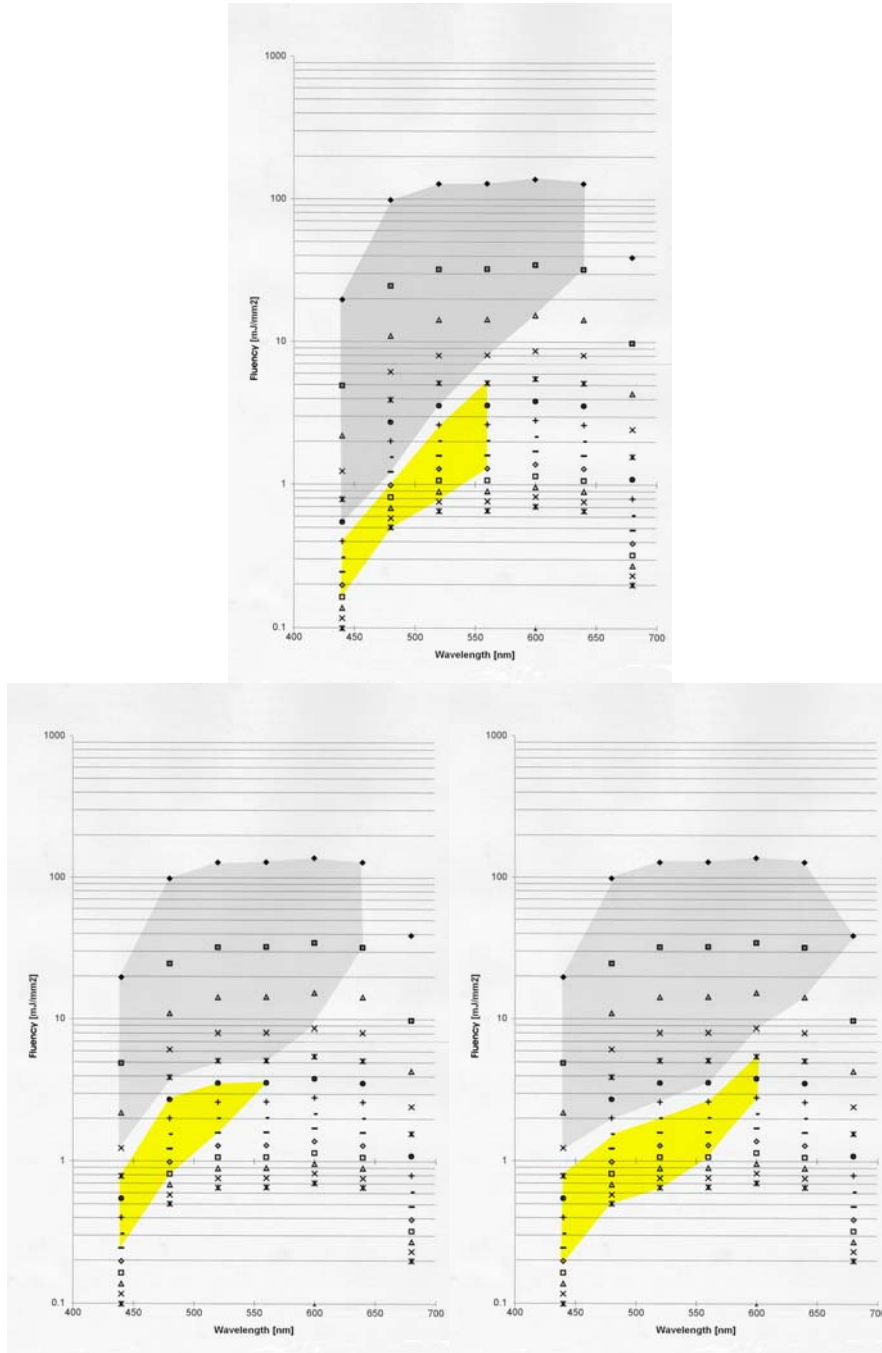
Figure 6.18: Process sheet lacquers, Top: cromophtal yellow HRP ,Left: lacquer + cromophtal yellow AGR, Right lacquer +paliotol yellow K2270. Yellow = bleaching.
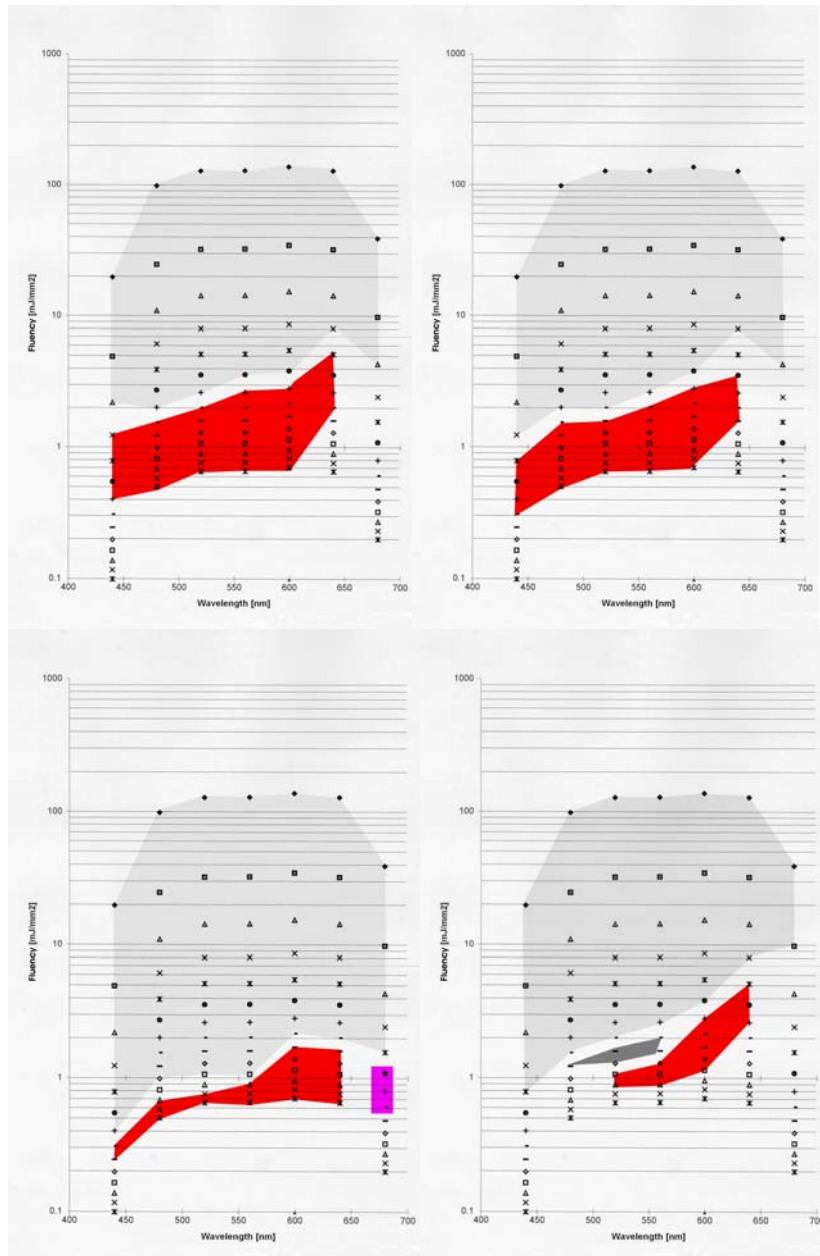
Figure 6.19: Process sheets lacquers, Top left, lacquer + cinq. Red B-RT-195 D, Top right lacquer + cinq. magenta RT-235 D. Red = colour darker, Light grey = structuring surface. Bottom left, lacquer + crom. red BN, Bottom right, lacquer + fast red HF 4B. Red = bleaching, light grey = structuring surface, dark grey = carbonization, purple = darker colour.

The irgalite green GFNP has a form which is almost the opposite of the irgalite blue BSP. The green lacquer (green GFNP) shows at its maximum reflection no bleaching. At the maximum reflection (550 nm) no darkening is visible. At lower levels in the blue and red regions a darkening effect is observed. This could be explained by the absorption curve: because of the higher absorption more energy is deposited inside the system, and will structure or ablate the lacquer more easily, see Figure 6.20. The cromophtal blue A3R shows a broad bleachable area without any selectivity, see Figure 6.21.
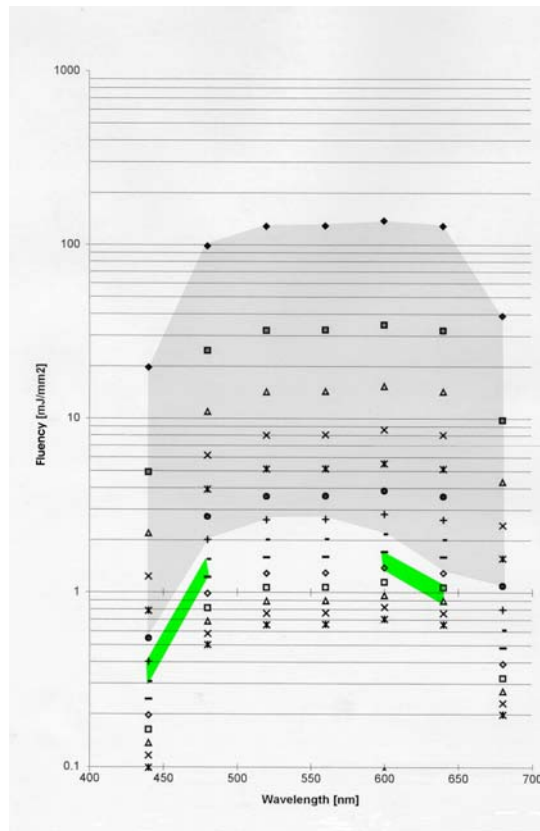
Figure 6.20: Lacquer + irgalite green GFNP.
Green = bleaching
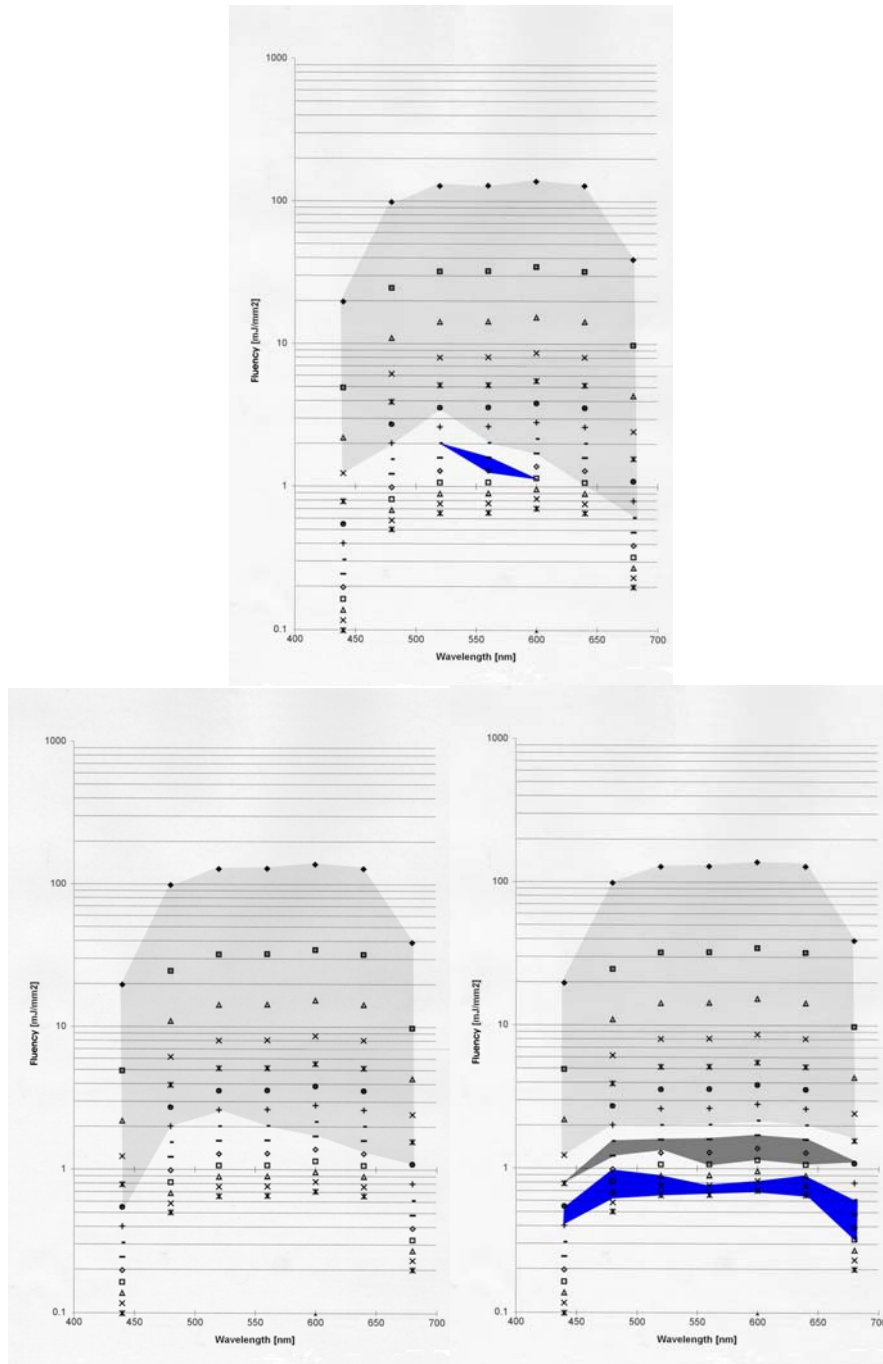
Figure 6.21: Process sheet lacquers, Top, lacquer + Irgalite Blue BSP. Bottom left, lacquer + Irgalite Blue GBP. Bottom right, lacquer +Crom. Blue A3R
Blue = bleaching, Light grey = structuring surface, Dark grey =carbonization.

6.9.2   **Industrial lacquers with a whitener.**

The two different white materials have two main differences:

1.   The level of carbonisation with TiO_2 is twice as low as with lithopoon.
2.   No carbonisation with lithopoon was observed, although TiO_2 had a lot of carbonisation.

The weight percentage used was around 30% in a dry material. No bleaching was observed.
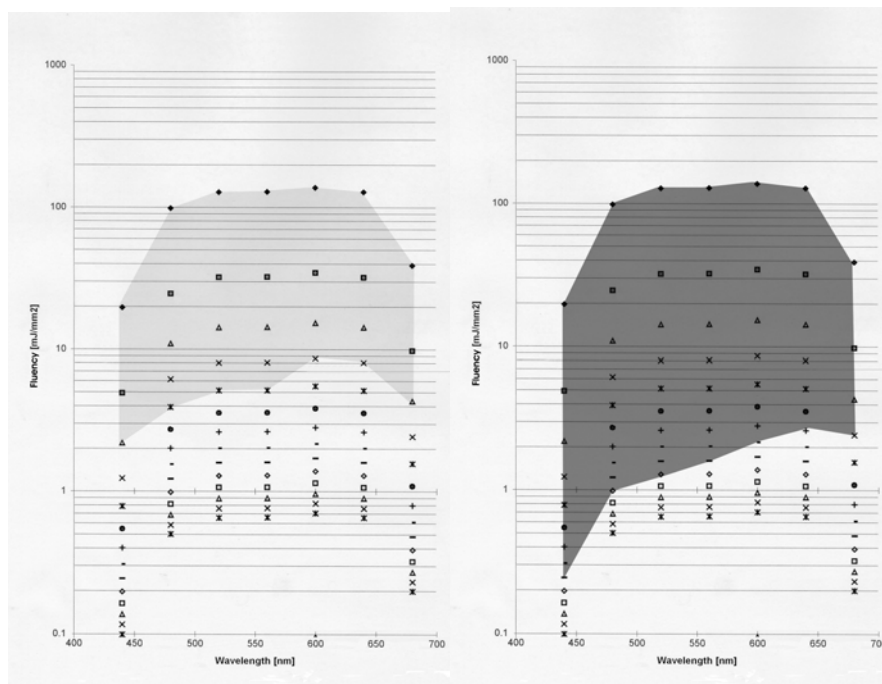
Figure 6.22: Left, lacquer + lithopoon (ZnS). Right, lacquer + TiO₂ (Kronos RN 2059).
Light grey = surface structuring, Dark grey = carbonisation.
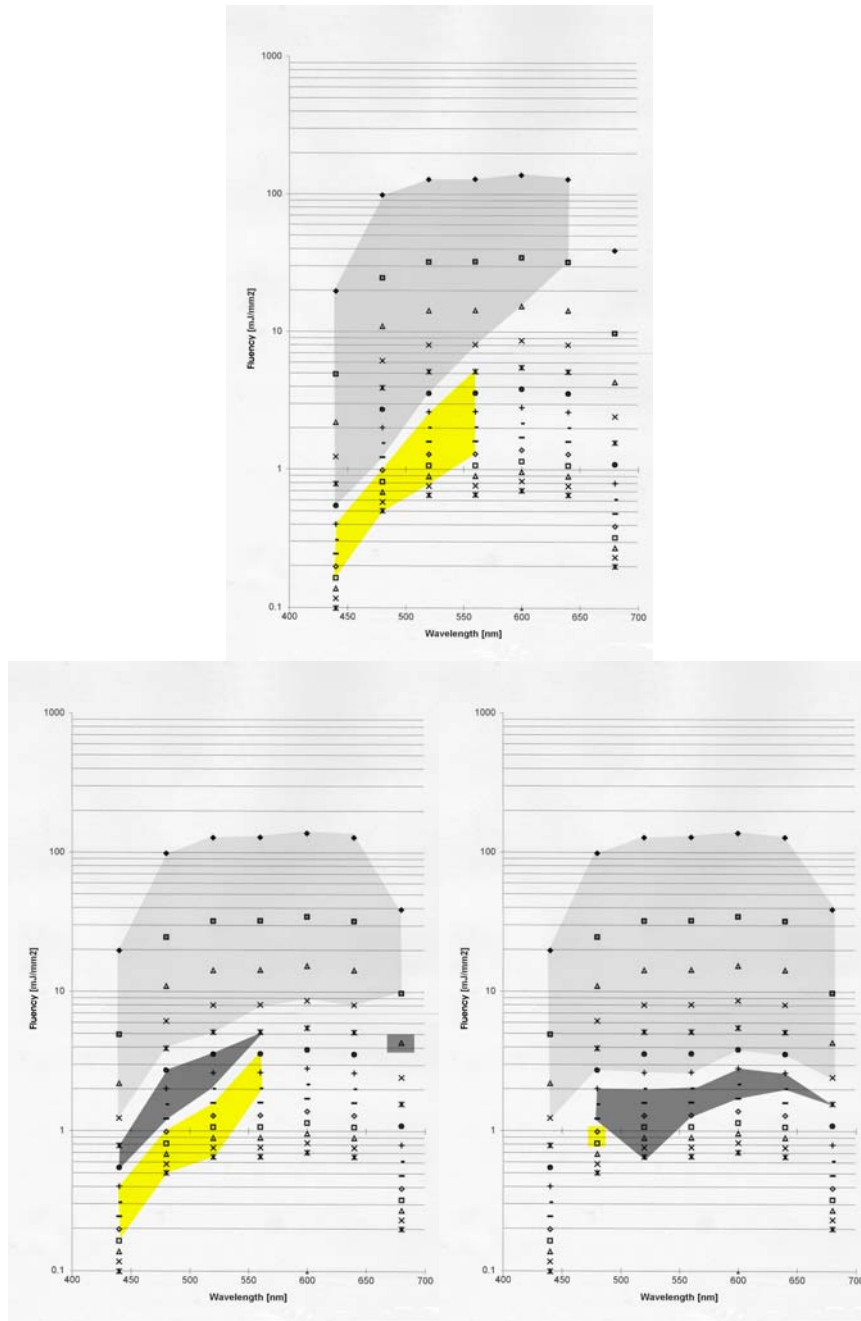
Figure 6.23: Top, lacquer + crom. yellow HRP. Bottom left, lacquer + crom. yellow HRP.+Lithopoon. Bottom right, lacquer + crom. yellow HRP + TiO$_2$ Kronos 2059. Yellow = bleaching, Light grey = surface structuring, Dark grey = carbonization.

Figure 6.24: Top, lacquer + paliotol yellow K2270. Left, lacquer + K2270.+ lithopoon.
Right, lacquer + K2270 + TiO$_2$ Kronos 2059.
Yellow = bleaching, Light grey = surface structuring, Dark grey = carbonization.

6.9.3   Industrial Lacquers with one pigment and a whitener

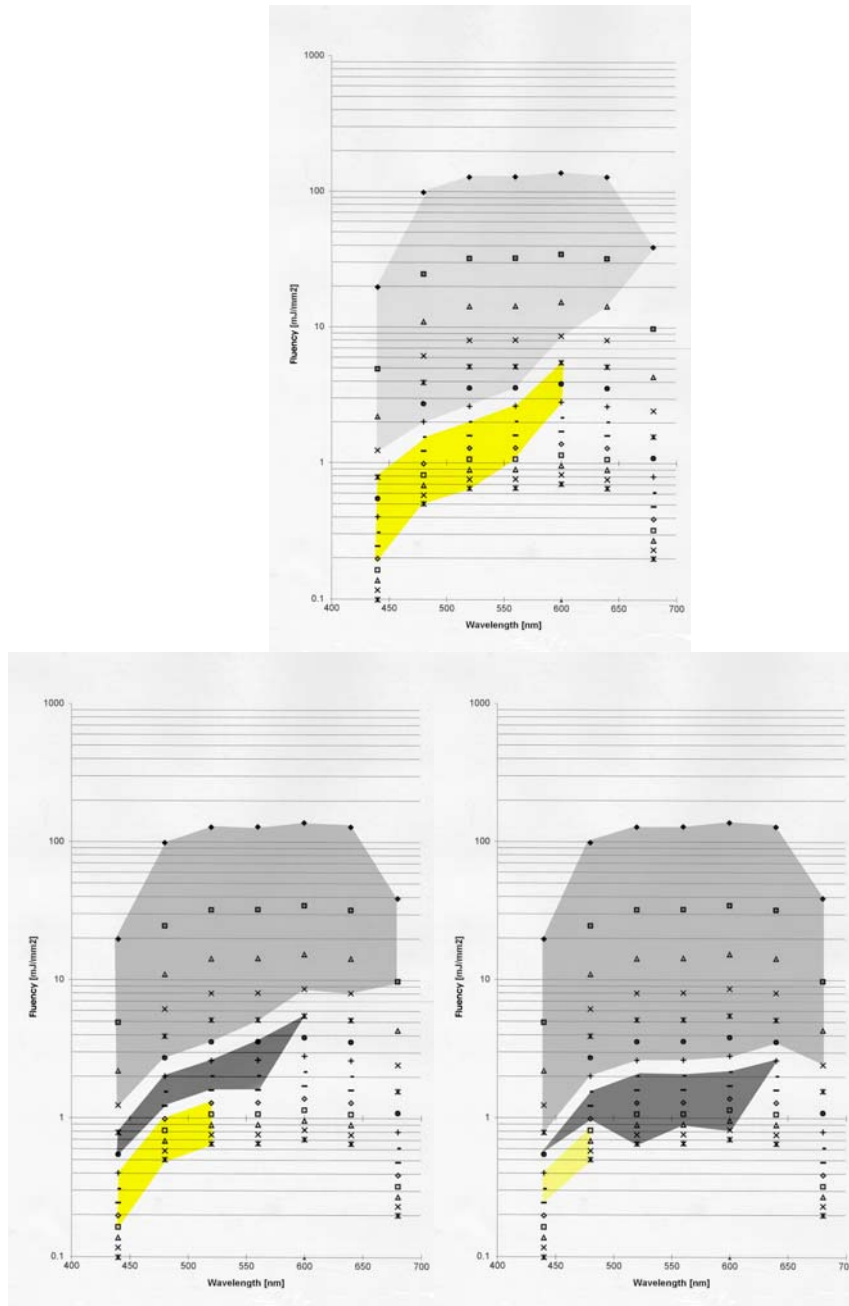For all tested pigments, adding a whitener changes the process sheet when compared to the mono-colour. For crom. yellow HRP the ablation threshold drops. Also carbonisation is observed over the complete tested wavelength range. Bleaching for the TiO_2 is reduced to a very small area, see Figure 6.23 right. The main conclusion from these three process sheets is that lithopoon does not have the same effect on bleaching as TiO_2. It promotes carbonisation but the change for this combination in the bleaching process area is very small. Paliotol yellow K2270 shows the same effect as the crom. yellow HRP, see Figure 6.24. The shape of the process sheets is almost the same. Only with TiO_2 does the paliotol Yellow have more bleaching area left than the crom. yellow with TiO_2. With different loads of whitener the same effect occurs.

6.10 Conclusions

The model shows the specific limitations of bleaching. If side band absorption is taken into account the possible difference in reflection reduces. Bleaching as a technique for full colour laser-decoration is not realistic with these pigments. The markings are readable and enable a certain colour range.

Bleaching is a mix of different possible processes, such as carbonisation of the polymer, pigment fragmentation and photo-oxidation. The balance between the different processes strongly depends on the polymer matrix and pigment type.

The desired base colour determines the pigments and pigment concentration. If three colours (red, green and blue) are used this will lead to dark brown, grey and purple base colours.

Chapter 7 Laser marking of titanium dioxide containing polymers

7.1 Introduction

Under normal laser conditions polymers like polypropylene (PP), polymethylmeta-acrylate (PMMA), LDPE, HDPE, do not change to a uniform charred structure when exposed to high temperatures introduced by laser irradiation. With conventional solid-state lasers the marking of polypropylene is a difficult process especially PP is difficult to mark due to its diffuse structure and its low absorption. The size of the structure influences the marking result. A finer crystal structure gives a better result (finer details visible) as the course structure does, see Figure 7.1.
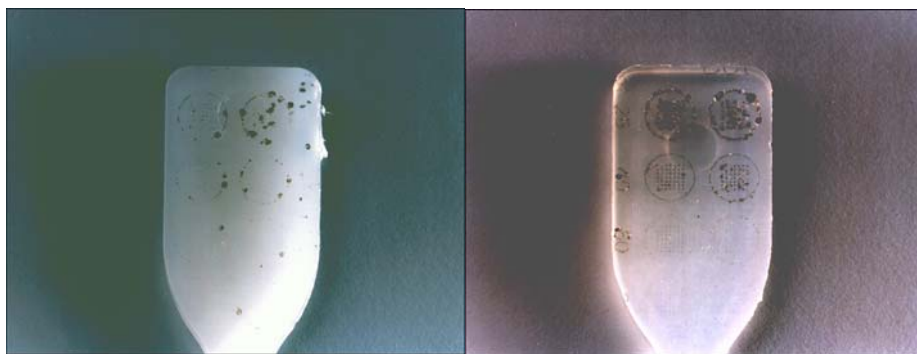
Figure 7.1: Pure PP with coarse crystal structure (left) and fine crystal structure (right)
marked by 1064 nm Q-switched Vanadate laser, t_p = 9 ns.

Both Mearl and Merck supply additives with the ability to absorb the laser energy and in this way concentrate the energy to obtain a local thermal degradation in which the pigment plays the dominant role. Although polypropylene (PP) does not turn to a black charred structure, the formation of gas bubbles will give some contrast. The mark has a highly irregular form, and some PP samples show a light brown shade.

PP is a cheap material that is used for an increasing number of applications. It is difficult to laser-mark and to print. The material has to be pre-processed for printing. Processes like flame and corona exposure can modify the surface structure prior to printing. Even laser exposure with UV is sometimes used as pre-treatment. The pre-treatment produces radical groups at the surface, which increase the adhesion of inks. The introduction of industrial UV laser-marking systems opens up an alternative marking method. The use of titanium dioxide (TiO_2) as an active additive is necessary for obtaining any form of mark on materials; it does not carbonize.

Figure 7.2: PP with 1.5% Mearl UFL and 1% TiO$_2$ marked
by 1064 nm Q-switched Vanadate laser, t$_p$ = 9 ns.

7.2   TiO$_2$ as additive

TiO$_2$ is an additive that is used very often. It is the most important whitener for polymers. It has a good thermal and chemical stability. The high refractive index makes it an ideal whitener for polymer systems. There are two basic crystals forms of TiO$_2$: the rutile form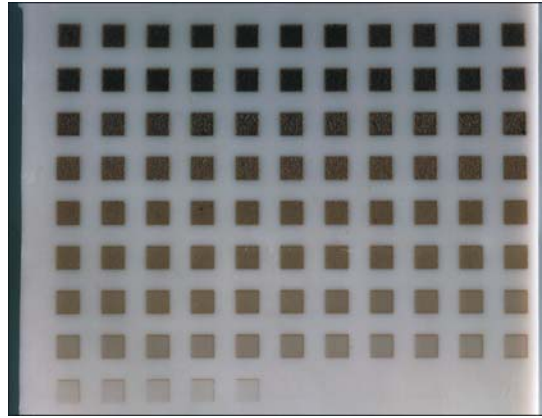, which has a higher opacity and a refractive index of 2.7, and the anatase form with a refractive index of 2.5, which is normally used for papers and elastomers. The rutile form is less photocatalytically active than the anatase and is used in polymers. But still the pure form of TiO$_2$ will degrade the polymer by its photocatalytic effect. The surrounding polymer will show a loss of gloss and a chalking effect. Therefore all TiO$_2$ has a surface treatment. It is coated by Alumina or combinations with Silica, and this coating reduces the opacity and tinting strength of TiO$_2$. The coating acts as a physical barrier. TiO$_2$ absorbs UV so it can also be used as an UV stabilizer. It transforms UV radiation into heat.

7.3   Industrial UV laser-marking.

The question arises whether UV lasers are industrial mature with regard to polymer marking. The generation of the third-harmonic energy has a limited yield. And if a fundamental solid-state laser can generate the same gray-tone in a white polymer the complexity of third-harmonic generation is not appreciated in production. Every part, which has not a specific role in the process, should be left out because of higher risks of failures. To be able to asses the effect of UV-marking in an industrial environment a comparison is made between a fundamental solid-state laser and a third-harmonic solid-state laser.

The fundamental solid-state is a commercially available Vanadate laser from Spectra Physics (T20) integrated by Rofin Sinar, for laser specifications see Table 5.2. The third-harmonic system, also a Vanadate from Spectra Physics, has the same integration by Rofin Sinar. Besides this system another third-harmonic system supplied by Nanolase was included in the test. This

system has a passive Q-switch build-up and had only an average power of 50 mW, see for laser specifications Table 5.3.

Due to the passive Q-switch build-up, the Q-switch frequency depends on the pumping power. In principle the laser starts to generate the pulse when the passive Q-switch is set to its higher excitation state. The material used absorbs the fundamental wavelength of the laser in its lower state and becomes transparent in its excited state. The generic names for these materials are saturable absorbers. The time needed to get the material in this state depends on the pumping intensity. A higher intensity will need less time to get the Q-switch transparent. The Q-switch will become transparent at a constant inversion level which can be translated into a constant pulse form and pulse energy (Koechner 1992). After the pulse the absorber returns to the closed form because there is no emission for a short period.

7.3.1   Materials

Three materials were chosen for evaluation with both the fundamental and third-harmonic systems. The percentage TiO_2 is representative for commercially used polymers. All these TiO_2 are coated. The materials also contain other additives beside the TiO_2. The supplier will not disclose the content of the materials. As this the normal situation in practice the decision was made to use three test materials that are widely used within Philips. The PP is used in its white form for irons and different other domestic appliances. PS is a material that is used for packaging. ABS is a copolymer that is a physical mixture of three different polymers and is used for example in shavers, mobile telephones and vacuum cleaners.

Table 7.1: CFT Polymer indexes.

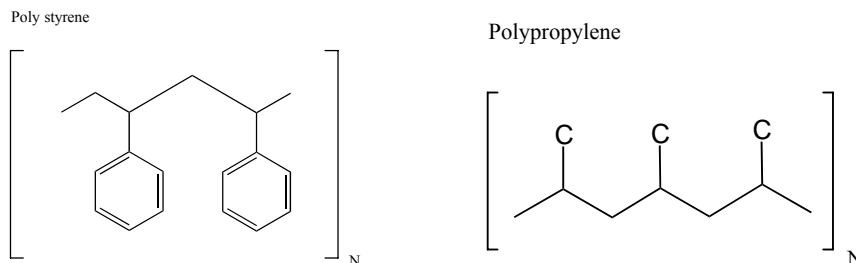|	Material	Char forming index
PP	Polypropylene	0
PS	Polystyrene	2
ABS	Acrylonitrile Butadiene Styrene (co polymer)	2

Figure 7.3: Chemical structures of Polystyrene and Polypropylene.

PP without any additives cannot be marked by either the 355 nm and 1064 nm solid-state lasers. PS and ABS both show a tendency to carbonization, and can be marked to a limited extent by both the fundamental and third-harmonic wavelengths.

7.4   Experiments and results.

The tests on the materials were performed according to the single-pulse strategy with exception of the dual-chip laser, which, due to the passive Q-switching and relative high frequency, could not be used for single exposures. This approach was chosen because the fastest way to mark polymers is by a single pulse. If more pulses are necessary to start the process this will always be slower than a single pulse. The gray-tones obtained by a single pulse can be lower in intensity than a multiple-pulse marking. These experiments were done to obtain the difference in material behavior for the fundamental (1064 nm) and third harmonic (355 nm) wavelengths.

The experiments were according to the CIELAB colour space. This standard colour space is used to express the difference a standard human will see under the standard illumination with a D65 illumination source, see appendix E. The measurements were done with a microflash colour meter (6 mm aperture) with a D65 standard illumination source. The microflash measures the wavelength dependence reflection of a 6 mm diameter circle using a standard flash illumination and integrating sphere.

The markings were made in focus with a fθ lens with 160 mm focal length and spot diameter of 100 μm for the 103D and 103D UV. The filling of the squares are 100 dots per inch (DPI).

Table 7.2: Marking result, Maximum DE* (D65 / 10 deg, microflash aperture 6.0 mm).

	103D 1064 nm, 9 ns	103D UV 355 nm, 8 ns	Dual chip 351 nm, 1 ns
PP	No marking	1.7 - 42.0	2.3 - 14.9
PS	2.4 - 10.8	0.4 - 36.4	5.2 - 14.3
ABS	1.2 - 17.0	0.4 - 28.7	2.9 - 10.9

The DE* difference is with regard to the colour of the unmarked test plate. The DE* can therefore be used to differentiate for the same material.
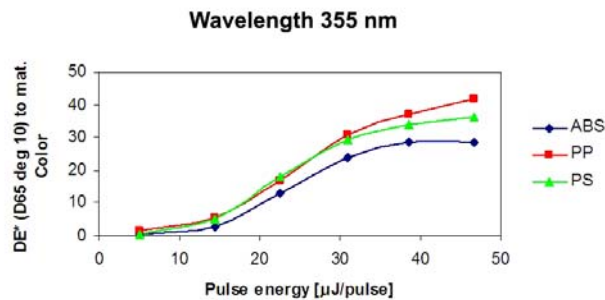

Figure 7.4: DE* relative to base material colour as function of the pulse energy
(wavelength 355 nm, , t_p = 8 ns, pulse diameter 100 μm).
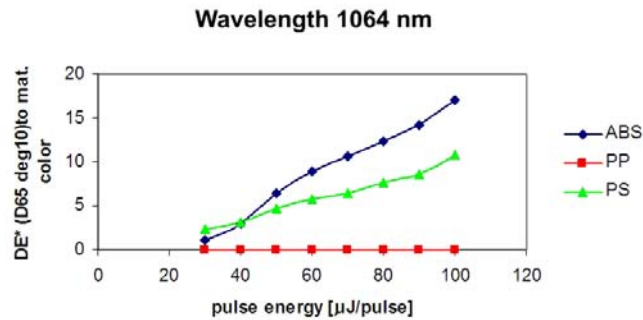
Wavelength 1064 nm

Figure 7.5 DE* relative to base material colour as function of the pulse energy
(wavelength 1064 nm, , t_p = 9 ns, pulse diameter 100 μm).

The maximum colour difference is for all three materials higher at 355 nm than for the 1064 nm. Polypropylene can only be marked with the 355 nm. The DE[*] results of the 355 nm experiments are obtained at a much lower pulse energy level than the 1064 nm experiments. The maximum DE[*] value for the ABS at 355 nm is reached at 40 μJ/pulse. Increasing the pulse to 50 μJ does not give a higher DE[*] value. For PP and PS the DE[*] value also tends to go to a maximum.

7.4.1   Colour spaces PP,PS and ABS

The absence of any mark on the PP irradiated by 1064 nm is rather striking because this laser can deliver 3W at a spot for which the dual-chip laser has only 50 mW at its disposal and could make a visible marking, see Table 7.2. At the higher pulse energies the colour changes a little towards the green blue. The change in DE[*] value for 1064 nm is small compared to the change at 355 nm.

Table 7.3: Pulse energy [μJ] for 1064 nm and 355 n, f_Q 10 kHz.
,used in the colour spaces in Figures 7.6, 7.7, 7.8

Laser vs.	1.	2.	3.	4.	5.	6.	7.	8.
103D 1064 nm	30	40	50	60	70	80	90	100
103D 355 nm	5	14.5	22.5	31	38.5	46.7		

PP white

Figure 7.6: LAB Colour space plot for PP
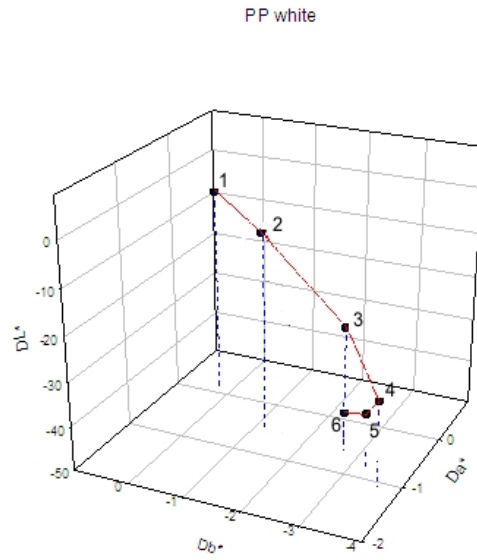*■ 355 nm, t_p = 9 ns*
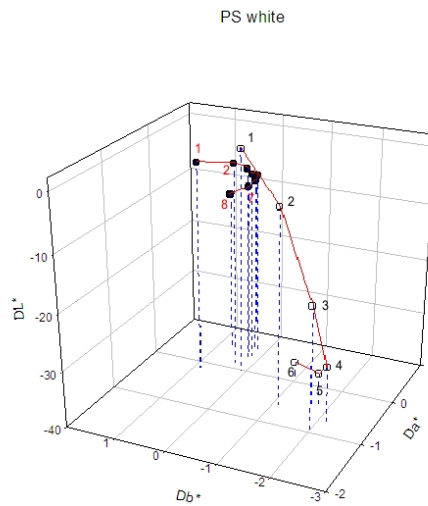*Pulse energies, see Table 7.3.*

PS white

Figure 7.7: Colour space plot for PS,
■1064 nm , t_p = 9 ns, red numbers,
□ 355 nm , t_p = 8 ns, black numbers,
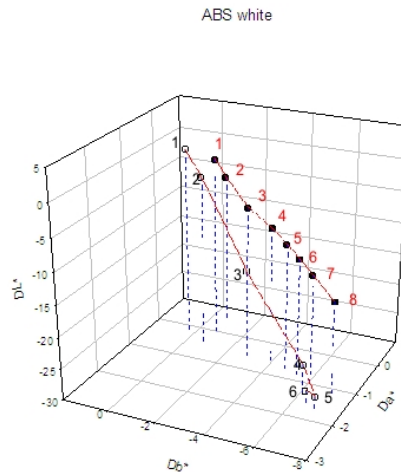*Pulse energies, see Table 7.3.*

Figure 7.8: Colour space plot for ABS,
■1064 nm, t_p = 9 ns, red numbers,
□ 355 nm, t_p = 8 ns, black numbers,
Pulse energies see Table 7.3.

7.5 Conclusions

TiO_2 changes dramatically the laser-marking of PP for 355 nm. With the near-infrared wavelength of 1064nm no mark can be made, but with the 355 nm a single low-energy pulse is able to mark the material. For the other materials like ABS and PS this effect is also present, but both materials can also be marked by the 1064 nm wavelength. This effect is often called the reduction of TiO_2 assuming the reduction to TiO or Ti. Both materials are black/grayish. The effect was not noticed when marking pure TiO_2. To create the black/grayish colour the reduction of the TiO_2 doesn't have to be complete, see Chapter 2.9.7 and (Dance 1990).

Because TiO_2 is surrounded by the polymer and absorbs the UV wavelength it is likely that the additive interacts with the polymer, and due to this interaction the polymer starts to become black by carbonization. TiO_2 has a known photo-catalytic effect on polymers and is therefore coated. The degradation products of polypropylene (PP) are reported to be saturated and unsaturated hydrocarbons from C_2 upwards, with a monomer yield of 0.17% for the temperature range of 321-410 °C (Madorky 1954). When the temperature is increased to 1200 °C the yield of small fragments increases at expense of large fragments (Day 1962). Experiments with high UV (355 nm) intensities on PP without additives showed no carbonization just below the ablation threshold. Therefore it is unlikely that even small energies as used for these experiments would enable the carbonization of PP. For ABS and PS the carbonization is a possible degradation route and will be present when the pulse energy is above a certain threshold.

Chapter 8   Review, conclusions and suggestions

8.1   Review and conclusions

Laser marking of polymers has a lot of aspects that I tried to describe and to show in this thesis. The low conductivity of polymers combined with the high transparency makes the laser an ideal tool to get energy where it is needed. By adding absorbing elements into the polymers the energy distribution can be controlled even further because the absorption coefficient changes. The high temperature of small absorbing particles during short laser pulses (pulse width ~ 10 ns) and the low conductivity of the polymers enable bleaching of these particles without destroying the polymer. I showed in Chapter 6 that the contrast is low due to the poor selectivity caused by side band absorption. This reduces the use of the selective bleaching of pigments for laser marking. If the pigments are concentrated in thin stacked layers a better contrast is expected. The bleached layer reveals the layer underneath. The stacked configuration adds an extra way of selectivity. The laser can stop if the colour changes. The high concentration and stacked configuration limits the use to foils.

 Further it was shown that the structure of the polymer is directly related to its ability to carbonize. The strategies of laser marking are described and expanded to new strategies. The way a marking is made has influence on the appearance of this marking. An analytical thermal model was made that can be used to analyze laser marking and its strategies. This model can calculate the thermal diffusion between pulses placed in a pattern in time. Also new strategies are introduced that use this effect to include surface texture in the marking.

The characteristics of solid-state lasers make it possible to reduce the amount of experiments done with these lasers. Instead of all combinations of lamp or diode current and frequency a reduced set with respect to pulse energy and pulse width can be used. A fixed relationship between pulse energy and pulse width reduces the combinations. The use of colour measurements show directly the differences between UV (355 nm) and infrared marking (1064 nm) if the amount of marked surfaces is kept constant.

8.2   New developments in laser marking and its use in the future

The possibility to use a non contact way to mark a product will always have a magical way regardless if it is applied for marking of apples or for marking condensators. The limited colour range is a minor set back but could be increased by using additives, different wavelengths or other pulse lengths. For example laser mass transfer could be used to transfer materials onto 3D

product skins. After a post treatment this could be used for small batch production as well as for mass customization.

The development of laser marking is still underway and will go on for the next 10 years and more. The use of concentrated energy with the ability to use it flexible and specific, invite new ideas.

The technology to transfer components has already been developed for placement but could for example also be used to print small pixels (leds) on a 3D product together with transfer of copper wires this would be the first real 3D display on products. Light effects will be a normal appearance of our products in the near future. The use of laser written lightguides in polymers would enable 3D light effects inside product skins.

Laser mass printing structured logos would not only give a visual but also a tactile experience. The light effects on such a 3D build up marking would integrate the logo with the complete appearance.

The marking of polarization markers is already used for anti counterfitting marking where a stretched foil is locally heated, where it will relax and give a polarization change in the material transmission. Laser marking of holographic codes would give more light effects and dynamic possibilities than the ones currently used. Latent marking for anti counterfeiting can also be made.

The speed of laser writing will increase. The laser frequencies are now in order of 50 kHz. 100 kHz is already available but also the powers will increase. It is expected that the development is going to 500 kHz. These high frequencies demands also faster scanners. The current type of scanners using galvanic motors is too slow for 500 kHz. An acousto-optic scanner could be the answer.

A higher scan resolution enables a spot size reduction through smaller wavelengths like the 5th harmonic. Xiton already has a 5th harmonic (213 nm) that could be used for small prints and 3D micromachining. The industrial use of optical parametric oscillators (OPO) will expand the available wavelengths even more. The wavelength will become a real parameter.

Laser tweezers can be used to change the pigment orientation locally in wet paints. After curing the marking is fixed.

And there will be more ideas using laser energy to create markings and decorations for consumer products. We only have to think about 'pico and femto seconds', concentrating the energy even further with respect to time while reducing the average power. The isolation properties of the polymer matrix will keep the energy concentrated.

Appendix A Thermal models, thermal balance

A.1   Introduction

We assume that all the energy that is absorbed during the laser pulse is converted into heat. To derive the heat balance first the absorption side is calculated. From this the temperature can be calculated.

A.2   Absorption side

Lambert's absorption law is based upon the equal absorption in each layer of equal thickness.

$$\frac{dI}{dz} = \alpha I \tag{A.1}$$

$$I = I_0 e^{-\alpha z} \qquad \text{laser intensity} \qquad [\text{W/cm}^2] \tag{A.2}$$

The fraction of intensity absorbed at depth z will be:

$$\frac{(I_0 - I)}{I_0} = \frac{I_0(1 - e^{-\alpha z})}{I_0} = 1 - e^{-\alpha z} \tag{A.3}$$

The differential fraction of intensity absorbed is:

$$\frac{d\frac{(I_0 - I)}{I_0}}{dz} = \frac{d(1 - e^{-\alpha z})}{dz} = \alpha e^{-\alpha z} \tag{A.4}$$

And the absorption per unit volume for one square pulse with pulse width t_p can be described as:

$$\varepsilon I_0 t_p \alpha e^{-\alpha z} = dE \tag{A.5}$$

With ε the emissivity of the material.

A.3   Energy side

The energy stored per unit volume for a temperature rise of T:

$$\rho c_p T = dE \tag{A.6}$$

The thermal balance can be written as:

$$\varepsilon I_0 t_p \alpha e^{-\alpha z} = \rho c_p T \tag{A.7}$$

From this the temperature with respect to the absorption coefficient and depth without heat diffusion can be written as:

$$T(z) = \frac{\varepsilon \cdot \alpha \cdot I_0 \cdot t_p \cdot e^{-\alpha \cdot z}}{c_p \cdot \rho} \tag{A.8}$$

Equation A.8 is expanded to three dimension with the introduction of the laser beam intensity distribution in the spatial domain. The intensity distribution of a Gaussian beam is:

$$I(x,y) = I_0 \cdot e^{\left(\frac{-2(x^2+y^2)}{w^2}\right)} \tag{A.9}$$

 Equation A.9 combined with A.8 gives the three dimensional initial temperature distribution used in Chapter 3.

$$T(x,y,z) = \frac{\varepsilon \cdot \alpha \cdot I_0 \cdot e^{\left(\frac{-2(x^2+y^2)}{w^2}\right)} \cdot t_p \cdot e^{-\alpha \cdot z}}{c_p \cdot \rho} \tag{A.10}$$

In the case of no diffusion during the laser pulse the intensity representation can be changed to the laser fluency form.

$$T(x,y,z) = \frac{\varepsilon \cdot \alpha \cdot F_0 \cdot e^{\left(\frac{-2(x^2+y^2)}{\omega^2}\right)} \cdot e^{-\alpha \cdot z}}{C_p \cdot \rho} \tag{A.11}$$

Appendix B The temporal pulse shape of Q-switched pulses

B.1   Introduction

The understanding of the temporal pulse-shape of Q-switched solid state systems is important for an effective process design. It makes comparison of different types of solid-state systems for one specific process possible. This method is an effective way of representing a solid state Q-switched laser and we will prove that the characterization represents the relationship between pulse-time and pulse width and the thermal stability of the complete system.

B.2   Temporal pulse shape

We examined the underlying theory for a solid-state laser with regard to the relation of the pulse width and the pulse energy. Starting from two well-known equations from "Koechner" (Koechner 1992), basically only the notation of some parameters are modified. This results in some new and more practical predictions. The two original equations are:

$$\frac{dn}{dt} = -nc\Phi\sigma \tag{B.1}$$

and

$$\frac{d\Phi}{dt} = nc\Phi\sigma\frac{l}{L} - \frac{\Phi}{\tau} \tag{B.2}$$

n = inversion population density,
Φ = laser photon density in the resonator,
c = speed of light,
σ = cross-section for radiative transition,
l = length of amplification medium,
L = optical length of the resonator,
τ = resonator decay time

The resonator decay time t is given by the losses ε per transit time. We assume that these losses are concentrated at the outcoupling mirror for simplicity. They consist of the outcoupling losses (1-R) and a smaller contribution representing other resonator losses (R_{loss}). We have thus:

$$\frac{1}{\tau} = \varepsilon \frac{c}{2L}; \varepsilon \approx (1-R) + R_{loss} \tag{B. 3}$$

We consider now, in place of the abstract photon density Φ, the resulting laser power P. Assuming that the resonator is filled by a column of photons with the transversal area A. On average, half of the photons travel at the speed of light into the positive, and half of them into the negative, longitudinal directions of the resonator. Per time interval a number of c × A × Φ/2 photons thus arrive at the outcoupling mirror, where a fraction ε is lost for the resonator. This fraction is converted into "intrinsic" laser power P', from which a small part is lost by scattering, but the predominant part can be measured as useful laser power P. The relation between the latter is simply:

$$P = \frac{(1-R)}{R_{loss} + (1-R)} P' \tag{B. 4}$$

And we have:

$$P' = \frac{\varepsilon \cdot \Phi A \cdot c \cdot h\nu}{2} = \frac{\Phi A \cdot h\nu \cdot L}{\tau} \tag{B. 5}$$

Correspondingly, the inversion population density n, is replaced by the energy E', stored in the form of inversion in the laser medium within the interaction volume A × l:

It is given by:

$$E' = n \cdot Al \cdot h\nu \tag{B. 6}$$

In place of the original equations, we have now:

$$\frac{dP'}{dt} = E' P' C - \frac{P'}{\tau} \tag{B.7}$$

$$\frac{dE'}{dt} = -E' P' C\tau \tag{B.8}$$

Where the "coupling factor" C, is given by:

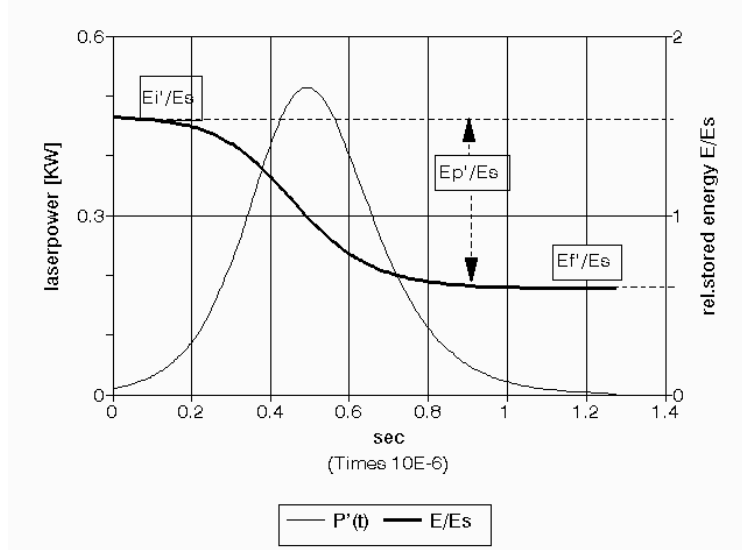$$C = \frac{c\sigma}{AL \cdot h\nu} \tag{B.9}$$

Figure B.1: Increase of the laser power and decrease of the stored energy according to coupled Equations B.7 and B.8.

At the start of the pulse the inversion is at its maximum, and the stored energy has a certain starting value, E'_i. After opening of the Q-switch the pulse swells, and more and more of the stored inversion energy is converted to laser energy. E' decreases continuously because the pumping during the pulse can be neglected. At the peak of the pulse, E' has reached the steady-state value E'_s, as the derivative of P' is zero (in both cases). We have there:

$$E' \xrightarrow{\frac{dP'}{dt}=0} E'_s = \frac{1}{C\tau} \tag{B.10}$$

After this moment the stored inversion energy drops below the steady state value, and the optical amplification cannot compensate the resonator losses any longer. The slope of the pulse becomes negative.

From a division of Equation B.7 by Equation B.8, we obtain the relation:

$$\tau \frac{dP'}{dE'} = -(1 - \frac{E'_s}{E'(t)}) \tag{B.11}$$

This can be integrated to:

$$\frac{\tau P'(t)}{E'_s} = [\frac{E'_i}{E'_s} - \ln(\frac{E'_i}{E'_s})] - [\frac{E'(t)}{E'_s} - \ln(\frac{E'(t)}{E'_s})] \tag{B.12}$$

At the maximum of the pulse, where $E' = E'_s$, we have:

$$\frac{\tau P'_{max}}{E'_s} = [\frac{E'_i}{E'_s} - \ln(\frac{E'_i}{E'_s})] - 1 \tag{B.13}$$

At the end of the pulse, E' has reached its final value E'_f, and we have (because of P'=0):

$$[\frac{E'_i}{E'_s} - \ln(\frac{E'_i}{E'_s})] = [\frac{E_f'}{E'_s} - \ln(\frac{E'_f}{E'_s})] \tag{B.14}$$

The total energy converted to "intrinsic" laser pulse energy E'_p is then the difference between the initial and the final values of E':

$$E'_p = E'_i - E'_f \tag{B.15}$$

Again, a small part of E'_p is lost by intrinsic resonator losses, but the predominant part can be measured as useful laser pulse energy E_p:

$$E_p = \frac{(1-R)}{R_{loss} + (1-R)} E'_p \tag{B.16}$$

With Equation B.15, we can substitute E'_f in Equation B.14 and obtain a relation for the starting value E'_i. As function of the (normalized) pulse energy E'_p / E'_s only:

$$\frac{E'_i - E'_f}{E'_s} = \frac{E'_p}{E'_s} = \ln(\frac{E'_i}{E'_i - E'_p}) \text{ or} \tag{B.17}$$

$$\frac{E'_i}{E'_s} = \frac{E'_p}{E'_s} \frac{1}{1 - \exp(-\frac{E'_p}{E'_s})} \tag{B.18}$$

B.3   Prediction of a pulse shape.

With the knowledge of the numerical values of the constants C and τ, and the starting value E'_i as a function of the desired pulse energy E_p by Equation B.16 and Equation B.18, we can now

perform a numerical integration of Equations B.7 and B.8. The following numerical constants have to be used:

Table B.1: Constants for the prediction of the pulse shape.

cross-section	σ:	$6.5 \cdot 10^{-19}\,\mathrm{cm}^2$
outcoupling mirror	R:	10 %
resonator loss	R_{loss}:	0.8 %
length of resonator	*L*:	103 cm
beam diameter (21A)	d:	1.5 mm

This prediction of the pulse shape is surprisingly accurate, as is shown in the comparison with real, measured pulses in Figure B.2. This comparison shows the measured and the predicted pulse shapes for pulses at 21A and at 10 kHz (0.552 mJ), 15 kHz (0.368 mJ), and 25 kHz (0.258 mJ). The only inputs for the theory are the parameters in Table B.1 and the pulse energies after the laser.
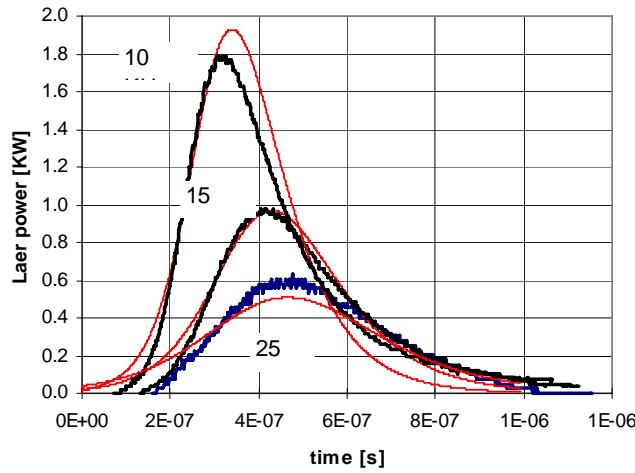
Figure B.2: Measured and (smooth lines) predicted pulse shapes for 21A and 10 kHz, 15 kHz, and 25 kHz.

To obtain an analytical expression for t_p, we can now substitute $E_i^{'}$ by $E_p^{'}$ in Equation B.13 for $P_{max}^{'}$ and obtain, with $x = \dfrac{E'_p}{E'_s}$:

$$\tau \frac{P'_{max}}{E'_p} = \tau \frac{P_{max}}{E_p} = \frac{1}{1-\exp(-x)} - \frac{1}{x}\ln(\frac{1}{1-\exp(-x)}) - \frac{1}{x} \approx \frac{1}{8}x(1-\frac{x^2}{72}+.....)$$

(B.19)

Neglecting higher order terms of x, the result is:

$$\frac{P_{max}}{E_p} \approx \frac{E'_p}{8\tau E'_s} = \frac{E'_p C}{8} = E_p (\frac{1 - R + R_{loss}}{1 - R}) \cdot \frac{c\sigma}{8h\nu} \cdot \frac{1}{AL} \tag{B.20}$$

If we take the ratio E_p / P_{max} as an approximate measure for the temporal pulse width t_p, we end up with the statement:

$$E_p \cdot t_p \approx (\frac{1 - R}{1 - R + R_{loss}}) \cdot \frac{8h\nu}{c\sigma} \cdot A \cdot L \tag{B.21}$$

This means that pulses with higher energy are proportionally shorter, and that the product of pulse energy and pulse time is basically constant for a Q-switched Nd:YAG laser with a given resonator, and can be predicted from first principles. The product depends only weakly on the mirror transmission (as long as $(1-R) \gg R_{loss}$) and the laser-current settings (which influence the value of A via the thermal lens effect).

$$t_p \approx C_{laser} \cdot \frac{1}{E_p} \tag{B.22}$$

Where the factor C_{laser}, is given by:

$$C_{laser} \approx (\frac{1 - R}{1 - R + \xi}) \cdot \frac{8h\nu}{c\sigma} \cdot A \cdot L \tag{B.23}$$

Under these conditions the pulse width t_p variation is directly related to the laser pulse energy E_p variation.

B.4   Thermal effects on temporal pulse shape.

If the resonator losses are much smaller than the outcoupling losses ($(1-R) \gg R_{loss}$) Equation B.23 will reduce to:

$$C_{laser} \approx \frac{8h\nu}{c\sigma} \cdot A \cdot L \tag{B.24}$$

The Equation B.4 will be almost one. The "intrinsic" laser power P' will be equal to the measured laser power. The cross-section (σ) is for a specific transition constant. Thus the laser constant can only change by either a change in the optical resonator length (L) or a decrease or increase of the transversal area (A). This change in the transversal area can be done by thermal lensing.

If a laser shows a single line with respect to Equation B.23 than the thermal lensing is constant. Some thermal lensing could still be there but will not have an effect on the performance during production. If the complete operational area of a laser system is characterized by a single curve no change in thermal lensing will have an effect on the production. If however the thermal lensing changes during the characterization due to different energy levels a shift of the line will be visible. The amount of line shift can be used to get an idea of the amount of change in thermal

lensing. A laser system with a high level of thermal lensing (broad range of possible combinations) will need more experiments for a good characterization.

The effect of the temperature on the resonator losses is still unclear. The effect on the optical resonator length is very small (YAG, $Y_3Al_5O_{12}$, $dN_r /dT = 7.3$ $10-6$ /°C, N_r ,(Ifflaender 1990).

Appendix C Material properties

C.1   Materials

Group	Description	Name
Polyolefins	PE	Polyethylene
	LDPE	Low density polyethylene
	HDPE	High density polyethylene
	PP	Polypropylene
	PIB	Polyisobuthylene
	PMP	Polymethylpentene
	PES	Polyethersulfone
	COC	Cyclic Olefin co-polymer
	COP	Cyclic Olefin polymer
Styrene Polymers	PS	Polystyrene
	ABS	Acrylonitrile/butadiene/styrene copolymer
	SAN	Styrene-acrylonitrile copolymer
	ASA	Acrylonitrile/styrene/acrylate copolymer
Halogen-containing Homopolymers	PVC	Polyvinylchloride
	PTFE	Polytetrafluorethylene (Teflon)
	ETFE	Ethylene-tetrafluorethylene
Poly(meth)acrylates	PMMA	Polymethylmethacrylate (Plexiglas)
Heteropolymers	POM	Polyoxymethylene
	PPE_{mod}	Polyphenyleneether modification
	PC	Polycarbonate

PA		Polyamides (Nylon)
PBT		Polybutylene terephthalate
PI		Polyimides (Kapton)
PET		Polyethylene terephthalate
PEN		Polyethylene naphthalate
PPS		Polyphenylene Sulfide
PEEK		Polyetheretherketone
Polyamide	PA 6	Nylon 6
	PA4/6	Nylon4/6 (stanyl,dsm)
Silicones	SI	Silicone rubber

C.2   Material properties

Table C.2: Material properties.

Property	PE	LDPE	HDPE
ρ [g/cm3]	0.89 – 0.93	0.92	0.95
c_p [J/gK]	1.84	1.9	2.2
α [cm-1] ($\delta_0 = \alpha^{-1}$)	6.73$^{(10.6\ \mu m)}$		
k [W/cmK] Conductivity	0.0034	0.0033	0.0045-0.0052
a [cm2/s] diffusivity	0.0021	0.0019	0.0025
Tdecomp oxidative	335- 450		
refractive index	1.49	1.51	1.54
LOI	17	17	17
Crys. / amorphous	C		

	SAN	PS	PES	PMP	PIB	PB	PP	
ρ [g/cm3]	1.08	1.04 – 1.08	1.37	0.83	0.92	0.90	0.85 – 0.92	ρ [g/cm3]
c_p [J/gK]	1.7	1.21 / 1.8	1	2	1.948	1.8	1.926	c_p [J/gK]
α [cm-1] ($\delta_0=\alpha^{-1}$)	0.42	$77.4^{(10.6\ \mu m)}$ / 1.43					$0.847^{(vis)}$ / $24.3^{(10.6\mu m)}$	α [cm-1] ($\delta_0=\alpha^{-1}$)
k [W/cmK] Conductivity	0.0014	0.00142	0.0013-0.0018	0.0017	0.0052	0.002	0.00117	k [W/cmK] Conductivity
a [cm2/s] diffusivity		0.001118					0.000677	a [cm2/s] diffusivity
Tdecomp oxydative		360 / 300 - 400					435 / 328 - 410	Tdecomp oxidative
refractive index		1.591	1.65	1.463			1.49	refractive index
LOI		19	34-41	17		<23	18	LOI
Crys./amorphous			A	A			C	Crys./amorphous

	POM	PMMA	ETFE	PTFE	PVC	ASA	ABS	
ρ [g/cm3]	1.41 – 1.43	1.16 – 1.20	1.7	2.15	1.39	1.04	1.04 – 1.06	ρ [g/cm3]
c_p [J/gK]	1.5	1.42	1.05	1.4	0.95	1.3	1.4	c_p [J/gK]
α [cm-1] ($\delta_0 = \alpha^{-1}$)		2.72 0.336					1.42 3.12	α [cm-1] ($\delta_0 = \alpha^{-1}$)
k [W/cmK] Conductivity	0.0022-0.0024	0.0019	0.0024	0.0019 0.0025	0.0016	0.0018	0.0025	k [W/cmK] Conductivity
a [cm2/s] diffusivity		0.0012		0.002067	0.001212		0.001717	a [cm2/s] diffusivity
Tdecomp oxydative	222			600 - 700	200 - 300			Tdecomp oxydative
refractive index		1.490		1.35	1.539			refractive index
LOI	15	17-20		95	47		19	LOI
Crys. / amorphous	C	A		C	C	C	C	Crys. / amorphous

	PBT	PA 12	PA 11	PA 6.6	PA 6	**PC**	PPE$_{mod}$	
ρ [g/cm3]	1.35	1.02	1.04	1.14	1.13	1.2 – 1.22	1.06	ρ [g/cm3]
c_p [J/gK]	2	1	2	1.70	1.6	1.2-1.4	1.40	c_p [J/gK]
α [cm-1] ($\delta_0=\alpha^{-1}$)						1.33-2.23 0.48		α [cm-1] ($\delta_0=\alpha^{-1}$)
k [W/cmK] Conductivity	0.0022	0.003	0.003	0.0025	0.0024-0.0028	0.0021 0.0019 -	0.0023	k [W/cmK] Conductivity
a [cm2/s] diffusivity						0.00125		a [cm2/s] diffusivity
Tdecomp oxydative								Tdecomp oxydative
refractive index				1.53	1.53	1.59		refractive index
LOI	19	21	22	23	25	27		LOI
Crys./ amorphous	A	C	C	C	C	A	C	Crys./ amorphous

	SI	PEEK	PPS	PEN	PET	PI
ρ [g/cm3]	1.8-1.9	1.45	1.35	1.36	1.34 – 1.41	1.42
c_p [J/gK]	0.8-0.9	2.16	1[(11)]		1.13	1.09
α [cm-1] ($\delta_0=\alpha^{-1}$)					1.56	
k [W/cmK] Conductivity	0.003 - 0.004	0.0025	0.003	0.0021	0.0037 0.0015-	0.0016 0.0010-
a [cm2/s] diffusivity					0.00143	0.001174
Tdecomp oxydative						
refractive index					1.58 - 1.64	1.66
LOI					21	53
Crys./amorphous				A	A	

Sources:
Simple methods for Identification of Plastics, Dietrich Braun.
Modern Organic chemistry, John D. Roberts
Goodfellow, material suppliers www.goodfellow.com

C.3   Absorption coefficients polymers.

Table C.3: Absorption coefficient α [cm⁻¹] for standard wavelengths.

	351 nm	532 nm	1064 nm	1600 nm	1908 nm
PE (red dye)	23.81	14.80	5.38	3.30	4.81
PES	20.00	3.55	0.61	0.69	1.42
PS	3.65	0.79	0.70	0.84	1.98
ABS	17.40	1.17	0.74	0.85	2.42
SAN	5.02	1.66	0.82	1.06	2.25
PMMA	0.50	0.38	0.39	0.75	4.2
PC	1.65	0.82	0.70	0.90	1.85
PET	4.86	0.81	0.61	0.90	3.78

C.3.1   PE

PE Norsolor
Including red dye
Thickness sample 2 mm
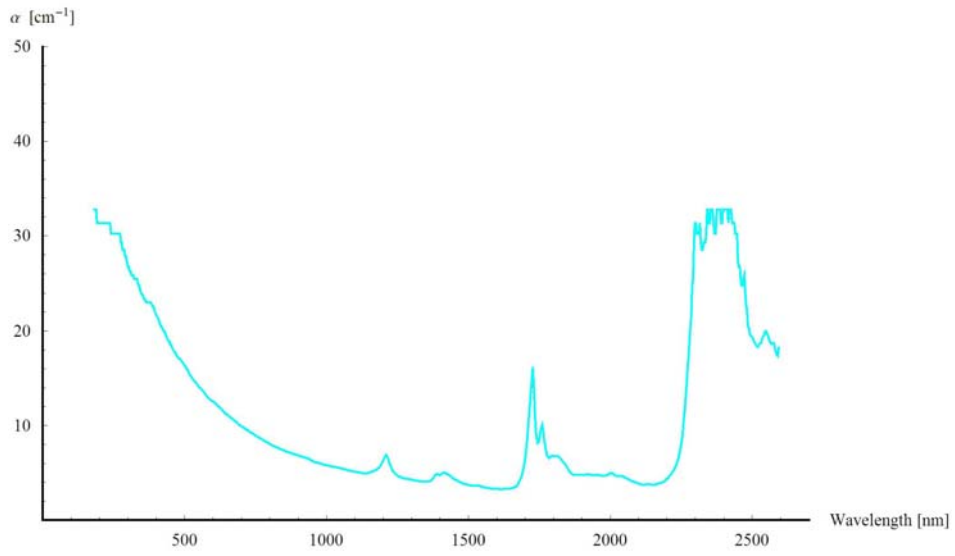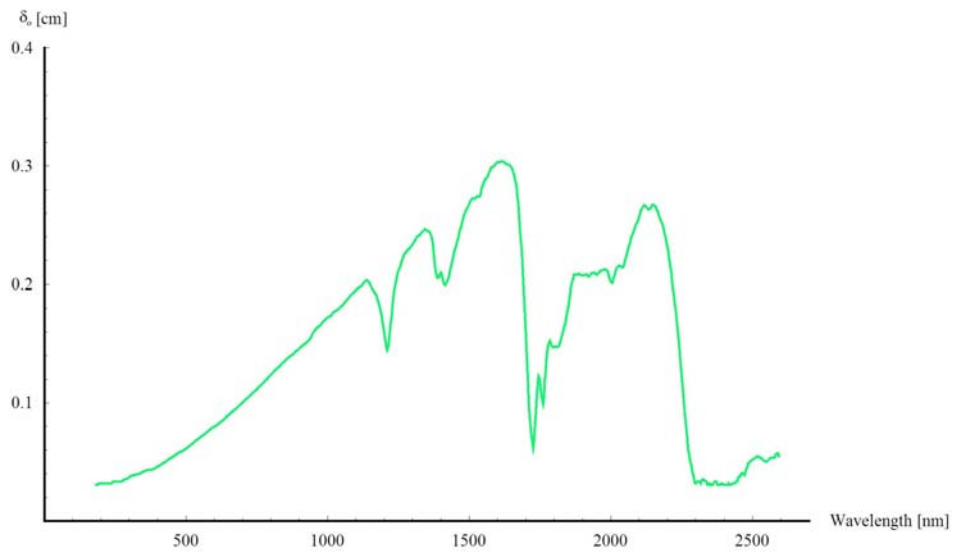

Figure C.1: Absorption coefficient PE.

Figure C.2: Optical penetration depth PE.

C.3.2 PES

Victrex PES
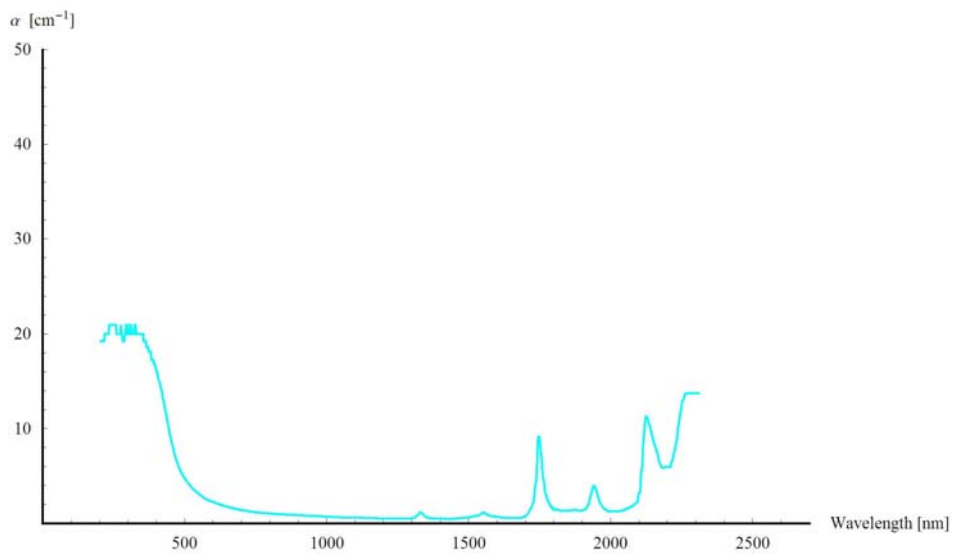Transparent
Thickness sample 3 mm

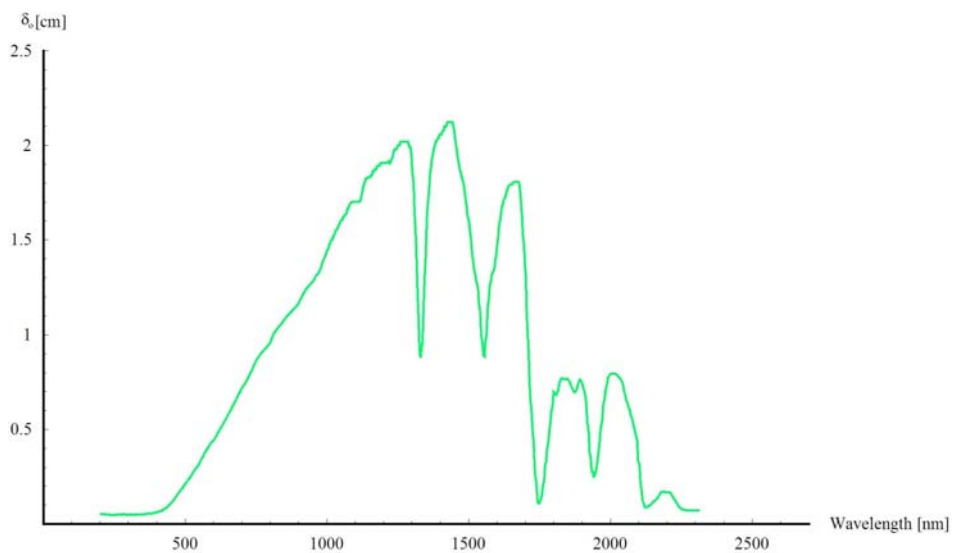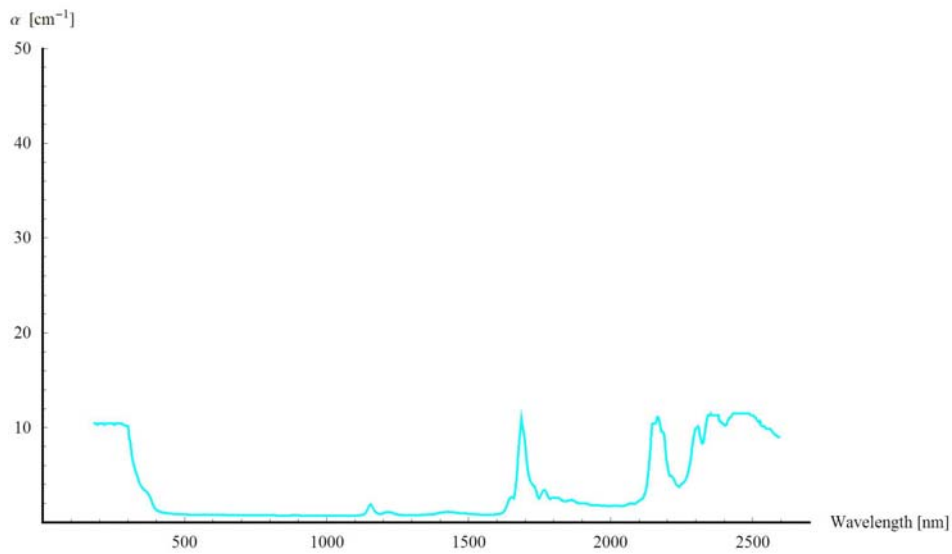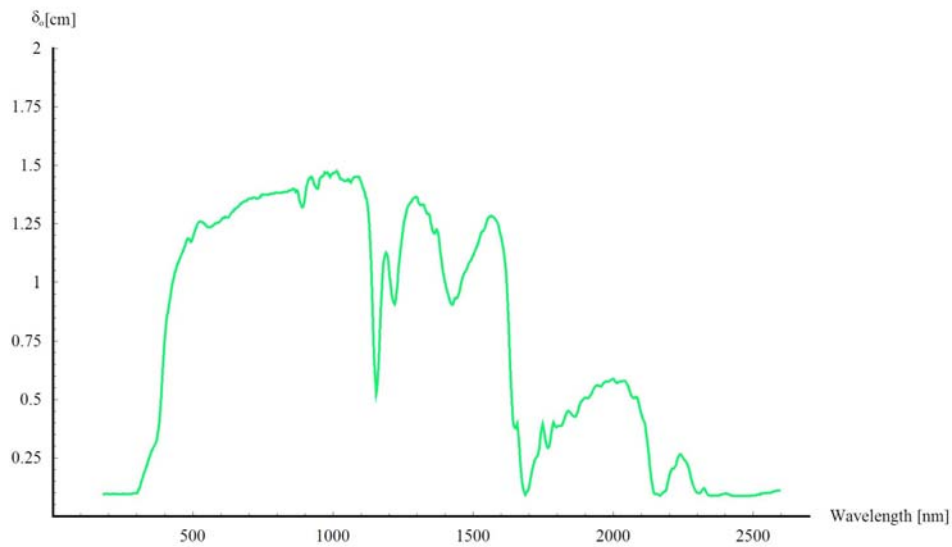*Figure C.3: Absorption coefficient PES.*

Figure C.4: Optical penetration depth PES.

C.3.3   PS

BASF PS
Transparent
Thickness sample 4.1 mm

Figure C.5: Absorption coefficient PS.

Figure C.6: Optical penetration depth PS.
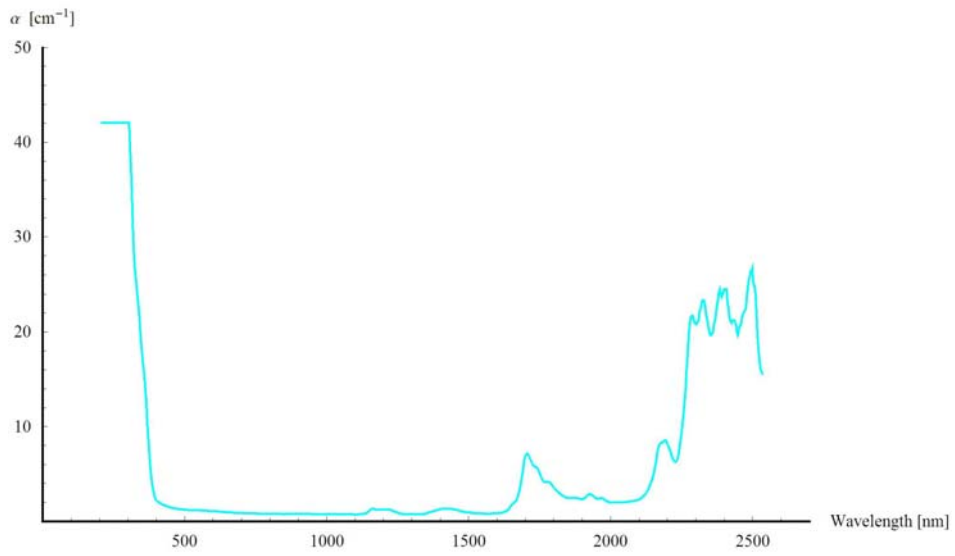
C.3.4   ABS

BASF Terluran 2802 TR
Thickness sample 1.5 mm

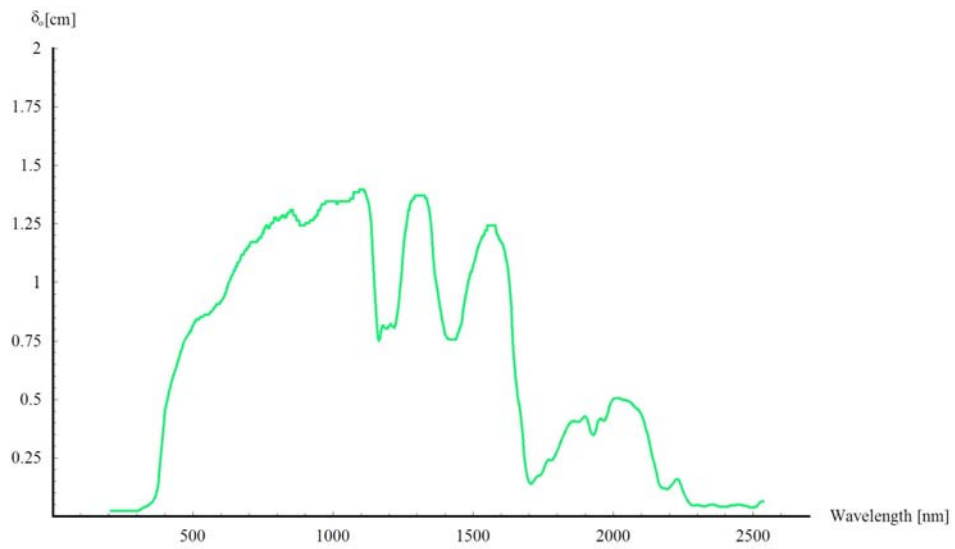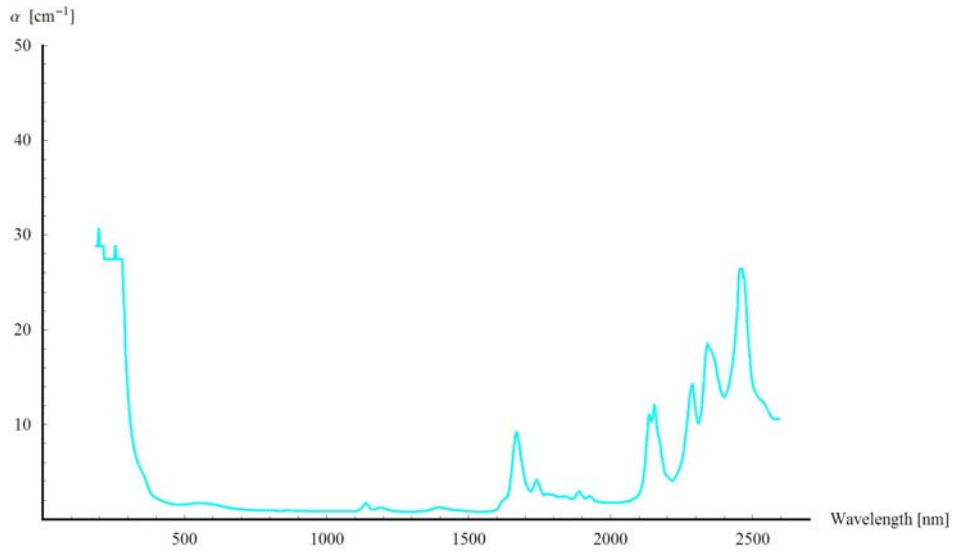*Figure C.7: Absorption coefficient ABS.*

Figure C.7: Optical penetration depth ABS.

C.3.5 SAN

BASF SAN
Thickness sample 2.1 mm

Figure C.8: Absorption coefficient SAN.

Figure C.9: Optical penetration depth SAN.

C.3.6 PMMA

PMMA Rohm
Thickness sample 4.1 mm

Figure C.10: Absorption coefficient PMMA.

Figure C.11: Optical penetration depth PMMA.

C.3.7   PC

PC BAYER
Thickness sample 2.0 mm

Figure C.12: Absorption coefficient PC.

Figure C.13: Optical penetration depth PC.

C.3.8 PET

PET AKZO
Thickness sample 4.1 mm
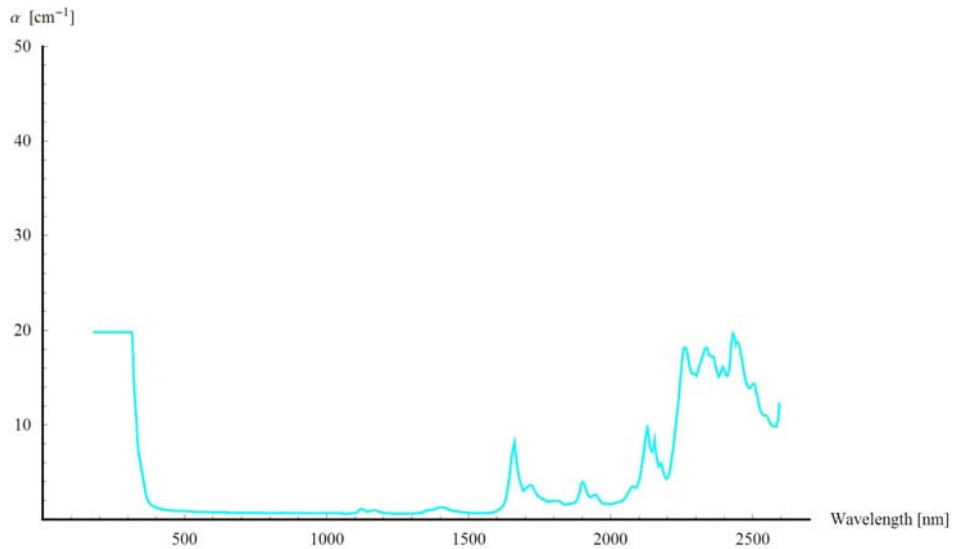
Figure C.14: Absorption coefficient PET.
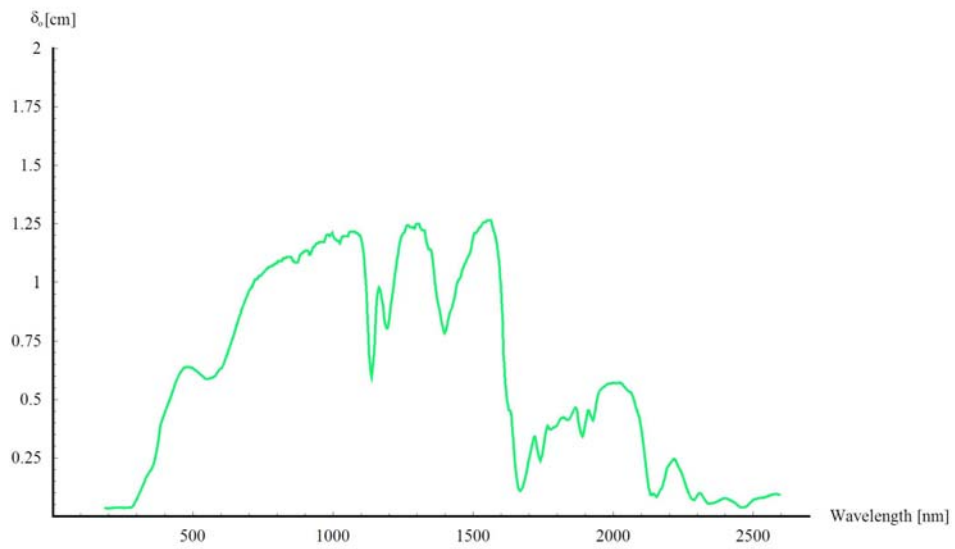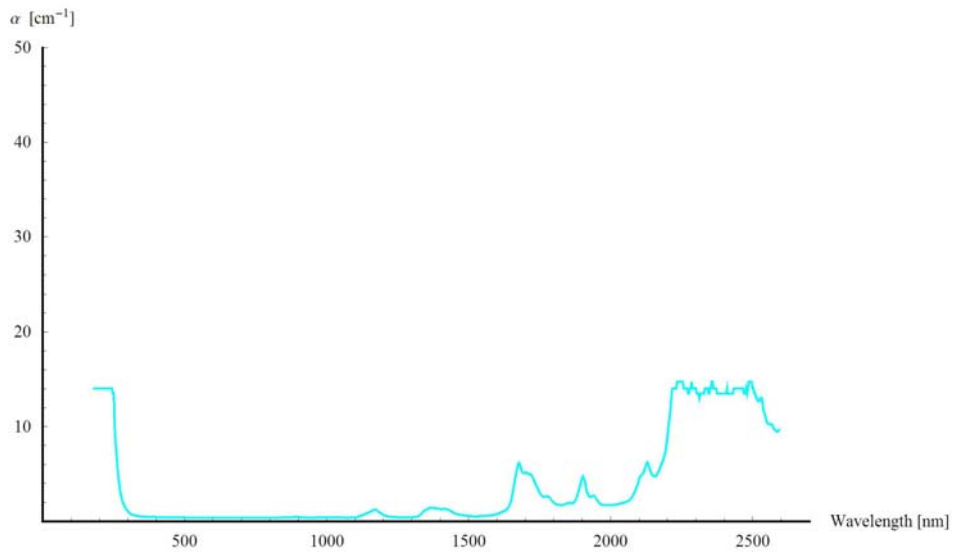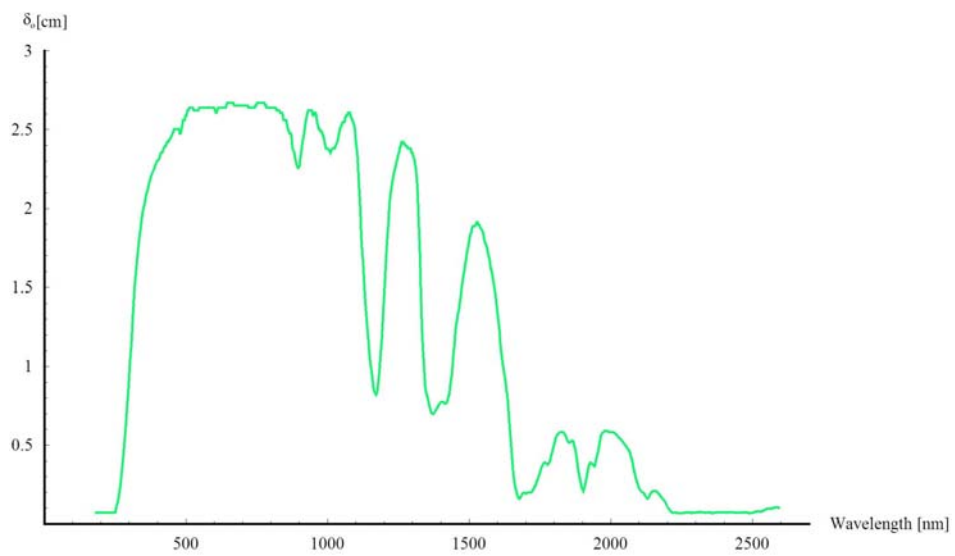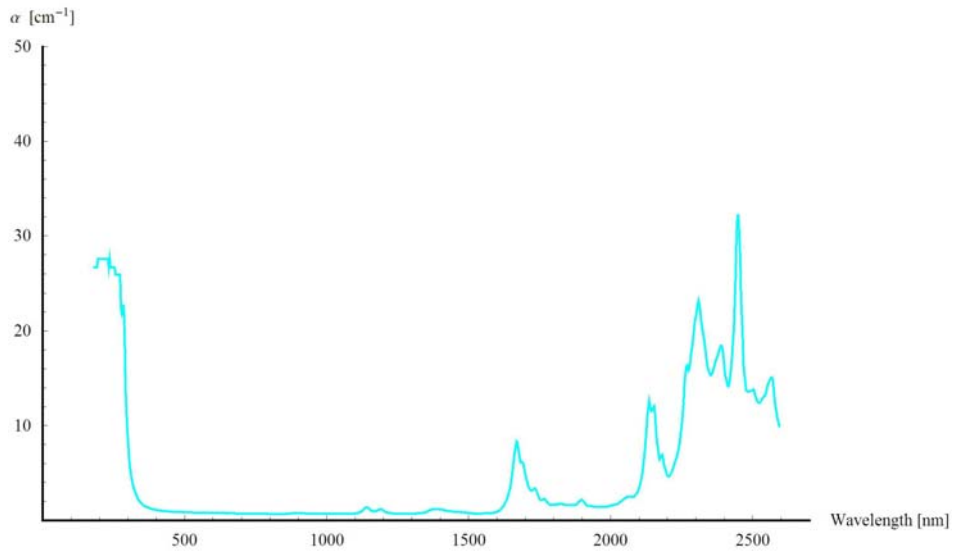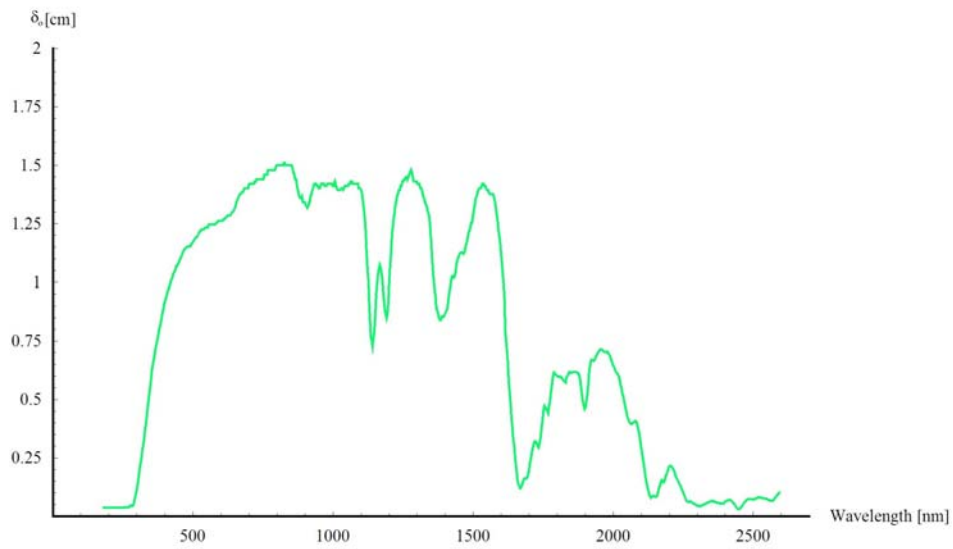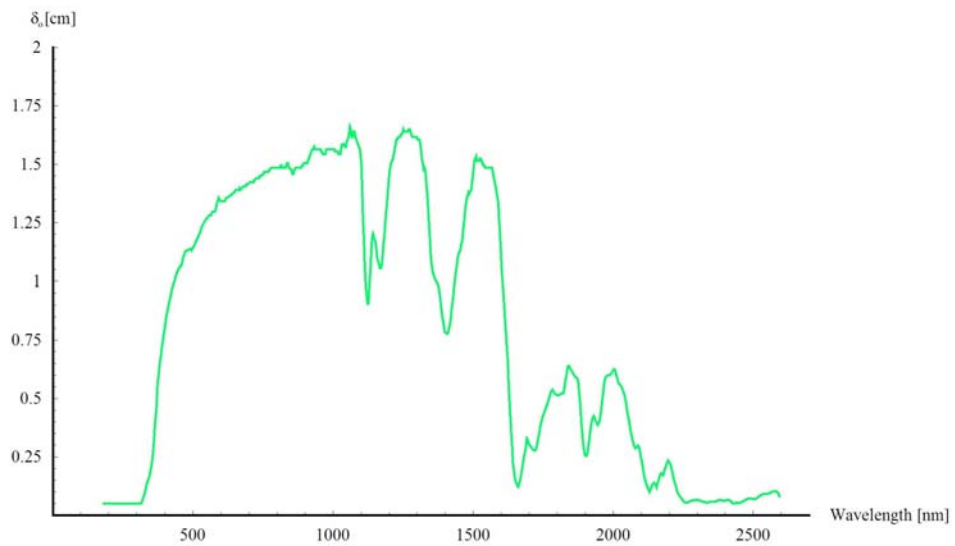

Figure C.15: Optical penetration depth PET.

C.4   Material properties ABS Chapter 6
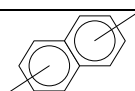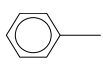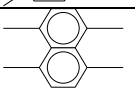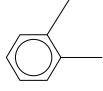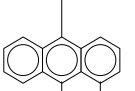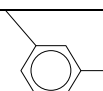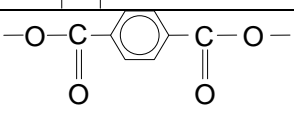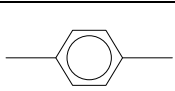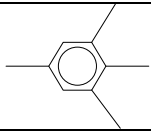
Table C.4: Pigment weight percentages of the ABS samples used in bleach experiment Chapter 6.

Plate	Cromophtal Yellow HRP	Cinquasia magenta RT-235D	Cromophtal blue 4GNP	TiO_2 (301)	Lithopoon D-S	ABS FG-50
1	0	0	0	0	0	100
2	0	0	0	2.5	0	97.5
3	0	0	0	0	3.75	96.25
4	0.05	0	0	0	0	99.95
5	0.05	0	0	2.5	0	97.45
6	0.05	0	0	0	3.75	96.2
7	0	0.05	0	0	0	99.95
8	0	0.05	0	2.5	0	97.45
9	0	0.05	0	0	3.75	96.2
10	0	0	0.05	0	0	99.95
11	0	0	0.05	2.5	0	97.45
12	0	0	0.05	0	3.75	96.2
13	0.05	0.05	0.05	2.5	0	97.35
14	0.1	0.05	0.05	2.5	0	97.3
15	0.2	0.1	0.1	2.5	0	97.1
16	0.05	0.05	0.05	0	3.75	96.1
17	0.1	0.05	0.05	0	3.75	96.05
18	0.2	0.1	0.1	0	3.75	95.85
19	0.05	0.05	0.05	0	0	99.85
20	0.1	0.05	0.05	0	0	99.8
21	0.2	0.1	0.1	0	0	99.6

C.5 CFT calculation

The char forming tendency of van Krevelen can be used if a material can degrade thermally into a carbonized structure. The CFT value is a statistical concept. If the CFT factor of a phenyl group is 1 it means that on the average only 1 out of 6 carbons ends up in the char residue. The other five carbons go into tar and gas. For example, the pyrolysis of polycarbonate gives a CFT value of 5, with a molecular weight of 254.3, the char residue will be 5 x 12g (1 mol carbon) = 60 g/ mol carbonate, which is 24%. Compared to POM (polyoxymethyleen) the CFT index is 0. No char forming is observed.

Table C.5: CFT calculation, without heterocyclic groups.

Group	CFT equivalent	Group	CFT equivalent
-CHOH	1/3		
All other aliphatic group without halogen	0		6
	1		10
	2		14
	3		1.25
	4		
	5		
Corrections due to disproportioning (H-shift): groups directly connected to aromatic nucleus			
$=CH_2$ and $=CH- CH_2$	-1		
- CH_3	-1.5		
$=C(CH_3)_2$	-3		
-$CH(CH_3)_2$	-4		

Appendix D Readability and scan speed tests.

D.1   Human readability test.

To test the readability of a code setup can be made using the similarity table. From this table different combinations can be used together with the three standard distributions, see Table D.1. This can be marked and shown to a human observer. The amount of failure readouts and non readouts can be used to optimize the speed and intensity of the laser process. The failure readouts are considered more dangerous than non readouts. But both are unacceptable.

Table D.:1 Readability test 5S.

Distribution	
Random	5SS55SS55S5S
Hidden	1234S67890
	TEXTTE5T
Uniform	5555S55555S5555
	SSS5SSSS5SSSSS
	5555555SSSSSSSS
	SSSSSS555555555

Table D.2: Similarity table.

Number					
1.	5	S			
2.	1	l	7	I	T
3.	0	O			
4.	U	V	W		
5.	6	b			
6.	8	B			
7.	N	M			
8.	9	g			
9.	0	Q			

D.2   Marking speed and scanner perfomance.

The marking speed is determined by the maximum speed a scanner can achieve. This maximum is dependent on the frequency bandwidth vs. the amplitude of the rotation of the scanner mirror and motor. Some suppliers don't publish these amplitude frequency characteristics. By testing a single motor these values can be measured. But still the translation to characters per second has to be done. Another approach is writing the desired patterns at different speeds and different amplitudes. The laser mark can be used to measure the performance of the scanner. At a frequency of 10 kHz the time interval between two pulses is 0.1 ms. To get an indication of the performance of the scanner a circle pattern can be written and measured afterwards. Also the total time of one mark can be measured and is often available in the standard software. Writing 100 circles with the same diameter results in an average time. When plotted we can see that the time doesn't have a linear relationship with speed. From this measurement we can calculate the real marking speed as a function of the amplitude and scan frequency.

D.3   Marking speed and characters per second.

Marking speed is often given in characters per second. All manufacturers have their own test. They all mention a number of characters per second together with the height of the character (1 or 2 mm).

To come to a more uniform test method a standard alphabet is combined with the human readability test of D.1. This ensures readable characters.

Four different standard patterns can be defined. The alphabet pattern which is the normal standard alphabet sequence repeated a number of times. For some application also numbers in combination with letters are used. For applications with only numbers the use of the number sequence is the best choice. In normal text not all letters are used in equal numbers. To have a more natural distribution a standard letter distribution for English texts can be used. From a large standard text a distribution is calculated and used to create a new list with the same character distribution. These smaller and constructed lists can be used for the tests.

Table D.3 Standard patterns

Pattern	Alphabet	abcdefghijklmnopqrstuvwxyz
	Alphabeth + numbers	abcdefghijklmnopqrstuvwxyz0123456789
	Numbers	0123456789
	Standard text distribution	Generated from a standard text distribution
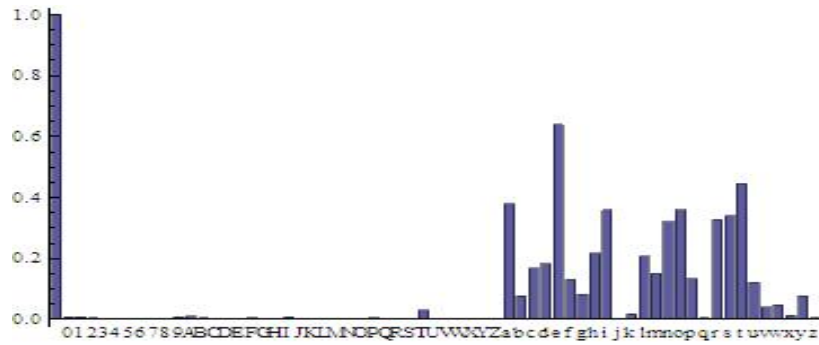
Figure D.1 Character distribution histogram extracted from part of this Thesis.

The character distribution can be extracted from a text. Table D.4. show the character distribution of a large part of this thesis. This distribution can be used to calculate the maximum amount of characters per second by measuring the amount of time it takes to write all characters.

Table D.4 Text character distribution % extracted from part of this thesis.

space	*16.662*		
a	*6.340*	*A*	*0.164*
b	*1.271*	*B*	*0.084*
c	*2.804*	*C*	*0.065*
d	*3.046*	*D*	*0.045*
e	*10.648*	*E*	*0.045*
f	*2.184*	*F*	*0.110*
g	*1.371*	*G*	*0.026*
h	*3.607*	*H*	*0.032*
i	*5.979*	*I*	*0.142*
j	*0.039*	*J*	*0.003*
k	*0.316*	*K*	*0.019*
l	*3.459*	*L*	*0.048*
m	*2.523*	*M*	*0.052*
n	*5.353*	*N*	*0.019*
o	*5.995*	*O*	*0.035*
p	*2.233*	*P*	*0.100*
q	*0.084*	*Q*	*0.006*
r	*5.476*	*R*	*0.023*
s	*5.672*	*S*	*0.052*
t	*7.418*	*T*	*0.510*
u	*2.039*	*U*	*0.026*
v	*0.665*	*V*	*0.026*
w	*0.774*	*W*	*0.029*
x	*0.216*	*X*	*0.006*
y	*1.281*	*Y*	*0.003*
z	*0.087*	*Z*	*0.003*

D.4   Standard alphabet and numbers

The text examples made in Chapter 4 uses a standard font (simple straight 2) from the SAM light program of SCAPS. This program is delivered with a few standard fonts. The definition of these fonts is published and based on the HPGL standard used for pen plotter systems. This simple language is effective for describing vector oriented patterns. SP1;PU defines a start of a sequence with pen up (PU). PD is pen down and PA is the absolute movement to a position. The area in which the character is placed is a square of 8000 x 8000 units. SI[AW][LSB],defines the position of the advanced width (AW) and the left side bearing (LSB). The baseline information is given in the third line of the file.

Simple straight 2 definition of the numbers 0 – 9:

```
// SCAPS FONT FILE
// VERSION 2.0
// BASELINE 2000
//
// CHAR 48 (0)
SI4640,640;SP1;PU;PA3760,7040;PD;PA3040,6800,2560,6080,2320,4880,2320,4160,2560,2960
,3040,2240,3760,2000,4240,2000,4960,2240,5440,2960,5680,4160,5680,4880,5440,6080,4960,6
800,4240,7040,3760,7040;PU;
// CHAR 49 (1)
SI2480,640;SP1;PU;PA3400,6080;PD;PA3880,6320,4600,7040,4600,2000;PU;
// CHAR 50 (2)
SI4640,640;SP1;PU;PA2560,5840;PD;PA2560,6080,2800,6560,3040,6800,3520,7040,4480,7040
,4960,6800,5200,6560,5440,6080,5440,5600,5200,5120,4720,4400,2320,2000,5680,2000;PU;
// CHAR 51 (3)
SI4640,640;SP1;PU;PA2800,7040;PD;PA5440,7040,4000,5120,4720,5120,5200,4880,5440,4640
,5680,3920,5680,3440,5440,2720,4960,2240,4240,2000,3520,2000,2800,2240,2560,2480,2320,2
960;PU;
// CHAR 52 (4)
SI4880,640;SP1;PU;PA4600,7040;PD;PA2200,3680,5800,3680;PU;SP1;PU;PA4600,7040;PD;P
A4600,2000;PU;
// CHAR 53 (5)
SI4640,640;SP1;PU;PA5200,7040;PD;PA2800,7040,2560,4880,2800,5120,3520,5360,4240,5360
,4960,5120,5440,4640,5680,3920,5680,3440,5440,2720,4960,2240,4240,2000,3520,2000,2800,2
240,2560,2480,2320,2960;PU;
// CHAR 54 (6)
SI4400,640;SP1;PU;PA5320,6320;PD;PA5080,6800,4360,7040,3880,7040,3160,6800,2680,6080
,2440,4880,2440,3680,2680,2720,3160,2240,3880,2000,4120,2000,4840,2240,5320,2720,5560,3
440,5560,3680,5320,4400,4840,4880,4120,5120,3880,5120,3160,4880,2680,4400,2440,3680;PU
;
// CHAR 55 (7)
```

SI4640,640;SP1;PU;PA5680,7040;PD;PA3280,2000;PU;PA2320,7040;PD;PA5680,7040;PU;
// CHAR 56 (8)
SI4640,640;SP1;PU;PA3520,7040;PD;PA2800,6800,2560,6320,2560,5840,2800,5360,3280,5120
,4240,4880,4960,4640,5440,4160,5680,3680,5680,2960,5440,2480,5200,2240,4480,2000,3520,2
000,2800,2240,2560,2480,2320,2960,2320,3680,2560,4160,3040,4640,3760,4880,4720,5120,520
0,5360,5440,5840,5440,6320,5200,6800,4480,7040,3520,7040;PU;
// CHAR 57 (9)
SI4400,640;SP1;PU;PA5560,5360;PD;PA5320,4640,4840,4160,4120,3920,3880,3920,3160,4160
,2680,4640,2440,5360,2440,5600,2680,6320,3160,6800,3880,7040,4120,7040,4840,6800,5320,6
320,5560,5360,5560,4160,5320,2960,4840,2240,4120,2000,3640,2000,2920,2240,2680,2720;PU
;

Appendix E Colour theory

E.1   Colour systems

Colours can be made by mixing different coloured light sources or a coloured pigment in a polymer matrix. These two methods represent two complementary colour systems. The mixing of different coloured light sources is called the additive system. The spectras are added together to form a new light source. In case of a pigment the incident light is partially absorbed and partially reflected. A part of the spectrum is subtracted. Therefore it is called the subtractive system. This subtractive system is also valid for the use of filters. Figure E.1 shows clearly the use of the different colour systems. Adding a red, green and blue light a white light is formed. By using a cyan, magenta and yellow filter all light from a white source is absorbed. The difference between pigments and colour filters lies not in the colour system because both are subtractive but in the physical distribution. This can be illustrated by making black. With colour filters this is an easy task. The stack of a cyan, magenta and yellow filter will absorb all light from the light source. In case of pigments this can only be achieved by one black pigment. Using a set of pigments would always give some reflection. This reflection is the result of the random distribution of the pigments in the polymer matrix. A yellow photon has a certain chance of being reflected directly out of the polymer matrix by a yellow pigment. This chance is not zero and therefore the colour of the polymer will not be black but more likely brown or dark purple.
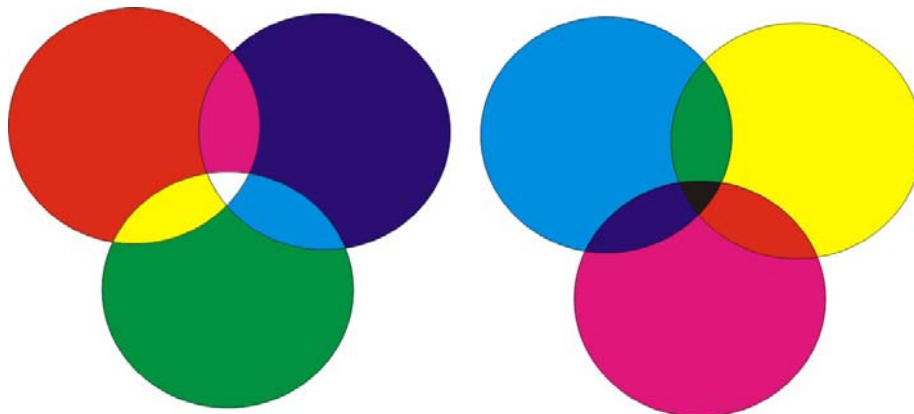

Figure E.1: Left, RGB additive (light sources). Right, CMY subtractive (filter colours).

Another example of the subtractive system is inkjet. It starts with a white paper and the inks acts as a filter; they absorb a small part of the visible spectrum. The light passes twice through these filters and the spectrum is altered according the combination of filters. If these filters are

constructed as Cyan, Magenta, and Yellow, all visible light can be filtered out. This gives the appearance of black. In reality it is difficult to get a real good black because inks are normally not exactly Cyan, Magenta, or Yellow. Small colour deviations turn the intended black into brown. This is the reason why a lot of ink-jet systems have an additional black. Black ink is also added to increase the speed. The use of pigments restricts the filter effect considerable. Filters are normally constructed using dye molecules. Dyes have a much better transmission than pigments.

E.2 Colour perception

There are three basic components of colour perception: the light source(s), the illuminated object, and the observer. All these three aspects are involved when we see a colour. If the light source is omitted no colour perception is possible. A change in light source will chance the colour perception as observed by the human observer. It is also true that different observers can have different perceptions about the colour of an illuminated object.
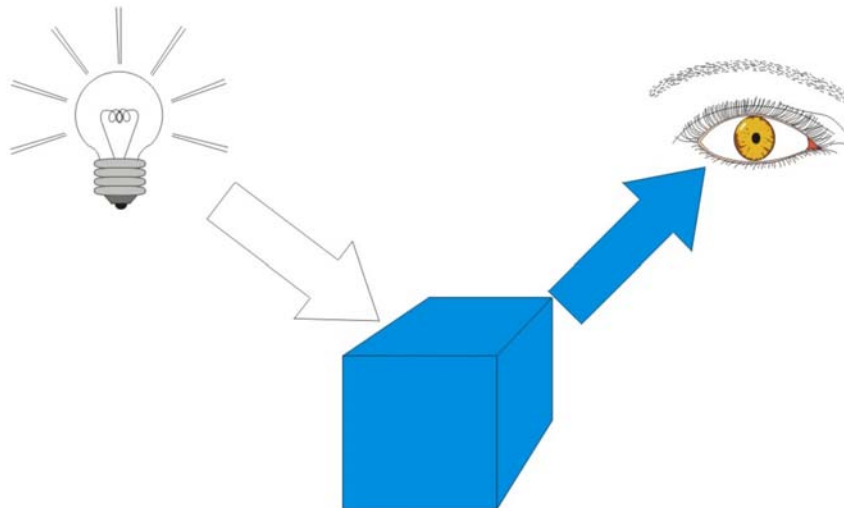
Figure E.2: The three aspects of vision (illumination, object and observer).

The retina is the light-sensitive surface of the eye. It is not uniform with respect to sensitivity over its area. Colour vision is limited to about 40 degree of the eye's axis. Outside this area the information gained is mainly used for detection of movement. The ability to have a sharp vision is limited to 1 degree of the diameter and has an offset of about 4 degrees to the eye's axis. This area of the retina is mainly covered with cones. There are three types of cones with different spectral sensitivity (r,g and b). Due to the different sensitivity the information gained from these three receptors is used for the colour perception. The rods are much more sensitive and are used for scoptopic (low level) vision. Compared to the photopic vision of the cones the scoptopic vision acts at luminances of less than one hundredths of candela per square meter (cd/m^2), while the photopic vision needs more than several candela per square meter.

The luminance level where both the contribution of the rods and cones is significant is called mesopic. By increasing the luminance level from scoptopic to photopic the average colour sensitivity of the eye chances from blue-green to red.

The colour discrimination is formed by the relative responses between the three different cones types where the intensity perception is formed by the strength of these signals. The focusing of an image on the retina is difficult because the lens is not corrected for chromatic aberration. The r and g cones have their maximum sensitive at 580 and 540 nm. The b cones have their maximum at 440 nm. Focusing at 560 nm gives a rather sharp image in the red and yellow region where the blue image is somewhat blurred. This is properly the reason why humans have a cone distribution ratio of 40:20 to 1 for r, g and b.
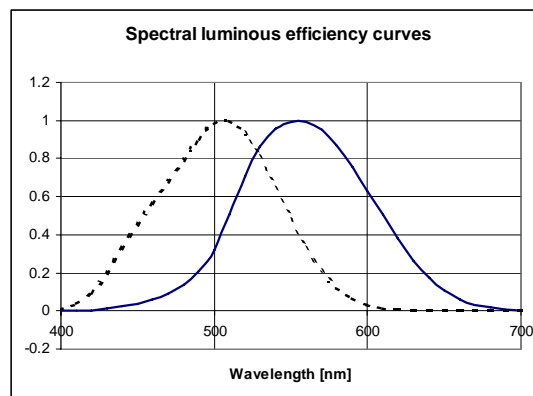
Figure E.3: The spectral luminous efficiency curves for scotopic vision (dashed, low luminance) and photopic vision (solid, high luminance).

The human vision has also a nonlinear response to brightness. Where brightness is defined by CIE as: "the attribute of a visual sensation according to which an area appears to exhibit more or less light". A source with a luminance of 18% of a reference source appears half as bright. All these aspects make our vision a rather complex system to model mathematically.

E.3   Colour measurement

Colour measurement is the translation of the spectral information to a colour coordinate system with respect to the human colour perception. The colour coordinate system presents the physical colours in a colour space. The horse shoe shaped diagram is one of the most known colour spaces. The x and y coordinates of this diagram are the result of the normalization of the XY values against the sum of the X,Y and Z values. The calculation of the XYZ values is defined as the summation of the power P in a small wavelength interval times the relative sensitive of the human eye for that wavelength interval. Because of the different sensitivity of the three types of cones, three colour matching functions are used. *k* is a constant to compensate for the intensity. The colour matching functions are defined by the CIE 1931 Standard Colourimetric Observer in 1931.

$$X = k \cdot \sum_{n=1}^{m} P_n \cdot \bar{x}(\lambda_n) \qquad\qquad\qquad\qquad (E.1)$$

$$Y = k \cdot \sum_{n=1}^{m} P_n \cdot \bar{y}(\lambda_n) \qquad\qquad\qquad\qquad (E.2)$$

$$Z = k \cdot \sum_{n=1}^{m} P_n \cdot \bar{z}(\lambda_n) \qquad\qquad\qquad\qquad (E.3)$$

With $\bar{x}, \bar{y}, \bar{z}$ the colour matching functions. The measurement is performed using an integrating sphere to measure the spectral distribution of the reflection from a sample illuminated by a standard light source. Two of these light sources are shown in Figure E.5. CIE standard illuminant A represents light from a radiator with temperature of 2856 K according to the Planck's radiation formula. Illuminant D65 is defined as natural daylight with a correlated colour temperature of 6504 K.
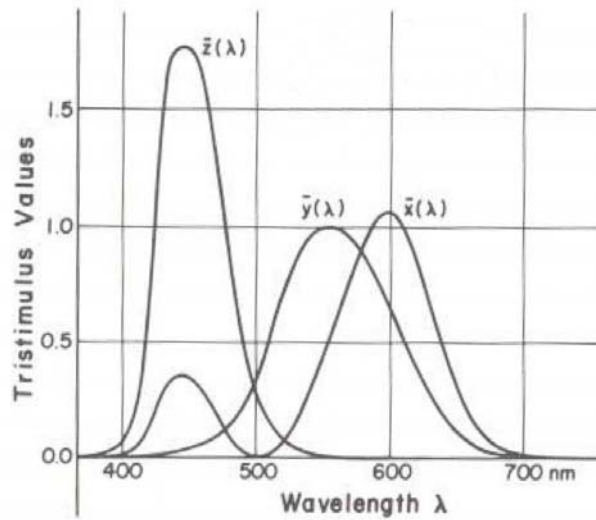
Figure E4: Colour matching functions

The transformation from X,Y, Z to *x ,y* reduces the three dimensions coming from the three cone types to a more practical 2D representation, see Equation E.4 and E.5.

$$x = \frac{X}{X + Y + Z} \qquad\qquad\qquad\qquad (E.4)$$

$$y = \frac{Y}{X + Y + Z} \qquad\qquad (E.5)$$

The main advantage of the horse diagram is that all physical colours are inside or on the boundary representing the monochromatic colours. It can be used to show graphically the combination of two colours, for example yellow (550 nm) and blue (470 nm) will give a white appearance. This is used in white leds using a phosphor to generate yellow from blue.
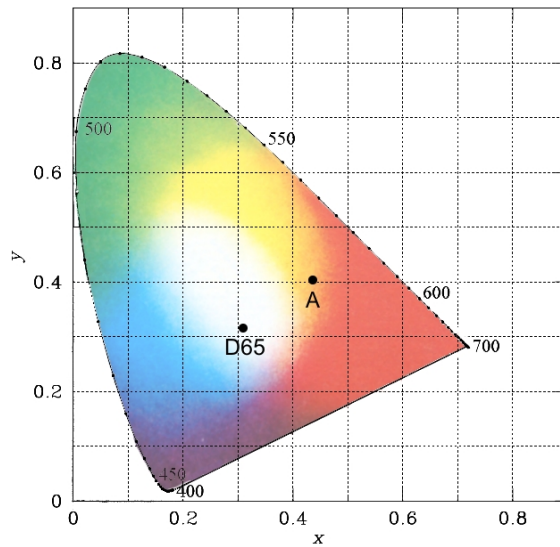
Figure E.5: Horse shoe shaped diagram.
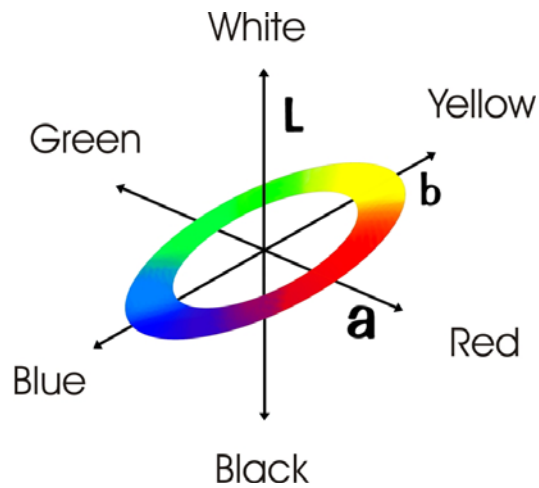
Figure E.6: CIELAB Lab colour space.

Another colour space is the Lab space. The Lab colour space has found its application field in the colour description of lacquers and polymers. The Lab colour space describes better the colour perception of human vision.

$$L^* = 116 \left(\frac{Y}{Y_n} \right)^{\frac{1}{3}} - 16 \qquad\qquad\qquad\qquad \text{(E.6)}$$

$$a^* = 500 \left(\left(\frac{X}{X_n} \right)^{\frac{1}{3}} - \left(\frac{Y}{Y_n} \right)^{\frac{1}{3}} \right) \qquad\qquad\qquad\qquad \text{(E.7)}$$

$$b^* = 500 \left(\left(\frac{Y}{Y_n} \right)^{\frac{1}{3}} - \left(\frac{Z}{Z_n} \right)^{\frac{1}{3}} \right) \qquad\qquad\qquad\qquad \text{(E.8)}$$

$$\text{DE}^* = \sqrt{ \left(\Delta L^* \right)^2 + \left(\Delta a^* \right)^2 + \left(\Delta b^* \right)^2 } \qquad\qquad\qquad\qquad \text{(E.9)}$$

The DE^* is defined to describe the amount of colour difference between two colours. The Lab colour space is defined for photopic vision ($Y / Y_n > 0.008856$). (Hunt 1987),(Voelz 1995),(science 1982),(Poyton 1997)

Appendix F 3D Thermal model

The thermal diffusion equation has no source term as t=0 is defined just after the pulse. This results in the thermal diffusion equation for an infinite space with the thermal diffusivity being a constant with respect to time, position and temperature:

$$\frac{\partial^2 T}{\partial x^2} + \frac{\partial^2 T}{\partial y^2} + \frac{\partial^2 T}{\partial z^2} = a^{-1}\frac{\partial T}{\partial t} \quad -\infty < x < \infty; -\infty < y < \infty; -\infty < z < \infty \quad \text{(E.1)}$$

The initial condition is given by the thermal balance just after the laser pulse:

$$T(x, y, z, 0) = f(x, y, z)$$

$$f(x, y, z) = \frac{\alpha F_0}{\rho c_p} \cdot e^{-z\alpha - \frac{2(x^2 + y^2)}{\omega^2}} \quad -\infty < x < \infty; -\infty < y < \infty; 0 \le z < \infty \quad \text{(E.2)}$$

Because the Fourier solution demands a continuous field the negative part of z has to be defined. Adding a temperature field preventing an energy flow across z=0 is often used. This is done by applying the same temperature field at the negative part mirrored at z=0. The complete temperature field becomes:

$$f(x, y, z) = \frac{\alpha F_0}{\rho c_p} \cdot e^{-|z|\alpha - \frac{2(x^2 + y^2)}{\omega^2}} \quad -\infty < x < \infty; -\infty < y < \infty; -\infty < z < \infty \quad \text{(E.3)}$$

The differential equation becomes written in the Fourier domain:

$$-(\xi^2 + \eta^2 + \varphi^2) \cdot T = a^{-1}\frac{\partial T}{\partial t} \quad\quad \text{(E.4)}$$

This can be re-arranged as:

$$\frac{\partial T}{\partial t} + a\ (\xi^2 + \eta^2 + \varphi^2)T = 0 \quad\quad \text{(E.5)}$$

The initial condition (E.2) transfers to the Fourier domain:

$$T(\xi,\eta,\varphi,0) = F(\xi,\eta,\varphi) \tag{E.6}$$

This gives the solution for T:

$$T(\xi,\eta,\varphi,t) = F(\xi,\eta,\varphi) \cdot e^{-a(\xi^2+\eta^2+\varphi^2)t} \tag{E.7}$$

This can be transformed to the time domain to yield the solution in this domain.

$$T(x,y,z,t) = F_{(3)}^{-1}\{F(\xi,\eta,\varphi) \cdot G(\xi,\eta,\varphi,t); x \to \xi, y \to \eta, z \to \varphi\} \tag{E.8}$$

Where:

$$G(\xi,\eta,\varphi,t) = e^{-a(\xi^2+\eta^2+\varphi^2)t} \tag{E.9}$$

The time domain representation of Equation E.9 becomes:

$$g(x,y,z,t) = (2\pi)^{-\frac{3}{2}} \int_{-\infty}^{\infty}\int_{-\infty}^{\infty}\int_{-\infty}^{\infty} G(\xi,\eta,\varphi) \cdot e^{-i(\xi x+\eta y+\varphi z)} d\xi d\eta d\varphi \tag{E.10}$$

or solved:

$$g(x,y,z,t) = \frac{e^{-\frac{x^2+y^2+z^2}{4at}}}{2\sqrt{2}(at)^{\frac{3}{2}}} \qquad -\infty < x < \infty; -\infty < y < \infty; -\infty < z < \infty \tag{E.11}$$

Using the convolution theorem the diffusion Equation E.8 is transformed to the time domain:

$$T(x,y,z,t) = (2\pi)^{-\frac{3}{2}} \int_{-\infty}^{\infty}\int_{-\infty}^{\infty}\int_{-\infty}^{\infty} f(x',y',z') \cdot g(x-x',y-y',z-z',t)\partial x'\partial y'\partial z' \tag{E.12}$$

Where :

$$f(x,y,z) = \frac{\alpha F_0}{\rho c_p} \cdot e^{-|z|\alpha - \frac{2(x^2+y^2)}{\omega^2}} \qquad -\infty < x < \infty; -\infty < y < \infty; -\infty < z < \infty \tag{E.13}$$

$$g(x,y,z,t) = \frac{e^{-\frac{x^2+y^2+z^2}{4at}}}{2\sqrt{2}(at)^{3/2}} \qquad -\infty < x < \infty; -\infty < y < \infty; -\infty < z < \infty \tag{E.14}$$

Using mathematica the equation for the temperature can be solved:

$$T(x, y, z, t) = \frac{\alpha \omega^2 F_0}{\rho c_p} \frac{-1}{2(8at + \omega^2)}$$

$$\left(e^{-z\alpha + at\alpha^2 - \frac{2(x^2 + y^2)}{8at + \omega^2}} \left(-2 + erfc\left(\tfrac{1}{2} \sqrt{\frac{1}{at}} (z - 2at\alpha) \right) - e^{2z\alpha} erfc\left(\tfrac{1}{2} \sqrt{\frac{1}{at}} (z + 2at\alpha) \right) \right) \right)$$

$$t > 0 \hspace{6cm} \text{(E.15)}$$

References

Adams, R., (2005), Barcode -1 2 Dimensional Bar Code Page,Internet page,

Agadjanov, V. V., 1971,"Method of making decorative articles", -, SU321422, 18-01-1972,

Arnold, N., N. Bityurin, et al. (1999). "Laser-induced thermal degradation and ablation of polymers." Appl. Surf. Sci. **138 - 139**: 212 -217.

Azuma, K. and M. Sakaki, 1987,"Method of laser marking", Mitsubishi Denki Kabushiki Kaisha, US 4861620, 22-10-1987,

Bastue, J. and F. O. Olsen (1996).Energy enhancer for mask based laser material processing, Personal Communication

Bauerle (1986). Laser processing and chemistry, Springer. 3-540-60541-X

Berman, M. R. (1992). "Excimer laser darkening of ETFE polymer films." Journal of applied Polymer science **45**: 111-117.

Bityrin, N., N. Arnold, et al. (1998). "Bulk model of laser ablation of polymers." Applied surface Science **127-129**: 164-170.

Blanchet, G. B. (1996). "Laser ablation and the unzipping of addition polymer." J. Appl. Phys. **80**(7): 4082-4089.

Boden, G., E. Richter, et al., 1983,"Verfahren zur fabrigen Dekoration auf Glass", Akademie der Wissenschaften der DDR, DDR 229493 8, 26-01-1983, DDR Amt fuer Erfindungs und Patentwesen

Boden, G., E. Richter, et al., 1983,"Verfahren zur herstellung farbiger Dekorationen auf Glass", Akademie der Wissenschaften der DDR, DDR 2331526, 06-04-1983, Deutsche Demokratische Republik Amt fuer Erfindungs und Patentwesen

Bosman, J., 1996,"Method of producing a patterned surfacial marking on a transparent body", Philips, US 5987920, 19-09-1996, US patent

Bosman, J., 2003,"Method of manufacturing an electronic component and electronic component obtained by means of said method", WO2003031193,

Bosman, J. and v. Dooren, 1998,"Method of selectively removing a metallic layer from a non- metallic substrate", Philips, US 5759416,

Breuer, J. (1995). "Photolytic surface modification of polymers with UV laser radiation." Journal of adhesion science and technology **9**(3): 351 - 363.

Brimrose, (2003), Introduction to A-O Deflectors/Scanners,Internet,

Bruton, N. J. (1997). "Profiling laser coding in the packaging industry." Opt. Photonics News **8(5)**: 24-30.

Butenin, a. V. and B. Y. Kogan (1976). "Mechanism of damage of transparent polymer materials due to multiple exposure to laser pulses." Sov. J. Quant Electron **6**(5): 611-613.

Chan, J. H. (1995). The thermal degradation of polypropylene and the effect of infrared-laser irradiation. Chemical Engineering and Applied Chemistry. Toronto, Univ. of Toronto**:** 219.

Cicala, E., D. Zsivanov, et al. (1998). "Off line multiresponse optimization of gas jet assisted, CO(2) laser cutting of PMMA." Proc. SPIE Int. Opt. Eng. 1998 (fifth conference on Optics 1997) **3405**: 293-298.

Clement, R. M., N. R. Ledger, et al., 1993,"Sub-surface marking", United Distillers PLC, WO 92/03297, 14-08-1991,

Cornish, P. (1997). Laser beam absorption and mark depth of laser marked wires. Bridgend, Spectrum Technologies Limited**:** 13.

Dance, B. (1990). "Excimer-laser system marks rapidly moving wire." Industrial Laser review **October**: 15.

Daniels, E. and H. Schuerle, 1989,"Verfahren zum Erzeugen einer Kennzeichnung und/oder Markiering auf einer Brillenlinse", Fa. Carl Zeiss, DE 3731398, 6-04-1989, Deutches Patentamt

Day, J. H. (1962). "Thermochromism." Chemical review **63**: 65 - 80.

Decker, C. (1980). "Laser -induced degradation of polyvinyl chloride." Journal Photochemistry **15**(1981): 221-228.

Dickinson, P., S. Williams, et al., 1988,"Laser marking", Britisch Aerospace PLC, 0 329 884 A1, 17-06-1988, European patent office

Dickmann, K. and E. Dik (1995). "Innenbearbeitung von Glas mit Nd:YAG-Laser." Laser magazin **1**: 16-19.

Dijk, J. (2004).Lasermarkeren CO_2 Laser, Personal Communication

Dmitriev, V., S. Oshemkov, et al. (2000). "Material processing applications of lasers using optical breakdown."

Drouillard, G. and R. W. Kanner, 1999,"Produce marking system", Atrion Medical Product Inc., US5897797, 27 April 1999,

Dufour, A., 1974,"Procedes et dispositifs de traitement thermique en profondeur de produits et produits traites ainsi obtenus", FR2195408, 1972-08-11,

Edginger, E. and G. Kohler, 1980,"Verfahren zur Herstellen von mit verschiedenen Zeichen versehenen gleichartigen Kunststoffteilen, insbesondere Kunststoff Geraetetasten durch Spritzgiessen." Siemens AG, DE 3044722 C2, 27-11-1980, Deutches Patent Amt

Edler, G. (1989). Laser markierung von Kunststoffen mit Hilfe von Perlglanzpigmenten, Merck**:** 1-6.

Elshout, W. v. d. and O. Aagaard (1996). "Process for the manufacture of an object with a coloured marking."

Erokhin, A., 1993,"Method and Apparatus for creating an image by a pulsed laser beam inside a transparent material", Podarok International, US5637244, 19 aug 1993, United state Patent office

F.Kuhn-Kuhnenfeld, J. Kramler, et al., 1984,"Method of marking reference surface markings on semiconductor wafers by laser beam", Wacker-Chemitronic, US 4,522,656, 26-04-1984, US patent opffice

Feng, K., 1997,"Controlled color laser marking of plastics", M.A. Hannacolor, WO 98 56,594, 13 juni 1997, World intellectual property organization

Fillaud, C., 1987,"Procede de traitment thermique d'un produit alimentaire, notamment fromager ou charcutier." Bongrain S.A., FR2621529, 1987-10-9, Institut national de la properiete industrielle

Frick, T., S. Polster, et al. (2004). Simulation des Laserstrahl-Kunststoffschweissens. Laserstrahl-Kunststoffschweissen, Duesseldorf, Bayerisches Laserzentrum.

Fujiura, K. (2005). <u>KTN optical devices with an extremely large electro-optic effect</u>. Passive components and fiber-based devices, SPIE. 5623

Fujiura, K. (2007).KTN based scanner, Personal Communication

G.E.Jellison (1984). "Optical and electrical properties of pulsed laser annealed silicon." <u>Semiconductors and semimetals</u> **23**(Pulsed laser processing of semiconductors).

Gaissinsky, 2003,"<u>Method and apparatus for generating color images in a transparent medium</u>", US20030015509, 23 jan. 2003, United States Patent Office

Gao, F., D. Price, et al. (1997). "Laser pyrolysis of polymers and its relation to polymer fire behaviour." <u>j. Anal. Appl. Pyrolysis</u> **40-41**: 217-231.

Graydon, O. (2005). Laser turn clothes into works of art. <u>Optics.org</u>.

Guskov, A., 1984,"<u>Laser glass marker focuses beam on interface of glass substrate and carbon powder for their fusion</u>", SU1106798-A, 07-aug-1984,

Hafez, M., T. Slider, et al. (2000). "Design, Simulations and experimental investigations of tip/tilt scanner." <u>Mechatronics</u> **10**: 741-760.

Hamano, K. and H. Kato, 1994,"<u>Ornamental parts and their production</u>", Citizen Watch Co Ltd., JP 06,256,993, 13-9-1994, Japanse patent office

Hare, D. E. and D. D. Dlott (1997). <u>Pulse duration dependence for laser photothermal imaging media</u>. IS&T's 50th Annual conference.

Harrison, P. W., 2000,"<u>High contrast surface marking</u>", Thermark, US 6075223, 8-09-1997, United states Patent office

Hei, v. d. (1990). Spectra van de licht transmissie in het UV+VIS+IR gebied (200 nm - 20 um). Eindhoven, Philips PMF**:** 35.

Heller (1995). Minutes of a meeting held to discuss final details of the syladec (BE96-3503) proposal. Eindhoven, Philips CFT.

Herkt-Maetzky, C. (1994). "Weiss auf schwarz, Laserbeschriften." <u>Kunststoffe 84</u> **7**: 872-875.

Heumann, E., J. Kleinschmidt, et al. (1985). Einschreiben von Information in das Volumen transparenter Plastmaterialen mittels Laserstrahlung. Laser 85, Muenchen, Springer.

Hofmann, H., R. C. Sykes, et al. (1987). High contrast and intact surface - a challenge in laser marking of plastics. Lasers in motion for industrial applications, Los Angeles, SPIE. 744

Hofmann, M. and F. Herren, 1989,"Laserbeschriftung von keramischen Materialen, Glasuren, keramische Glaesern and Glaesern", Ciba-Geigy AG, EP 0 391 848 A1, 28-03-90, European Patent Office

Hopp, B., Z. Marton, et al. (1998). Investigation of changes in optical properties of excimer laser irradiated polymers. Modern optics, SPIE. 3573

Hulst, H. C. v. d. (1957). Light scattering by small particles, Wiley, New York.

Hunt, R. W. G. (1987). Measuring colour. ISBN0-7458-0125-0

Ifflaender (1990). FestKoerperlaser zur Materialbearbeitung, Springer-Verlag. ISBN 3-540-52150 X

Kahn, N., 2002,"Laser coding", Sherwood Technology LTD., WO02/068205, 27 February 2002,

Kantor, Z., Z. Toth, et al. (1994). "Deposition of micrometer-sized tungsten patterns by laser transfer technique." Appl. Phys. Lett. **64(25)**: 3506-3508.

Kanzaki, 1973,"Improvements in or relating to colouring techniques using lasers", Kansai Paint Company, 1 459 799, 11-12-1972, Patent office London

Kato, H., 1994,"Resin compositions for laser marking", GE Plastics, 0 675 001 A1, 29-03-94, European patent office

Kaufmann, S. and A. Otto (1999). Lasergestuetzte Fuegeverfahren fuer die Lichtwellenleiter Technik. Laser in der Elektronikproduction & Feinwerktechnik (LEF 99).

Kern, W. (1997). "Laser engraving of rubbers." raw materials and applications **10**: 710 - 715.

Kichelhain, J., G. Kusnezow, et al., 1998,"Method for making a marking in a glass body", LPKF Laser & Electronics AG, WO oo/32531, 2 -12-1998,

Kleinschmidt, P., G. Mader, et al., 1987,"Device for laser transfer printing", Siemens AG, WO 88 / 07450, 27-03-1987,

Klimt, B. H. (1988). "Review of Laser Marking and Engraving." Laser & Optronics **September 1988**: 61 - 67.

Koechner (1992). Solid-state laser engineering, Springer-Verlag. 0-387-53756-2

Krevelen, D. W. v. (1976). Chemical degradation of polymers. Properties of polymers, their estimation and correlation with chemical structure, elsevier. **chap. 22:** 467-472.

Krevelen, D. W. v. (1976). Thermal decomposition. Properties of polymers, their estimation and correlation with chemical structure, elsevier. **chap. 21:** 459-465.

Kuntze, T., M. Panzner, et al. (2003). New excimer laser marking method using MMD. Fourth International Symposium on Laser Precision Microfabrication, Munich, SPIE. 5063

Kuwahara, K., K. Sasaki, et al., 1997,"Laser beam marking of wafers and chips", Hitachi, JP 10 211,593, 29-01-1997, Japan Patent Office

Kvapil, J., B. Perner, et al., 1990,"Verfahren zur Beschriftung oder Dekoration von transparenten Substraten mit einem Laser", Glas und Laser applikation Systeme, 0 531 584 A1, 03-12-1991, european patent office

Laakmann, P. (1990). "A Bright future for small, sealed CO(2) Lasers." Photonics Spectra (reprinted by Laurin Publishing Co. Inc.)(October 1990).

Laakmann, P. (1991). "CO(2) Lasers mark color on Aluminum." Industrial Laser Review **June**: 11 - 14.

Laakmann, P., 1993,"Method and apparatus for multi-color laser engraving", Laser Color Marking, US 5215864, 1 june 1993,

Lau, S. T. (1997). User applied markings on wires working towards perfect legibility. SAE Aerospace Electrical Interconnect Systems Conference, Williamsburg, West Virginia, Spectrum Technologies Limited.

Lenk, A., T. Witke, et al. (1998). Laser precision machining of glass. ECLAT, European Conference on Laser Treatment of Materials.

Lenk, A., T. Witke, et al. (1998). Q-switched and mode-locked solid state laser for precision machining of transparent materials. High Power laser ablation, Santa Fe New Mexico, SPIE. 3343

Leyen, D. v. (1971). Waermeuebertragung. Berlin,Muenchen, Siemens Aktiengesellschaft.

Lippert, T. (1997). "Laser ablation of doped polymer systems." Adv. Mater. (Weinheim, Ger.) 9(2): 105-119.

Lucchesi, M. and J. Padiou, 1996,"Method for laser marking glass objects and the marked objects obtained", Cabinet Bonnet Thririon, WO 96/32221, 17-10-1996,

Luehs (2005). Apple trift Laser. Trumpf express. 05: 28-31.

Lumonics (1992). Electronics, semiconductors play key role in marking. Industrial Laser review: 7-9.

Madorky, S. L. (1954). J.Res. Natl. Bur. Std. 53(361).

Mann, C. O., 1983,"Materialstueck aus Aluminium, vorzugsweise Aluminiumschild und verfahren zur Herstellung desselben", Carl Baasel Lasertechnik GmbH, EP0,121,150, 09-03-84, European patent office

Masashi, I., 1995,"Method of driving liquid crystal mask marker", K.K. Komatsu Seisakusho, WO 9521718, 17-08-95, Japanese patent office

McKee, T. and J. Scaroni (1997). "A close look at laser marking of silicon wafers." Solid state technology 06-1997: 245-251.

Meier, M. and W. Weinfurtner, Eds. (1990). Lasern Beschriften fast alles. Laser Praxis, Carl Hanser Verlag Muenchen.

Meijer, J. (2002). Laser Micromachining, Marcel Dekker, Inc. 0-8247-0644-7

Meneghini, F. A., 1995,"Transfer printing medium", Markem Coorperation, wo 97/20696, 6-12-1995, World intellectual property organisation

Michl, P. (1992). Beschriften mit Lasern, VDI Verlag. 3-18-400990-4

Miller, A., 2006, MieTab Scattering for Windows, 8.34.03, Windows computer program

Moisan, J. (1985). Effects of Oxygen Permeation and Stabiliser Migration on Polymer Degradation. Plymer Permeability. J. Comyn. Leceister, Elsevier Applied Science**: 119 - 176.

Sub-surface marking, 2002, Boards of appeal of the european patent office, 4-02-2002, T 0345/00 3.2.5

Murphy, J. (1996). Additives for Plastics, Elsevier Science Pub Co. ISBN 185617 281 3

Nagata, I., T. Nakanishi, et al., 1994,"Decorative treatment of metal surfaces comprising irradiation with laser beam and coating with oxide or nitride film." Osaka Fuji Kogyo Kk, JP 06,212,451, 11-01-1993, Japanese Patent Office

Nanai, L., R. Vajtai, et al. (1996). "Laser-induced oxidation of metals: state of the art." Thin Solid Films **298**(1997): 160-164.

Nilson, J. A. (1982). Laser marking via mask projection. ICALEO 1982, LIA. 31

Pan, C. T. and H. Hocheng (1997). "Prediction of laser-induced thermal damage of fiber mat and fiber matUD reinforced polymers." Journal of materials engineering and performance **7**(6): 751-756.

Parts, L. P., J. Pinsky, et al., 1971,"Method for selectively foaming the surface of a thermoplastic article by use of a laser", Monsanto Research Corporation, US 3,627,858, 14-12-1971, United State Patent

Perry, D. V. and W. H. Huffines (1986). Quality evaluation of CO_2 and Nd:YAG Laser Marking of ceramic chip capacitors, IEEE. 0569-5 503/86/0000

Pinner, S. and A. J. Swallow, 1956,"Causing colour changes in polymer plastics by irradiation", TI limited, 835120, 20-07-1956, Patent office London

Pique, A., J. Fitz-Gerald, et al. (2000). Direct writing of electronic materials using a new Laser assisted transfer/annealing technique. Laser Applications in Microelectronic and Optoelectronic Manufacturing V, SPIE. 3933

Pique, A., J. Fitz-Gerald, et al. (1999). "A novel laser transfer process for direct writing of electronic and sensor materials." Appl. Phys. A **A69**: 279-284.

Popat, A. H. and M. R. Edwards, 1996,"Process for forming a colored three-dimensional article", Zeneca limited,
US6133336, 30-08-1996, United States Patent Office

Potente, H., J. Korte, et al. (1998). <u>Laser transmission welding of thermoplastics analysis of the heating phase.</u> Antec 98. 1

Poyton, C., (1997), Poynton's Colour FAQ, http://www.poyton.com/PDFs/ColorFAQ.pdf

Prahl, S., M. Keijzer, et al. (1989). <u>A Monte Carlo model of light propagation in tissue</u>. Dosimetry of Laser dosimetry of laser radiation in medicine and biology radiation in medicine and biology, SPIE.

Prichystal, J. P., H. N. Hansen, et al. (2005). <u>Invisible display in aluminum</u>. Photonics West 2005, San Jose, SPIE. 5713

Rabek, J. (1996). <u>Photodegradation of polymers</u>, Springer-Verlag. ISBN 3-540-60716-1

Reyna, L. (1994). "Laser ablation of multilayer polymer films." <u>J. Appl. Phys.</u> **76(7)**: 4367-4371.

Reyna, L. G. (1995). "Repetition rate effect on the laser ablation of polymer structures." <u>J. Appl. Phys.</u> **78**(5): 3423 -3427.

Rhothor, (2007), XY2-100 Interface technical datasheet,http://www.newson.be/Files/TD_XY2-100_R0608.pdf,

Sato, T. and K. Kaminaga (1995). <u>Pattern marking on transparent materials by YAG laser</u>. Surf. Modif. Technol VIII 8th 1994, The institute of Materials, London.

Sayed, A. E., F. Gerling, et al., 1994,"<u>Polymerformmassen zur partiellen farblichen Veranderung durch Laserenergie, Insbesondere zur erzeugung bunter Zeichen.</u>" Bayer AG, 0 675 168 A1, 17-03-1995, Europen patent office

Scanlab, (2004), Specification HS& datasheet,

Schildbach, K. (1990). "Solid-state laser pulse shape."

Schott, (2004), Optical Glass Catalog, www.schott.com/optics_devices/english/products/flash/abbediagramm_flash.html,

Schultze, V. and M. Wagner (1991). "Laser-induced forward transfer of aluminium." <u>Applied surface science</u> **52**: 303-309.

Schumacher, B., 1985,"Verfahren zum Dekorieren, Markieren und Gravieren odgl. von Gegenstaenden mit emaillierten Oberflaechen mittels Laserstrahl", VEB Berlin, 10-7-1986, Deutches Patent Amt

science, C. (1982). Color science: concepts and methods. ISBN 0-471-02106-7

Scruby, C. B. and L. E. Drain (1990). Laser ultrasonics, Adam Hilger. 0-7503-0050-7

Seth, A. and J. Scaroni (1986). "Ceramic component Marking with YAG Lasers." Semiconductor International(October): 80 - 83.

Simoes, F. D. S., J. P. Coelho, et al., 1996,"Method for colouring effects of rock by laser rays", WO 96/12684, 2-05-1996, PCT

Smith, J. and M. Cooper, 2001,"Marking diamond", Gersan Establishment, US6187213, 13 feb 2001, United states patent office

Staupendahl, G. and P. Gerling (1997). Laser material processing of glasses with CO(2) lasers. Lasers in Material Processing, SPIE. 3097

Tokarev, V. N. (1994). "Clean processing of polymers and smoothing of ceramics by pulsed laser melting." J. Appl. Phys. **77 (9)**: 4714-4723.

Toth, Z., B. Hopp, et al. (1999). Pulsed Laser ablation mechanisms of thin metal films. Europto, Computer controlled Micro shaping, Muenchen, SPIE. 3822

Troitski, I., 2002,"Method for creating laser-induced color images within three-dimensional transparent media." Troitski, US6664501, 13 june 2002, United States Patent Office

Veiko, V. P., E. A. Shahno, et al. (1996). Local Laser-induced film transfer: theory and applications. Lasers as tools for manufacturing of durable goods and microelektronics, SPIE. 2703

Voelz, H. G. (1995). Industrial colour testing. ISBN 3-527-28643-8

Vorst, 1980,"Method of marking a synthetic material surface and to an object having the marked synthetic material surface", EP0036680, 25-03-1980, European Patent Office

Weinfurtner, W. W. (1995). Licht Schreibt, beschriften mit dem Laser in der Industrie. 3-8169-1237-0

Weisser, h. and H. Mueller, 1996,"Verfahren zum indirekten Beschriften von transparenten Materialien", Jenoptik, DE 19637255, 13-09-1996, Deutsches Patent Amt

Wielstra, 1994,"Method for marking a surface of an object by means of a laser", Philips, EP0628424, European patent application

Wood, R. (1995). Pulse duration dependence of laser damage. Laser induced damage in optical materials, SPIE. 2428

Yeo, K. K., 2004,"Marking of an anodized layer of an aluminium object", Philips, US6777098, 17-08-2004, United States Patent Office

Zelensky, S. (1999). "Laser-induced heat radiation of suspended particles: a method for temperature estimation." J. Opt. A **1**(Pure Appl. Opt.): 454-458.